

Mathematical Modeling of Atom Transfer Radical Polymerization

by

Mamdouh Al-Harhi

A thesis

presented to the University of Waterloo

in fulfillment of the

thesis requirement for the degree of

Doctor of Philosophy

in

Chemical Engineering

Waterloo, Ontario, Canada, 2006

© Mamdouh al-Harhi, 2006

I hereby declare that I am the sole author of this thesis. This is a true copy of the thesis, including any required final revisions, as accepted by my examiners.

I understand that my thesis may be made electronically available to the public.

Abstract

Atom transfer radical polymerization is a new and important living polymerization mechanism because it can produce many different polymers with controlled microstructures and novel properties. The commercialization of these new polymers will require detailed polymer reaction engineering investigations. Mathematical models are essential in this stage because they can summarize our knowledge on polymers made by ATRP and help us to find the optimum conditions for their synthesis.

This thesis studies the polymerization kinetics of ATRP with mathematical models based on our own experimental work and experimental data published by other researchers. ATRP with both monofunctional and bifunctional initiators are considered. This is one of very few studies combining detailed mathematical models for polymerization kinetics and polymer microstructure and experimental results in the area of ATRP.

Fundamental mathematical models were used to study the main features of ATRP. Population balances and the method of moments were used to predict polymer average properties, while Monte Carlo models were used to predict the complete microstructural distributions. This type of comparison between different modeling techniques is seldom done in the literature, even for other polymerization techniques, and can lead to a better understanding of polymerization mechanisms and mathematical modeling techniques.

Since the discovery of ATRP, approximately ten years ago, little attention has been given to bifunctional initiators. This thesis tries to extend our knowledge on this important class of initiators. Comparison between monofunctional and bifunctional initiators, both through mathematical modeling and experimentally, showed that bifunctional initiators have some advantages over monofunctional initiators for ATRP. Polymers made with bifunctional initiators have narrow molecular weight distributions, higher molecular weight averages, and higher monomer conversion for the same polymerization time.

In addition to homopolymerization studies, this thesis presents mathematical models for copolymerization with ATRP and for processes combining ATRP and coordination polymerization. These models describe the detailed microstructures of these

copolymers and permit a better understanding of ATRP with its advantages and pitfalls. An interesting conclusion from these modeling studies in atom transfer radical copolymerization is that the Mayo-Lewis terminal model is applicable to ATRP and that the copolymer composition in ATRP is independent of the equilibrium constants (activation and deactivation).

In order to develop and validate these mathematical models, we collected experimental data in our own laboratories and also used experimental data available in the literature. Our experimental work focused on the homopolymerization and copolymerization of styrene, because of the commercial importance of this monomer and also due to the relative simplicity of its polymerization. Experimental data collected from the literature covered the following systems: bulk homopolymerization of styrene, solution polymerization of styrene, solution polymerization of methyl methacrylate, bulk polymerization of n-butyl acrylate, bulk copolymerization of styrene and n-butyl acrylate. Different characterization techniques were used to determine polymer properties. Molecular weight and molecular weight distribution were measured using gel permeation chromatography (GPC); copolymer chemical composition was determined with nuclear magnetic resonance (NMR) and Fourier-transform infrared (FTIR). We have also done copolymerization with styrene and acrylonitrile (SAN) because it is one of the least understood ATRP system and also because its potential industrial importance.

The ability to synthesize polymers with novel molecular architectures is one of the advantages of living polymerization techniques. In this thesis, we used ATRP to produce amphiphilic copolymers composed of polystyrene and polyethylene glycol methacrylate macromonomers. We have shown that ATRP can produce these very interesting polymers with two different types of macroinitiators.

Acknowledgments

My unqualified gratitude is to Allah, the Almighty who guided me in every facet of this work in his infinite wisdom and bounties.

For this dissertation, I am deeply indebted to Professor. Joao Soares and Professor. Leonardo Simon who served as my supervisor. This dissertation would never have been accomplished without there priceless support, constant encouragement, and valuable advice throughout my academic journey.

I would like to express my thanks to my supervisory committee members: Professor Michael Cunningham, Professor Jean Duhamel, Professor Thomas A. Duever, and Professor Xianshe Feng

I would also like to take this opportunity to thank my colleagues, lab technicians, and the co-op students for their assistance throughout this work.

I would also acknowledge the financial support from King Fahad University of Petroleum & Minerals (KFUPM) and the Natural Science and Engineering Research Council of Canada (NSERC).

Finally, my deep thanks go to my parents and my wife for their love, support and encouragement for their invaluable help and motivation.

Table of Contents

Abstract.....	iii
Acknowledgments.....	v
Table of Contents.....	vi
List of Figures.....	x
List of Tables.....	xvi
NOMENCLATURE.....	xvii
List of Publications.....	xix
1 Introduction.....	1
1.1 Motivation.....	1
1.2 Objectives.....	2
1.3 Thesis contents.....	3
2 Background and Literature Review.....	5
2.1 Free radical polymerization.....	5
2.2 Copolymerization.....	6
2.2.1 Introduction.....	6
2.2.2 Copolymerization models.....	8
2.3 Living radical polymerization.....	10
2.4 Atom transfer radical polymerization.....	12
2.4.1 Mechanism.....	12
2.4.2 Copolymerization via ATRP.....	14
2.5 Coordination polymerization.....	15
2.6 Modeling of ATRP.....	19
2.7 References.....	21
3 Methods and Materials.....	23
3.1 Mathematical modeling.....	23
3.2 Experimental.....	25
3.2.1 Materials.....	25
3.2.2 Polymerization and polymer purifications.....	25
3.2.3 Polymer characterization.....	29
3.3 References.....	31
4 Dynamic Monte Carlo Simulation of Atom-Transfer Radical Polymerization.....	32
4.1 Abstract.....	32
4.2 Introduction.....	32
4.3 Model description.....	33
4.4 Results and discussions.....	40
4.4.1 Effect of control volume size.....	40
4.4.2 Effect of the equilibrium constant.....	44
4.4.3 Simulation of the complete MWD.....	47
4.4.4 Model validation.....	51
4.5 Conclusions.....	53
4.6 References.....	55
4.7 Appendix.....	57
Chapter 5.....	61

5	Mathematical Modeling of Atom-Transfer Radical Polymerization Using Bifunctional Initiators	61
5.1	Abstract	61
5.2	Introduction	61
5.3	Model development	63
5.3.1	Reaction mechanism	63
5.3.2	Population balances	65
5.3.3	Kinetics parameters	66
5.3.4	Method of moments	67
5.4	Results and discussion	68
5.4.1	Comparison between monofunctional and bifunctional initiators	68
5.4.2	Effect of the equilibrium constant	71
5.4.3	Effect of the propagation rate constant	73
5.4.4	Effect of the termination constant	76
5.4.5	Effect of catalyst and initiator concentration	78
5.5	Conclusions	82
5.6	References	84
5.7	Appendices	86
6	Modelling of Atom Transfer Radical Polymerization with Bifunctional Initiators: Diffusion Effects and Case Studies	90
6.1	Abstract	90
6.2	Introduction	91
6.3	Model development	91
6.3.1	Diffusion control	92
6.3.2	Free volume theory	92
6.3.3	Model parameters	94
6.4	Results and discussion	95
6.4.1	Diffusion effects	95
6.4.2	Case studies – model validation	104
6.5	Conclusions	114
6.6	References	116
	Chapter 7	117
7	Dynamic Monte Carlo Simulation of ATRP with Bifunctional Initiators	117
7.1	Abstract	117
7.2	Introduction	118
7.3	Model description	118
7.3.1	Kinetics parameters	122
7.4	Results and discussion	123
7.4.1	Comparison of Monte Carlo simulation with the method of moments ..	123
7.4.2	Comparison between monofunctional and bifunctional initiators	125
7.4.3	Characteristics of the dynamic Monte Carlo simulation	129
7.5	Conclusions	138
7.6	References	140
	Chapter 8	141
8	Atom-Transfer Radical Polymerization of Styrene with Bifunctional and Monofunctional Initiators: Experimental and Mathematical Modeling Results	141

8.1	Abstract.....	141
8.2	Introduction.....	142
8.3	Experimental section.....	142
8.4	Model development.....	143
8.4.1	Reaction mechanism.....	143
8.4.2	Diffusion effects.....	145
8.5	Results and discussion.....	147
8.5.1	Effect of thermal initiation and elimination reactions.....	147
8.5.2	Comparison of benzal bromide with 1-bromo ethyl benzene.....	148
8.6	Conclusions.....	160
8.7	References.....	161
9	Atom Transfer Radical Polymerization (ATRP) of Styrene and Acrylonitrile with Monofunctional and Bifunctional Initiators.....	162
9.1	Abstract.....	162
9.2	Introduction.....	162
9.3	Experimental.....	164
9.4	Results and discussion.....	166
9.5	Conclusion.....	179
9.6	References.....	181
	Chapter 10.....	182
10	Mathematical Modeling of Atom Transfer Radical Copolymerization.....	182
10.1	Abstract.....	182
10.2	Introduction.....	182
10.3	Model development.....	184
10.3.1	Polymerization mechanism.....	184
10.3.2	Pseudo-Kinetic constants.....	185
10.3.3	Polymerization rate constants.....	188
10.3.4	Method of moment equations.....	188
10.4	Results and discussion.....	191
10.4.1	Model validation.....	191
10.4.2	Effect of ATRP parameters on copolymer sequence lengths.....	196
10.5	Conclusions.....	201
10.6	References.....	202
	Chapter 11.....	211
11	Dynamic Monte Carlo Simulation of Graft Copolymers Made with ATRP and Metallocene Catalysts.....	211
11.1	Abstract.....	211
11.2	Introduction.....	211
11.3	Model development.....	214
11.3.1	ATRP mechanism.....	214
11.3.2	Coordination polymerization mechanism.....	214
11.3.3	Principles of Monte Carlo simulation.....	215
11.4	Modeling macromonomer formation.....	217
11.5	Modeling of graft copolymer formation.....	217
11.6	Conclusion.....	221
11.7	References.....	222

12	Amphiphilic Copolymers of PS and PEGMA using ATRP	224
12.1	Abstract	224
12.2	Introduction.....	224
12.3	Experimental	226
12.4	Results and discussion	227
12.5	Conclusion	232
12.6	References.....	233
13	Conclusions and Recommendations	235

List of Figures

FIGURE 2.1 GENERAL COPOLYMERIZATION REACTION SCHEME.	7
FIGURE 2.2 TYPES OF COPOLYMER TOPOLOGIES.....	7
FIGURE 2.3 GENERAL LFRP MECHANISM.	11
FIGURE 2.4 GENERAL NMP MECHANISM. <i>D</i> : DORMANT SPECIES; R^\bullet : PROPAGATING RADICAL; <i>X</i> : THE NITROXIDE GROUP.	11
FIGURE 2.5 ATRP MECHANISM. <i>RX</i> : DORMANT SPECIES (ALKYL HALIDE); M_i^n / L : ACTIVATOR (METAL COMPLEX); R^\bullet : PROPAGATING RADICAL; $X - M_i^{n+1} / L$: DEACTIVATOR; <i>M</i> : MONOMER; <i>P</i> : DEAD CHAIN.	12
FIGURE 2.6 ILLUSTRATION OF TRIBLOCK COPOLYMER. <i>XRX</i> : BIFUNCTIONAL INITIATOR; [<i>A</i>]: MONOMER A; [<i>B</i>]: MONOMER B.....	15
FIGURE 2.7 ATRP INITIATOR FOR SYNTHESIZING STAR POLYMERS.	15
FIGURE 2.8 TACTICITY OF POLYSTYRENE.....	16
FIGURE 2.9 GENERALIZED STRUCTURE OF A METALLOCENE CATALYST PRECURSOR. <i>M</i> – TRANSITION METAL CENTER; <i>X</i> – HALOGEN; <i>R</i> – ALKYL OR AROMATIC LIGAND; <i>B</i> – BRIDGING GROUP.	17
FIGURE 2.10 TYPES OF GRAFT COPOLYMERS.	18
FIGURE 3.1 PICTURE OF THE REACTION MIXTURE IN THE REACTOR DURING THE POLYMERIZATION. THE BROWN COLOUR IS CAUSED BY THE PRESENCE OF CuBr(I).	27
FIGURE 3.2 ALUMINIUM OXIDE AFTER FILTERING THE POLYMER SOLUTION. THE GREEN COLOR IS CAUSED BY THE PRESENCE OF CuBr(II).	27
FIGURE 3.3 LIQUID-LIQUID EXTRACTION OF THE CATALYST FROM THE ORGANIC PHASE TO THE WATER PHASE. (A) BEFORE THE EXTRACTION (B) AFTER THE EXTRACTION.	28
FIGURE 4.1 ALGORITHM FOR MONTE CARLO SIMULATION OF ATRP.....	38
FIGURE 4.2 EFFECT OF THE CONTROL VOLUME ON THE MOLECULAR WEIGHT DISTRIBUTION AT <i>X</i> =0.1: (A) $V = 1 \times 10^{-21}$ L, (B) $V = 1 \times 10^{-20}$ L, (C), $V = 1 \times 10^{-19}$ L, AND (D) $V = 1 \times 10^{-18}$ L.....	43
FIGURE 4.3 EFFECT OF THE CONTROL VOLUME ON THE POLYMERIZATION TIME (THE RATE CONSTANTS ARE SHOWN IN TABLE 1, $[C]_0/[I]_0/[M]_0$ MOLE RATIO: 1:1:100).	44
FIGURE 4.4 EFFECT OF EQUILIBRIUM CONSTANT (K_{EQ}) ON (A) MONOMER CONVERSION, (B) DEGREE OF POLYMERIZATION AND (C) POLYDISPERSITY INDEX. ($K_p = 1516 \text{ L mol}^{-1} \text{ s}^{-1}$, $K_t = 0.5 \text{ L mol}^{-1} \text{ s}^{-1}$, $K_{TC} = 3.469 \times 10^8 \text{ L mol}^{-1} \text{ s}^{-1}$, $K_{TD} = 0$, $K_{TR} = 0.22$, $V = 1 \times 10^{-19}$, $[C]_0/[I]_0/[M]_0$ MOLE RATIO: 1:1:100).	46
FIGURE 4.5 EFFECT OF EQUILIBRIUM CONSTANT (K_{EQ}) ON MOLECULAR WEIGHT DISTRIBUTION AT CONVERSION 0.3 AND CONTROL VOLUME 1×10^{-19} . ($K_p = 1516 \text{ L mol}^{-1} \text{ s}^{-1}$, $K_t = 0.5 \text{ L mol}^{-1} \text{ s}^{-1}$, $K_{TC} = 3.469 \times 10^8 \text{ L mol}^{-1} \text{ s}^{-1}$, $K_{TD} = 0$, $K_{TR} = 0.22$ $[C]_0/[I]_0/[M]_0$ MOLE RATIO: 1:1:100).....	46
FIGURE 4.6 NUMBER AVERAGE MOLECULAR WEIGHT (M_n) VERSUS MONOMER CONVERSION FOR ATRP PREDICTED BY MONTE CARLO SIMULATION AND THE METHOD OF MOMENTS (THE RATE CONSTANTS ARE SHOWN IN TABLE 1 AND $[C]_0/[I]_0/[M]_0$ MOLE RATIO: 1:1:100).	48
FIGURE 4.7 POLYDISPERSITY INDEX VS. MONOMER CONVERSION FOR ATRP PREDICTED BY MONTE CARLO SIMULATION AND THE METHOD OF MOMENTS. (THE RATE CONSTANTS ARE SHOWN IN TABLE 1 AND $[C]_0/[I]_0/[M]_0$ MOLE RATIO: 1:1:100).	49
FIGURE 4.8 COMPARISON BETWEEN THE CLD OF POLYSTYRENE MADE WITH ATRP AND CONVENTIONAL FREE RADICAL (CFR) POLYMERIZATION AT 50 % CONVERSION (THE KINETIC RATE CONSTANTS ARE SHOWN IN TABLE 1). THE INITIATOR TO MONOMER RATIOS ARE 1:100 (ATRP LEFT PEAK), 1:500 (ATRP RIGHT PEAK), AND 1:1000 (CFR).	49
FIGURE 4.9 MWD OF POLYSTYRENE MADE WITH ATRP: A) NUMBER DISTRIBUTION, B) WEIGHT DISTRIBUTION, AND C) Z DISTRIBUTION, AT DIFFERENT MONOMER CONVERSIONS. THE MONOMER CONVERSIONS, FROM LEFT TO RIGHT, ARE 10 %, 50%, AND 99%.....	51
FIGURE 4.10 COMPARISON BETWEEN MODELS PREDICTIONS (MONTE CARLO AND METHOD OF MOMENTS) AND EXPERIMENTAL DATA FOR STYRENE POLYMERIZATION IN BULK AT 110 °C: (A) $\ln([M_0]/[M])$, (B) NUMBER AVERAGE MOLECULAR WEIGHT, AND (C) POLYDISPERSITY INDEX. (POLYMERIZATION CONDITIONS: $[M]/[I]/[CAT]=100:1:1$ (MOLAR RATIO), REACTION TEMPERATURE $T = 110^\circ\text{C}$. KINETIC PARAMETERS ARE SHOWN IN TABLE 4.1). EXPERIMENTAL DATA FROM MATYJASZEWSKI ET AL. ^[30] ...	53

FIGURE 5.1 EFFECT OF MONO AND BIFUNCTIONAL INITIATORS ON MONOMER CONVERSION (X) AS A FUNCTION OF TIME (T). ($K_p=1000 \text{ L MOL}^{-1} \text{ S}^{-1}$, $K_{TC}=1 \times 10^7 \text{ L MOL}^{-1} \text{ S}^{-1}$, $K_{TD}=0$, $K_D=1 \times 10^7 \text{ L MOL}^{-1} \text{ S}^{-1}$, $K_A=0.01 \text{ L MOL}^{-1} \text{ S}^{-1}$, $[C]_0/[I]_0/[M]_0$ MOLE RATIO: 1:1:100).....	69
FIGURE 5.2 EFFECT OF MONO AND BIFUNCTIONAL INITIATORS ON NUMBER AVERAGE CHAIN LENGTH (RN) AS A FUNCTION OF TIME (T) ($K_p=1000 \text{ L MOL}^{-1} \text{ S}^{-1}$, $K_{TC}=1 \times 10^7 \text{ L MOL}^{-1} \text{ S}^{-1}$, $K_{TD}=0$, $K_D=1 \times 10^7 \text{ L MOL}^{-1} \text{ S}^{-1}$, $K_A=0.01 \text{ L MOL}^{-1} \text{ S}^{-1}$, $[C]_0/[I]_0/[M]_0$ MOLE RATIO: 1:1:100).....	70
FIGURE 5.3 EFFECT OF MONO AND BIFUNCTIONAL INITIATORS ON POLYDISPERSITY INDEX (PDI) AS A FUNCTION OF TIME (T) ($K_p=1000 \text{ L MOL}^{-1} \text{ S}^{-1}$, $K_{TC}=1 \times 10^7 \text{ L MOL}^{-1} \text{ S}^{-1}$, $K_{TD}=0$, $K_D=1 \times 10^7 \text{ L MOL}^{-1} \text{ S}^{-1}$, $K_A=0.01 \text{ L MOL}^{-1} \text{ S}^{-1}$, $[C]_0/[I]_0/[M]_0$ MOLE RATIO: 1:1:100).....	70
FIGURE 5.4 EFFECT OF THE EQUILIBRIUM CONSTANT (K_{EQ}) ON THE POLYDISPERSITY INDEX ($K_p=2000 \text{ L MOL}^{-1} \text{ S}^{-1}$, $K_A=0.01 \text{ L MOL}^{-1} \text{ S}^{-1}$, $K_{TC}=1 \times 10^7 \text{ L MOL}^{-1} \text{ S}^{-1}$, $K_{TD}=0$, $[C]_0/[I]_0/[M]_0$ MOLE RATIO: 1:1:100).....	72
FIGURE 5.5 EFFECT OF EQUILIBRIUM CONSTANT (K_{EQ}) ON MONOMER CONVERSION ($K_p=2000 \text{ L MOL}^{-1} \text{ S}^{-1}$, $K_A=0.01 \text{ L MOL}^{-1} \text{ S}^{-1}$, $K_{TC}=1 \times 10^7 \text{ L MOL}^{-1} \text{ S}^{-1}$, $K_{TD}=0$, $[C]_0/[I]_0/[M]_0$ MOLE RATIO: 1:1:100).....	72
FIGURE 5.6 EFFECT OF EQUILIBRIUM CONSTANT (K_{EQ}) ON NUMBER AVERAGE CHAIN LENGTH ($K_p=2000 \text{ L MOL}^{-1} \text{ S}^{-1}$, $K_A=0.01 \text{ L MOL}^{-1} \text{ S}^{-1}$, $K_{TC}=1 \times 10^7 \text{ L MOL}^{-1} \text{ S}^{-1}$, $K_{TD}=0$, $[C]_0/[I]_0/[M]_0$ MOLE RATIO: 1:1:100).....	73
FIGURE 5.7 EFFECT OF THE PROPAGATION CONSTANT (K_p) ON MONOMER CONVERSION ($K_D=1 \times 10^7 \text{ L MOL}^{-1} \text{ S}^{-1}$, $K_A=0.01 \text{ L MOL}^{-1} \text{ S}^{-1}$, $K_{TC}=1 \times 10^7 \text{ L MOL}^{-1} \text{ S}^{-1}$, $K_{TD}=0$, $[C]_0/[I]_0/[M]_0$ MOLE RATIO: 1:1:100).....	74
FIGURE 5.8 EFFECT OF THE PROPAGATION CONSTANT (K_p) ON NUMBER AVERAGE CHAIN LENGTH ($K_D=1 \times 10^7 \text{ L MOL}^{-1} \text{ S}^{-1}$, $K_A=0.01 \text{ L MOL}^{-1} \text{ S}^{-1}$, $K_{TC}=1 \times 10^7 \text{ L MOL}^{-1} \text{ S}^{-1}$, $K_{TD}=0$, $[C]_0/[I]_0/[M]_0$ MOLE RATIO: 1:1:100).....	75
FIGURE 5.9 EFFECT OF THE PROPAGATION CONSTANT (K_p) ON POLYDISPERSITY INDEX ($K_D=1 \times 10^7 \text{ L MOL}^{-1} \text{ S}^{-1}$, $K_A=0.01 \text{ L MOL}^{-1} \text{ S}^{-1}$, $K_{TC}=1 \times 10^7 \text{ L MOL}^{-1} \text{ S}^{-1}$, $K_{TD}=0$, $[C]_0/[I]_0/[M]_0$ MOLE RATIO: 1:1:100).....	75
FIGURE 5.10 EFFECT OF THE TERMINATION BY COMBINATION CONSTANT (K_{TC}) ON MONOMER CONVERSION ($K_D=1 \times 10^7 \text{ L MOL}^{-1} \text{ S}^{-1}$, $K_A=0.01 \text{ L MOL}^{-1} \text{ S}^{-1}$, $K_p=2000 \text{ L MOL}^{-1} \text{ S}^{-1}$, $K_{TD}=0$, $[C]_0/[I]_0/[M]_0$ MOLE RATIO: 1:1:100).....	76
FIGURE 5.11 EFFECT OF THE TERMINATION BY COMBINATION CONSTANT (K_{TC}) ON NUMBER AVERAGE CHAIN LENGTH ($K_D=1 \times 10^7 \text{ L MOL}^{-1} \text{ S}^{-1}$, $K_A=0.01 \text{ L MOL}^{-1} \text{ S}^{-1}$, $K_p=2000 \text{ L MOL}^{-1} \text{ S}^{-1}$, $K_{TD}=0$, $[C]_0/[I]_0/[M]_0$ MOLE RATIO: 1:1:100).....	77
FIGURE 5.12 EFFECT OF THE TERMINATION BY COMBINATION CONSTANT (K_{TC}) ON POLYDISPERSITY INDEX ($K_D=1 \times 10^7 \text{ L MOL}^{-1} \text{ S}^{-1}$, $K_A=0.01 \text{ L MOL}^{-1} \text{ S}^{-1}$, $K_p=2000 \text{ L MOL}^{-1} \text{ S}^{-1}$, $K_{TD}=0$, $[C]_0/[I]_0/[M]_0$ MOLE RATIO: 1:1:100).....	77
FIGURE 5.13 EFFECT OF INITIAL CATALYST CONCENTRATION ON MONOMER CONVERSION ($K_p=2000 \text{ L MOL}^{-1} \text{ S}^{-1}$, $K_D=1 \times 10^7 \text{ L MOL}^{-1} \text{ S}^{-1}$, $K_A=0.01 \text{ L MOL}^{-1} \text{ S}^{-1}$, $K_{TC}=1 \times 10^7 \text{ L MOL}^{-1} \text{ S}^{-1}$, $K_{TD}=0$, $[C]_0/[M]_0$ MOLE RATIO: 1:100, THE MOLE RATIO OF $[C]_0$ VARIES AS IN THE LEGEND).....	79
FIGURE 5.14 EFFECT OF INITIAL CATALYST CONCENTRATION ON NUMBER AVERAGE CHAIN LENGTH ($K_p=2000 \text{ L MOL}^{-1} \text{ S}^{-1}$, $K_D=1 \times 10^7 \text{ L MOL}^{-1} \text{ S}^{-1}$, $K_A=0.01 \text{ L MOL}^{-1} \text{ S}^{-1}$, $K_{TC}=1 \times 10^7 \text{ L MOL}^{-1} \text{ S}^{-1}$, $K_{TD}=0$, $[C]_0/[M]_0$ MOLE RATIO: 1:100, THE MOLE RATIO OF $[C]_0$ VARIES AS IN THE LEGEND).....	79
FIGURE 5.15 EFFECT OF INITIAL CATALYST CONCENTRATION $[C]_0$ ON POLYDISPERSITY AS A FUNCTION OF TIME (T) ($K_p=2000 \text{ L MOL}^{-1} \text{ S}^{-1}$, $K_D=1 \times 10^7 \text{ L MOL}^{-1} \text{ S}^{-1}$, $K_A=0.01 \text{ L MOL}^{-1} \text{ S}^{-1}$, $K_{TC}=1 \times 10^7 \text{ L MOL}^{-1} \text{ S}^{-1}$, $K_{TD}=0$, $[C]_0/[M]_0$ MOLE RATIO: 1:100, THE MOLE RATIO OF $[C]_0$ VARIES AS IN THE LEGEND).....	80
FIGURE 5.16 EFFECT OF THE INITIAL INITIATOR CONCENTRATION ON MONOMER CONVERSION ($K_p=2000 \text{ L MOL}^{-1} \text{ S}^{-1}$, $K_D=1 \times 10^7 \text{ L MOL}^{-1} \text{ S}^{-1}$, $K_A=0.01 \text{ L MOL}^{-1} \text{ S}^{-1}$, $K_{TC}=1 \times 10^7 \text{ L MOL}^{-1} \text{ S}^{-1}$, $K_{TD}=0$, $[C]_0/[M]_0$ MOLE RATIO: 1:100, THE MOLE RATIO OF $[I]_0$ VARIES AS IN THE LEGEND).....	81
FIGURE 5.17 EFFECT OF THE INITIAL INITIATOR CONCENTRATION ON NUMBER AVERAGE CHAIN LENGTH ($K_p=2000 \text{ L MOL}^{-1} \text{ S}^{-1}$, $K_D=1 \times 10^7 \text{ L MOL}^{-1} \text{ S}^{-1}$, $K_A=0.01 \text{ L MOL}^{-1} \text{ S}^{-1}$, $K_{TC}=1 \times 10^7 \text{ L MOL}^{-1} \text{ S}^{-1}$, $K_{TD}=0$, $[C]_0/[M]_0$ MOLE RATIO: 1:100, THE MOLE RATIO OF $[I]_0$ VARIES AS IN THE LEGEND).....	81
FIGURE 5.18 EFFECT OF THE INITIAL INITIATOR CONCENTRATION ON POLYDISPERSITY INDEX ($K_p=2000 \text{ L MOL}^{-1} \text{ S}^{-1}$, $K_D=1 \times 10^7 \text{ L MOL}^{-1} \text{ S}^{-1}$, $K_A=0.01 \text{ L MOL}^{-1} \text{ S}^{-1}$, $K_{TC}=1 \times 10^7 \text{ L MOL}^{-1} \text{ S}^{-1}$, $K_{TD}=0$, $[C]_0/[M]_0$ MOLE RATIO: 1:100, THE MOLE RATIO OF $[I]_0$ VARIES AS IN THE LEGEND).....	82
FIGURE 6.1 EFFECT OF DIFFUSION LIMITATION ON THE TERMINATION RATE CONSTANT: (A) DEGREE OF POLYMERIZATION, (B) MONOMER CONVERSION, AND (C) POLYDISPERSITY INDEX. ($B_A=B_D=B_P=0$, $K_{A0}=0.5 \text{ L MOL}^{-1} \text{ S}^{-1}$, $K_{D0}=1 \times 10^5 \text{ L MOL}^{-1} \text{ S}^{-1}$, $K_{P0}=1578 \text{ L MOL}^{-1} \text{ S}^{-1}$, $K_{TC0}=3.475 \times 10^8 \text{ L MOL}^{-1} \text{ S}^{-1}$, $K_{TD0}=0$, $[C]_0/[I]_0/[M]_0$ MOLE RATIO: 2:1:100) OTHER PARAMETERS ARE SHOWN IN TABLE 6.1.....	98
FIGURE 6.2 EFFECT OF DIFFUSION LIMITATION ON THE DEACTIVATION RATE CONSTANT: (A) DEGREE OF POLYMERIZATION, (B) MONOMER CONVERSION, AND (C) POLYDISPERSITY INDEX. ($B_T=0.1$, $B_P=B_A=0$, $K_{A0}=0.5 \text{ L MOL}^{-1} \text{ S}^{-1}$, $K_{D0}=1 \times 10^5 \text{ L MOL}^{-1} \text{ S}^{-1}$, $K_{P0}=1578 \text{ L MOL}^{-1} \text{ S}^{-1}$, $K_{TC0}=3.475 \times 10^8 \text{ L MOL}^{-1} \text{ S}^{-1}$, $K_{TD0}=0$, $[C]_0/[I]_0/[M]_0$ MOLE RATIO: 2:1:100). OTHER PARAMETERS ARE SHOWN IN TABLE 6.1.....	100

FIGURE 6.3 EFFECT OF DIFFUSION LIMITATION ON THE ACTIVATION RATE CONSTANT: (A) DEGREE OF POLYMERIZATION, (B) MONOMER CONVERSION, AND (C) POLYDISPERSITY INDEX. ($B_T=0.1, B_P=0, B_D=0.05, K_{A0}=0.5 \text{ L MOL}^{-1} \text{ S}^{-1}, K_{D0}=1 \times 10^5 \text{ L MOL}^{-1} \text{ S}^{-1}, K_{P0}=1578 \text{ L MOL}^{-1} \text{ S}^{-1}, K_{TC0}=3.475 \times 10^8 \text{ L MOL}^{-1} \text{ S}^{-1}, K_{TD0}=0, [C]_0/[I]_0/[M]_0$ MOLE RATIO: 2:1:100). OTHER PARAMETERS ARE SHOWN IN TABLE 6.1.	101
FIGURE 6.4 EFFECT OF DIFFUSION LIMITATION ON THE PROPAGATION RATE CONSTANT: (A) DEGREE OF POLYMERIZATION, (B) MONOMER CONVERSION, AND (C) POLYDISPERSITY INDEX. ($B_A=B_D=0.5, B_T=0.1, K_{A0}=0.5 \text{ L MOL}^{-1} \text{ S}^{-1}, K_{D0}=1 \times 10^5 \text{ L MOL}^{-1} \text{ S}^{-1}, K_{P0}=1578 \text{ L MOL}^{-1} \text{ S}^{-1}, K_{TC0}=3.475 \times 10^8 \text{ L MOL}^{-1} \text{ S}^{-1}, K_{TD0}=0, [C]_0/[I]_0/[M]_0$ MOLE RATIO: 2:1:100). OTHER PARAMETERS ARE SHOWN IN TABLE 6.1.	103
FIGURE 6.5 COMPARISON BETWEEN MODEL PREDICTIONS AND EXPERIMENTAL DATA FOR STYRENE POLYMERIZATION IN BUTYL ACETATE AT 130 °C WITH DCT AS INITIATOR: (A) MONOMER CONVERSION, (B) NUMBER AVERAGE MOLECULAR WEIGHT, (C) $\text{LN}([M_0]/[M])$, AND (D) POLYDISPERSITY. (POLYMERIZATION CONDITIONS: $[St]_0=4.35 \text{ MOL/L}, [St]/[I]/[Cat]=100:1:1$ (MOLAR RATIO), REACTION TEMPERATURE $T=130 \text{ °C}$. KINETIC PARAMETERS ARE SHOWN IN TABLE 6.1). EXPERIMENTAL DATA FROM HOCKER ET AL. ^[1]	107
FIGURE 6.6 COMPARISON BETWEEN MODEL PREDICTIONS AND EXPERIMENTAL DATA FOR ATRP OF METHYL METHACRYLATE IN TOLUENE AT 90 °C WITH 1,3-BIS{1-METHYL-(2,2,2-TRICHLOROETHOXY) CARBONYLAMINO}ETHYL} BENZENE AS INITIATOR: (A) MONOMER CONVERSION, (B) NUMBER AVERAGE MOLECULAR WEIGHT, (C) $\text{LN}([M_0]/[M])$, AND (D) POLYDISPERSITY. (POLYMERIZATION CONDITIONS: $[MMA]_0=4.5 \text{ MOL/L}, [MMA]/[I]/[Cat]=100:1:1$ (MOLAR RATIO), REACTION TEMPERATURE $T=90 \text{ °C}$. KINETIC PARAMETERS ARE GIVEN IN TABLE 6.2). EXPERIMENTAL DATA FROM VLCEK ET AL. ^[2]	110
FIGURE 6.7 COMPARISON BETWEEN MODEL PREDICTIONS AND EXPERIMENTAL DATA FOR N-BA POLYMERIZATION IN BULK AT 90 °C: (A) MONOMER CONVERSION, (B) NUMBER AVERAGE MOLECULAR WEIGHT, (C) $\text{LN}([M_0]/[M])$, AND (D) POLYDISPERSITY. (POLYMERIZATION CONDITIONS: $[M]/[I]/[Cat]=465:1:1$ (MOLAR RATIO), REACTION TEMPERATURE $T=90 \text{ °C}$. KINETIC PARAMETERS ARE SHOWN IN TABLE 6.3). EXPERIMENTAL DATA FROM MATYJASZEWSKI ET AL. ^[3]	113
FIGURE 7.1 ALGORITHM FOR MONTE CARLO SIMULATION OF ATRP WITH BIFUNCTIONAL INITIATORS.....	121
FIGURE 7.2 COMPARISON BETWEEN MONTE CARLO SIMULATION AND METHOD OF MOMENTS FOR ISOTHERMAL BATCH POLYMERIZATION: (A) MONOMER CONVERSION, (B) NUMBER AVERAGE CHAIN LENGTH, (C) POLYDISPERSITY INDEX ($V=1 \times 10^{-19} \text{ L}$).	124
FIGURE 7.3 COMPARISON BETWEEN MONO- AND BIFUNCTIONAL INITIATORS: MONOMER CONVERSION (x) AS A FUNCTION OF TIME. ($V=1 \times 10^{-19} \text{ L}$).	126
FIGURE 7.4 NUMBER AVERAGE CHAIN LENGTH (R_n) AS A FUNCTION OF (A) TIME AND (B) CONVERSION FOR POLYMER MADE WITH MONO- AND BIFUNCTIONAL INITIATORS ($V=1 \times 10^{-19} \text{ L}$).	126
FIGURE 7.5 POLYDISPERSITY INDEX (PDI) AS A FUNCTION OF (A) TIME AND (B) CONVERSION FOR POLYMER MADE WITH MONO- AND BIFUNCTIONAL INITIATORS ($V=1 \times 10^{-19} \text{ L}$).	127
FIGURE 7.6 COMPARISON BETWEEN MONO- AND BIFUNCTIONAL INITIATORS: CHAIN LENGTH DISTRIBUTION FOR CONVERSION $x=0.5$ ($V=1 \times 10^{-19} \text{ L}$) (A) WEIGHT FRACTION (B) NUMBER FRACTION.	128
FIGURE 7.7 EVOLUTION OF THE CLD OF POLYMER MADE WITH A BIFUNCTIONAL INITIATOR AS A FUNCTION OF MONOMER CONVERSION ($V=1 \times 10^{-19} \text{ L}$).	129
FIGURE 7.8 EFFECT OF THE SIZE OF THE CONTROL VOLUME ON SIMULATION TIME. ($x=0.5$).	130
FIGURE 7.9 EFFECT OF THE SIZE OF THE CONTROL VOLUME ON MONOMER CONVERSION.	131
FIGURE 7.10 EFFECT OF THE SIZE OF THE CONTROL VOLUME ON NUMBER AVERAGE CHAIN LENGTH.	131
FIGURE 7.11 EFFECT OF THE SIZE OF THE CONTROL VOLUME ON POLYDISPERSITY INDEX.	131
FIGURE 7.12 EFFECT OF USING A SMALL CONTROL VOLUME ON THE CHAIN LENGTH DISTRIBUTION ($V=1 \times 10^{-20} \text{ L}, x=0.3$).	132
FIGURE 7.13 EFFECT OF USING LARGE CONTROL VOLUMES ON THE CHAIN LENGTH DISTRIBUTION ($x=0.3$).	132
FIGURE 7.14 EFFECT OF REPEATING THE SIMULATION SEVERAL TIMES AND AVERAGING THE FINAL RESULTS FOR CLD PREDICTION ($V=1 \times 10^{-20} \text{ L}, x=0.3$).	133
FIGURE 7.15 EFFECT OF CONTROL VOLUME SIZE ON COMPUTATIONAL TIME (SOLID LINE) AND CLD NOISE (DASHED LINE) ($x=0.5$).	134
FIGURE 7.16 EFFECT OF NUMBER OF REPETITIONS ON COMPUTATIONAL TIME (SOLID LINE) AND CLD NOISE (DASHED LINE) ($V=1 \times 10^{-19} \text{ L}, x=0.5$).	135
FIGURE 7.17 EFFECT OF THE EQUILIBRIUM RATE CONSTANT ON SIMULATION TIME. ($V=1 \times 10^{-18} \text{ L}, x=0.3$).	136

FIGURE 7.18 EFFECT OF THE EQUILIBRIUM RATE CONSTANT ON POLYMERIZATION TIME ($V = 1 \times 10^{-18}$ L, $x = 0.3$).....	136
FIGURE 7.19 EFFECT OF THE EQUILIBRIUM RATE CONSTANT ON MONOMER CONVERSION ($V = 1 \times 10^{-18}$ L) .	136
FIGURE 7.20 EFFECT OF THE EQUILIBRIUM RATE CONSTANT ON NUMBER AVERAGE CHAIN LENGTH ($V = 1 \times 10^{-18}$ L).....	137
FIGURE 7.21 EFFECT OF THE EQUILIBRIUM RATE CONSTANT ON POLYDISPERSITY INDEX ($V = 1 \times 10^{-18}$ L) .	137
FIGURE 7.22 EFFECT OF THE EQUILIBRIUM RATE CONSTANT ON CHAIN LENGTH DISTRIBUTION ($V = 1 \times 10^{-18}$ L, $x = 0.5$).....	137
FIGURE 7.23 EFFECT OF MONOMER CONVERSION ON SIMULATION TIME ($V = 1 \times 10^{-18}$ L).....	138
FIGURE 8.1 EFFECT OF THERMAL INITIATION AND ELIMINATION REACTIONS ON (A) DEGREE OF POLYMERIZATION, AND (B) CHAIN LENGTH DISTRIBUTION. MODEL PARAMETERS ARE LISTED IN TABLE 8.1.....	148
FIGURE 8.2 ATRP OF STYRENE USING 1-BROMOETHYL BENZENE AND BENZAL BROMIDE.....	149
FIGURE 8.3 EXPERIMENTAL DATA AND MODEL PREDICTIONS FOR MONOMER CONVERSION AS A FUNCTION OF TIME FOR THE BULK ATRP OF STYRENE WITH BENZAL BROMIDE AND 1-BROMO ETHYL BENZENE AT 110 °C. MODEL PARAMETERS ARE SHOWN IN TABLE 8.1 AND $[M]_0/[I]_0/[C]_0 = 100/1/1$	151
FIGURE 8.4 EXPERIMENTAL DATA AND MODEL PREDICTIONS FOR (A) NUMBER AVERAGE MOLECULAR WEIGHT VERSUS CONVERSION; (B) NUMBER AVERAGE MOLECULAR WEIGHT VERSUS TIME FOR THE BULK ATRP OF STYRENE WITH BENZAL BROMIDE AND 1-BROMO ETHYL BENZENE AT 110 °C. MODEL PARAMETERS ARE SHOWN IN TABLE 8.1 AND $[M]_0/[I]_0/[C]_0 = 100/1/1$	152
FIGURE 8.5 EXPERIMENTAL DATA AND MODEL PREDICTIONS FOR (A) POLYDISPERSITY INDEX AGAINST TIME, (B) POLYDISPERSITY INDEX AGAINST CONVERSION FOR THE BULK ATRP OF STYRENE WITH BENZAL BROMIDE AND 1-BROMO ETHYL BENZENE AT 110 °C. MODEL PARAMETERS ARE SHOWN IN TABLE 8.1 AND $[M]_0/[I]_0/[C]_0 = 100/1/1$	153
FIGURE 8.6 COMPARISON OF MONTE CARLO SIMULATION (SQUARE DOTS) AND EXPERIMENTAL MOLECULAR WEIGHT DISTRIBUTIONS (SOLID LINE) FOR THE BULK ATRP OF STYRENE WITH 1-BROMOETHYL BENZENE AT 110 °C. MODEL PARAMETERS ARE SHOWN IN TABLE 8.1 AND $[M]_0/[I]_0/[C]_0 = 100/1/1$	155
FIGURE 8.7 COMPARISON OF MONTE CARLO SIMULATION (DIAMOND DOTS) AND EXPERIMENTAL MOLECULAR WEIGHT DISTRIBUTIONS (SOLID LINE) FOR THE BULK ATRP OF STYRENE WITH BENZAL BROMIDE AT 110 °C. MODEL PARAMETERS ARE SHOWN IN TABLE 8.1 AND $[M]_0/[I]_0/[C]_0 = 100/1/1$	156
FIGURE 8.8 ¹ H NMR SPECTRUM OF POLYSTYRENE CHAINS OBTAINED IN THE FILTRATE AFTER POLYMERIZATION FOR 30 MINUTES USING MONOFUNCTIONAL INITIATOR. THE ARROW INDICATES THE BROMIDE END (DORMANT CHAIN) IN THE POLYSTYRENE MOLECULE ^[9]	158
FIGURE 8.9 COMPARISON BETWEEN CONVERSION MEASURED WITH GRAVIMATRY AND ¹ H NMR FOR ATRP OF STYRENE USING 1-BROMO ETHYLBENZENE AS INITIATOR AT 110 °C (DATA FROM TABLE 8.2).....	159
FIGURE 9.1 CHEMICAL STRUCTURES OF THE INITIATORS USED IN THIS STUDY.....	164
FIGURE 9.2 COMPARISON OF BATCH ATRP OF STYRENE AND ACRYLONITRILE USING A MONOFUNCTIONAL AND A BIFUNCTIONAL INITIATOR WHEN BOTH COMONOMERS ARE ADDED SIMULTANEOUSLY: (A) MONOMER CONVERSION, X; (B) NUMBER AVERAGE MOLECULAR WEIGHT, MN. (POLYMERIZATION CONDITIONS: $[M]_0/[I]_0/[C]_0 = 100/1/1$. TEMPERATURE = 90 °C).....	167
FIGURE 9.3 MECHANISM FOR THE FORMATION OF AN UNSYMMETRICAL INITIATOR INACTIVE FOR ACRYLONITRILE PROPAGATION.....	168
FIGURE 9.4 PROPOSED MECHANISM FOR THE FORMATION OF PS-B-SAN AND SAN-B-PS-B-SAN COPOLYMER USING MONOFUNCTIONAL (TOP) AND BIFUNCTIONAL (BOTTOM) INITIATORS IN THE SEQUENTIAL POLYMERIZATION APPROACH.....	169
FIGURE 9.5 COMPARISON OF ATRP OF STYRENE AND ACRYLONITRILE USING A MONOFUNCTIONAL AND A BIFUNCTIONAL INITIATOR WHEN ACRYLONITRILE IS ADDED 20 MINUTES AFTER THE INITIATION OF THE POLYMERIZATION WITH STYRENE: (A) MONOMER CONVERSION, X; AND (B) LN($[M]_0/[M]$) VS. TIME (POLYMERIZATION CONDITIONS: $[M]_0/[I]_0/[C]_0 = 100/1/1$).....	171
FIGURE 9.6 COMPARISON OF ATRP OF STYRENE AND ACRYLONITRILE USING A MONOFUNCTIONAL AND A BIFUNCTIONAL INITIATOR WHEN ACRYLONITRILE IS ADDED 20 MINUTES AFTER THE INITIATION OF THE POLYMERIZATION WITH STYRENE: (A) MN VS. TIME; AND (B) MN VS CONVERSION, X (POLYMERIZATION CONDITIONS: $[M]_0/[I]_0/[C]_0 = 100/1/1$).....	172
FIGURE 9.7 COMPARISON OF ATRP OF STYRENE AND ACRYLONITRILE USING A MONOFUNCTIONAL AND A BIFUNCTIONAL INITIATOR WHEN STYRENE IS ADDED 20 MINUTES BEFORE ACRYLONITRILE: (A) PDI VS. TIME; AND (B) PDI VS. CONVERSION, X (POLYMERIZATION CONDITIONS: $[M]_0/[I]_0/[C]_0 = 100/1/1$)..	173

FIGURE 9.8 ^{13}C -NMR SPECTRUM OF A REPRESENTATIVE SAN COPOLYMER MADE BY SEQUENTIAL COPOLYMERIZATION.....	174
FIGURE 9.9 SAN COPOLYMER COMPOSITION MEASURED WITH ^{13}C NMR: (A) STYRENE FRACTION VS. POLYMERIZATION TIME FOR BOTH INITIATORS; AND (B) ACRYLONITRILE FRACTION VS. POLYMERIZATION TIME FOR BOTH INITIATORS. POLYMERIZATION CONDITIONS: $[\text{M}]_0/[\text{I}]_0/[\text{C}]_0 = 100/1/1$. TEMPERATURE = 90°C	175
FIGURE 9.10 DN/DC RATIOS OF SAN POLYMERIZED WITH ATRP AT 90°C USING MONOFUNCTIONAL AND BIFUNCTIONAL INITIATORS AS A FUNCTION OF POLYMERIZATION TIME. (POLYMERIZATION CONDITIONS: $[\text{M}]_0/[\text{I}]_0/[\text{C}]_0 = 100/1/1$). THE ERROR BARS REPRESENT ONE STANDARD DEVIATION FROM TWO REPLICATES DONE FOR EACH SAMPLE.	178
FIGURE 9.11 FTIR SPECTRA FOR PURE POLYSTYRENE AND TWO SAN COPOLYMER SAMPLES WITH DIFFERENT FRACTIONS OF ACRYLONITRILE. (SPECTRA PRESENTED IN TRANSMITTANCE UNITS, CURVES SHIFTED HORIZONTALLY FOR CLARITY).....	179
FIGURE 10.1 COMPARISON BETWEEN MODEL PREDICTIONS AND EXPERIMENTAL DATA FOR THE BATCH COPOLYMERIZATION OF STYRENE AND N-BUTYL ACRYLATE FROM AREHART ET AL. ⁽³¹⁾ : (A) MONOMER CONVERSION, (B) POLYDISPERSITY, (C) NUMBER AVERAGE MOLECULAR WEIGHT, AND (D) CUMULATIVE COPOLYMER COMPOSITION.	194
FIGURE 10.2 COMPARISON BETWEEN MODEL PREDICTIONS AND EXPERIMENTAL DATA FOR THE BATCH COPOLYMERIZATION OF SAN (FROM CHAPTER 9) ⁽³¹⁾ : (A) MONOMER CONVERSION, (B) NUMBER AVERAGE MOLECULAR WEIGHT, (C), AND POLYDISPERSITY INDEX.	196
FIGURE 10.3 TOTAL COMONOMER CONVERSION VERSUS THE RATIO OF INSTANTANEOUS COPOLYMER COMPOSITION (IF) FOR THREE ATRP SYSTEMS AT 110°C . THE INITIAL FEED MONOMERS ARE $F_{0,\text{ST}}=0.25$, $F_{0,\text{B}}=0.75$. (THE SUBSCRIPT <i>B</i> STANDS FOR THE SECOND MONOMER THAT COPOLYMERIZES WITH STYRENE: AN, N-BA OR MMA)	198
FIGURE 10.4 RATIO OF INSTANTANEOUS COPOLYMER COMPOSITION (IF) AS A FUNCTION OF TOTAL COMONOMER CONVERSION FOR THE COPOLYMERIZATION OF STYRENE AND N-BUTYL ACRYLATE AT 110°C WITH VARIOUS INITIAL FEED MONOMER.....	199
FIGURE 10.5 RATIO OF INSTANTANEOUS COPOLYMER COMPOSITION (IF) AS A FUNCTION OF TOTAL COMONOMER CONVERSION FOR FICTITIOUS COMONOMERS WITH REACTIVITY RATIOS EQUAL TO ONE AND VARIOUS INITIAL FEED MONOMER.	199
FIGURE 10.6 RATIO OF INSTANTANEOUS COPOLYMER COMPOSITION (IF) AS A FUNCTION OF TOTAL COMONOMER CONVERSION FOR THE COPOLYMERIZATION OF STYRENE AND N-BUTYL ACRYLATE: (A) VARIOUS VALUES OF K_p AND (B) VARIOUS VALUES OF K_t	200
FIGURE 11.1 <i>GRAFTING-TO</i> APPROACH.	212
FIGURE 11.2 <i>GRAFT-FROM</i> APPROACH.	213
FIGURE 11.3 ALGORITHM FOR MONTE CARLO SIMULATION.	216
FIGURE 11.4 ALLYL BROMIDE (LEFT) AND ALLYL CHLORIDE (RIGHT).	217
FIGURE 11.5 AVERAGE NUMBER OF EX-SITU MACROMONOMER BRANCHES PER POLYMER CHAIN AS A FUNCTION OF TIME.	219
FIGURE 11.6 AVERAGE NUMBER OF IN-SITU MACROMONOMER BRANCHES PER POLYMER CHAIN AS A FUNCTION OF TIME.	219
FIGURE 11.7 EFFECT OF EX-SITU MACROMONOMER CONCENTRATION AND POLYMERIZATION TIME ON POLYDISPERSITY INDEX.	220
FIGURE 11.8 EFFECT OF EX-SITU MACROMONOMER CONCENTRATION ON THE CLD FOR TEN MINUTES OF POLYMERIZATION	221
FIGURE 12.1 ^1H NMR SPECTRA FOR PEGMA POLYMERIZED WITH PS MACROINITIATOR AT DIFFERENT CONVERSION (<i>x</i>). (POLYMERIZATION CONDITIONS: $[\text{PEGMA}]_0/[\text{PS}]_0/[\text{C}]_0 = 17/1/1$ (MOLAR RATIO). PEGMA/XYLENE = 3:1 (VOLUME RATIO) TEMPERATURE = 110°C).	228
FIGURE 12.2 CONVERSION OF PEGMA AS A FUNCTION OF TIME USING MONOFUNCTIONAL AND BIFUNCTIONAL MACROINITIATORS. (POLYMERIZATION CONDITIONS: $[\text{PEGMA}]_0/[\text{PS}]_0/[\text{C}]_0 = 17/1/1$ (MOLAR RATIO). PEGMA/XYLENE = 3:1 (VOLUME RATIO) TEMPERATURE = 110°C).	228
FIGURE 12.3 IDEAL MECHANISM TO FORM AMPHIPHILIC BLOCK COPOLYMER OF POLYSTYRENE AND PEGMA.	230
FIGURE 12.4 POLYDISPERSITY INDEX VERSUS CONVERSION OF PEGMA USING MONOFUNCTIONAL AND BIFUNCTIONAL MACROINITIATORS. (POLYMERIZATION CONDITIONS: $[\text{PEGMA}]_0/[\text{PS}]_0/[\text{C}]_0 = 17/1/1$ (MOLAR RATIO). PEGMA/XYLENE = 3:1 (VOLUME RATIO) TEMPERATURE = 110°C).	231

FIGURE 12.5 NUMBER AVERAGE MOLECULAR WEIGHT VERSUS CONVERSION OF PEGMA USING MONOFUNCTIONAL AND BIFUNCTIONAL MACROINITIATORS. (POLYMERIZATION CONDITIONS: [PEGMA] ₀ /[PS] ₀ /[C] ₀ = 17/1/1 (MOLAR RATIO). PEGMA/XYLENE = 3:1 (VOLUME RATIO) TEMPERATURE = 110 °C).....	231
FIGURE 12.6 COMPARISON OF EXPERIMENTAL AND THEORETICAL MOLECULAR WEIGHTS OF PEGMA POLYMERIZED WITH POLYSTYRENE BIFUNCTIONAL MACROINITIATOR. (POLYMERIZATION CONDITIONS: [PEGMA] ₀ /[PS] ₀ /[C] ₀ = 17/1/1 (MOLAR RATIO). PEGMA/XYLENE = 3:1 (VOLUME RATIO) TEMPERATURE = 110 °C).....	232

List of Tables

TABLE 2.1 SOME ATRP SYSTEM COMPONENTS.....	14
TABLE 4.1 PARAMETERS USED IN ATRP OF STYRENE AT $T=110^{\circ}\text{C}$	39
TABLE 4.2 EFFECT OF CONTROL VOLUME SIZE (RATE CONSTANTS ARE SHOWN IN TABLE 4.1).....	41
TABLE 5.1 KINETIC RATE CONSTANTS USED IN THE SIMULATIONS	67
TABLE 6.1 PARAMETERS USED IN ATRP OF STYRENE.	97
TABLE 6.2 PARAMETERS USED IN SOLUTION ATRP OF MMA AT 90°C	108
TABLE 6.3 PARAMETERS USED IN BULK ATRP OF N-BA AT 90°C	114
TABLE 7.1 KINETIC PARAMETERS AND INITIAL CONCENTRATIONS USED IN THE SIMULATIONS	122
TABLE 7.2 EFFECT OF CONTROL VOLUME ON SIMULATION TIME AND CLD NOISE ($\chi=0.5$)	134
TABLE 7.3 EFFECT OF NUMBER OF REPETITIONS ON SIMULATION TIME AND CLD NOISE ($V=1\times 10^{-19}\text{L}$, $\chi=0.5$).....	134
TABLE 8.1 PARAMETERS USED IN ATRP OF STYRENE AT 110°C	147
TABLE 8.2 COMPARISON BETWEEN CONVERSION (χ) MEASURED WITH GRAVIMETRY AND ^1H NMR FOR ATRP OF STYRENE USING 1-BROMO ETHYLBENZENE AS INITIATOR AT 110°C	159
TABLE 9.1 MOLAR FRACTION OF ACRYLONITRILE IN THE SAN COPOLYMER. CUMULATIVE COPOLYMER COMPOSITION (FROM ^{13}C NMR) AND CORRECTED FRACTION EXCLUDING BLOCK OF POLYSTYRENE MADE DURING THE FIRST 20 MINUTES OF POLYMERIZATION.	176
TABLE 10.1 THE FINAL MODEL EQUATIONS USED IN THE MODEL AND THEIR INITIAL CONDITIONS	189
TABLE 10.2 KINETIC RATE CONSTANTS AND PHYSICAL PROPERTIES FOR THE STYRENE -N-BUTYL ACRYLATE COPOLYMERIZATION.....	208
TABLE 10.3 KINETIC RATE CONSTANTS AND PHYSICAL PROPERTIES FOR THE STYRENE-ACRYLONITRILE COPOLYMERIZATION.....	209
TABLE 10.4 KINETIC RATE CONSTANTS AND PHYSICAL PROPERTIES FOR THE STYRENE-METHYL METHACRYLATE COPOLYMERIZATION.	210
TABLE 11.1 SUMMARY OF POLYMERIZATION KINETIC PARAMETERS.....	218

NOMENCLATURE

A_x	Frequency factor for reaction x in Arrhenius equation (x = activation, deactivation, propagation and termination)
B_x	Adjustable parameter of reaction x (x = activation, deactivation, propagation and termination)
C	Catalyst in its lower oxidation state
CX	Catalyst in its higher oxidation state
DP	Degree of polymerization
E_x	Activation energy of reaction x (x = activation, deactivation, propagation and termination) (cal mol^{-1})
I	Initiator
K_{eq}	Equilibrium rate constant
$k_p, k_{p,0}$	Rate constant for monomer propagation (superscript “0” for value at initial conditions) ($\text{L mol}^{-1}\text{s}^{-1}$)
$k_{tc}, k_{tc,0}$	Rate constant for termination by combination (superscript “0” for value at initial conditions) ($\text{L mol}^{-1}\text{s}^{-1}$)
$k_{td}, k_{td,0}$	Rate constant for termination by disproportionation (superscript “0” for value at initial conditions) ($\text{L mol}^{-1}\text{s}^{-1}$)
$k_a, k_{a,0}$	Rate constants for activation (superscript “0” for value at initial conditions) ($\text{L mol}^{-1}\text{s}^{-1}$)
$k_d, k_{d,0}$	Rate constants for deactivation (superscript “0” for value at initial conditions) ($\text{L mol}^{-1}\text{s}^{-1}$)
L	Ligand
M	Monomer
M_n	Number average molecular weight
M_w	Weight average molecular weight
PDI	Polydispersity index
R	Universal gas constant, $R=1.987 \text{ cal mol}^{-1} \text{ K}^{-1}$
r_n	Number average chain length
r_w	Weight average chain length

t	Time
T	Reaction temperature (K)
T_g	Glass transition temperature of component i (i = monomer, polymer, solvent), (K)
V_t	Total reaction volume (L)
V_i	Volume of component i (i =monomer, polymer, catalyst and solvent), L
v_f, v_{f0}	Free volume of the reaction mixture (superscript "0" for value at initial conditions)
x	Monomer conversion
α_i	Thermal expansion coefficient for species i (i =monomer, polymer, solvent) (K^{-1})
$\lambda_{i,j}$	J^{th} moment for species i

List of Publications

Journal publications

- 1- M. Al-Harhi, J. Soares, L. Simon, *Macromol. Theory Simul*, 2006, 15, 198-214.
- 2- M. Al-Harhi, J. Soares, L. Simon, *Macromol. Chem. Phys.*, 2006, 207, 469-483.
- 3- M. Al-Harhi, J. Soares, L. Simon, *Macromol. Mat. Eng.*, 2006, 291, 993-1003.
- 4- M. Al-Harhi, J. Soares, L. Simon, "Dynamic Monte Carlo Simulation of ATRP with Bifunctional Initiators", *Macromol. React. Eng.*, accepted.
- 5- M. Al-Harhi, J. Soares, L. Simon "Dynamic Monte Carlo Simulation of Graft Copolymers Made with ATRP and Metallocene Catalysts", *Macromol. Symp.*, accepted.
- 6- M. Al-Harhi, L.Cheng, J. Soares, L. Simon "Atom Transfer Radical Polymerization of Styrene with Bifunctional and Monofunctional Initiators: Experimental and Mathematical Modeling Results", *J. Polym. Sci., Part A Polym. Chem.* accepted
- 7- M. Al-Harhi, A. Sardashti, J. Soares, L. Simon "Atom transfer radical polymerization (ATRP) of styrene and acrylonitrile with monofunctional and bifunctional initiators", *Polymer* submitted.
- 8- M. Al-Harhi, J. Soares, L. Simon "Mathematical Modeling of Atom Transfer Radical Copolymerization", *J. Appl. Polym. Sci.*, submitted.
- 9- M. Al-Harhi, J. Soares, L. Simon "Amphiphilic Copolymers of PS and PEGMA using ATRP", *Macromol. Rapid Commun.*, submitted.

Oral presentations

- 1- Mamdouh Alharhi; Leonardo, Simon; Joao Soares. Mathematical Model for Controlled Free Radical Polymerization Using Multimodal Initiators. 55th Canadian Chemical Engineering Conference. Toronto, Canada. 16-19 October (2005).

Poster presentations

- 1- Mamdouh Alharhi; Leonardo, Simon; Joao Soares. Mathematical model for block and random copolymers using ATRP. 3rd European Conference on the Reaction Engineering of Polyolefins. Lyon, France. 20-24 June (2005).
- 2- Mamdouh Alharhi; Leonardo, Simon; Joao Soares. Dynamic Monte Carlo Simulation of Atom Transfer Radical Polymerization, Polymer Reaction Engineering VI May 21-26, 2006 Halifax, Nova Scotia, Canada
- 3- Mamdouh Alharhi; Leonardo, Simon; Joao Soares. Dynamic Monte Carlo Simulation of Graft Copolymers Made With ATRP and Metallocene Catalysts,. Polymer Reaction Engineering VI May 21-26, 2006 Halifax, Nova Scotia, Canada

Chapter 1

1 Introduction

1.1 Motivation

Polymers, either synthetic or natural, are present in every aspect of our daily lives. Many modern functional materials, pharmaceutical equipments, electronic devices, automobile parts, etc., have polymeric components. Polymers are replacing traditional materials because of their low cost and special applications. Our lives have been thoroughly changed with the advent of mobile phones, computers, refrigerators, electrical domestic appliances, television, etc.; all of these appliances have parts made of synthetic polymeric materials to a large extent. Polymeric materials are also everywhere in our homes: floor carpeting, glue, pipes, paint, wallpaper, foils, electric insulation and moldings are examples of components based on synthetic polymers. The development of new polymers and the modification and enhancement of the old ones are goals of many researchers in both industry and academia.

Polymers can be synthesized via several different methods, such as free radical polymerization, anionic and cationic polymerization, ring-opening polymerization, and coordination polymerization. Of the above mentioned techniques, free radical polymerization is the most widely used industrially. This technique is much simpler than the others and is applicable to a wide variety of monomers. However, free radical polymerization offers poor control over the molecular weight and polydispersity index of the resulting polymer. In addition, it is impossible to make polymer with complex and well defined macromolecular architectures, such as block copolymers, with conventional free radical polymerization.

Living free radical polymerization techniques (LFRP) are promising solutions for the limitations of conventional free radical polymerization. Although LFRP processes generally have low rates of polymerization, they can make polymers that are well defined with respect to:

1. Topology: linear, star-shaped, and comb-shaped chains.
2. Terminal functionalities.

3. Comonomer composition and intramolecular distribution: statistical, periodic, block, graft, and gradient copolymers.
4. Molecular weight: predetermined by the ratio of monomer concentration to initiator, having polydispersity index close to one.

LFRP methods are very useful for the synthesis of macromonomers having terminal functional groups for further polymerization. They are important to produce polymers with complex architectures such as block, graft, hyperbranched and star-shaped copolymers. Among several types of controlled free radical polymerization, atom transfer radical polymerization (ATRP) is one of the most promising techniques. Although ATRP received great attention from a wide range of polymer groups all over the world, less effort was spent in developing mathematical models for it. Building a mathematical model can help researchers understand the polymerization kinetics and optimize process operating conditions. In this thesis we developed several mathematical models for ATRP and validated them with laboratory data to enhance our understanding of ATRP.

1.2 Objectives

The objectives of this thesis research work can be summarized as follows:

- 1- Apply the method of moments to model:
 - a- ATRP with monofunctional initiators.
 - b- ATRP with bifunctional initiators.
 - c- ATRP copolymerization.
- 2- Develop Monte Carlo models to:
 - a- ATRP with monofunctional initiators.
 - b- ATRP with bifunctional initiators.
 - c- Graft copolymerization with ATRP and coordination polymerization.
- 3- ATRP synthesis of:
 - a- Polystyrene using monofunctional and bifunctional initiators.

b- Styrene-acrylonitrile copolymers using monofunctional and bifunctional initiators.

c- Amphiphilic block copolymers.

1.3 Thesis contents

This thesis is divided into twelve chapters. The first three chapters present introductory information on background and experimental methods. The basics of free radical polymerization, controlled free radical polymerization and atom transfer radical polymerization are presented in Chapter 2. This is followed by an outline of the research methodologies used in this thesis in Chapter 3. More details about specific experimental and modeling methodologies are given in the following chapters. Chapters 4 to 12 are based on journal papers that have been published or submitted for publication. To avoid repetition, some sections originally present in the journal papers may have been omitted or simplified in the chapters. General conclusions and recommendations are discussed in Chapter 13.

Chapters 4 to 7 show mathematical modeling results for atom transfer radical homopolymerization with monofunctional and bifunctional initiators using the method of moments and Monte Carlo methods. All mathematical models were validated with experimental data from the literature.

Polystyrene was used as a model polymer in this thesis because it has been made extensively with ATRP and its kinetic parameters are well researched in the literature. In Chapter 8 we use the model developed in Chapters 4 to 7 to describe the ATRP of polystyrene produced in our laboratories.

Chapters 9 to 12 focus on atom transfer radical copolymerization. Experimental polymerization kinetics of styrene-acrylonitrile (SAN) copolymers with two types of initiators is presented in Chapter 9. A model for atom transfer radical copolymerization is developed in Chapter 10 using the method of moments and pseudo-kinetic rate constants. The model was validated with two case studies and used to show qualitative results for ATRP. A mathematical model for a novel polyolefin copolymer that can be prepared in two steps (ATRP and coordination polymerization) is presented in Chapter 11. In this

chapter, we describe a process where ATRP is used to prepare macromonomers with controlled properties (molecular weight and molecular weight distribution) and coordination polymerization is used to incorporate these chains into the polyolefin backbones. Chapter 12 shows an experimental study of amphiphilic copolymers prepared via ATRP. This amphiphilic copolymer is composed of polystyrene and polyethylene glycol methacrylate macromonomers.

Chapter 2

2 Background and Literature Review

2.1 Free radical polymerization

Polymerization is the formation of long chains of covalently bonded monomer units, and it is commonly subdivided into condensation and chain growth polymerization. Herein we will concentrate on the chain growth polymerization mechanisms.

Free-radical polymerization (FRP) is one type of chain growth polymerization technique and it is a very useful method for large scale production of a variety of polymers. Most of the vinyl polymers can be produced industrially by free-radical polymerization. Compared to other polymerization techniques, free radical polymerization is much less sensitive to impurities; it is not sensitive to water and, actually, sometimes it is carried out in aqueous media.

Free radical polymerization, like other chain growth polymerization mechanisms, has mainly three classes of reactions: initiation, propagation, and termination.

Initiation in free radical polymerization consists of two steps. First (Equation 1), the initiator (I) decomposes to form two radical species ($I \bullet$).



In the second step of the initiation, a monomer molecule (M) reacts with the initiator radical (Equation 2), forming a monomer radical.



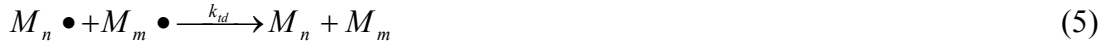
The propagation step is the growth of the active (free radical) chain by sequential addition of monomers. The monomers are added to the active chain in subsequent propagation steps as indicated in equation 3.



The propagation reaction will continue until some termination process occurs. One obvious termination mechanism occurs when two propagating radical chains react to form a single dead chain (Equation 4). This termination mechanism is called termination by combination.



Termination can also occur by a disproportionation reaction to give two dead chains. One of the dead chains will have an unsaturated chain end while the other will have a saturated chain end. Equation 5 illustrates the mechanism of termination by disproportionation.



The termination step produces dead polymer chains: the growth of the polymer chain is terminated and the active centers are irreversibly annihilated. This implies that it is impossible to form block copolymers by adding a new monomer and re-activating the polymerization system.

In addition to termination by combination and disproportionation, another mechanism of termination is chain transfer by hydrogen abstraction from any H-containing reactant present in the system (Equation 6).



where TH represents monomer, initiator, solvent, polymer or any substance in the reaction media that can have a hydrogen atom abstracted by the polymer radical chain [1,2].

2.2 Copolymerization

2.2.1 Introduction

There are several ways of changing the properties of a polymeric material. For example, additives can be used to incorporate desirable properties into an existing polymer material for new applications. Another approach is to combine the properties of different polymer structures. The simplest way to achieve this is to blend two polymers to give a material with mechanical and rheological properties that are better than those of the individual polymers. However, because few polymers are miscible, they tend to phase separate in most blends which, consequently, often have poor physical properties due to inadequate interfacial strength between the phases.^[3] An alternative way is to copolymerize different monomers into a single polymeric material (Figure 2.1).

Copolymerization is the best way to produce a polymer with properties that are intermediate between the properties of the respective homopolymers. It is an important process from a commercial point of view because it can produce new polymers with completely different properties. An unlimited number of polymeric structures with a wide range of properties and applications can be synthesized via copolymerization of a few different types of comonomers.

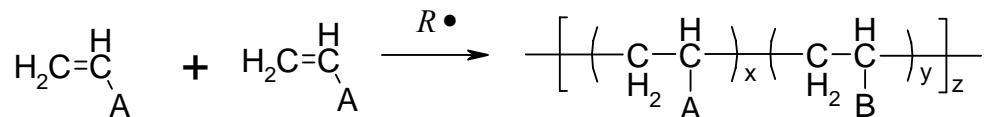


Figure 2.1 General copolymerization reaction scheme.

One way to categorize copolymers is based on their architecture. Figure 2.2 shows how copolymers are classified as statistical, alternating, block, and graft. In statistical or random copolymers, the placement of the comonomers in the chain is random. In alternating copolymers, comonomer molecules alternate in the chain. If long sequences of one comonomer are followed by long sequences of the other comonomer, the resultant copolymer is called block copolymer. Block copolymers can be diblock, triblock or multiblock depending on the number of comonomer types used during polymerization. Graft copolymers are branched polymers where the backbone is made of one copolymer type and the branches are made of another copolymer type.

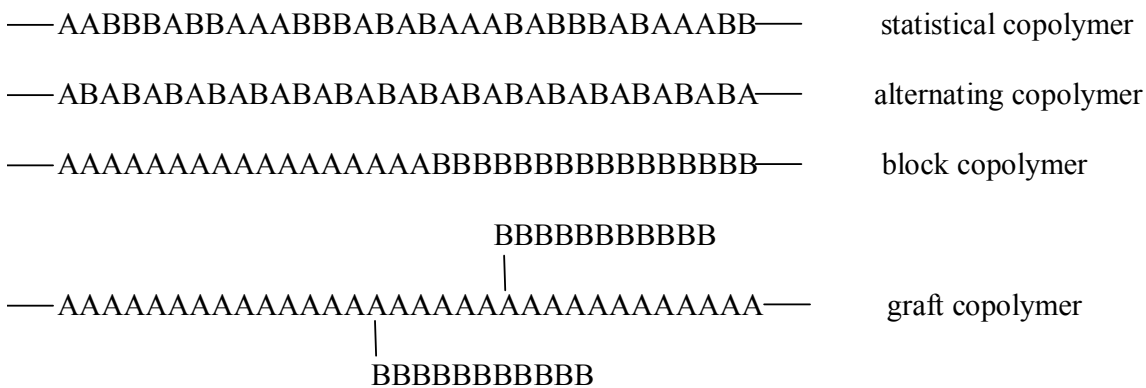


Figure 2.2 Types of copolymer topologies.

2.2.2 Copolymerization models

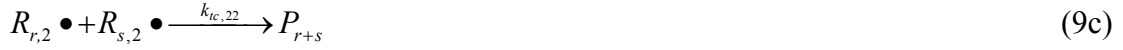
The terminal model to describe copolymerization was first suggested by Dostal in 1936.^[4] The terminal model is based upon the assumption that the chemical reactivity of a propagating polymer chain is independent of the size or composition of the chain and is only influenced by the chemical nature of the active end group.^[5] When two monomers, M_1 and M_2 , are copolymerized in free radical polymerization, four propagation reactions are relevant according to the terminal model, as shown in equation 7.



where $k_{p,11}$ is the rate constant for the addition of a propagating chain ending in M_1 adding to monomer M_1 , $k_{p,12}$ is the rate constant for the addition of a propagating chain ending in M_1 adding to monomer M_2 , and so on. Monomer reactivity ratios, r_1 and r_2 , quantify these relative rates of copolymerization reactions, where $r_1 = k_{p,11}/k_{p,12}$ and $r_2 = k_{p,22}/k_{p,21}$. From the values of the reactivity ratios, different types of copolymerization behaviors can be distinguished. Random copolymerization occurs when $r_1 = r_2 = 1$ due to the equal reactivity of the monomers toward both types of propagating chain ends and the resulting copolymer composition will directly reflect the comonomer feed. When $r_1 r_2 = 1$ (ideal polymerization), the two different types of propagating chain ends add preferentially to one of the monomers. Block copolymers are formed when r_1 and r_2 are much greater than one and alternating copolymerization happens when $r_1 r_2 = 0$.

Termination reactions in copolymerization are similar to the ones in homopolymerization. Equations 8 to 10 illustrate these reactions for the terminal model.





The terminal model is useful to approximate copolymer compositions that are dependent on the comonomer feed ratio and the reactivities of the comonomers. The Mayo-Lewis equation^[6] was derived from the terminal model using the assumption of the steady-state radical approximation. It can be used to describe the instantaneous copolymer composition:

$$\frac{d[M_1]}{d[M_2]} = \frac{[M_1](r_1[M_1] + [M_2])}{[M_2](r_2[M_2] + [M_1])} \quad (11)$$

The Mayo-Lewis equation can be also written as follows:

$$F_1 = \frac{r_1 f_1^2 + f_1 f_2}{r_1 f_1^2 + 2 f_1 f_2 + r_2 f_2^2} \quad (12)$$

where F_i is the mole fraction of M_i in the copolymer and f_i is the mole fraction of M_i in the monomer mixture.

2.3 Living radical polymerization

The control of macromolecular structure can lead to the development of new polymer products with improved and/or new materials properties. Of all polymerization techniques, living polymerization offers the best control over macromolecular structure. During living polymerization, polymer chains grow without permanent chain termination or transfer reactions. The absence (or reduction) of termination reactions leads to polymers with narrow molecular weight distributions (MWD) if initiation reactions are fast. The width of the MWD is commonly measured as the ratio of the weight average molecular weight to the number average molecular weight (M_w/M_n) and called polydispersity index (PDI). In living polymerization, PDI approaches one ($1 < \text{PDI} < 1.2$). In addition, living polymerization also provides end-group control and therefore enables the synthesis of polymers with various chain end functionalities. Finally, block copolymers can be made with living polymerization by sequentially polymerizing comonomer of different types in the same reactor ^[7].

Living ionic (anionic or cationic) polymerization has perfect control over molecular architecture because chain ends having a similar electrostatic charge repel each other. This repulsion between the chain ends prevents them from combining in termination reactions. However, living ionic polymerization techniques have some disadvantages: The growing carbonium ion is extremely reactive toward traces of oxygen, water, or carbon dioxide. Therefore, the polymerization system should be totally devoid of these impurities. Even when the concentration of these impurities is at levels of parts per million, they can markedly affect the polymerization. Therefore, these systems require great care in purification and drying of solvent and monomers and in handling the initiator solution. The polymerization temperature is another disadvantage for living ionic polymerizations: High reaction temperatures are not suitable and the optimum temperature range is very low, varying from $-20\text{ }^\circ\text{C}$ to $-78\text{ }^\circ\text{C}$.^[8] Instead of living ionic polymerization, living free radical polymerization (LFRP) was found to be more suitable to produce living/controlled polymers ^[7].

The concept of LFRP is based on the reduction of termination reactions by decreasing radical concentration. The approach to reduce the radical concentration and to protect the polymer chains from termination reactions is based on a reversible

activation/deactivation process. Figure 2.3 illustrates this concept. In LFRP, while a polymer radical ($R\bullet$) propagates monomers (M), it can also be deactivated, forming a dormant chain (D).

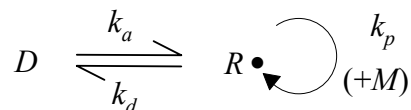


Figure 2.3 General LFRP mechanism.

Nitroxide mediated polymerization (NMP) is one of the earliest methods of LFRP. Figure 2.4 shows the general mechanism of NMP, where X represents the nitroxide group, D is the dormant species, $R\bullet$ is the polymer radical, k_a is the dissociation constant, and k_d is the coupling constant. At low temperatures, the dormant chain is stable and therefore the nitroxide group behaves as an inhibitor. However, at elevated temperatures, the dormant chain may undergo homolytic cleavage (dissociate), leading to polymer radicals and nitroxide groups. The polymer radical can grow, terminate or couple with the nitroxide group again to form the dormant species. As we will discuss later in more detail, this equilibrium between active and dormant species leads to the production of polymer chains with controlled molecular weight and narrow MWDs.

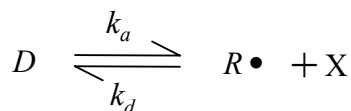


Figure 2.4 General NMP mechanism. D : dormant species; $R\bullet$: propagating radical; X : the nitroxide group.

Reversible addition-fragmentation chain transfer (RAFT) and atom transfer radical polymerization (ATRP) can be applied to a wider range of temperatures and monomer types than NMP. Since ATRP is the main focus of this thesis, the following section will describe it in more detail.

2.4 Atom transfer radical polymerization

2.4.1 Mechanism

Since 1995 (the year of the independent discoveries of ATRP by Matyjaszewski's group^[9] and Sawamoto's group^[10]) the technical literature on this process has been growing very rapidly. Several reviews, books, and book chapters summarize hundreds of papers that appeared in the literature on ATRP of a large variety of monomers^[11-15]. ATRP can synthesize various polymers with controlled molecular weight and narrow MWD. It can be carried out in a wide range of polymerization temperatures and is not very sensitive to the presence of oxygen and other inhibitors.^[16]

Figure 2.15 is the general mechanism of ATRP. In addition to the monomer, the ATRP system consists of an initiator that has an easily transferable halide atom (RX) and a catalyst. The catalyst (or activator) is a lower oxidation state metal halide ($M_t^n X$) with a suitable ligand (L). Polymerization starts when the halide atom transfers from the initiator to the catalyst to form a free radical ($R\bullet$) and a higher oxidation state metal halide $M_t^{n+1}X$ (deactivator). This step is called activation or forward reaction. The deactivation step or backward reaction pushes the reaction to form dormant species (RX) rather than the radicals ($R\bullet$). The reaction of monomer molecules (M) in the propagation step is similar to conventional free radical polymerization.

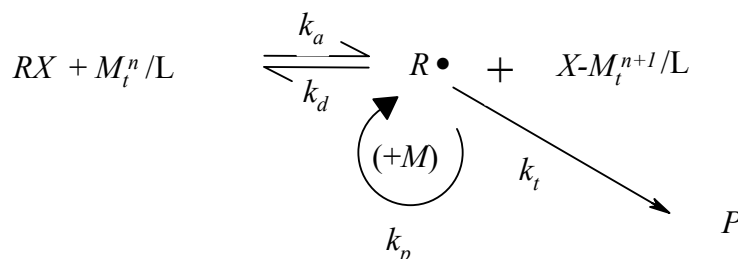


Figure 2.5 ATRP Mechanism. RX : dormant species (alkyl halide); M_t^n/L : activator (metal complex); $R\bullet$: propagating radical; $X-M_t^{n+1}/L$: deactivator; M : monomer; P : dead chain.

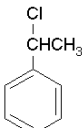
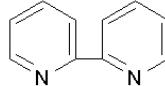
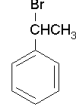
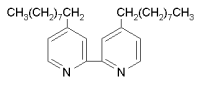
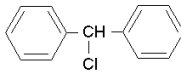
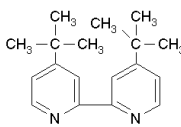
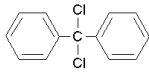
Termination reactions may occur in ATRP, especially in the beginning of the polymerization. Transfer reactions may also occur in ATRP. Fast initiation and rapid reversible deactivation will lead to better control and narrow MWD. The equilibrium constant is the ratio between the activation constant and the deactivation constant

($K_{eq}=k_a/k_d$). If the equilibrium constant is too small, ATRP will not occur or it will occur very slowly. Additionally, as the equilibrium constant increases, the concentration of radicals increases.

Usually alkyl halides with substituents on the α -carbon such as aryl, carbonyl or allyl groups are used as initiators in ATRP. The carbon halide bond must be weak so that the halogen atom can be easily transferred between the dormant species and the catalyst. Most of the ATRP initiators use either chlorine or bromine, but some investigations used iodine as the halogen atom in the initiator.^[17, 18] Polyhalogenated initiators were found to act as bifunctional initiators.^[19] Structural similarity between the initiator and the monomer has a considerable effect in ATRP. For instance, although methyl methacrylate is more reactive than styrene, benzyl halides are more active towards styrene polymerization than methyl methacrylate polymerization due to their similar structures.^[20]

Compared to conventional free radical polymerization, the new and the key component in ATRP is the catalyst. Suitable ligands should complex with a metal halide to form the ATRP catalyst. The metal halide should have at least two oxidation states and should have good affinity toward halogen atoms. ATRP systems using Cu,^[21] Rh,^[22] Ni,^[23] Pd,^[24] and Fe,^[25] transition metals in conjunction with suitable ligands such as substituted and unsubstituted bipyridines, and amines^[26] have been used as catalysts. Table 2.1 shows some ATRP initiators, metal halides and ligands.

Table 2.1 Some ATRP system components.

Initiators	Metal halide	Ligand
	CuCl	
	CuBr	
		
		

2.4.2 Copolymerization via ATRP

Shortly after its discovery, it was found out that most of the vinyl monomers could be copolymerized through ATRP. While conventional free radical polymerization produces copolymers with broader chemical composition distribution because of the termination reactions, the living nature of ATRP leads to the production of copolymers with narrow chemical composition distribution. In fact, ATRP (and other living polymerizations) can make copolymers with backbone compositions varying from random to gradient by varying the composition of the comonomer during the polymerization.^[27] While the synthesis of block copolymers is difficult in conventional free radical polymerization, LFRP techniques are ideally suited for the synthesis of block copolymers.

Various block copolymers have been synthesized by ATRP using the *macroinitiator method*. In this method, the first monomer type is polymerized with an initiator having the proper end carbon halide, yielding polymer chains with end carbon halide bonds (macroinitiators) that can be used to initiate the polymerization of the second monomer type to produce AB block copolymers.

Bifunctional initiators can also be used to prepare ABA triblock copolymers. They can polymerize the first monomer type to produce chains that have two functional

end groups (difunctional macroinitiators). The produced macroinitiator can be used to polymerize the second monomer type to form ABA triblock copolymers. Figure 2.6 illustrates this idea.

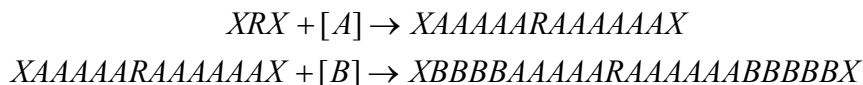


Figure 2.6 Illustration of triblock copolymer. XRX: bifunctional initiator; [A]: monomer A; [B]: monomer B

Star polymers can also be prepared via ATRP. The use of multifunctional initiators to synthesize star polymers was introduced by Matyjaszewski et al. in 1995. Figure 2.7 shows an example of an initiator that can be used to form star polymers.^[28]

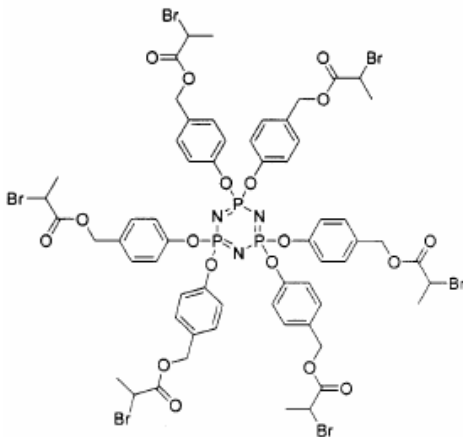


Figure 2.7 ATRP initiator for synthesizing star polymers.

2.5 Coordination polymerization

Coordination polymerization is an effective catalytic route for the production of high polymers. Unlike free radical polymerization, the growing polymer chain is bonded to the catalyst metal atom. The monomer double bond coordinates to the metal and is inserted between the catalyst and the growing macromolecule, permitting a very high degree of control during monomer insertion (site control). Like in free radical polymerization, propagation and transfer reactions are also present but there are no

termination reactions by combination or disproportionation in coordination polymerization.

In addition, because coordination polymerization is site-controlled, it is possible to design coordination catalysts that are stereo and regio-selective, thus favoring the production of atactic, isotactic or syndiotactic chains. Stereoregularity is important in controlling the properties of polymer molecules. During the polymerization of vinyl monomers ($\text{CH}_2=\text{CHR}$) depending on the insertion arrangement, atactic, isotactic and syndiotactic polymers can be formed. For example, in the case of styrene, random arrangement of the phenyl groups along the backbone results in atactic polystyrene. When all the phenyl groups are on the same side, the structure is isotactic and when the phenyl groups alternate positions above and below the backbone, the structure is named syndiotactic polystyrene^[29] (Figure 2.8).

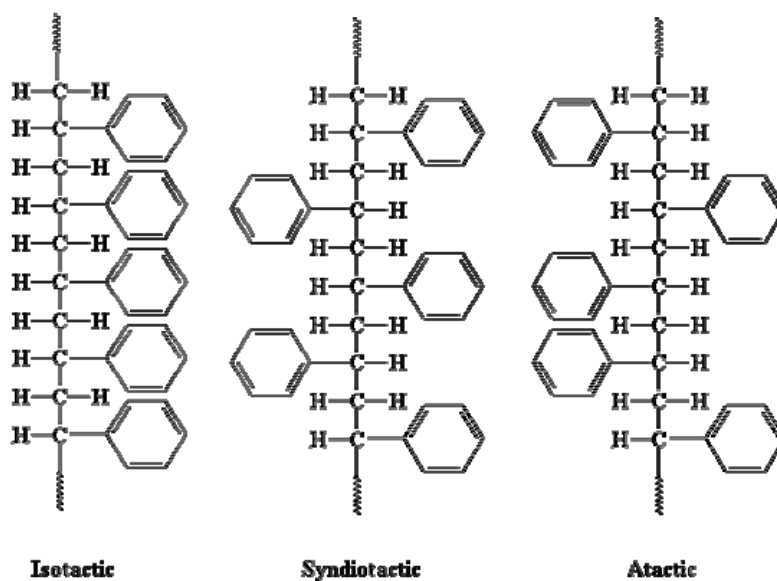


Figure 2.8 Tacticity of polystyrene.

Compared to heterogeneous Ziegler-Natta catalysts, many metallocenes produce polymers with much narrower MWD and a theoretical PDI of 2.^[30]

Several different transition metals have been used in metallocene catalysts, but zirconium and titanium are the most common choices.

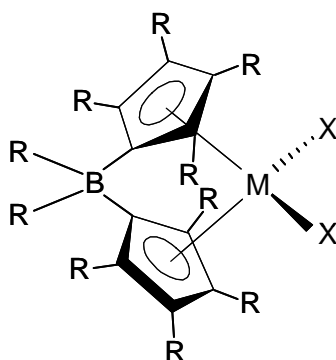


Figure 2.9 Generalized structure of a metallocene catalyst precursor. M – transition metal center; X – halogen; R – alkyl or aromatic ligand; B – bridging group.

The most widely used metallocene catalysts consist of two bent cyclopentadienyl ligands (Cp_2MX_2) such as illustrated in Figure 2.9. Fluorenyl and indenyl groups can be used as a ligand instead of cyclopentadienyl. The ligands can be connected by a bridge (B) such as ethyl and silyl bridge. The transition metal (M) is bonded to two atoms (X) which are usually chlorine atoms.

Metallocene catalysts are used with strong Lewis acid cocatalysts. The most typical cocatalyst used with metallocenes is methylaluminoxane (MAO). The cocatalyst abstracts a halide atom from the catalytic complex and leaves the metal with vacant site that will be used for monomer coordination and propagation. The growing chains can be terminated by transfer reactions or catalyst deactivation. The transfer reactions produce dead polymer chains and active sites that can grow another polymer chain. On the other hand, deactivation reactions produce dead polymer chains and deactivated active centers. β -Hydride elimination is a common transfer reaction with metallocenes, leading to polymer chains with unsaturated end groups. Transfer to monomer or β -alkyl elimination reactions (for polypropylene and higher α -olefins) gives dead chains with terminal unsaturations. Hydrogen is the most common chain transfer agent used with metallocenes. It is used to regulate polymer molecular weight and forms polymer chains that have saturated end groups.

If chains containing unsaturated chain ends (macromonomers) react with a growing chain, polymers containing long chain branches (graft copolymers) can be produced. These graft copolymers can be classified as homogeneous or heterogeneous grafts. If the backbone and the side chains are composed of the same type of monomer,

the resultant polymer is a homogeneous graft copolymer. On the other hand, if they are different the resultant polymer is a heterogeneous graft copolymer (Figure 2.10).

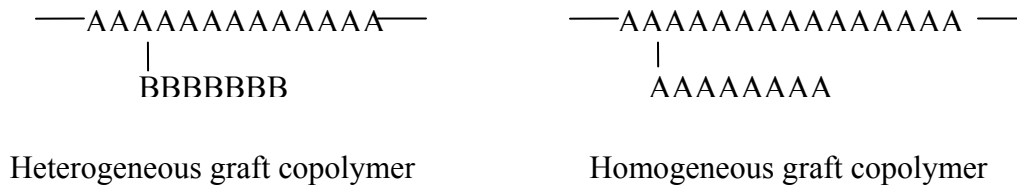


Figure 2.10 Types of graft copolymers.

There are two approaches to produce graft copolymers with metallocenes via macromonomer incorporation: in-situ and ex-situ techniques.

The ex-situ technique requires two polymerization steps. The macromonomers are produced in the first step and then copolymerized or "grafted to" the backbones of another polymer in the second step. The two steps usually performed in two separate reactors.^[31] The molecular weight, MWD and other properties of the macromonomers can be characterized before the second incorporation step.

The two steps used in the ex-situ procedure can be combined in one single step using mixed catalysts. This procedure is known as in-situ procedure. Choosing the catalyst pair is important in order to synthesize graft copolymers with mixed catalysts. One of the catalysts should have the ability to form polymer chains with unsaturated ends (macromonomers) and the second catalyst should copolymerize the macromonomers with the monomer to form grafted chains.

The polymerization conditions for macromonomer incorporation are also important. The main factors are high macromonomer concentration and low monomer concentration. The end group selectivity and/or copolymerization tendency may also be influenced by the polymerization temperature, reaction medium and monomer and hydrogen concentration.^[32-34]

2.6 Modeling of ATRP

As mentioned above, a great number of studies have been done to understand and utilize ATRP. Most of these studies are experimental. One valuable tool that can be used to capture the mechanistic chemistry of any process is the mathematical model. More understanding of polymer structures, polymer kinetics, and polymer properties can be achieved through mathematical modeling.

There have been several models published in the literature for various controlled radical polymerization systems. Some models are general for any controlled radical polymerizations and some are utilized for specific processes.

Efforts have been done to model several controlled free radical polymerizations using the method of moments. Zhu proposed a detailed kinetic models for NMP,^[35] ATRP,^[36] and RAFT^[37] in batch reactors. Although they were not validated with experimental results, his models are capable of showing the effects of rate constants and reactant concentrations on the kinetic data. Free volume theory was incorporated to the ATRP model^[36] in order to study the diffusion limitation.^[38] Three case studies were presented. Integrated model of free volume theory with the method of moments for NMP was presented by Vivaldo-Lima and Mendoza-Fuentes.^[39] Similarly, Butte et al. used the method of moments and an empirical expression for diffusion-controlled termination to develop a kinetic model for NMP and ATRP.^[40] The NMP model was validated with an experimental data of styrene polymerization. Bonilla et. al. presented detailed modeling and parameter estimation of nitroxide mediated living free radical polymerization of styrene. They validated their model with an experimental data from the literature.^[41] All of the previous models are for polymerizations in batch reactor. Zhang and Ray published a series of papers on the modeling of living polymerizations (including anionic, NMP, ATRP, and RAFT).^[42-45] They applied their models to batch, semibatch, continuous tank reactors, and plug flow reactors and validated their models with an experimental data.

Monte Carlo simulation was used in the modeling of controlled radical polymerizations to give more understanding about these processes especially about the molecular weight distribution of the polymer. He et. al.^[46] applied Monte Carlo simulation to nitroxide mediated polymerization. The predicted molecular weight

distribution was as narrow as expected in living polymerizations. The model was used to study the effect of the equilibrium rate constants and reactant concentrations on polymer properties. Recently Tobita ^[47] presented another Monte Carlo simulation for NMP and compared it with the method of moments.

Along with the previous modeling strategies, the commercially available program PREDICI has been used extensively to model controlled free radical polymerizations. Barner-Kowollik and coworkers simulate RAFT process using PRIDICI. ^[48,49] Chaffey-Millar et al. ^[50] described (using PREDICI) computational strategy for the simulation of star polymerization with RAFT. Matyjaszewski's group ^[51] has modeled the polymerization of styrene with NMP considering thermal initiation and neglecting diffusion-controlled reactions. Also they used PREDICI to study the chain-end functionality of polystyrene ^[52] the polymerization kinetics, ^[53] and the importance of diffusion-controlled reactions ^[54] in ATRP.

2.7 References

- [1] G. Odian, Principles of polymerization, 3rd edition, **1990**, p. 198.
- [2] A. Rudin, The element of polymer science and engineering, **1999**, p.189.
- [3]. O. Olabisi, L. M. Robeson, M. T. Shaw, Polymer-Polymer Miscibility; Academic Press: New York, N.Y., **1979**.
- [4]. H. Dostal, Monatsh. Chem. **1936**, 69, 424.
- [5]. L. M. Morris, T. P. Davis, R. P. Chaplin, Polymer **2000**, 42, 941.
- [6]. F. P. Mayo, F. M. Lewis, J. Am. Chem. Soc. **1944**, 66, 1594.
- [7] K. Matyjaszewski, Controlled/living radical polymerization : progress in ATRP, NMP, and RAFT . **2000**.
- [8]. T. Kitayama, K. Ute, K. Hatada, Polym. J. **1990**, 23, 5.
- [9] J. S. Wang, K. Matyjaszewski, J. Am. Chem. Soc. **1995**, 117, 5614
- [10] M. Kato, M. Kamigaito, M. Sawamoto, T. Higashimura, Macromolecules **1995**, 28, 1721.
- [11] K. Matyjaszewski, J. Xia, Chem. Rev. **2001**, 101, 2921.
- [12] M. Kamigaito, T. Ando, M. Sawamoto, Chem. Rev. **2001**, 101, 3689.
- [13] K. Matyjaszewski, ACS Symp. Ser. **2002**, 854, 2.
- [14].J. Jagur-Grodzinski, “Living and Controlled Polymerization: Synthesis, Characterization and Properties of the Respective Polymers and Copolymers” **2005**,1.
- [15]. K. Davis, K. Matyjaszewski, Statistical, gradient, block and graft copolymers by controlled/living radical polymerization, **2002**.
- [16]. K. Matyjaszewski, S. Coca, S. Gaynor, B. Woodworth, Macromolecules **1998**, 31, 5967.
- [17]. Y. Kotani, M. Kamigaito, M. Sawamoto, Macromolecules **1999**, 32, 2420.
- [18]. Y. Kotani, M. Kamigaito, M. Sawamoto, Macromolecules **2000**, 33, 6746.
- [19]. M. Destarac, K. Matyjaszewske, B. Boutevin, Macromol. Chem. Phys. **2000**, 201, 265.
- [20]. K. Matyjaszewske, J. L. Wang, T. Grimaud, D. A. Shipp, Macromolecules **1998**, 31, 1527.
- [21]. J. S. Wang, K. Matyjaszewski, Macromolecules **1995**, 28, 7572.
- [22]. V. Percec, B. Barboiu, A. Neumann, J. C. Ronda, M. Zhao, Macromolecules **1996**, 29, 3665.
- [23]. C. Granel, P. Dubois, R. Jerome, P. Teyssie, Macromolecules **1996**, 29, 8576.
- [24]. P. Lecomte, I. Drapier, P. Dubois, P. Teyssie, R. Jerome, Macromolecules **1997**, 30, 7631.
- [25]. T. Ando, M. Kamigaito, M. Sawamoto, Macromolecules **1997**, 30, 4507.
- [26]. J. Xia, X. Zhang, K. Matyjaszewske ACS Symp. Ser. **2000**, 760, 207.
- [27].D. Greszta, K. Matyjaszewski, Polym. Prepr. (Am. Chem. Soc. Div. Polym. Chem.) **1996**, 37(1), 569.
- [28]. J. S. Wang, D. Greszta, K. Matyjaszewski, Polym. Mater. Sci. Eng. **1995**, 73, 416.
- [29] T. Meyer, J. Keurentjes, Hnabook of polymer reaction engineering”, vol 1, **2005**, P. 365.

- [30]. H. Sinn, E. Kaminsky, *Adv. Organomet. Chem.*, **1980**, 18, 99.
- [31]. E. Kolodka, S. Zhu, A. Hamielec, *Macromol. Rapid Commun.* **2003**, 24, 311.
- [32]. E. Markel, W. Weng, A. Peacock, A. Dekmezian, *Macromolecules* **2000**, 33, 8541.
- [33]. A. Malmberg, E. Kokko, P. Lehmus, B. Löfgren, J. Seppälä, *Macromolecules* **1998**, 31, 8448.
- [34]. F. Zhu, Y. Fang, H. Chen, S. Lin, *Macromolecules* **2000**, 33, 5006.
- [35] S. Zhu, *J. Polym. Sci. Part B: Polym. Phys.* **1999**, 37, 2692.
- [36] S. Zhu, *Macromol. Theory. Simul.* **1999**, 8, 29.
- [37] A. Wang, S. Zhu, *J. Polym. Sci. Part A: Polym. Chem.* **2003**, 41, 1553.
- [38] O. Delgadillo-Velazquez, E. Vivaldo-Lima, I. Quintero-Ortega, S. Zhu, *AIChE J.* **2002**, 48(11), 2597.
- [39] E. Vivaldo-Lima, A. Mendoza-Fuentes, *Polym. React. Eng.* **2002**, 4, 10, 193.
- [40] A. Butte, G. Storti, M. Morbidelli, *Chem. Eng. Sci.* **1999**, 54, 3225.
- [41] J. Bonilla, E. Saldivar, A. Flores-Tlacuahuac, E. Vivaldo-Lima, R. Pfaendner, F. Tiscareno-Lechuga, *Polymer Reaction Engineering*, **2002**, 10, 4, 227.
- [42] M. Zhang, H. Ray, *Journal of applied polymer science* **2002**, 86, 1630.
- [43] M. Zhang, H. Ray, *Journal of applied polymer science* **2002**, 86, 1047.
- [44] M. Zhang, H. Ray, *Industrial and Engineering Chemistry Research*, 40, **2001**, 4336.
- [45] M. Zhang, Ph. D. Thesis, University of Wisconsin at Madison, **2001**.
- [46] J. He, H. Zhang, J. Chen, Y. Yang, *Macromolecules* **1997**, 30, 8010.
- [47] H. Tobita, *Macromol. Theory Simul.* **2006**, 15, 23.
- [48] C. Barner-Kowollik, J. F. Quinn, D. R. Morsley, T. P. Davis, *J. Polym. Sci., Polym. Chem. Ed.* **2001**, 39, 1353.
- [49] C. Barner-Kowollik, J. F. Quinn, T. L. Uyen Nguyen, T. P. Davis, *Macromolecules* **2001**, 34, 7849.
- [50] H. Chaffey-Millar, M. Busch, T. P. Davis, M. H. Stenzel, C. Barner-Kowollik, *Macromol. Theory Simul.* **2005**, 14, 143.
- [51] D. Greszta, K. Matyjaszewski, *Macromolecules* **1996**, 29, 7661.
- [52] J. Lutz, K. Matyjaszewski, *Macromol. Chem. Phys.* **2002**, 203, 1385.
- [53] D. Shipp, K. Matyjaszewski, *Macromolecules* **2000**, 33, 1553.
- [54] D. Shipp, K. Matyjaszewski, *Macromolecules* **1999**, 32, 2948.

Chapter 3

3 Methods and Materials

3.1 Mathematical modeling

Mathematical models can describe both the physical and chemical phenomena during polymerization based on our understanding of the polymerization mechanism or process. In this way, mathematical models are a compilation of the most important (at least from the modeller's point of view) information that has been acquired for a specific system. Once mathematical models are developed and validated by experimental data, they can be used to predict, explain and optimize certain polymer structures or properties.

Polymerizations can be described using several different mathematical modeling techniques. Two of these techniques are used in this thesis to model ATRP.

In the method of population balances, molar balance equations are defined for each species in the reactor based on the elementary reactions of the polymerization mechanism. This leads to a very large set of the ordinary differential equations that needs a large computational effort to solve. Therefore, it is common to combine population balances with the method of moments to solve only for the average molecular weights and the polydispersity index. Much less computational effort can be used by utilizing the method of moments. Zeroth, first, and second moments are sufficient to get the average number molecular weight (M_n), average weight molecular weight (M_w), and the polydispersity index (PDI). More detail of this technique (supported with case studies) is presented in Chapters Four and Five.

The second approach that is used in this thesis to model ATRP is Monte Carlo simulation. In this case, it is not necessary to solve any differential equation. The Monte Carlo technique used in this thesis is based on the general simulation method developed by Gillespie in 1977.^[1] The method requires the following steps:

- 1- Selection of a suitable simulation volume.
- 2- Transformation of macroscopic or experimental reaction constants (k^{exp}) to microscopic or Monte Carlo rate constants (k^{MC}).

- 3- Transformation of experimental concentration of the species to their number of molecules.
- 4- Generation of random numbers to choose the reaction step that takes place and the time interval elapsed between reactions.

Although Monte Carlo simulation is usually more time consuming than the method of moments, it can predict the full molecular weight distribution instead of only averages. More details of this technique (supported with case studies) is presented in Chapters Four, Five, Six and Eleven.

3.2 Experimental

General experimental details are described in this section. Details of experiments and materials that are specific for each Chapter will be described separately in those Chapters.

3.2.1 Materials

The monomers were obtained from Aldrich Chemical Co. After they were passed through an alumina column to remove the inhibitor, they were stored under nitrogen atmosphere at 0°C. Copper (I) bromide (99.999%), 2,2'-bipyridine (bpy, 99%), 1-bromoethyl benzene (97%), and benzal bromide (97%) were used as received (from Aldrich). Technical grade solvents (from VWR) were employed without further treatment.

3.2.2 Polymerization and polymer purifications

Standard ATRP procedures were followed in our laboratory with reproducibility of at least three times. The solid species (such as the metal halides, ligands or macroinitiators) were introduced initially to a round glass bottom flask (100 ml) used as reactor. To remove the air from the system, the reactor was evacuated and purged with nitrogen several times. The liquid species (such as the monomers and the initiators) were then introduced to the reactor with degassed syringes. The reactor was heated in an oil bath up to the set-point polymerization temperature according to the polymerization recipe. The reaction was stopped by exposure to air and by cooling in ice bath.

Although ATRP is very good to synthesize polymers with special topologies, compositions and functional chain ends, a challenging problem is the required high catalyst concentrations due to its low catalyst efficiency. Usually, the initiator to catalyst molar ratio was one. The molar fraction of metal halide (catalyst) in monomer can be sometimes as high as 1% (molar). Normally, the catalyst is not soluble in most of the polymerization media commonly used.^[2] Contamination of polymer due to catalyst residues is one of the disadvantages of ATRP. This residue changes the color of the polymer and makes it toxic. Passing the polymer solution through silica gel or alumina^[3] or dissolution and reprecipitation^[4] are some of the methods that have been used to remove the catalyst from the final product. In our laboratory, we used three ways to remove the catalyst from the final product:

- 1- CuBr (I) is soluble in ethanol and can be removed by adding excess of ethanol in the precipitation step. Figure 3.1 is a picture of the reaction mixture in the reactor during the polymerization. The brown color in the mixture is given by CuBr(I). After exposing the reaction to air, the reaction medium colour changes from brown to green due to the oxidation of CuBr(I) to CuBr(II). The green colored complex is not soluble in ethanol and needs another method to be removed from the polymer product. Beside its limitation in removing CuBr(II), this method of cleaning the catalyst requires a lot of ethanol to remove CuBr(I) completely.
- 2- THF was used as the solvent to dissolve the reaction mixture after the reaction, after the solution turned green due to the oxidization of CuBr (I) to CuBr(II). The solution was passed through a column containing aluminum oxide to remove the catalyst. The solution obtained was clear and the green particles were retained in the filter column (Figure 3.2).
- 3- The third method used to remove the catalyst from the product is the most interesting and least expensive one. The polymer mixture is dissolved in a good solvent that is immiscible with water. Liquid-liquid extraction was applied to extract the CuBr(II) from the organic phase to the water phase. Then the organic phase was collected and the polymer can recovered after evaporating the solvent. Dichloromethane is a good solvent because it is immiscible with water and very volatile. Toluene was also used in this study. Figure 3.3 shows the liquid-liquid extraction technique before and after the transfer of the catalyst from the organic phase to the water phase.



Figure 3.1 Picture of the reaction mixture in the reactor during the polymerization. The brown colour is caused by the presence of CuBr(I) .



Figure 3.2 Aluminium oxide after filtering the polymer solution. The green color is caused by the presence of CuBr(II) .

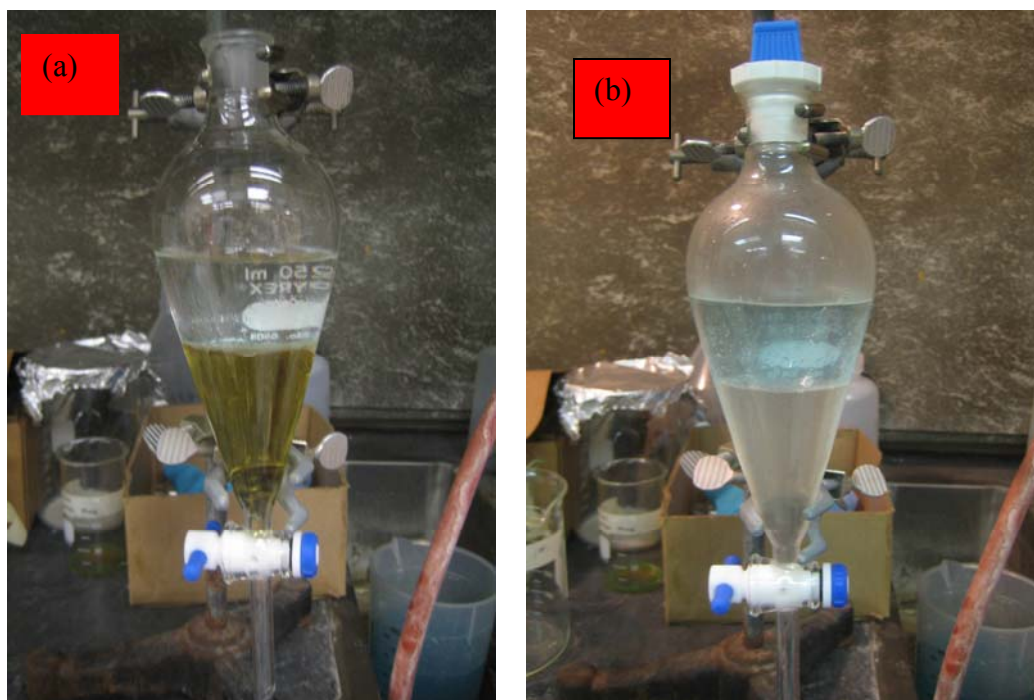


Figure 3.3 Liquid-liquid extraction of the catalyst from the organic phase to the water phase. (a) before the extraction (b) after the extraction.

3.2.3 Polymer characterization

Detailed characterization of polymer chains is very important for the synthesis of polymers with novel molecular architectures or for the modification of the microstructure of existing polymers. The level of characterization depends on the nature of the project and can achieve a great degree of sophistication. Generally, the concept of characterization is associated with the description of molecular structure in terms of molecular weight and chemical composition. Knowledge of the molecular structure is necessary for understanding the chemical mechanism involved during the synthesis and the final properties of the polymer material.

Molecular Weight

Molecular weight distribution is measured by gel permeation chromatography (GPC). This technique is also known as size exclusion chromatography (SEC). GPC is a fractionation method in which solvated polymer molecules are separated according to their sizes in solution. In this technique, a small volume of polymer solution is injected into one or more columns in series packed with particles with different pore radii. Polymer chains with smaller molecular weights have a longer retention time than chains with higher molecular weight. Under identical conditions, the sample of given polymer is compared with polymer standards of known molecular weight and narrow molecular weight distribution. A plot of concentration of polymer versus retention time can be transformed into a molecular weight distribution curve by using the universal calibration curve. Once a proper calibration curve is available to relate the elution volume to the molecular weight of the calibration standard, the direct calculation of all molecular weights and the polydispersity index is possible. ^[5]

In this study, molecular weights were obtained using a gel permeation chromatographer (Waters 590) operating at room temperature with an on-line refractive index (RI) detector and a multiangle laser light-scattering photometer system. THF was filtered and used as the eluent at a flow rate of 1.0 ml/min. Samples for analysis were prepared as 0.5% solutions in THF and filtered through 0.45 μm filters prior to injection. The dn/dc values used in the calculation of molecular weights were calculated

independently using a refractometer (Brice-Phoenix differential refractometer equipped with 632 nm band-pass interference filters, operated at 25 °C).

Chemical Composition

The average chemical composition of copolymers can be determined by Fourier transform-infrared spectroscopy (FTIR) or nuclear magnetic resonance spectroscopy (NMR). FTIR is based on the interaction of infrared electromagnetic radiation with the sample. The vibration of characteristic chemical groups at certain frequencies will absorb the incident infrared beam. The result of the analysis can be a spectrum of the transmittance as a function of wavelength. Each group can be identified in a range of band and an identical group in a molecule alters the relative strengths of the absorption bands. [6] For FTIR, Fourier transform-infrared spectroscopy was used to measure the composition of the copolymers. The polymer powder was dissolved in THF and a few drops of the solution were added onto a transparent KBr disk. After evaporation of the solvent, a thin polymer film was formed on the KBr disk. The samples were analyzed by FTIR and the spectra were reported after subtracting from a background spectrum for the plain KBr disk. The spectra were recorded from 400 to 4000 cm^{-1} , after 32 scans, with a resolution of 4 cm^{-1} .

Nuclear magnetic resonance is based on the interaction of an external magnetic field and the magnetic spin of the atomic nucleus. ^1H and ^{13}C are by far the most utilized NMR techniques; under suitable condition it is possible to identify the type of protons or carbons in the polymer chain, making this a powerful analytical tool for the characterization of the chemical composition of copolymers. The result of the analysis is a plot with intensity of nucleus as a function of chemical shift. The chemical shift is relative to a standard sample and permits identification of the nature of the atoms in the sample. [7]

A 300-MHz AC Bruker Fourier-Transform spectrometer was used to get ^1H and/or ^{13}C -NMR. The sample dissolved in deuterated chloroform at a concentration of 10–30 mg/ml. The operating conditions were as follows: temperature of the probe is 25°C and number of scans is 32 for ^1H NMR and 4092 for ^{13}C NMR. The relative amount of

comonomers incorporated into the copolymer was estimated from the integrated area under the appropriate peak intensities.

3.3 References

- [1] D. Gillespie, J. Phys. Chem. **1979**, 81, 2340
- [2] J. Wang, K. Matyjaszewski J. Am. Chem. Soc. **1995**, 117, 5614.
- [3] K. Matyjaszewski, T. Pintauer, S. Gaynor, Macromolecules **2000**, 33, 1476.
- [4] A. M. Kasko, A. M. Heintz, C. Pugh, Macromolecules **1998**, 31, 256.
- [5] A. Rudin, The element of polymer science and engineering, **1999**, p.103.
- [6] B. Smith, Fundamentals of fourier transform infrared spectroscopy, **1996**.
- [7] R. Ernst, G. Bodenhausen, A. Wokaun, Principles of nuclear magnetic resonance in one and two dimention, **1991**.

Chapter 4

4 Dynamic Monte Carlo Simulation of Atom-Transfer Radical Polymerization*

4.1 Abstract

A dynamic Monte Carlo model was developed to simulate atom-transfer radical polymerization (ATRP). The algorithm used to describe the polymerization includes activation, deactivation, propagation, chain transfer, and termination by combination and disproportionation reactions. Model probabilities are calculated from polymerization kinetic parameters and reactor conditions. The model was used to predict monomer conversion, average molecular weight, polydispersity index and the complete molecular weight distribution at any polymerization time or monomer conversion. The model was validated with experimental results for styrene polymerization and compared with simulation results from a mathematical model that uses population balances and the method of moments. The simulations agree well with experimental and theoretical results reported in the literature. We also investigated the control volume size and number of iterations to reduce computation time while keeping an acceptable noise level in the Monte Carlo results.

4.2 Introduction

Living free radical polymerization (LFRP) has attracted considerable interest because it combines the versatility of conventional free radical polymerization with the excellent microstructural control of living polymerization. Currently, the most attractive types of living free radical polymerization are reversible addition-fragmentation chain transfer (RAFT),^[1,2] nitroxide-mediated polymerization (NMP)^[3-5] and atom-transfer radical polymerization (ATRP).^[6, 7]

* This chapter has been published: M. Al-Harthi, J. Soares, L. Simon, *Macromol. Mat. Sci.* **2006** 291, 993-1003.

A large literature is available on the chemistry of LFRP and several of LFRP features have been elucidated with the help of mathematical models. For instance, the method of moments was used to describe NMP,^[8,9] ATRP,^[10-13] and RAFT^[14] in batch reactors, and NMP, ATRP^[15,16] and RAFT^[17] in semi-batch and continuous reactors; Predici was also used to study NMP,^[18] ATRP^[19-21] and RAFT^[22] in batch reactors.

Usually, LFRP models describe monomer conversion and number and weight average molecular weights as a function of polymerization time. It is very important, however, to determine the complete molecular weight distribution (MWD) of the polymer in order to uniquely define properties such as glass transition temperature, melting point, strength, and flow properties. Although the method of moments is very powerful and has been used widely to describe several polymerization mechanisms, it can not predict the MWD. Predici, and related numerical techniques for the integration of large sets of stiff differential equations is a powerful technique that can predict MWDs. Monte Carlo simulation has been used to model the MWD and other microstructural distributions for conventional free radical polymerization,^[23, 24] NMP^[25-27] and RAFT^[28] using only probabilities derived from the polymerization mechanism. In addition to being simple to implement, Monte Carlo simulation gives the most complete description of polymer microstructure, since the polymer chains are produced one-by-one throughout the simulation.

In the present investigation we study ATRP with a dynamic Monte Carlo model and compare our simulation results with the ones obtained with the method of moments as well as with experimental results. To our knowledge, this is the first time that a Monte Carlo model is used to describe ATRP and validated with experimental polymerization results.

4.3 Model description

Our simulation approach follows Gillespie's algorithm for dynamic Monte Carlo simulation.^[29] The algorithm defines a control volume V that contains a certain number of reactant molecules at time zero in a homogeneous reaction system. Several reactions may take place in the control volume. The experimental rates of these reactions – measured

macroscopically with established methods of polymerization kinetics – are transformed into stochastic rates based on the number of molecules of each reactant present in the control volume at a given reaction time. For instance, the number of monomer molecules (X_m) in the control volume at a given time equals the monomer molar concentration $[M]$ multiplied by Avogadro's number (N_A) and the size of the control volume:

$$X_m = [M] N_A V \quad (1)$$

Similarly, the number of initiator molecules (X_i) and catalyst molecules (X_c) are calculated as follows:

$$X_i = [I] N_A V \quad (2)$$

$$X_c = [C] N_A V \quad (3)$$

According to Gillespie,^[29] experimental rate constants are transformed into stochastic rate constants with the equations:

$$k^{MC} = k^{\text{exp}} \quad \text{for first order reactions} \quad (4)$$

$$k^{MC} = \frac{k^{\text{exp}}}{VN_A} \quad \text{for bimolecular reactions between different species} \quad (5)$$

$$k^{MC} = \frac{2k^{\text{exp}}}{VN_A} \quad \text{for bimolecular reactions between similar species} \quad (6)$$

The rationale for this transformation is explained in detail by Gillespie and involves the number of independent combinations of molecules participating in each reaction inside the control volume. Note that the stochastic rate constants have units of reciprocal time; this is why experimental rate constants for bimolecular reactions must be divided by the product VN_A .

The probability of any reaction (P_v) taking place at a given time can be calculated with the equation,

$$P_v = \frac{R_v}{\sum_{v=1}^N R_v} \quad (7)$$

where R_v is the reaction rate of v^{th} reaction.

The following relation is used to determine which reaction type will take place,

$$\sum_{\nu=1}^{\mu-1} P_{\nu} < r_1 < \sum_{\nu=1}^{\mu} P_{\nu} \quad (8)$$

where μ is the number of the selected reaction type and r_1 is a random number distributed uniformly in the interval [0, 1].

Another random number (r_2) is generated to determine the time interval (τ) between two consecutive reactions. The time step is related to the inverse of the total stochastic rates and the natural logarithmic of r_2 according to the equation:^[29]

$$\tau = \frac{1}{\sum_{\nu=1}^{\mu} R_{\nu}} \ln\left(\frac{1}{r_2}\right) \quad (9)$$

Conventional free-radical polymerization proceeds via a chain growth mechanism involving four different reaction types: 1) primary radical generation from non-radical species (initiation); 2) radical addition to a substituted alkene (propagation); 3) chain termination either by combination or by disproportionation; and 4) chain transfer to monomer, solvent and other small molecules.

The propagation step increases the length of polymer radicals by the sequential addition of monomer molecules. Propagation reactions will continue until some chain termination or transfer step occurs. Termination by combination occurs when two polymer radicals react to form a single dead chain, while termination by disproportionation produces two dead chains. In addition to these two termination processes, chain transfer by hydrogen abstraction from any hydrogen-containing reactant present in the system will also stop the growth of polymer radicals and generate another primary radical.

In living radical polymerization, active and dormant polymer chains exist in equilibrium. This equilibrium allows simultaneous, but slow, growth of several polymer chains, while keeping the concentration of active polymer chains low enough to minimize termination and transfer reactions.

Atom-transfer radical polymerization uses alkyl halides (initiator) and low valence transition metal complexes (catalyst) to minimize termination rates (by decreasing the radical concentration) during free radical polymerization. This decreases the ratio of termination to propagation, however the ratio of transfer to propagation rate does not change. The catalyst promotes the equilibrium between the polymer radicals and the dormant chains. In the activation step, one dormant chain reacts with one catalyst molecule (low valence transition metal complex), forming a polymer radical and a high valence transition metal complex. The reverse process happens in the deactivation step. Thermal initiation and other side reactions, such as elimination reactions, that may occur under some conditions were neglected because they have a negligible effect on the MWD of the polymer^[30] for the conditions used in the model as will be demonstrated below. The elementary reaction steps of ATRP used in the model are described below.

Equilibrium



Propagation



Transfer to monomer



Termination by combination



Termination by disproportionation



In Equations (10) to (15), C and CX is the catalyst in its low and high valence states, M is the monomer, $R_r \bullet$ is a polymer radical, P_r is a dead polymer chain, D_r is a

dormant polymer chain, k_p is the propagation rate constant, k_{tc} is the rate constant of termination by combination, k_{td} is the rate constant of termination by disproportionation, k_a is the activation rate constant, k_d is the deactivation rate constant, k_{tr} is the transfer rate constant, and the subscripts r and m indicate the number of monomer molecules in the chain.

The polymerization mechanism described by Equations (10) to (15) was used to make the flowsheet summarizing the Monte Carlo simulation procedure adopted in this investigation (Figure 4.1).

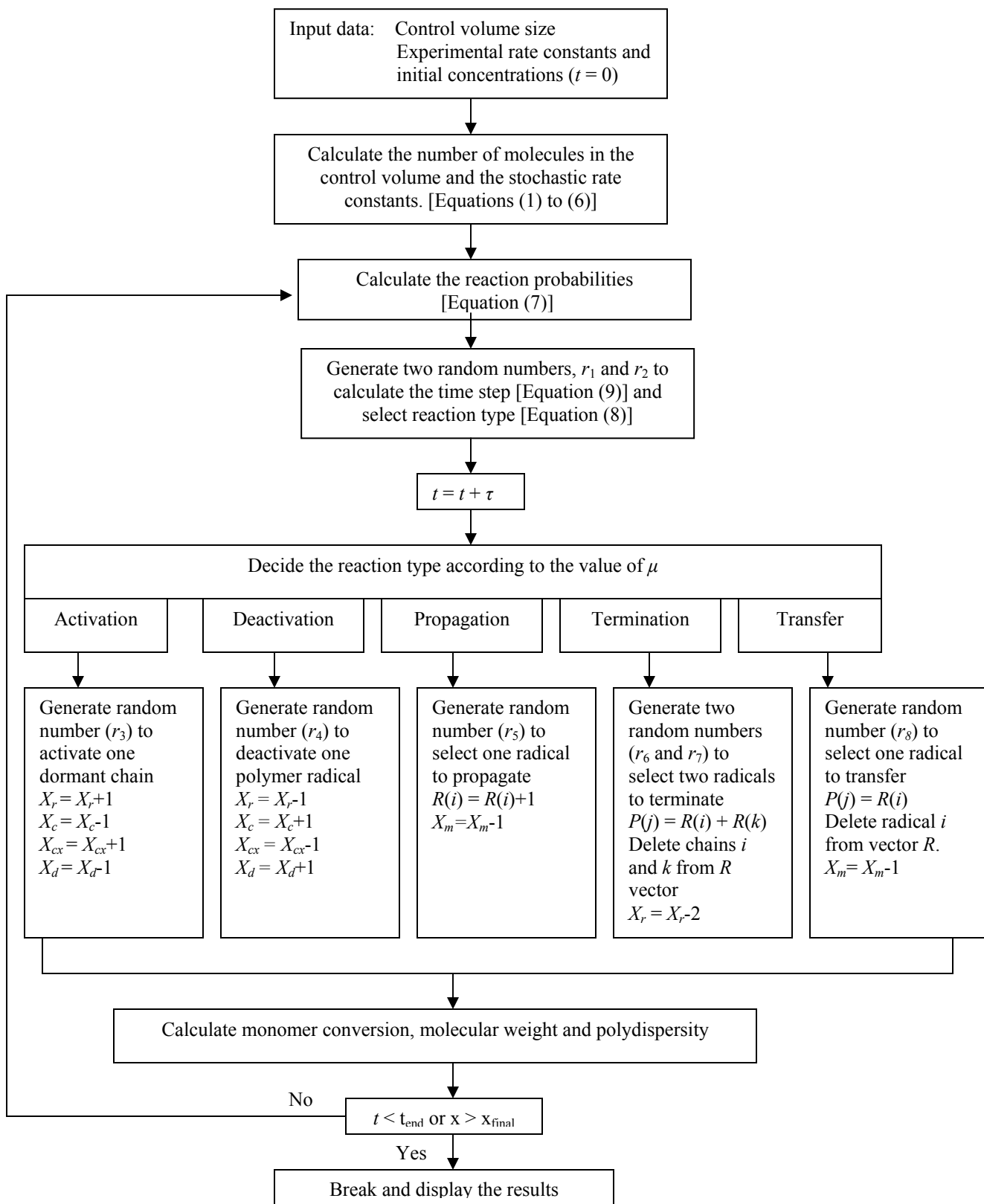


Figure 4.1 Algorithm for Monte Carlo simulation of ATRP.

A personal computer (Intel (R) Pentium(R) 4 with 2.8 GHz processor and 504 MB of RAM) was used in the simulations. The program was written in MATLAB version 7. The kinetic rate constants used in the model were selected from the literature for styrene polymerization at 110 °C and are listed in the Table 4.1. The molar ratio monomer:initiator:catalyst was kept at 100:1:1 in all simulations, unless mentioned otherwise.

Table 4.1 Parameters used in ATRP of styrene at $T=110$ °C

Parameter	Value	Reference
k_p (L.mol ⁻¹ . s ⁻¹)	1516	31
k_{tc0} (L.mol ⁻¹ . s ⁻¹)	3.469×10^8	32
k_{td0} (L.mol ⁻¹ . s ⁻¹)	0	
k_{tr} (L.mol ⁻¹ . s ⁻¹)	0.22	32
k_a (L.mol ⁻¹ . s ⁻¹)	0.45	33
k_d (L.mol ⁻¹ . s ⁻¹)	1.1×10^7	33
	(unless mentioned otherwise)	

Gel Effect

In free radical polymerization, the termination rate constant becomes diffusion controlled at high conversion; this phenomenon is known as the gel effect. The relevance of this phenomenon in living free radical polymerization is still debatable. Some studies suggest that only the termination constant may be affected by diffusion limitations at high monomer conversions,^[15-17] but others claim that all rate constants may be affected.^[11,34] In this study, we assumed that diffusion limitations affected only termination reactions, since they involve the reaction of large molecules that are more likely to be diffusion-limited. To account for the diffusion limitation on termination reactions, the empirical

correlation, relating k_{tc} to monomer conversion, X , and temperature, T , suggested by Husain and Hamielec^[32] was used in our model:

$$k_{tc} = k_{tc0} \exp[-2(A_1X + A_2X^2 + A_3X^3)] \quad (16)$$

$$A_1 = 2.57 - 5.05 \times 10^{-3} T \quad (17)$$

$$A_2 = 9.56 - 1.76 \times 10^{-2} T \quad (18)$$

$$A_3 = -3.03 + 7.85 \times 10^{-3} T \quad (19)$$

4.4 Results and discussions

4.4.1 Effect of control volume size

The first step in the simulation is the selection of the size of the control volume (Figure 4.1). The size of this control volume affects the simulation time and the CPU memory required to store the simulation data. In this study, the chain lengths (r) of dormant chains (D_r), polymer radicals ($R_r\bullet$), and dead chains (P_r) are stored in vectors **D**, **R**, and **P**, respectively. As the control volume increases, the number of species that the simulation must keep track of increases, and so do the sizes of vectors **D**, **R**, and **P**.

Because of the ATRP mechanism, large vectors will be required if the size of the control volume is large. Equation (2) shows that the number of dormant species increases linearly with the size of the control volume; it can increase up to millions of molecules (vector positions) for a control volume of 1×10^{-17} L. Therefore, the size of the dormant vector (**D**) will be in order of millions, increasing CPU memory requirements and computation time.

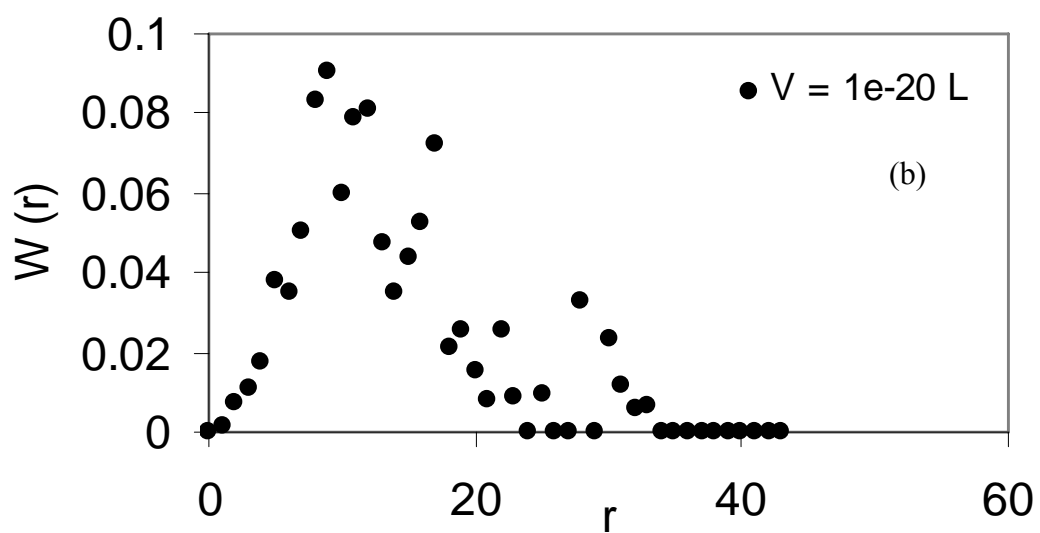
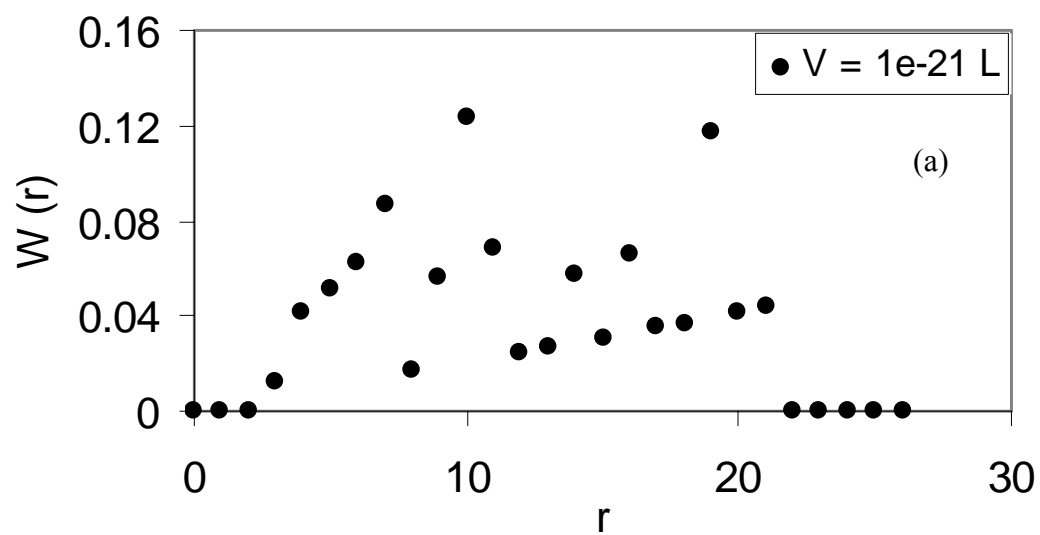
Table 4.2 shows the CPU time needed to reach 30 percent monomer conversion for several control volume sizes. Varying the control volume from 1×10^{-21} to 1×10^{-18} has no appreciable effect on the degree of polymerization (DP) and polydispersity index (PDI) but increases the computation time by several hours. It is clear that, to calculate only DP and PDI , small control volume is enough to give a feeling about the predicted values.

Table 4.2 Effect of control volume size (rate constants are shown in Table 4.1)

V (L)	X	DP	PDI	CPU time (h:m:s)
1×10^{-21}	0.3	30.2	1.09	0:0:1
1×10^{-20}	0.3	30.7	1.08	0:0:9
1×10^{-19}	0.3	30.8	1.07	0:2:14
1×10^{-18}	0.3	30.8	1.07	4:48:28

Figure 4.2 compares the molecular weight distribution (MWD) of polymer produced at a monomer conversion of 0.1 for several control volume sizes. The MWD predicted with the two smallest control volumes (1×10^{-21} and 1×10^{-20} L) is very noisy and not adequate for an accurate representation of MWD. The two largest control volumes (1×10^{-19} and 1×10^{-18} L) generate very smooth MWD, but the computation time for $V = 1 \times 10^{-19}$ L is much smaller than for $V = 1 \times 10^{-20}$ L. Therefore, we selected $V = 1 \times 10^{-19}$ L as the control volume size for the subsequent simulations. Unfortunately, this “optimum” value is not general for all systems; instead, it applies only to this set of simulation conditions.

The relation between monomer conversion and time can be simulated separately from the part of the model that relates monomer conversion to polymer properties. In order to determine monomer conversion at a given polymerization time, or vice-versa, the program needs to keep track only of the number of the reactant molecules present in the system and all chain property vectors can be removed from the code. The data stored in these vectors are important to determine the polymer properties but do not affect the polymerization time. Therefore, if we just want to calculate how monomer conversion varies with polymerization time, we can use a larger control volume without having to worry about the large data storage space needed for the vectors **D**, **P**, and **R**.



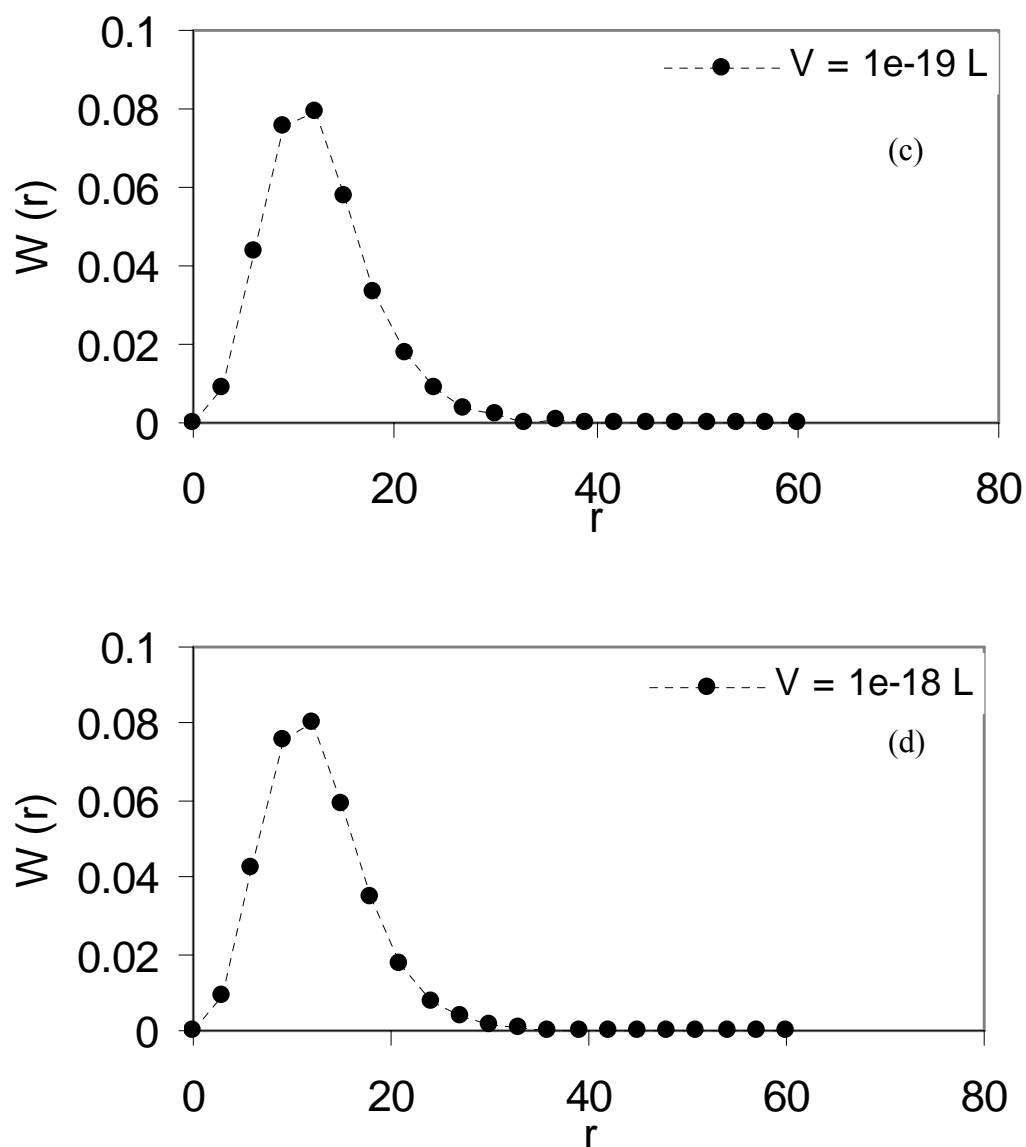


Figure 4.2 Effect of the control volume on the molecular weight distribution at $X = 0.1$: (a) $V = 1 \times 10^{-21} \text{ L}$, (b) $V = 1 \times 10^{-20} \text{ L}$, (c), $V = 1 \times 10^{-19} \text{ L}$, and (d) $V = 1 \times 10^{-18} \text{ L}$.

Figure 4.3 shows the results of conversion versus time for several control volumes. The Monte Carlo results are also compared with a solution obtained using a population balance approach ^[10] (See the appendix for the model equations). If the control volume is greater than 1×10^{-19} , good agreement is obtained between the population balance approach and the Monte Carlo simulations; for smaller volumes, some

differences between the two methods are observed because of the random fluctuations of the Monte Carlo method.

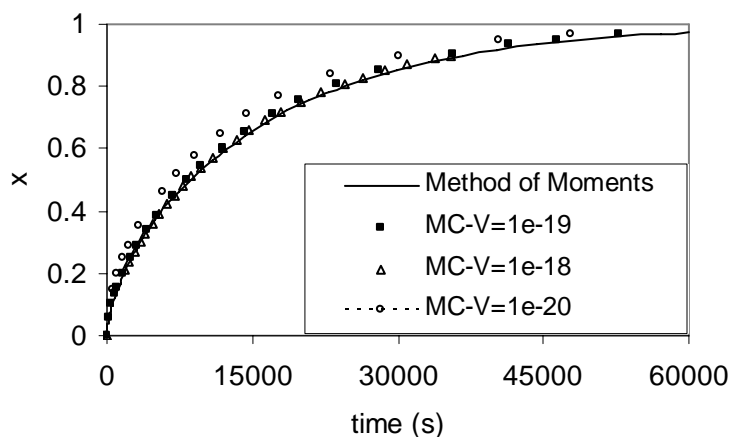
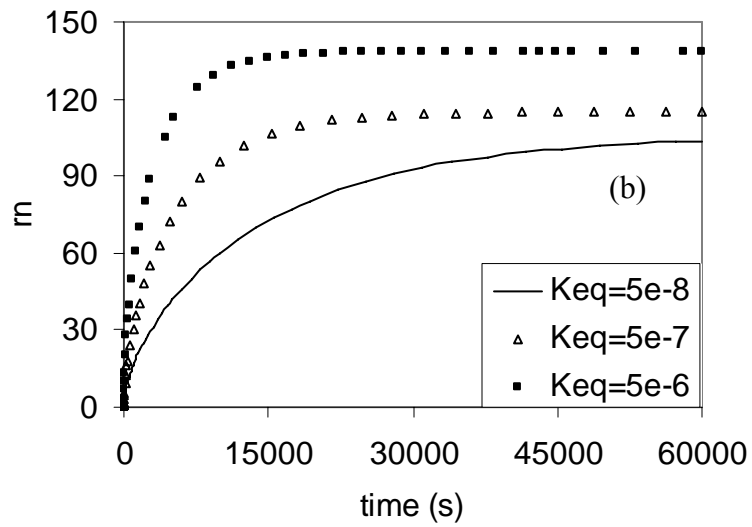
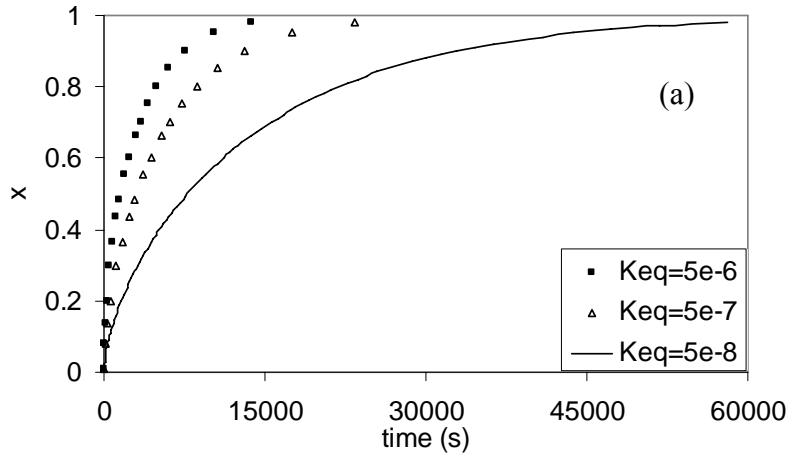


Figure 4.3 Effect of the control volume on the polymerization time (The rate constants are shown in Table 1, $[C]_0/[I]_0/[M]_0$ mole ratio: 1:1:100).

4.4.2 Effect of the equilibrium constant

The rate constants in conventional free radical polymerization are function of monomer and chain end type, and polymerization temperature. In addition to the propagation, termination and transfer reactions, ATRP also has the equilibrium reaction between dormant chains and polymer radicals. The rate constant of the equilibrium reactions depends on monomer and chain end type, polymerization temperature, catalyst type and polymerization medium. The equilibrium constant (K_{eq}) is the ratio of the activation (k_a) to the deactivation (k_d) rate constants. Figures 4.4 and 4.5 show the effect of K_{eq} on monomer conversion (x), degree of polymerization (r_n), polydispersity index (PDI) and molecular weight distribution. In these figures, k_d was changed while k_a was kept constant. By increasing k_d , the equilibrium is shifted towards higher dormant chain concentrations. Having more dormant chains in the system decreases monomer conversion and degree of polymerization (for the same time). On the other hand, a higher k_d improves the control over the chain length distribution and, hence, produces polymers

with smaller polydispersity indices and narrower molecular weight distributions, as illustrated in Figure 4.5.



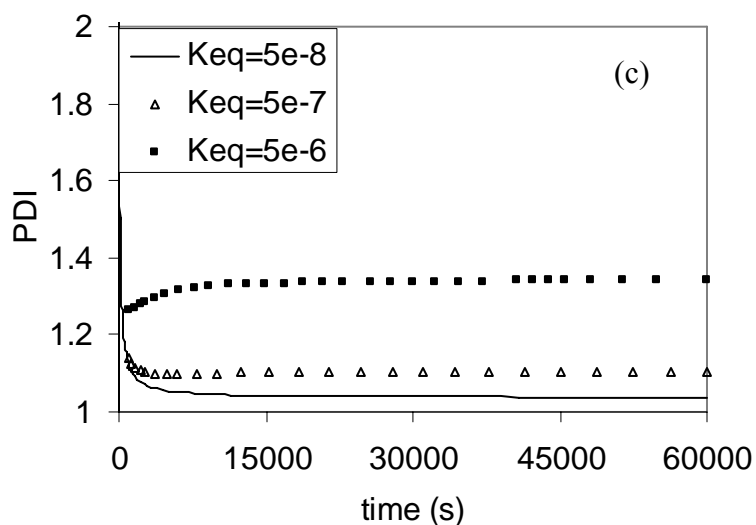


Figure 4.4 Effect of equilibrium constant (K_{eq}) on (a) monomer conversion, (b) degree of polymerization and (c) polydispersity index. ($k_p = 1516 \text{ L mol}^{-1} \text{ s}^{-1}$, $k_a = 0.5 \text{ L mol}^{-1} \text{ s}^{-1}$, $k_{tc} = 3.469 \times 10^8 \text{ L mol}^{-1} \text{ s}^{-1}$, $k_{td} = 0$, $k_{tr} = 0.22$, $V = 1 \times 10^{-19}$, $[C]_0/[I]_0/[M]_0$ mole ratio: 1:1:100).

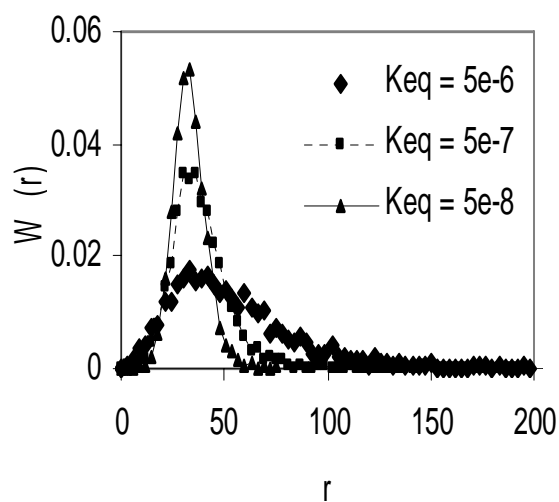


Figure 4.5 Effect of equilibrium constant (K_{eq}) on molecular weight distribution at conversion 0.3 and control volume 1×10^{-19} . ($k_p = 1516 \text{ L mol}^{-1} \text{ s}^{-1}$, $k_a = 0.5 \text{ L mol}^{-1} \text{ s}^{-1}$, $k_{tc} = 3.469 \times 10^8 \text{ L mol}^{-1} \text{ s}^{-1}$, $k_{td} = 0$, $k_{tr} = 0.22$ $[C]_0/[I]_0/[M]_0$ mole ratio: 1:1:100).

The value of the equilibrium rate constant affects the simulation time: the simulation time needed to reach a monomer conversion of 0.3 decreases from almost five hours to fifteen minutes by decreasing the deactivation rate constant from 1.1×10^7 to 1.1×10^5 , for a control volume of 1×10^{-18} . This result is expected because increasing the deactivation rate constants increases the number of dormant chains in vector **D**, and manipulating large vectors is a time consuming operation. On the other hand, when small values of the deactivation rate constant are used, many species will be present as polymer radicals (vector **R**), increasing the probability of chain termination and the size of vector **P**, while the size of vector **D** decreases. However, the size of vector **P** does not affect the computation time because once the chain is terminated it does not participate in the simulation anymore, but smaller vectors **D** are faster to simulate.

4.4.3 Simulation of the complete MWD

In the ideal case, living polymerizations make polymers with degrees of polymerization predetermined by the ratio of the concentration of monomer to initiator, polydispersity index near to one, and chain length distribution close to the Poisson distribution. A linear relation between the molecular weight average and monomer conversion is one of the features of ATRP, indicating fast initiation and negligible termination reactions. The polymer number average molecular weight is proportional to both polymerization time and the molar ratio between the monomer and the initiator. Monte Carlo simulation can predict this feature as shown in Figure 4.6. The straight line indicates that there are a constant number of polymer radicals in the reactor.

Another key feature of ATRP is the low polydispersity index. In conventional free radical polymerization, termination by combination and disproportionation leads to the production of polymer with instantaneous polydispersity indices varying from 1.5 to 2. In ATRP, however, the polydispersity index approaches one. As shown in Figure 4.7, our Monte Carlo simulation predicts this phenomenon accurately. As usual in ATRP, the polydispersity index is high at very low monomer conversion but then rapidly decreases to values below 1.1 at higher monomer conversions.

More importantly, Monte Carlo simulation can predict the complete chain length distribution (CLD) at any conversion in a relatively simple way. Other options to obtain the complete CLD as a function of time require solving the complete set (or discretized set, as done in Predici) of differential equations resulting from the population balance for all living and dead species, which is a much more involved numerical procedure. Compared to conventional free radical polymerization, ATRP produces polymers with much narrower CLDs (Figure 4.8). Also, as shown in Figure 4.9, the CLD peak position increases with monomer conversion, differently from classical free radical polymerization. All types of distributions (number, weight, and z) can be easily calculated using Monte Carlo simulation for any monomer conversion as shown in Figure 4.9.

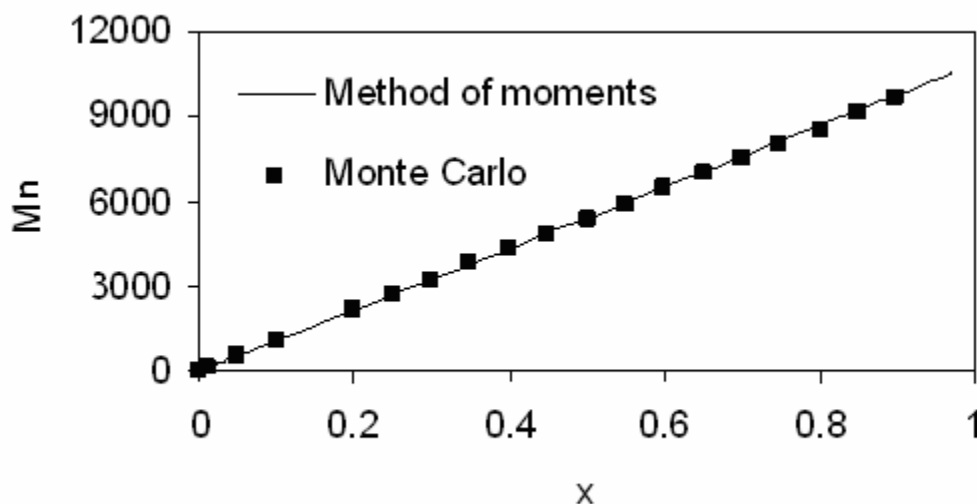


Figure 4.6 Number average molecular weight (M_n) versus monomer conversion for ATRP predicted by Monte Carlo simulation and the method of moments (The rate constants are shown in Table 1 and $[C]_0/[I]_0/[M]_0$ mole ratio: 1:1:100).

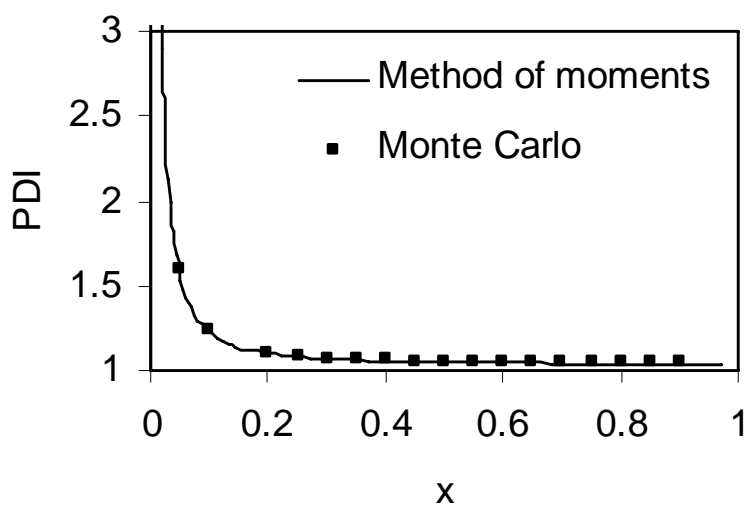


Figure 4.7 Polydispersity index vs. monomer conversion for ATRP predicted by Monte Carlo simulation and the method of moments. (The rate constants are shown in Table 1 and $[C]_0/[I]_0/[M]_0$ mole ratio: 1:1:100).

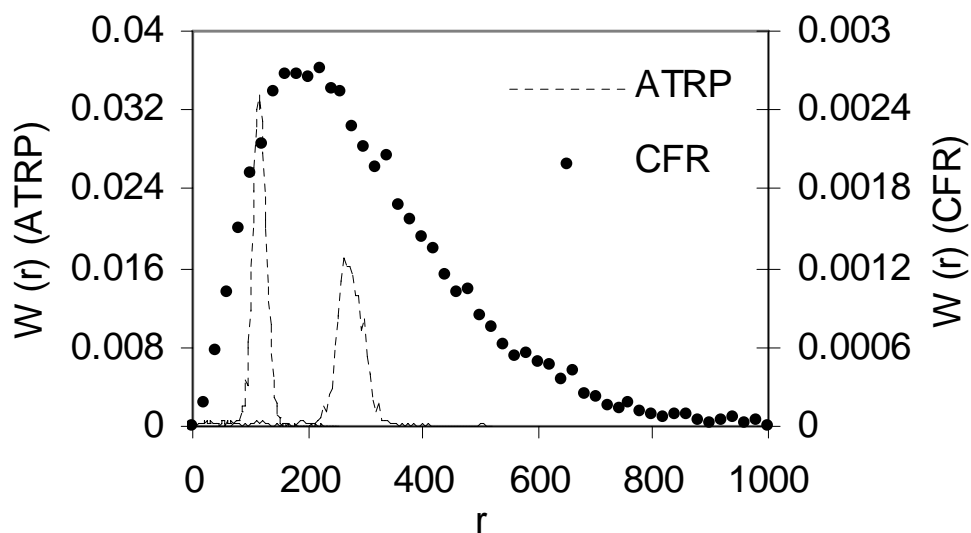
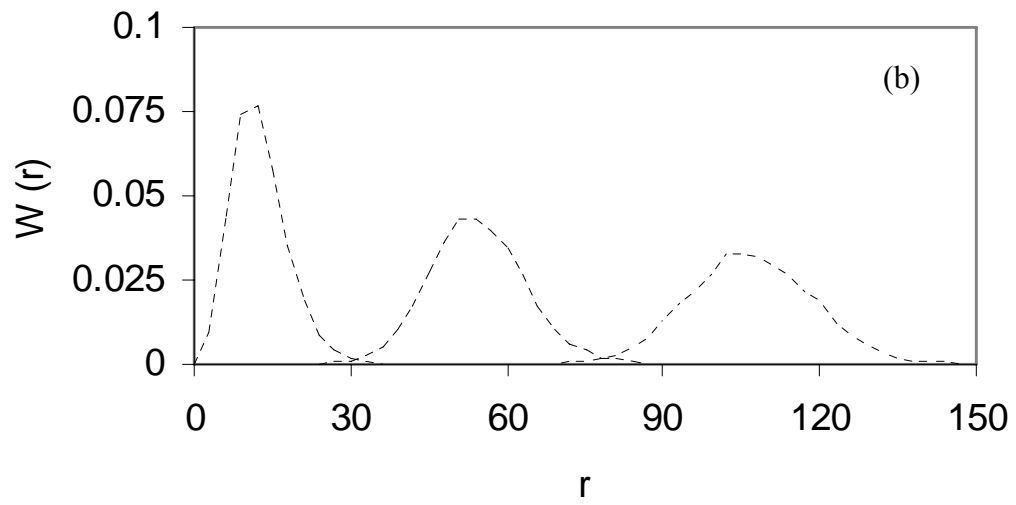
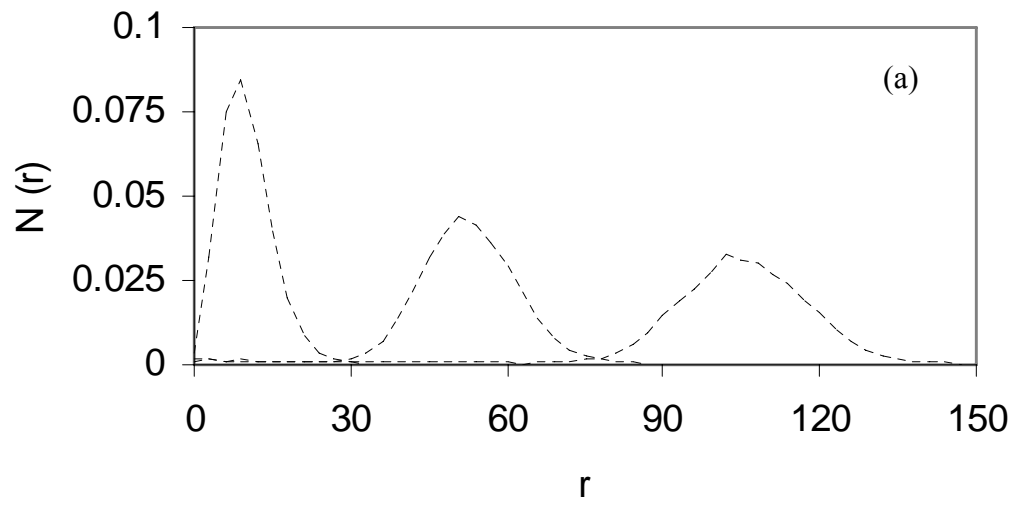


Figure 4.8 Comparison between the CLD of polystyrene made with ATRP and conventional free radical (CFR) polymerization at 50 % conversion (The kinetic rate constants are shown in Table 1). The initiator to monomer ratios are 1:100 (ATRP left peak), 1:500 (ATRP right peak), and 1:1000 (CFR).



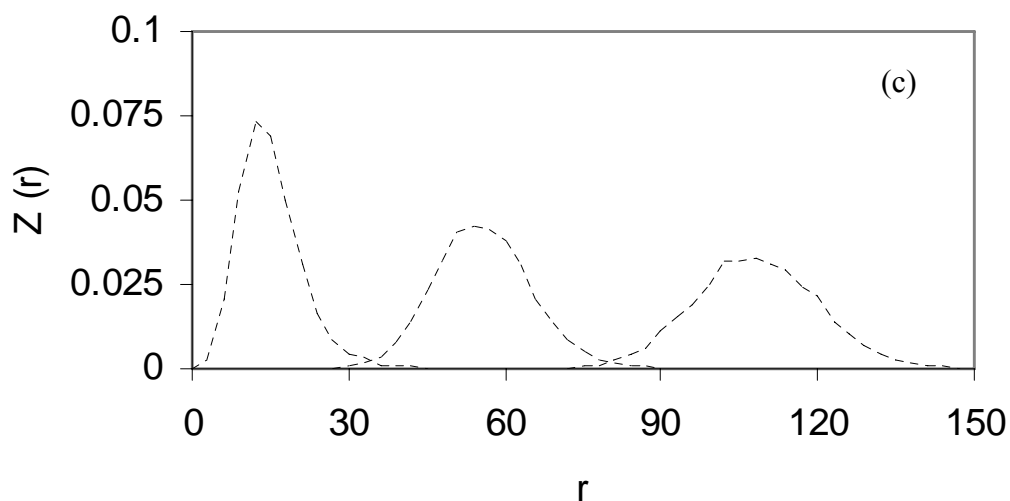


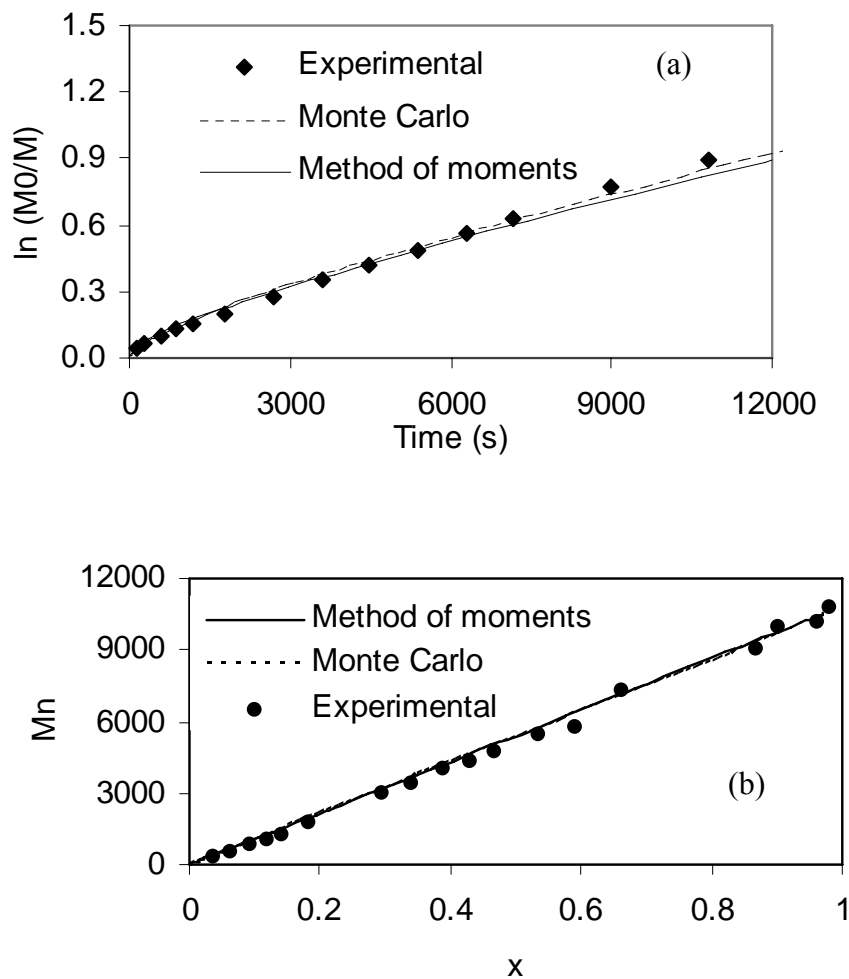
Figure 4.9 MWD of polystyrene made with ATRP: a) number distribution, b) weight distribution, and c) z distribution, at different monomer conversions. The monomer conversions, from left to right, are 10 %, 50%, and 99%.

4.4.4 Model validation

The atom-transfer radical polymerization of several monomers has been studied extensively. Styrene polymerization using copper bromide/4,4'-di(5-nonyl)-2,2'-bipyridine as the ATRP catalyst and methyl 2-bromopropionate as the initiator was chosen to validate our Monte Carlo simulation because of the availability of the kinetic data in the literature.^[30] Styrene was polymerized in batch mode with an initial concentration of 8.7 mol/L and a molar ratio of monomer, initiator and catalyst of 100:1:1. The polymerization temperature was 110 °C. The simulation was validated with the experimental data under the same conditions using the parameters shown in Table 4.1.

The Monte Carlo and experimental results were also compared with simulation results using the method of moments for completeness. Both models, using the Monte Carlo approach or the method of moments, agree very well with the experimental data. Notice that we used kinetic parameters that were available in the literature without any adjustment. Figure 4.10.a shows the rate of styrene consumption due to polymerization as

a function of time. The almost linear relationship between $\ln[M_0]/[M]$ and time indicates that there is a constant number of active sites in the system and that monomer propagation is first order with respect to the monomer concentration. The number average molecular weight increases linearly with monomer conversion (Figure 4.10.b), in excellent agreement with the experimental results. The polydispersity index decreases with monomer conversion and approaches one as indicated in Figure 4.10.c. The agreement between model predictions and the experimental data is very good, considering that no adjustable parameters were used. The slight deviation at high monomer conversion may be caused by neglecting diffusion limitations on propagation and equilibrium reactions during model development.



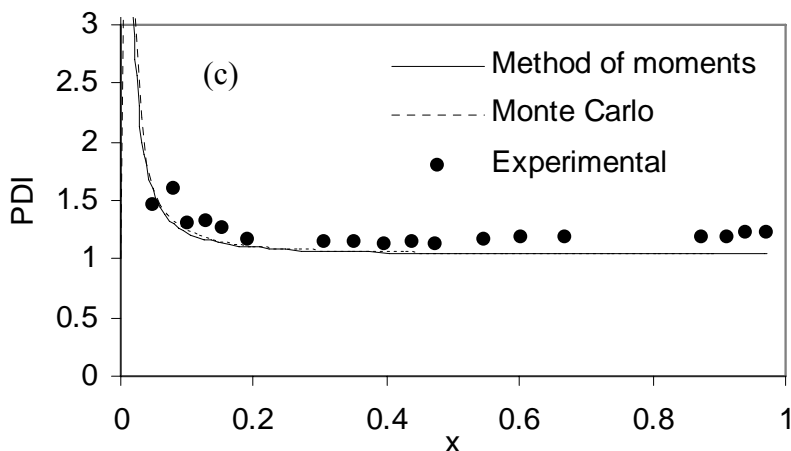


Figure 4.10 Comparison between models predictions (Monte Carlo and method of moments) and experimental data for styrene polymerization in bulk at 110 °C: (a) $\ln([M_0]/[M])$, (b) number average molecular weight, and (c) polydispersity index. (Polymerization conditions: $[M]/[I]/[Cat]=100:1:1$ (molar ratio), reaction temperature $T = 110$ °C. Kinetic parameters are shown in Table 4.1). Experimental data from Matyjaszewski et al. ^[30]

4.5 Conclusions

The Monte Carlo simulation presented in this study can describe ATRP very well and predict complete molecular weight distributions as a function of polymerization time or monomer conversion. All the main elementary reactions proposed for ATRP are included in our simulation. The effect of the control volume on the polymer properties, polymerization time and the CPU time is presented in this study. Increasing the control volume will increase computational time and improve the results slightly. We have also shown how to select an adequate control volume that gives good results (free of excessive stochastic variation) and acceptable CPU time.

The simulation was used to predict the effect of the equilibrium constant ($K_{eq} = k_a/k_d$) on monomer conversion and polymer properties. The narrow molecular weight distributions and smaller polydispersity index obtained with high equilibrium constants come at the expense of lower conversions and molecular weight averages. Longer polymerization and computational times are required to reach high conversions and

molecular weight averages as the value of the equilibrium constant decreases (by increasing the deactivation rate constant).

The Monte Carlo simulation can predict all the features of ATRP, including the linear increase of the molecular weight with conversion and the production of polymers with narrow MWD. The Monte Carlo simulation was compared with the method of moments and found to be more versatile than the latter because it can predict the complete MWD of the polymer, despite its higher computation time. We have also shown that the Monte Carlo predictions agree well with the experimental values for monomer conversion, average molecular weight and polydispersity for the atom-transfer radical polymerization of styrene.

4.6 References

- [1] J. Chiefary, YK. Chong, F. Ercole, C. Moad , G. Moad, E. Rizzardo, SH. Thang, *Macromolecules* **1998**, 31, 5559.
- [2] G. Moad, J. Chiefary, YK. Chong, J. Krstina, RTA. Mayadunne, A. Postma, E. Rizzardo, SH. Thang,. *Polym Int* **2000**, 49, 993.
- [3] MK. Georges, RPN. Veregin, PM. Kazmaier, GK. Hamer, *Macromolecules* **1993**, 26, 2987.
- [4] D. Benoit, V. Chaplinski, R. Braslau, CJ. Hawker, *J Am Chem Soc* **1999**, 121, 3904.
- [5] M. Rodlert, E. Harth, I. Rees, CJ. Hawker, *J Polym Sci, Polym Chem Ed* **2000**, 38, 4749.
- [6] K. Matyjaszewski, J. Xia, *Chem Rev* **2001**,101, 2921.
- [7] M. Kamigaito, T. Ando, M. Sawamoto, *Chem Rev* **2001**, 101, 3689.
- [8] S. Zhu, *J. Polym. Sci. Part B: Polym. Phys.* **1999**, 37, 2692.
- [9] J. Bonilla, E. Saldivar, A. Flores-Tlacuahuac, E. Vivaldo-Lima, R. Pfaendner, F. Tiscareno-Lechuga, *Polymer Reaction Engineering*, **2002**, 10, 4, 227.
- [10] S. Zhu, *Macromol. Theory Simul.* **1999**, 8, 29.
- [11] O. Delgadillo-Velazquez, E. Vivaldo-Lima, I. Quintero-Ortega, S. Zhu, *AIChE Journal*, **2002**, 48,11, 2597.
- [12] M. Al-Harhi, J. Soares, L. Simon, *Macromol. Theory Simul*, **2006**, 15, 198.
- [13] M. Al-Harhi, J. Soares, L. Simon, *Macromol. Chem. Phys.*, **2006**, 207,469.
- [14] A. Wang, S. Zhu, *J. Polym. Sci. Part A: Polym. Chem.* **2003**, 41, 1553.
- [15] M. Zhang, H. Ray, *Journal of applied polymer science* **2002**, 86, 1630.
- [16] M. Zhang, H. Ray, *Journal of applied polymer science* **2002**, 86, 1047.
- [17] M. Zhang, H. Ray, *Ind. Eng. Chem. Res.* **2001**, 40, 4336.
- [18] D. Greszta, K. Matyjaszewski, *Macromolecules* **1996**, 29, 7661.
- [19] A. Shipp, K. Matyjaszewski, *Macromolecules* **1999**, 32, 2948.
- [20] A. Shipp, K. Matyjaszewski, *Macromolecules* **2000**, 33, 1553.
- [21] J. Lutz, K. Matyjaszewski, *Macromol. Chem. Phys.* **2002**, 203, 1385.
- [22] C. Barner-Kowollik, J.F. Quinn, D. R. Morsley, T.P. Davis, *J. Polym. Sci., Polym. Chem. Ed.* **2001**, 39, 1353.
- [23] H. Tobita, *Macromol. Theory Simul.* **2003**, 12, 32.
- [24] J. He, H. Zhang, Y. Yang, *Macromol. Theory Simul.* **1993**, 2, 747.
- [25] J. He, L. Li, Y. Yang, *Macromol. Theory Simul.* **2000**, 9, 463.
- [26] J. He, H. Zhang, J. Chen, Y, Yang, *Macromolecules* **1997**, 30, 8010.

- [27] H. Tobita, *Macromol. Theory Simul.* **2006**, 15, 23.
- [28] L. Li, J. He, Y. Yang, *Chem. J. Chin. Univ.* **2000**, 21, 1146.
- [29] D. Gillespie, *J. Phys. Chem.* **1979**, 81, 2340.
- [30] J. Luitz, k. Matyjaszewski, *J. Polym. Sci. Part A: Polym. Chem.* **2005**, 43, 897.
- [31] M. Buback, R. Gilbert, R. Hutchinson, B. Klumperman, F. Kuchata, B. Manders, K. O'Driscoll, G. Russell, J. Schweer, *Macromol. Chem. Phys.* **1995**, 196, 3267.
- [32] A. Hui, E. Hamielec, *J. Appl. Polym. Sci.* **1976**, 16, 749.
- [33] K. Ohno, A. Goto, T. Fukuda, J. Xia, K. Matyjaszewski, *Macromolecules* **1998**, 31, 2699.
- [34] D. Peclak, A. Butte, G. Storti, M. Morbidelli, *J. Polym. Sci. Part A: Polym. Chem.* **2006**, 44, 1071.

4.7 Appendix

Population balances

The molar population balances for ATRP in a batch reactor are given by the following equations:

Dormant chains :

$$\frac{d[D_r]}{dt} = -k_d[D_r][C] + k_d[R_r \bullet][CX] \quad (A1)$$

Polymer radicals :

$$\begin{aligned} \frac{d[R_r \bullet]}{dt} = & k_p[R_{r-1} \bullet]M - k_p[R_r \bullet]M \\ & - k_{tr}[R_r \bullet]M - k_t[\lambda_{R,0}][R_r \bullet] \\ & + k_d[\lambda_{D,r}][C] - k_d[R_r \bullet][CX] \end{aligned} \quad (A2)$$

Dead polymer from transfer and disproportionation reactions:

$$\frac{d[P_r]}{dt} = k_{tr}[R_r \bullet]M + k_{td}[R_r \bullet][\lambda_{R,0}] \quad (A3)$$

Dead polymer from combination reactions:

$$\frac{d[PP_r]}{dt} = \frac{k_{tc}}{2} \sum_{i=1}^{r-1} [R_i \bullet][R_{r-i} \bullet]$$

Assuming the long chain approximation (monomer is consumed mainly by propagation reactions), the monomer concentration varies as a function of the residence time in the batch reactor according to the following equation:

$$\frac{dM}{dt} = -k_p M [\lambda_{R,0}] \quad (A4)$$

The non-polymeric species in the system are described with the following equations:

$$[C] = [C]_0 - [CX] \quad (A5)$$

$$[CX] = [I]_0 - [\lambda_{D,0}] \quad (A6)$$

Method of moments

Number (r_n) and the weight (r_w) average chain lengths are calculated using the method of moments. The j^{th} moments of the chain length distributions for the several polymer species present in the reactor are given by the equations:

$$[\lambda_{D,j}] = \sum_{r=1}^{\infty} r^j [D_r] \quad (\text{A7})$$

$$[\lambda_{R,j}] = \sum_{r=1}^{\infty} r^j [R_r] \quad (\text{A8})$$

$$[\lambda_{P,j}] = \sum_{r=1}^{\infty} r^j [P_r] \quad (\text{A9})$$

$$[\lambda_{PP,j}] = \sum_{r=1}^{\infty} r^j [PP_r] \quad (\text{A10})$$

The zeroth moment of the dormant species (D) is given by :

$$[\lambda_{D,0}] = \sum_{r=1}^{\infty} [D_r] = D_1 + \sum_{r=2}^{\infty} D_r \quad (\text{A11})$$

Therefore

$$\frac{d[\lambda_{D,0}]}{dt} = \frac{d[D_1]}{dt} + \sum_{r=2}^{\infty} \frac{d[D_r]}{dt} \quad (\text{A12})$$

The population balances equation (equation A1) was substituted in the above equations.

After some simplifications the equation for the zeroth moment of the distribution of chain length for the dormant species was obtained:

$$\frac{d[\lambda_{D,0}]}{dt} = -k_a [\lambda_{D,0}] [C] + k_d [\lambda_{R,0}] [CX] \quad (\text{A13})$$

Similarly, the first moment of dormant species is given by,

$$[\lambda_{D,1}] = \sum_{r=1}^{\infty} r [D_r] = D_1 + \sum_{r=2}^{\infty} r D_r \quad (\text{A14})$$

and:

$$\frac{d[\lambda_{D,1}]}{dt} = \frac{d[D_1]}{dt} + \sum_{r=2}^{\infty} r \frac{d[D_r]}{dt} \quad (\text{A15})$$

Substituting the population balances, and simplifying the resulting expression, we obtain:

$$\frac{d[\lambda_{D,1}]}{dt} = -k_a [\lambda_{D,1}] [C] + k_d [\lambda_{R,1}] [CX] \quad (\text{A16})$$

The second moment of dormant species is given by,

$$[\lambda_{D,2}] = \sum_{r=1}^{\infty} r^2 [D_r] = D_1 + \sum_{r=2}^{\infty} r^2 D_r \quad (\text{A17})$$

and:

$$\frac{d[\lambda_{D,2}]}{dt} = \frac{d[D_1]}{dt} + \sum_{r=2}^{\infty} r^2 \frac{d[D_r]}{dt} \quad (\text{A18})$$

Substituting the population balances and simplifying the resulting expression, we obtain:

$$\frac{d[\lambda_{D,2}]}{dt} = -k_a[\lambda_{D,2}][C] + k_d[\lambda_{D,2}][CX] \quad (\text{A19})$$

Similarly, the method of moments was applied to the other species and we obtain the following equations:

Polymer Radicals:

Zeroth moments

$$\frac{d[\lambda_{R,0}]}{dt} = k_a[\lambda_{D,0}][C] - k_d[\lambda_{R,0}][CX] - k_t[\lambda_{R,0}][\lambda_{R,0}] - k_{tr}[M][\lambda_{R,0}] \quad (\text{A20})$$

First moments

$$\begin{aligned} \frac{d[\lambda_{R,1}]}{dt} = & k_p[\lambda_{R,0}][M] + k_a[\lambda_{D,1}][C] - k_d[\lambda_{R,1}][CX] \\ & - k_t[\lambda_{R,1}][\lambda_{R,0}] - k_{tr}[M][\lambda_{R,1}] \end{aligned} \quad (\text{A21})$$

Second moments

$$\begin{aligned} \frac{d[\lambda_{R,2}]}{dt} = & k_p[\lambda_{R,0}][M] + 2k_p[\lambda_{R,1}][M] + k_a[\lambda_{D,2}][C] - k_d[\lambda_{R,2}][CX] \\ & - k_t[\lambda_{R,0}][\lambda_{R,2}] - k_{tr}[M][\lambda_{R,2}] \end{aligned} \quad (\text{A22})$$

Dead Polymers:

Zeroth moments

Dead polymers via combination

$$\frac{d[\lambda_{PP,0}]}{dt} = \frac{k_{tc}}{2} [\lambda_{R,0}][\lambda_{R,0}] \quad (\text{A23})$$

Dead polymers via disproportionation

$$\frac{d[\lambda_{P,0}]}{dt} = k_{td}[\lambda_{R,0}][\lambda_{R,0}] + k_{tr}[M][\lambda_{R,0}] \quad (\text{A24})$$

First moments

Dead polymers via combination

$$\frac{d[\lambda_{PP,1}]}{dt} = k_{tc}[\lambda_{R,1}][\lambda_{R,0}] \quad (\text{A25})$$

Dead polymers via disproportionation

$$\frac{d[\lambda_{P,1}]}{dt} = k_{td}[\lambda_{R,0}][\lambda_{R,1}] + k_{tr}[M][\lambda_{R,1}] \quad (\text{A26})$$

Second moments

Dead polymers via combination

$$\frac{d[\lambda_{PP,2}]}{dt} = k_{tc}[\lambda_{R,0}][\lambda_{R,2}] + k_{tc}[\lambda_{R,1}][\lambda_{R,1}] \quad (\text{A27})$$

Dead polymers via disproportionation

$$\frac{d[\lambda_{P,2}]}{dt} = k_{td}[\lambda_{R,0}][\lambda_{R,2}] + k_{tr}[M][\lambda_{R,2}] \quad (\text{A28})$$

The polydispersity index is given by

$$PDI = \frac{r_w}{r_n} \quad (\text{A29})$$

where r_n is the number average chain length, given by

$$r_n = \frac{[\lambda_{R,1}] + [\lambda_{D,1}] + [\lambda_{P,1}] + [\lambda_{PP,1}]}{[\lambda_{R,0}] + [\lambda_{D,0}] + [\lambda_{P,0}] + [\lambda_{PP,0}]} \quad (\text{A30})$$

and r_w is the weight average chain length, given by

$$r_w = \frac{[\lambda_{R,2}] + [\lambda_{D,2}] + [\lambda_{P,2}] + [\lambda_{PP,2}]}{[\lambda_{R,1}] + [\lambda_{D,1}] + [\lambda_{P,1}] + [\lambda_{PP,1}]} \quad (\text{A31})$$

Chapter 5

5 Mathematical Modeling of Atom-Transfer Radical Polymerization Using Bifunctional Initiators*

5.1 Abstract

Bifunctional initiators can produce polymers with higher molecular weight and smaller polydispersity index than monofunctional initiators. In this study, we developed a mathematical model for atom-transfer radical polymerization (ATRP) with bifunctional initiators. The most important reactions in ATRP were included in the model. The method of moments was used to predict monomer conversion, average molecular weights and polydispersity index as a function of polymerization time in batch reactors. The model was used to understand the mechanism of ATRP and to quantify how polymerization conditions affect monomer conversion and polymer properties by examining the effect of several rate constants (activation, deactivation, propagation and chain termination) and of catalyst and initiator concentration on polymerization kinetics and polymer properties. When compared to monofunctional initiators, bifunctional initiators not only produce polymers with higher molecular weight averages at higher polymerization rates, but also control their molecular weight distributions more effectively.

5.2 Introduction

The design of macromolecules with defined topology, composition and functionality is an attractive field in polymer science and engineering because polymers with designed macromolecular structures can lead to products with improved or new properties. Of all polymerization techniques, living polymerization offers the best control over polymer microstructure. During living polymerization, polymer chains grow without

* This chapter has been published: M. Al-Harhi, J. Soares, L. Simon, *Macromol. Theory Simul.* **2006** *15*, 198-214.

permanent chain termination or transfer reactions. Polymers with narrow molecular weight distributions (MWD) are produced without termination reactions provided that the rate of initiation is fast and all the chains start growing at approximately the same time.

Living anionic and cationic polymerizations control polymer microstructure well but are very sensitive to impurities present in the reaction medium. On the other hand, living free-radical polymerization (LFRP) is less affected by impurities. The most efficient types of LFRP are reversible addition-fragmentation chain transfer (RAFT),^[1,2] nitroxide-mediated polymerization (NMP)^[3-5] and atom-transfer radical polymerization (ATRP).^[6,7] Among them, ATRP is considered by some researchers the most attractive technique.^[8]

There have been several mathematical models published in the literature for living free-radical polymerization systems. Some models are general for any living free-radical polymerizations and some are specific for a particular process. Zhu et al. developed mathematical models for NMP^[9], ATRP^[10,11] and RAFT^[12] in batch reactors using the method of moments. Zhang and Ray developed a mathematical model for living free-radical polymerization in batch, semi-batch, continuous stirred-tank and plug-flow reactors.^[13,14] They applied their model to both NMP and ATRP. Fischer investigated persistent radical effects in various types of LFRP.^[15,16] Shipp and Matyjaszewski modeled the ATRP of styrene using an empirical expression for diffusion-controlled termination.^[17] Lutz and Matyjaszewski modeled the production of polymers with chain-end functionality by ATRP.^[18]

It is not possible to increase simultaneously the rate of polymerization and the polymer molecular weight with monofunctional initiators because an increase in radical concentration (thus increasing polymerization rate) inevitably leads to an increase in chain termination rates and a reduction in polymer molecular weight. Bifunctional initiators are a very interesting alternative to monofunctional initiators because the presence of two radicals per polymer chain leads to higher polymerization rates and molecular weights.^[19] Moreover, when bifunctional initiators are used in living free-radical polymerizations, ABA triblock copolymers can be synthesized:^[20-22] first, monomer type B is polymerized to produce chains with functional end groups called

bifunctional macro-initiators; then, the macro-initiators are used to polymerize monomer type A to form ABA triblock copolymers.

In ATRP, bifunctional initiators are those initiators that contain two labile groups (two halide atoms). In general there are two types of bifunctional initiators: initiators that have two identical labile groups are called symmetrical initiators; unsymmetrical bifunctional initiators have two different labile groups.

Several bifunctional initiators were used to polymerize many common monomers using ATRP.^[23-27] However, to our knowledge, the mathematical models published in the literature are applicable only to monofunctional initiators. For the most efficient use of bifunctional initiators in ATRP, it is essential to have a kinetic model that can provide a greater insight into the polymerization process, such as the one developed in this investigation.

5.3 Model development

5.3.1 Reaction mechanism

ATRP is based on the equilibrium between polymer radicals (active species) and dormant chains (non-active species). The monomer propagation step is similar to that in conventional free-radical polymerization. Termination reactions may also occur in ATRP and they follow the same mechanism as in conventional free-radical polymerization. The unique step in ATRP involves the dynamic equilibrium between active and dormant polymer chains. A low oxidation-state metal halide – CuBr, for example – complexed with ligands undergoes one-electron oxidation and abstracts a halogen atom from the dormant chain end – producing CuBr₂, for example – to generate a polymer radical. The radical activation and metal oxidation reactions are reversible. The abstracted halogen atom can easily go back to cap a polymer radical. This dynamic equilibrium is responsible for the control of the polymerization. This general feature of ATRP is common for mono-, bi-, and multifunctional initiators. The proposed elementary reactions for bifunctional initiators, that form the basis of our model, are listed in Equations (1) to (21).

Activation



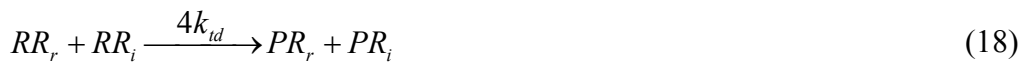
Deactivation



Propagation



Termination



In Equations (1) to (21), C is the catalyst in its lower oxidation state, CX is the catalyst in its higher oxidation state, M is the monomer, DD is a chain with two dormant ends, DR is a chain with a dormant end and a free-radical end, RR is a chain with two free-radical

ends, PP is a chain with two dead ends, PD is a chain with a dormant end and a dead end, PR is a chain with a free-radical end and a dead end and r is the chain length.

5.3.2 Population balances

The molar balances for the ATRP mechanism with bifunctional initiators in batch reactors are given by Equations (22) to (28):

$$\begin{aligned} \frac{d[DD_r]}{dt} = & -2k_a[DD_r][C] + k_d[DR_r][CX] \\ & + \frac{k_t}{2} \sum_{i=1}^{r-1} [DR_{r-i}][DR_i] \end{aligned} \quad (22)$$

$$\begin{aligned} \frac{d[DR_r]}{dt} = & 2k_a[DD_r][C] - k_a[DR_r][C] + 2k_d[RR_r][CX] - k_d[DR_r][CX] + k_p[M](DR_{r-1} - DR_r) \\ & - k_{tc}[DR_r] \sum_{i=1}^{\infty} [DR_r] - 2k_{tc}[DR_r] \sum_{i=1}^{\infty} [RR_r] + 2k_{tc} \sum_{i=1}^{r-1} [DR_{r-i}][RR_i] - k_{tc}[DR_r] \sum_{i=1}^{\infty} [PR_r] \\ & - k_{td}[DR_r] \sum_{i=1}^{\infty} [DR_r] - 2k_{td}[DR_r] \sum_{i=1}^{\infty} [RR_r] - k_{td}[DR_r] \sum_{i=1}^{\infty} [PR_r] \end{aligned} \quad (23)$$

$$\begin{aligned} \frac{d[RR_r]}{dt} = & k_a[DR_r][C] - 2k_d[RR_r][CX] + 2k_p[M](RR_{r-1} - [RR_r]) \\ & - 2k_{tc}[RR_r] \sum_{i=1}^{\infty} [DR_r] - 4k_{tc}[RR_r] \sum_{i=1}^{\infty} [RR_r] + 2k_{tc} \sum_{i=1}^{r-1} [RR_{r-i}][RR_i] - 2k_{tc}[RR_r] \sum_{i=1}^{\infty} [PR_r] \\ & - 2k_{td}[RR_r] \sum_{i=1}^{\infty} [DR_r] - 4k_{td}[RR_r] \sum_{i=1}^{\infty} [RR_r] - 2k_{td}[RR_r] \sum_{i=1}^{\infty} [PR_r] \end{aligned} \quad (24)$$

$$\begin{aligned} \frac{d[PR_r]}{dt} = & k_a[PD_r][C] - k_d[PR_r][CX] + k_p[M](PR_{r-1} - [PR_r]) \\ & - k_{tc}[PR_r] \sum_{i=1}^{\infty} [PR_r] - 2k_{tc}[PR_r] \sum_{i=1}^{\infty} [RR_r] + 2k_{tc} \sum_{i=1}^{r-1} [PR_{r-i}][RR_i] - k_{tc}[PR_r] \sum_{i=1}^{\infty} [DR_r] \\ & + 2k_{td}[DR_r] \sum_{i=1}^{\infty} [RR_r] + 4k_{td}[RR_r] \sum_{i=1}^{\infty} [RR_r] - k_{td}[PR_r] \sum_{i=1}^{\infty} [PR_r] \\ & + -2k_{td}[PR_r] \sum_{i=1}^{\infty} [RR_r] + 2k_{td}[PR_r][RR_r] - k_{td}[PR_r] \sum_{i=1}^{\infty} [DR_r] \end{aligned} \quad (25)$$

$$\begin{aligned} \frac{d[PD_r]}{dt} = & -k_a[PD_r][C] + k_d[PR_r][CX] \\ & + k_{tc} \sum_{i=1}^{r-1} [PR_{r-i}][DR_i] \\ & + k_{td}[DR_r] \sum_{i=1}^{\infty} [DR_r] + 2k_{td}[DR_r] \sum_{i=1}^{\infty} [RR_r] + k_{td}[DR_r] \sum_{i=1}^{\infty} [PR_r] \end{aligned} \quad (26)$$

$$\begin{aligned} \frac{d[PP_r]}{dt} = & \frac{k_{tc}}{2} \sum_{i=1}^{r-1} [PR_{r-i}][PR_i] + k_{td}[PR_r] \sum_{i=1}^{\infty} [PR_r] \\ & + 2k_{td}[PR_r] \sum_{i=1}^{\infty} [RR_r] + k_{td}[PR_r] \sum_{i=1}^{\infty} [DR_r] \end{aligned} \quad (27)$$

The long chain approximation (monomer is consumed mainly by propagation reactions) is assumed for monomer consumption. Thus, the monomer concentration varies as a function of the residence time in the batch reactor according to the following equation:

$$\frac{d[M]}{dt} = -k_p[M] \left(\sum_{r=1}^{\infty} [DR_r] + 2 \sum_{r=1}^{\infty} [RR_r] + \sum_{r=1}^{\infty} [PR_r] \right) \quad (28)$$

The concentrations of non-polymeric species in the system are described with the expressions:

$$[C] = [C]_0 - [CX] \quad (29)$$

$$[CX] = 2[I]_0 - 2\lambda_{DD,0} - \lambda_{DR,0} \quad (30)$$

The zeroth moments of living polymer, $\lambda_{DD,0}$ and $\lambda_{DR,0}$, will be defined later in Equations (31) and (32).

5.3.3 Kinetics parameters

Kinetics parameters in free-radical polymerization depend on monomer type and polymerization temperature. They may also depend on monomer conversion especially at high conversions when diffusion effects may limit the rate of several elementary reactions. In this study, the values of these parameters are varied over the range commonly used for most monomers^[28] (see Table 5.1). However, all polymerization kinetic constants were kept constant during the simulations, that is, we neglected diffusion effects in all our simulations.

Table 5.1 Kinetic rate constants used in the simulations

Parameters	Range of numerical values
k_p (L mol ⁻¹ s ⁻¹)	10 ² -10 ³
k_{tc} (L mol ⁻¹ s ⁻¹)	10 ⁶ -10 ⁸
k_{td} (L mol ⁻¹ s ⁻¹)	10 ⁶ -10 ⁸
k_a (L mol ⁻¹ s ⁻¹)	0.01
k_d (L mol ⁻¹ s ⁻¹)	10 ⁶ -10 ⁸

5.3.4 Method of moments

The number (r_n) and the weight (r_w) average chain lengths are calculated using the method of moments. The j^{th} moments of the chain length distributions for the several polymer species present in the reactor are given by the equations:

$$[\lambda_{DD,j}] = \sum_{r=1}^{\infty} r^j [DD_r] \quad (31)$$

$$[\lambda_{DR,j}] = \sum_{r=1}^{\infty} r^j [DR_r] \quad (32)$$

$$[\lambda_{RR,j}] = \sum_{r=1}^{\infty} r^j [RR_r] \quad (33)$$

$$[\lambda_{PR,j}] = \sum_{r=1}^{\infty} r^j [PR_r] \quad (34)$$

$$[\lambda_{PD,j}] = \sum_{r=1}^{\infty} r^j [PD_r] \quad (35)$$

$$[\lambda_{PP,j}] = \sum_{r=1}^{\infty} r^j [PP_r] \quad (36)$$

The moment equations are obtained by combining the moment definitions given in Equations (31) to (36) with the molar balance shown in Equations (22) to (27). The final moment equations are summarized in the Appendix. The resulting set of ordinary differential equations was solved using MATLAB version 7. Since these ordinary differential equations are stiff, the ode15s solver, based on Gear's method,^[29] was used.

Average chain lengths

Number and weight average chain lengths and polydispersity index are calculated dynamically using the ratio of the moments at a given polymerization time:

$$r_n = \frac{[\lambda_{DD,1}] + [\lambda_{RR,1}] + [\lambda_{DR,1}] + [\lambda_{PD,1}] + [\lambda_{PR,1}] + [\lambda_{PP,1}]}{[\lambda_{DD,0}] + [\lambda_{RR,0}] + [\lambda_{DR,0}] + [\lambda_{PD,0}] + [\lambda_{PR,0}] + [\lambda_{PP,0}]} \quad (37)$$

$$r_w = \frac{[\lambda_{DD,2}] + [\lambda_{RR,2}] + [\lambda_{DR,2}] + [\lambda_{PD,2}] + [\lambda_{PR,2}] + [\lambda_{PP,2}]}{[\lambda_{DD,1}] + [\lambda_{RR,1}] + [\lambda_{DR,1}] + [\lambda_{PD,1}] + [\lambda_{PR,1}] + [\lambda_{PP,1}]} \quad (38)$$

$$PDI = \frac{r_w}{r_n} \quad (39)$$

where r_n , r_w , and PDI are the number average chain length, the weight average chain length, and polydispersity index, respectively. Number and weight average molecular weights can be calculated by multiplying their respective average chain lengths by the molecular weight of the repeating unit.

5.4 Results and discussion

5.4.1 Comparison between monofunctional and bifunctional initiators

In bulk and solution free-radical polymerization processes with monofunctional initiators, it is impossible to increase the polymerization rate and molecular weight simultaneously. Bifunctional initiators can be used to overcome this limitation since they allow higher polymerization rates without lowering the molecular weights of the final product. In addition, the molecular weight distribution is narrower if bifunctional initiators are used.^[19] The same behavior was reported experimentally in the literature for monofunctional and multifunctional initiators in ATRP.^[30]

In our first set of simulations, we compared the microstructures of polymers produced with bifunctional initiators with those made with monofunctional initiators under the same conditions. The model for ATRP using monofunctional initiators is based on models available in the literature.^[10,11] In living polymerization, monomer conversion and polymer chain length averages increase as a function of time using both monofunctional and bifunctional initiators. However, when bifunctional initiators are used,

higher monomer conversions are achieved and polymers with higher molecular weights are produced for the same polymerization time because of the dual functionality of bifunctional initiators, as illustrated in Figures 5.1 and 5.2. In addition, the polydispersity index of polymers made with bifunctional initiators is smaller than of those made with monofunctional initiators (Figure 5.3). The effect on polydispersity index depicted in Figure 5.3 is interesting because it shows that the presence of two terminal free radicals per chain leads to a more uniform chain growth and therefore favors a tighter control of the molecular structure of these polymers.

To help the reader compare the behavior of mono- and bifunctional initiators in the next simulations, we added a comparative result for polymerization with a monofunctional initiator to all of the following figures in this study (Figures 5.4 to 5.18).

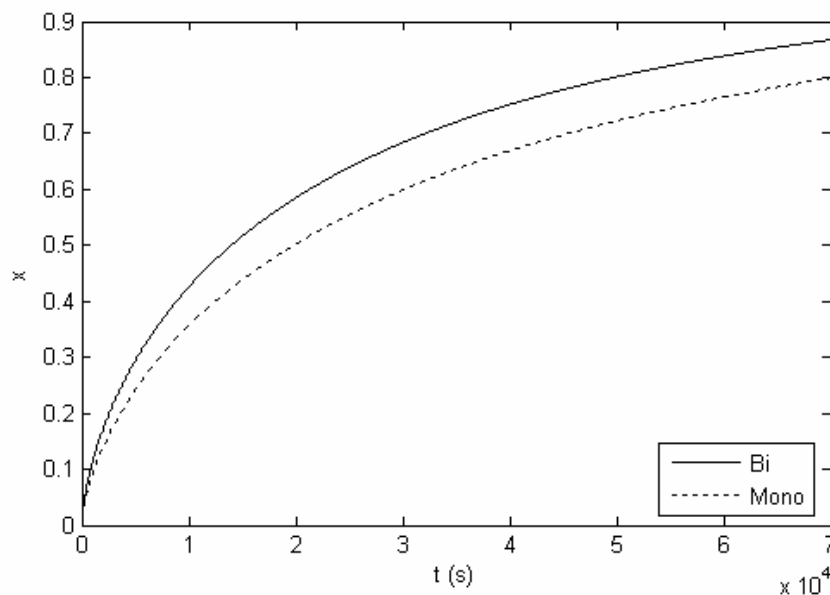


Figure 5.1 Effect of mono and bifunctional initiators on monomer conversion (x) as a function of time (t). ($k_p=1000 \text{ L mol}^{-1} \text{ s}^{-1}$, $k_{tc}=1 \times 10^7 \text{ L mol}^{-1} \text{ s}^{-1}$, $k_{td}=0$, $k_d=1 \times 10^7 \text{ L mol}^{-1} \text{ s}^{-1}$, $k_a=0.01 \text{ L mol}^{-1} \text{ s}^{-1}$, $[C]_0/[I]_0/[M]_0$ mole ratio: 1:1:100).

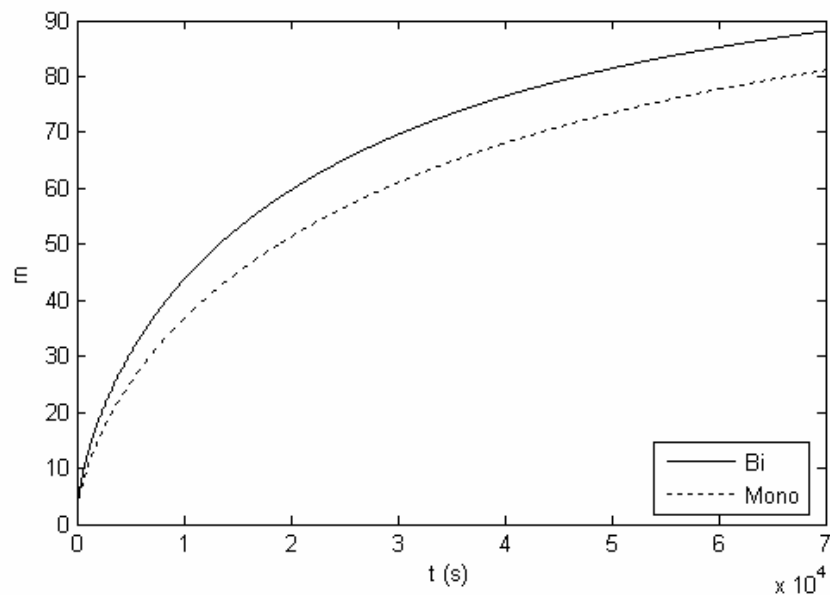


Figure 5.2 Effect of mono and bifunctional initiators on number average chain length (\bar{n}) as a function of time (t) ($k_p=1000 \text{ L mol}^{-1} \text{ s}^{-1}$, $k_{tc}=1 \times 10^7 \text{ L mol}^{-1} \text{ s}^{-1}$, $k_{td}=0$, $k_d=1 \times 10^7 \text{ L mol}^{-1} \text{ s}^{-1}$, $k_a=0.01 \text{ L mol}^{-1} \text{ s}^{-1}$, $[C]_0/[I]_0/[M]_0$ mole ratio: 1:1:100).

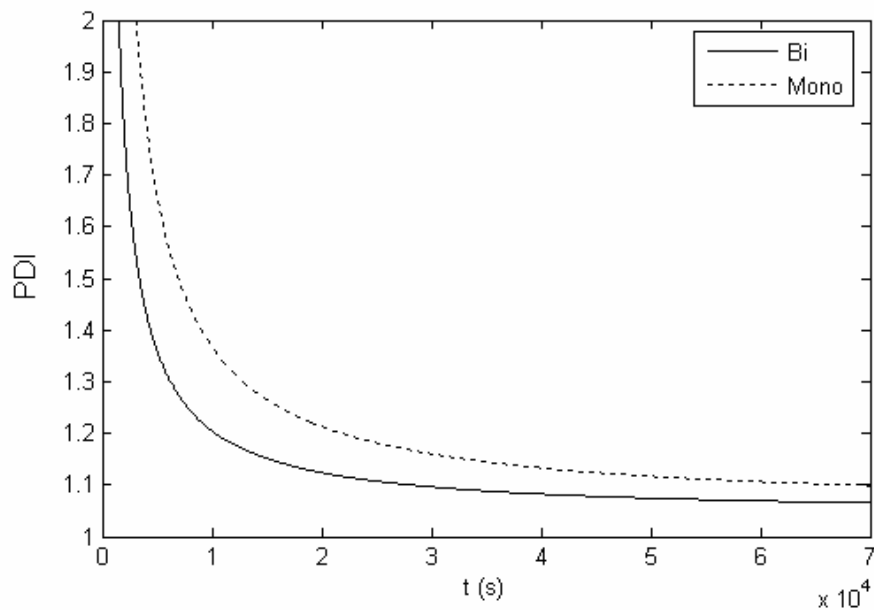


Figure 5.3 Effect of mono and bifunctional initiators on polydispersity index (PDI) as a function of time (t) ($k_p=1000 \text{ L mol}^{-1} \text{ s}^{-1}$, $k_{tc}=1 \times 10^7 \text{ L mol}^{-1} \text{ s}^{-1}$, $k_{td}=0$, $k_d=1 \times 10^7 \text{ L mol}^{-1} \text{ s}^{-1}$, $k_a=0.01 \text{ L mol}^{-1} \text{ s}^{-1}$, $[C]_0/[I]_0/[M]_0$ mole ratio: 1:1:100).

5.4.2 Effect of the equilibrium constant

It is difficult to change the rate constant for an elementary reaction in free-radical polymerization without changing all the other constants as well. For example, if we increase the polymerization temperature, all the rate constants will change according to their Arrhenius law expressions. On the other hand, in ATRP it is possible to change some rate constants while keeping the others unchanged. Different catalysts have distinct activation and deactivation rate constants, but the same propagation and termination rate constants, since the last two are a function of monomer and chain end type. Solvent type may also change the values of the activation and deactivation constants in ATRP: it was reported that those constants are a function of solvent polarity.^[31]

Compared to conventional free-radical polymerization, ATRP has small polymerization rates (compared to normal free radical polymerization) because of the equilibrium reaction between the polymer radicals and the dormant chains. In fact, during its life time, a chain spends most of its time as a dormant species in ATRP. This limitation is difficult to overcome because if the equilibrium is shifted towards the polymer radicals, polymer with broad MWDs will be produced. It is, therefore, important to shift the equilibrium towards the dormant chains in order to have controlled polymerization and hence narrow MWD.

The equilibrium constant (K_{eq}) is the ratio of the activation (k_a) to the deactivation (k_d) rate constant. Figures 5.4 to 5.6 show the effect of K_{eq} on monomer conversion, number average chain length and polydispersity index. In these figures, k_d was changed while k_a was kept constant. By increasing k_d , the equilibrium is shifted towards the dormant chain side. Having more dormant chains in the system decreases monomer conversion and chain length. On the other hand, a higher value k_d improves the control over the chain length distribution and hence produces polymers with smaller polydispersities index.

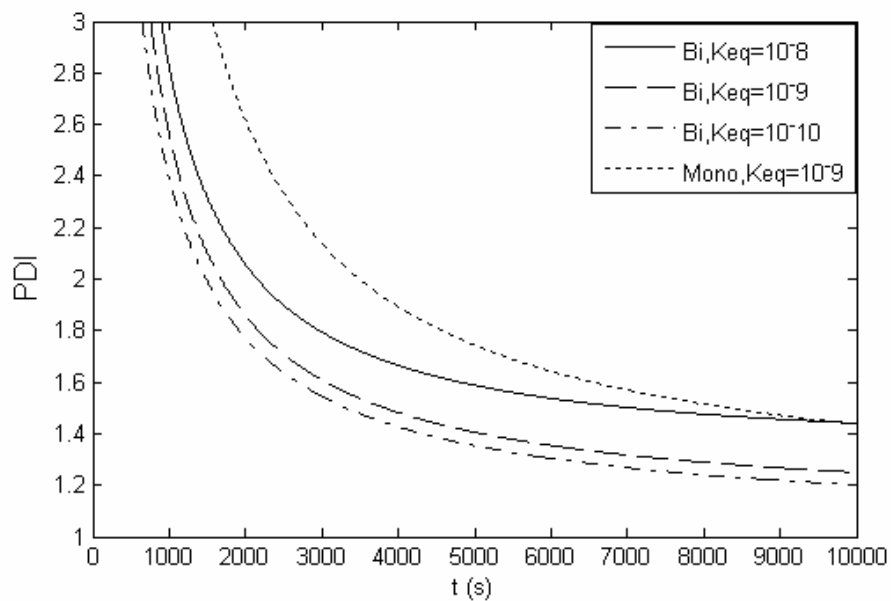


Figure 5.4 Effect of the equilibrium constant (K_{eq}) on the polydispersity index ($k_p=2000 \text{ L mol}^{-1} \text{ s}^{-1}$, $k_a=0.01 \text{ L mol}^{-1} \text{ s}^{-1}$, $k_{tc}=1 \times 10^7 \text{ L mol}^{-1} \text{ s}^{-1}$, $k_{td}=0$, $[C]_0/[I]_0/[M]_0$ mole ratio: 1:1:100).

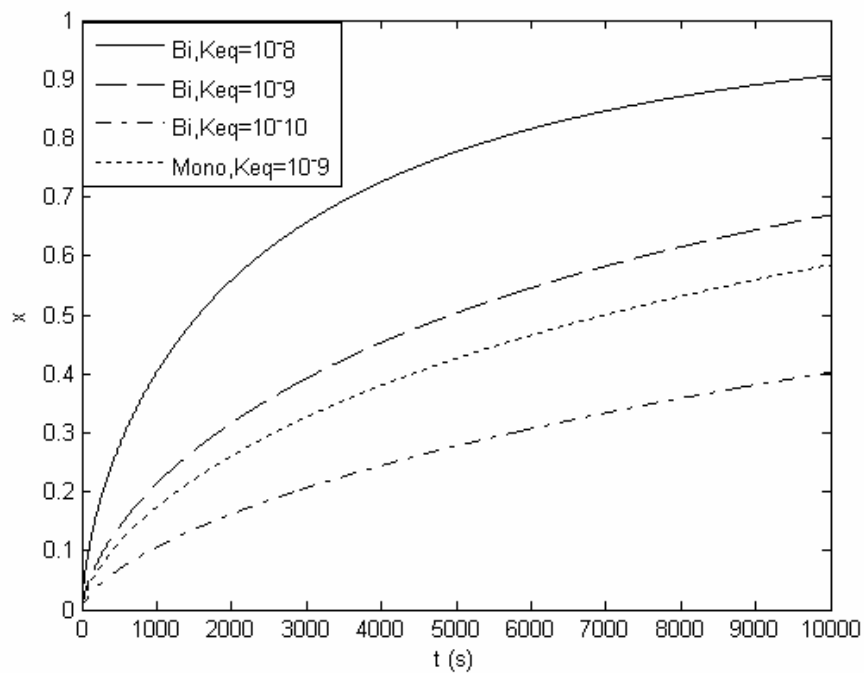


Figure 5.5 Effect of equilibrium constant (K_{eq}) on monomer conversion ($k_p=2000 \text{ L mol}^{-1} \text{ s}^{-1}$, $k_a=0.01 \text{ L mol}^{-1} \text{ s}^{-1}$, $k_{tc}=1 \times 10^7 \text{ L mol}^{-1} \text{ s}^{-1}$, $k_{td}=0$, $[C]_0/[I]_0/[M]_0$ mole ratio: 1:1:100).

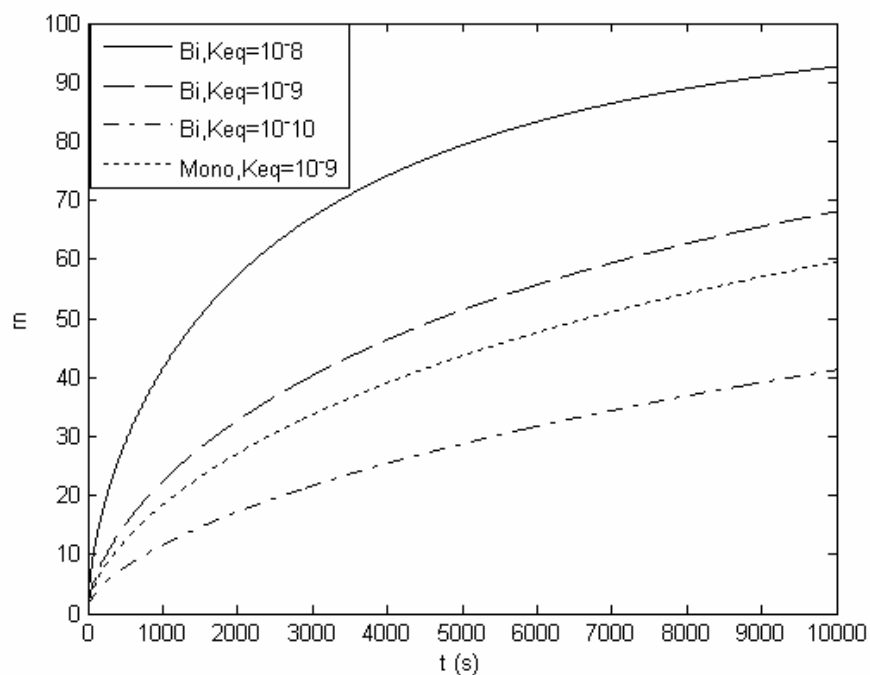


Figure 5.6 Effect of equilibrium constant (K_{eq}) on number average chain length ($k_p=2000$ L mol⁻¹ s⁻¹, $k_a=0.01$ L mol⁻¹ s⁻¹, $k_{tc}=1 \times 10^7$ L mol⁻¹ s⁻¹, $k_{td}=0$, $[C]_0/[I]_0/[M]_0$ mole ratio: 1:1:100).

5.4.3 Effect of the propagation rate constant

The rate of propagation is a function of the concentrations of monomer and free-radical initiators. Minimizing the concentration of free radicals by shifting the equilibrium reaction towards the dormant chains decreases the rate of propagation and monomer conversion for a given polymerization time. Therefore, rates of polymerization in living free-radical polymerizations are smaller than in conventional free-radical polymerizations. The rate of propagation is also a function of the propagation rate constant, k_p , that depends on polymerization temperature, monomer type, and may become a function of conversion at high monomer conversions. The value of the propagation rate constant in living free-radical polymerization is the same as in conventional free-radical polymerization. Values of the propagation rate constant for most monomers vary from 10^3 to 10^4 L.mol⁻¹.s⁻¹ under practical polymerization conditions.^[28] It is clear that increasing the propagation rate constant increases the rate of

addition of monomer to the growing polymer chains and therefore increases monomer conversion and degree of polymerization, as illustrated in Figures 5.7 and 5.8.

Ideally, polymer radicals should be activated and propagate one monomer unit only in each activation-deactivation cycle to have perfectly controlled polymerization. Figure 5.9 shows how increasing the propagation rate constant leads to a higher rate of monomer addition to the polymer radicals and to inadequate microstructural control as reflected by the higher polydispersity index values.

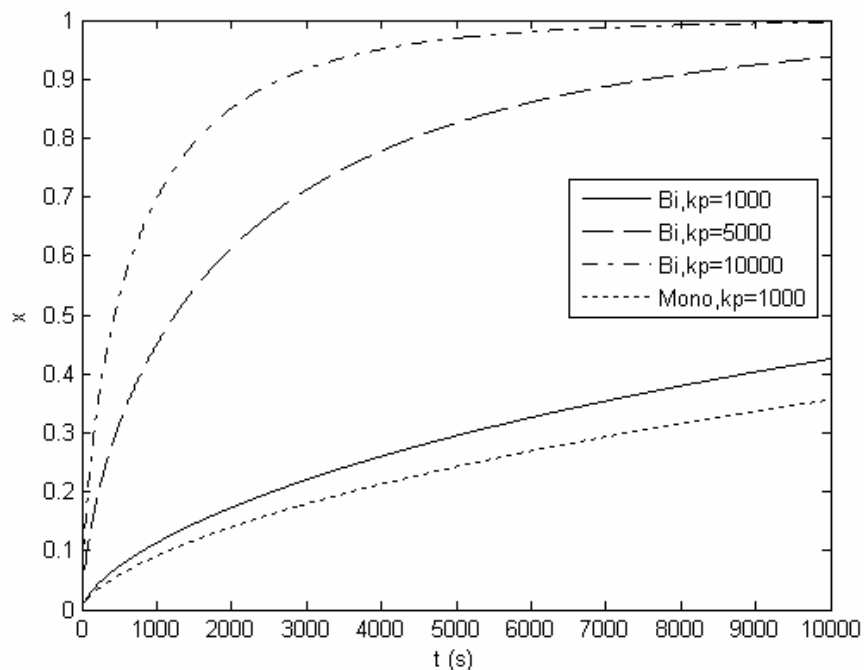


Figure 5.7 Effect of the propagation constant (k_p) on monomer conversion ($k_d=1 \times 10^7 \text{ L mol}^{-1} \text{ s}^{-1}$, $k_a=0.01 \text{ L mol}^{-1} \text{ s}^{-1}$, $k_{tc}=1 \times 10^7 \text{ L mol}^{-1} \text{ s}^{-1}$, $k_{td}=0$, $[C]_0/[I]_0/[M]_0$ mole ratio: 1:1:100).

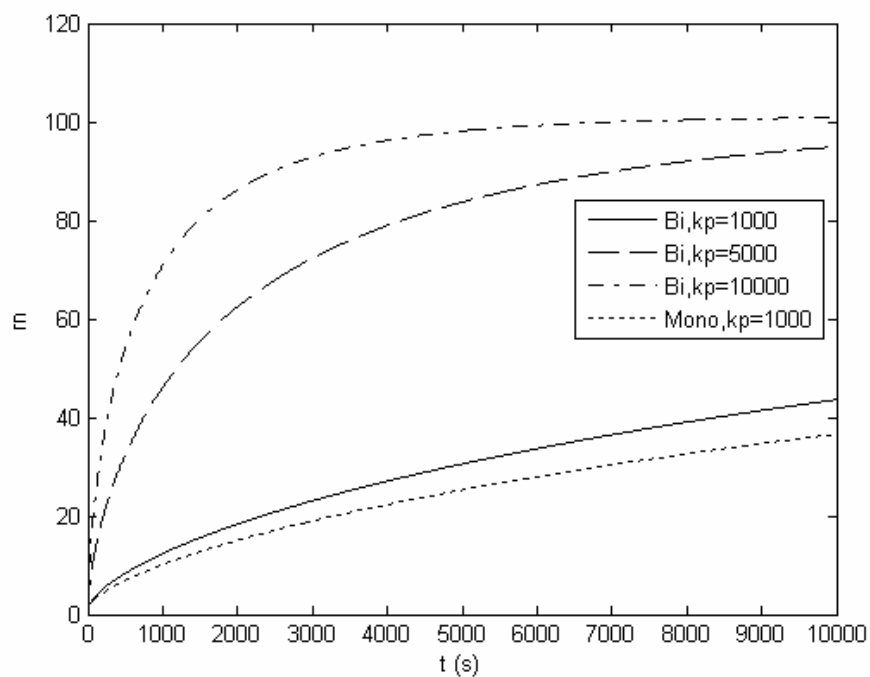


Figure 5.8 Effect of the propagation constant (k_p) on number average chain length ($k_d=1 \times 10^7 \text{ L mol}^{-1} \text{ s}^{-1}$, $k_a=0.01 \text{ L mol}^{-1} \text{ s}^{-1}$, $k_{tc}=1 \times 10^7 \text{ L mol}^{-1} \text{ s}^{-1}$, $k_{td}=0$, $[C]_0/[I]_0/[M]_0$ mole ratio: 1:1:100).

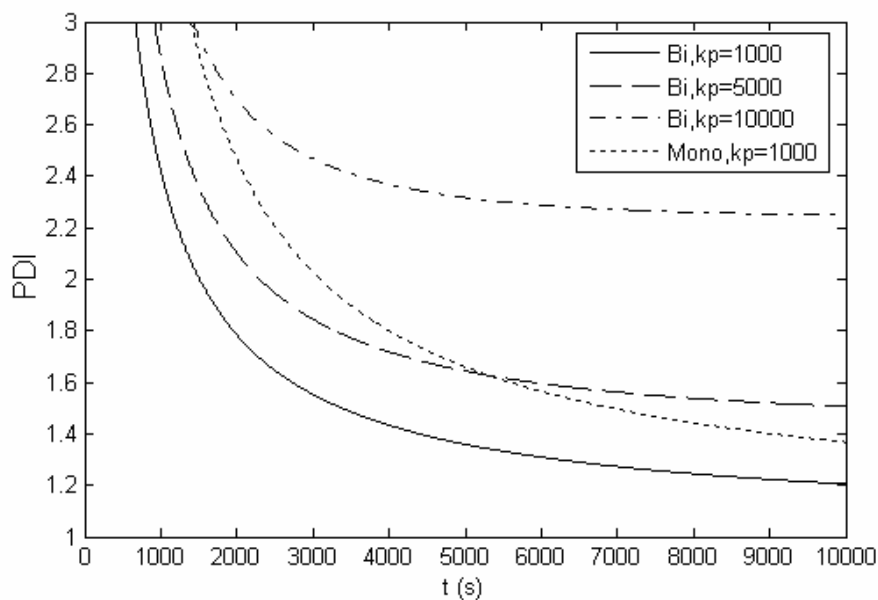


Figure 5.9 Effect of the propagation constant (k_p) on polydispersity index ($k_d=1 \times 10^7 \text{ L mol}^{-1} \text{ s}^{-1}$, $k_a=0.01 \text{ L mol}^{-1} \text{ s}^{-1}$, $k_{tc}=1 \times 10^7 \text{ L mol}^{-1} \text{ s}^{-1}$, $k_{td}=0$, $[C]_0/[I]_0/[M]_0$ mole ratio: 1:1:100).

5.4.4 Effect of the termination constant

Polymer radicals in conventional free-radical polymerization can terminate via combination and disproportionation reactions. Typical termination rate constants vary from 10^6 to 10^8 $\text{L}\cdot\text{mol}^{-1}\cdot\text{s}^{-1}$.^[28] Figures 5.10 and 5.11 show that monomer conversion and degree of polymerization decrease as the termination constants increase because of the reduction in the concentration of polymer radicals. The model shows that the polydispersity index becomes smaller as the termination rate constant increases (Figure 5.12). This somewhat unexpected behavior arises because chains that terminate by combination can grow again from both ends if they are made with bifunctional initiators. Moreover, termination by combination increases the concentration of dormant species. For example if two DR chains combine (chain with a dormant end and a free-radical end), they will form a chain with two dormant chain ends, DD.

The comparison of monofunctional and bifunctional initiators in Figures 5.10 to 5.12 agrees with the above conclusion. Under the same conditions, bifunctional initiators will make polymer with higher chain length averages and lower polydispersity indices at higher monomer conversion.

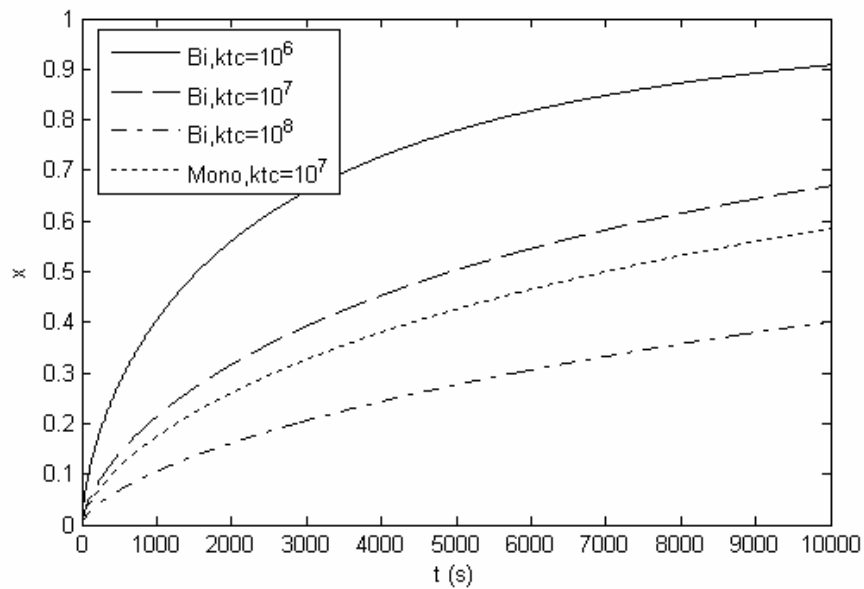


Figure 5.10 Effect of the termination by combination constant (k_{tc}) on monomer conversion ($k_d=1\times 10^7$ $\text{L mol}^{-1} \text{s}^{-1}$, $k_a=0.01$ $\text{L mol}^{-1} \text{s}^{-1}$, $k_p=2000$ $\text{L mol}^{-1} \text{s}^{-1}$, $k_{td}=0$, $[C]_0/[I]_0/[M]_0$ mole ratio: 1:1:100).

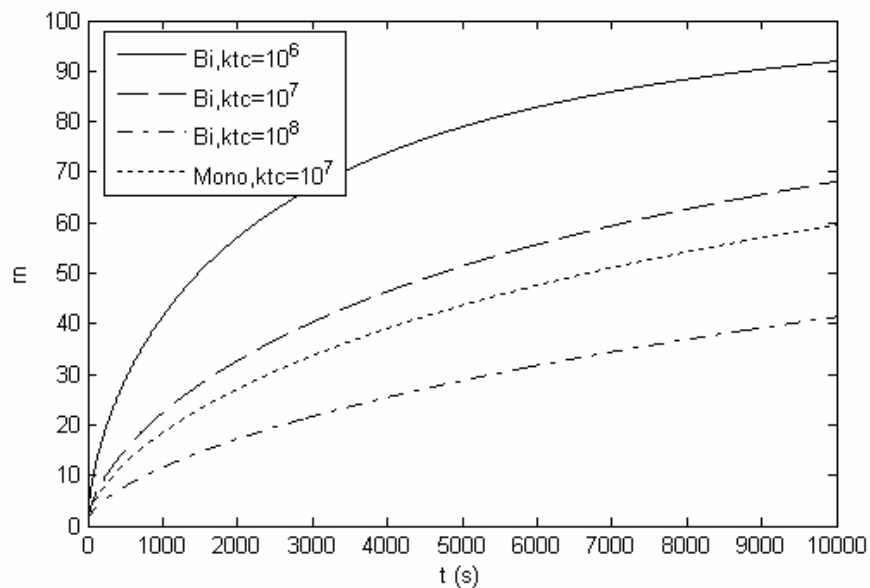


Figure 5.11 Effect of the termination by combination constant (k_{tc}) on number average chain length ($k_d=1 \times 10^7 \text{ L mol}^{-1} \text{ s}^{-1}$, $k_a=0.01 \text{ L mol}^{-1} \text{ s}^{-1}$, $k_p=2000 \text{ L mol}^{-1} \text{ s}^{-1}$, $k_{td}=0$, $[C]_0/[I]_0/[M]_0$ mole ratio: 1:1:100).

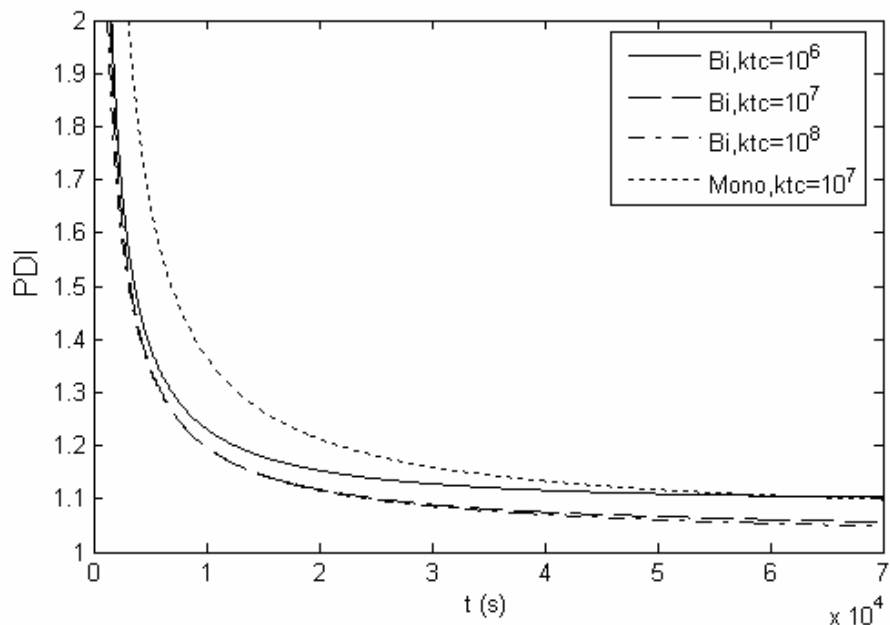


Figure 5.12 Effect of the termination by combination constant (k_{tc}) on polydispersity index ($k_d=1 \times 10^7 \text{ L mol}^{-1} \text{ s}^{-1}$, $k_a=0.01 \text{ L mol}^{-1} \text{ s}^{-1}$, $k_p=2000 \text{ L mol}^{-1} \text{ s}^{-1}$, $k_{td}=0$, $[C]_0/[I]_0/[M]_0$ mole ratio: 1:1:100).

5.4.5 Effect of catalyst and initiator concentration

The usual ATRP system contains, in addition to the monomer, initiator and catalyst molecules. It is important to adjust the ratios of all of these components in order to end up with living polymers with the desired microstructure. Our model can predict the effect of those species on monomer conversion, chain length and polydispersity index.

The catalyst is the most important component in ATRP. In its lower oxidation state, the catalyst activates the initiator (dormant species) to form uncapped species (polymer radicals) that propagate the monomer, whereas in its higher oxidation state the catalyst deactivates the polymer radicals and keeps the molecular weight distribution narrow. Figures 5.13 to 5.15 show the effect of catalyst concentration on ATRP. A higher catalyst concentration leads to a higher conversion of dormant to active species and thus increases monomer conversion and degree of polymerization. When catalyst is present in higher concentrations, many dormant species are activated simultaneously (fast activation), leading to polymer chains with well controlled sizes and lower polydispersity index.

Results for monofunctional initiators are included in Figures 5.13 to 5.15 for comparison with bifunctional initiators. ATRP with bifunctional initiators gives better control especially at low conversions, as shown in Figure 15, because the polymer chains can grow from both chain ends.

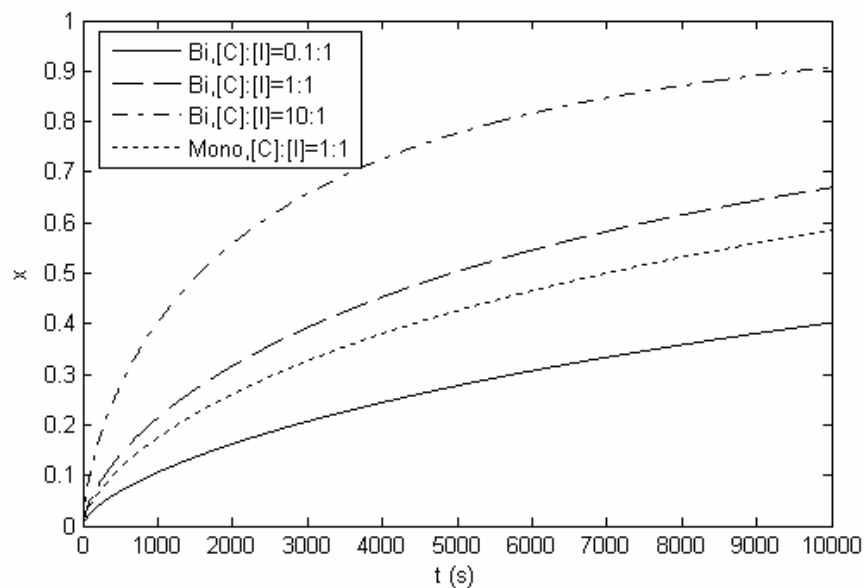


Figure 5.13 Effect of initial catalyst concentration on monomer conversion ($k_p=2000 \text{ L mol}^{-1} \text{ s}^{-1}$, $k_d=1 \times 10^7 \text{ L mol}^{-1} \text{ s}^{-1}$, $k_a=0.01 \text{ L mol}^{-1} \text{ s}^{-1}$, $k_{tc}=1 \times 10^7 \text{ L mol}^{-1} \text{ s}^{-1}$, $k_{td}=0$, $[C]_0/[M]_0$ mole ratio: 1:100, the mole ratio of $[C]_0$ varies as in the legend).

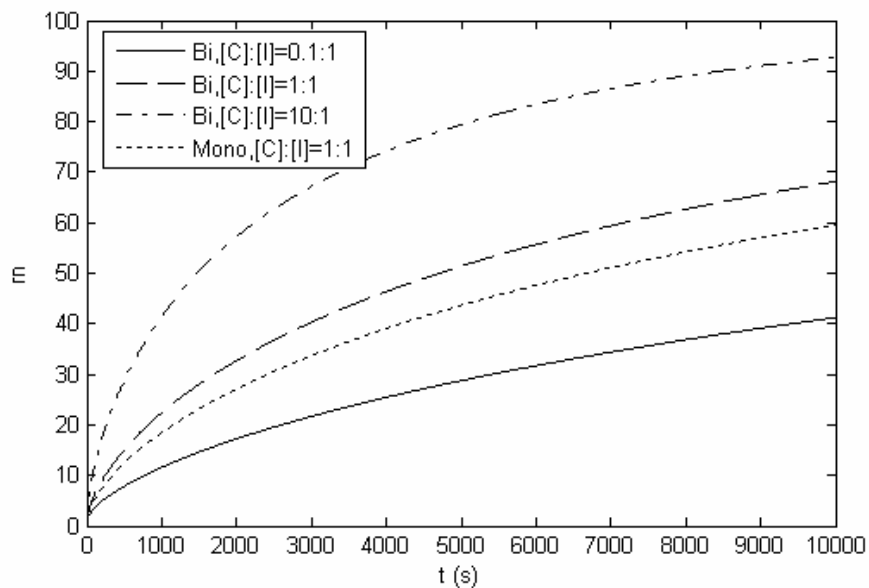


Figure 5.14 Effect of initial catalyst concentration on number average chain length ($k_p=2000 \text{ L mol}^{-1} \text{ s}^{-1}$, $k_d=1 \times 10^7 \text{ L mol}^{-1} \text{ s}^{-1}$, $k_a=0.01 \text{ L mol}^{-1} \text{ s}^{-1}$, $k_{tc}=1 \times 10^7 \text{ L mol}^{-1} \text{ s}^{-1}$, $k_{td}=0$, $[C]_0/[M]_0$ mole ratio: 1:100, the mole ratio of $[C]_0$ varies as in the legend).

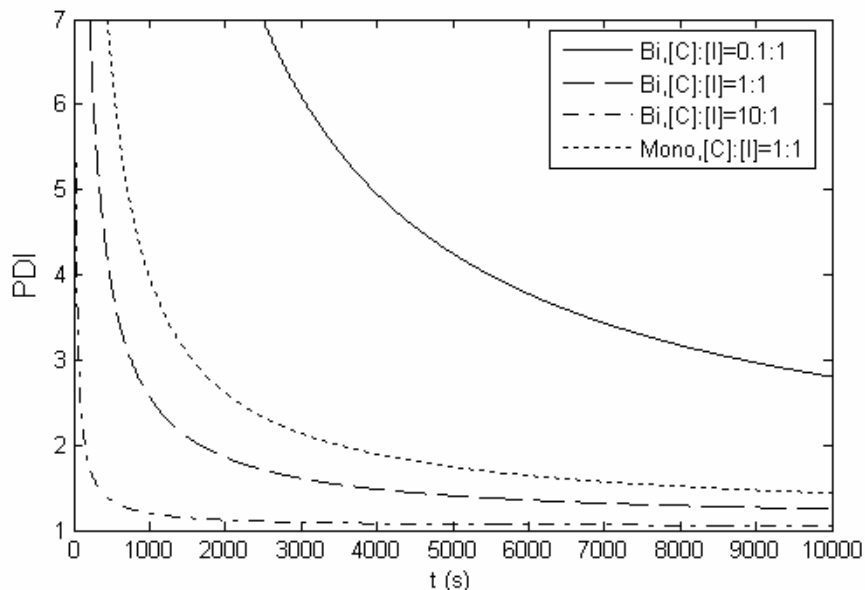


Figure 5.15 Effect of initial catalyst concentration $[C]_0$ on polydispersity as a function of time (t) ($k_p=2000 \text{ L mol}^{-1} \text{ s}^{-1}$, $k_d=1 \times 10^7 \text{ L mol}^{-1} \text{ s}^{-1}$, $k_a=0.01 \text{ L mol}^{-1} \text{ s}^{-1}$, $k_{tc}=1 \times 10^7 \text{ L mol}^{-1} \text{ s}^{-1}$, $k_{td}=0$, $[C]_0/[M]_0$ mole ratio: 1:100, the mole ratio of $[C]_0$ varies as in the legend).

Figures 5.16 to 5.18 show the effect of varying the concentration of initiator on monomer conversion, degree of polymerization and polydispersity index. Monomer consumption increases with increasing initiator concentration, as expected. The initiator also plays an important role in determining the number of living polymer chains in the reactor: increasing the initiator concentration decreases the number average chain length. This behavior is described by the theoretical molecular weight or degree of polymerization (DP) equation:

$$DP = \frac{[M]_0}{[\text{initiator}]_0} \times \text{conversion} \quad (40)$$

In addition, increasing the initiator concentration leads to more radical species. Therefore, the probability of termination reactions (formation of dead polymer chains) also increases, broadening the chain length distribution and increasing the polydispersity index of the polymer.

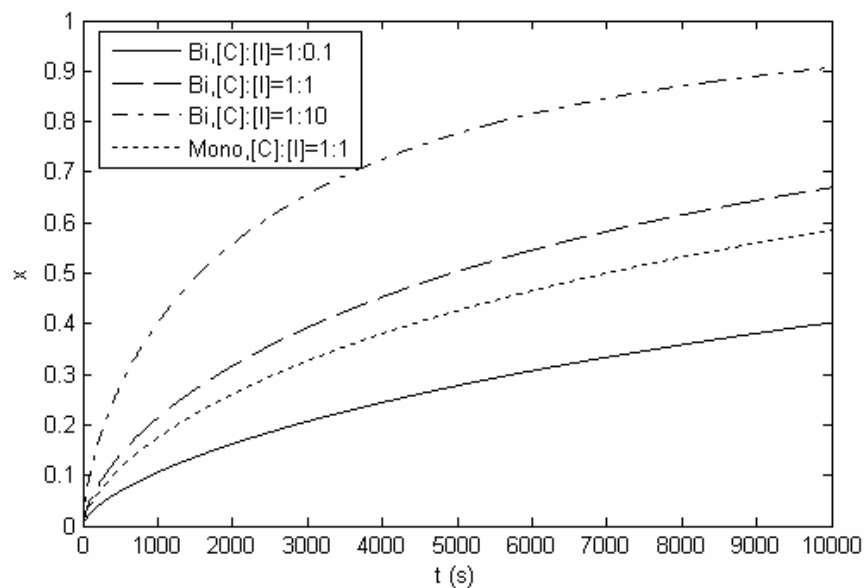


Figure 5.16 Effect of the initial initiator concentration on monomer conversion ($k_p=2000$ L mol⁻¹ s⁻¹, $k_d=1 \times 10^7$ L mol⁻¹ s⁻¹, $k_a=0.01$ L mol⁻¹ s⁻¹, $k_{tc}=1 \times 10^7$ L mol⁻¹ s⁻¹, $k_{td}=0$, $[C]_0/[M]_0$ mole ratio: 1:100, the mole ratio of $[I]_0$ varies as in the legend).

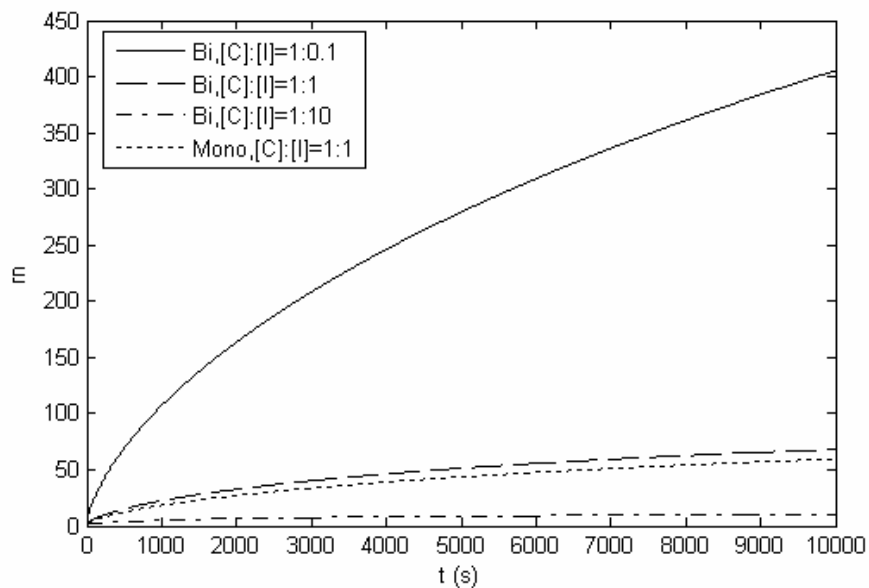


Figure 5.17 Effect of the initial initiator concentration on number average chain length ($k_p=2000$ L mol⁻¹ s⁻¹, $k_d=1 \times 10^7$ L mol⁻¹ s⁻¹, $k_a=0.01$ L mol⁻¹ s⁻¹, $k_{tc}=1 \times 10^7$ L mol⁻¹ s⁻¹, $k_{td}=0$, $[C]_0/[M]_0$ mole ratio: 1:100, the mole ratio of $[I]_0$ varies as in the legend).

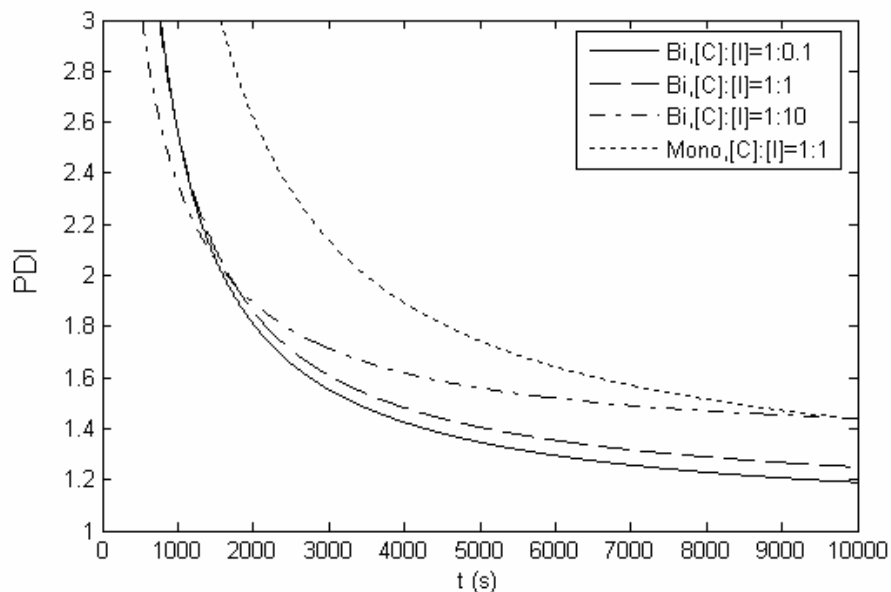


Figure 5.18 Effect of the initial initiator concentration on polydispersity index ($k_p=2000 \text{ L mol}^{-1} \text{ s}^{-1}$, $k_d=1 \times 10^7 \text{ L mol}^{-1} \text{ s}^{-1}$, $k_a=0.01 \text{ L mol}^{-1} \text{ s}^{-1}$, $k_{tc}=1 \times 10^7 \text{ L mol}^{-1} \text{ s}^{-1}$, $k_{td}=0$, $[C]_0/[M]_0$ mole ratio: 1:100, the mole ratio of $[I]_0$ varies as in the legend).

5.5 Conclusions

Atom-transfer radical polymerization using bifunctional initiators was studied with a fundamental mathematical model. The mathematical model represents a systematic way of storing the most important (at least from the modeller's point of view) information that has been acquired for a specific system. The model can be used to predict, explain and optimize polymer microstructure as a function of polymerization conditions.

A detailed comparison between monofunctional and bifunctional initiators showed that bifunctional initiators have some advantages over monofunctional initiators for ATRP. Under the same conditions, bifunctional initiators achieve higher monomer conversions, and make polymer with higher molecular weight averages and smaller polydispersity indices.

The equilibrium constant ($K_{eq} = k_a/k_d$) is an important factor for controlling the polymerization and regulating the “livingness degree” of the polymers made by ATRP. The narrow molecular weight distributions obtained with high equilibrium constants come at the expense of lower conversions and molecular weight averages. Longer

polymerization times are required in order to reach high conversions and molecular weight averages as the value of equilibrium constant decreases.

The effect of the propagation reactions was studied by varying the propagation rate constant. Higher k_p increases the conversion and the molecular weight but at the same time the polydispersity index increases up to the point that the polymerization stops being controlled ($PDI \sim 1.5$ or higher).

The relative concentration of the reactive species is also very important in ATRP. The model shows that the catalyst concentration has a very important effect. Keeping the catalyst concentration constant and increasing the initiator concentration with respect to the monomer concentration will lead to higher conversions, lower molecular weight averages and broader molecular weight distributions.

5.6 References

- [1] J. Chiefary, YK. Chong, F. Ercole, C. Moad, G. Moad, E. Rizzardo, SH. Thang, *Macromolecules* **1998**, 31, 5559.
- [2] G. Moad, J. Chiefary, YK. Chong, J. Krstina, RTA. Mayadunne, A. Postma, E. Rizzardo, SH. Thang, *Polym Int* **2000**, 49, 993.
- [3] MK. Georges, RPN. Veregin, PM. Kazmaier, GK. Hamer, *Macromolecules* **1993**, 26, 2987.
- [4] D. Benoit, V. Chaplinski, R. Braslau, CJ. Hawker, *J Am Chem Soc* **1999**, 121, 3904.
- [5] M. Rodlert, E. Harth, I. Rees, CJ. Hawker, *J Polym Sci, Polym Chem Ed* **2000**, 38, 4749.
- [6] K. Matyjaszewski, J. Xia, *Chem Rev* **2001**, 101, 2921.
- [7] M. Kamigaito, T. Ando, M. Sawamoto, *Chem Rev* **2001**, 101, 3689.
- [8] K. Matyjaszewski, *ACS Symp. Ser.* **2002**, 854, 2.
- [9] S. Zhu, *J. Polym. Sci. Part B: Polym. Phys.* **1999**, 37, 2692.
- [10] S. Zhu, *Macromol. Theory Simul.* **1999**, 8, 29.
- [11] O. Delgadillo-Velazquez, E. Vivaldo-Lima, I. Quintero-Ortega, S. Zhu, *AIChE Journal*, **2002**, 48,11, 2597.
- [12] A. Wang, S. Zhu, *J. Polym. Sci. Part A: Polym. Chem.* **2003**, 41, 1553.
- [13] M. Zhang, H. Ray, *Journal of applied polymer science* **2002**, 86, 1630.
- [14] M. Zhang, H. Ray, *Journal of applied polymer science* **2002**, 86, 1047.
- [15] H. Fischer, *Macromolecules* **1997**, 30, 5666.
- [16] H. Fischer, *J. Polym. Sci. Part A: Polym. Chem.* **1999**, 37, 1885.
- [17] A. Shipp, K. Matyjaszewski, *Macromolecules* **1999**, 32, 2948.
- [18] J. Lutz, K. Matyjaszewski, *Macromol. Chem. Phys.* **2002**, 203, 1385.
- [19] M. Villalobos, A. Hamielec, P. Wood, *Journal of applied polymer science* **1991**, 42, 629.
- [20] M. Mennicken, R. Nagelsdiek, H. Keul, H. Hocker, *Macromol. Chem. Phys.* **2004**, 205, 143.
- [21] X. Zhang, K. Matyjaszewski, *Macromolecules* **1999**, 32, 1763.
- [22] K. Matyjaszewski, D. Shipp, G. McMurtry, S. Gaynor, T. Pakula, *J. Polym. Sci., Part A: Polym. Chem.* **2000**, 38, 2023.
- [23] A. Malinowska, P. Vlcek, J. Kriz, L. Toman, P. Latalova, M. Janata, B. Masar, *Polymer*, **2005**, 46, 5.
- [24] M. Janata, B. Masar, L. Toman, P. Vlcek, P. Policka, J. Brus, P. Holler, *Reactive & Functional Polymers*, **2001**, 50, 67.
- [25] M. Destarac, J. Bessiere, B. Boutevin, *J. Polym. Sci., Part A: Polym. Chem.* **1998**, 36, 2933.
- [26] M. Destarac, B. Boutevin, K. Matyjaszewski, *Macromol. Chem. Phys.* **2000**, 201, 265.
- [27] M. Destarac, B. Boutevin, K. Matyjaszewski, *ACS Symp. Ser.* **2000**, 768, 234.
- [28] G. Odian, *Principles of polymerization*, 3rd edition, **1990**, pp. 206.

- [29].L. Shampine, M. Reichelt, "The MATLAB ODE Suite," SIAM Journal on Scientific Computing, **1997**, 18, 1.
- [30] K. Matyjaszewski, P. Miller, J. Pyun, G. Kickelbick, S. Diamanti, Macromolecules **1999**, 32, 6526.
- [31] G. Chambard, B. Klumperman, A. German, Macromolecules, **2000**, 33, 4417.

5.7 Appendices

Appendix A

The method of moments is an efficient method to calculate several chain length averages. Herein, moments of chain length distribution are calculated for all the polymeric species present in our system. The j^{th} moment of the polymeric species are defined in Equations (31) to (36).

The zeroth moment of the dormant species (DD) is given by :

$$[\lambda_{DD,0}] = \sum_{r=1}^{\infty} [DD_r] = DD_1 + \sum_{r=2}^{\infty} DD_r \quad (\text{A1})$$

Therefore

$$\frac{d[\lambda_{DD,0}]}{dt} = \frac{d[DD_1]}{dt} + \sum_{r=2}^{\infty} \frac{d[DD_r]}{dt} \quad (\text{A2})$$

The population balances equation (defined in Equation 22) was substituted in Equations (A.1) and (A.2) and after some simplifications the equation for the zeroth moment of the distribution of chain length for the dormant species was obtained:

$$\frac{d[\lambda_{DD,0}]}{dt} = -2k_a \lambda_{DD,0} [C] + k_d \lambda_{DR,0} [CX] + \frac{k_{tc}}{2} \lambda_{DR,0}^2 \quad (\text{A3})$$

Similarly, the first moment of dormant species (DD) is given by,

$$[\lambda_{DD,1}] = \sum_{r=1}^{\infty} r [DD_r] = DD_1 + \sum_{r=2}^{\infty} r DD_r \quad (\text{A4})$$

and:

$$\frac{d[\lambda_{DD,1}]}{dt} = \frac{d[DD_1]}{dt} + \sum_{r=2}^{\infty} r \frac{d[DD_r]}{dt} \quad (\text{A5})$$

Substituting the population balances, Equation (22), and simplifying the resulting expression, we obtain:

$$\frac{d[\lambda_{DD,1}]}{dt} = -2k_a \lambda_{DD,1} [C] + k_d \lambda_{DR,1} [CX] + k_{tc} \lambda_{DR,0} \lambda_{DR,1} \quad (\text{A6})$$

Finally, the second moment of dormant species (DD) is given by,

$$[\lambda_{DD,2}] = \sum_{r=1}^{\infty} r^2 [DD_r] = DD_1 + \sum_{r=2}^{\infty} r^2 DD_r \quad (\text{A7})$$

and:

$$\frac{d[\lambda_{DD,2}]}{dt} = \frac{d[DD_1]}{dt} + \sum_{r=2}^{\infty} r^2 \frac{d[DD_r]}{dt} \quad (\text{A8})$$

Substituting the population balances Equation (22) and simplifying the resulting expression, equation (A.8) becomes:

$$\frac{d[\lambda_{DD,2}]}{dt} = -2k_a \lambda_{DD,2}[C] + k_d \lambda_{DR,2}[CX] + k_{ic} (\lambda_{DR,0} \lambda_{DR,2} + \lambda_{DR,1}^2) \quad (\text{A9})$$

Similar equations can be derived for the rest of the polymeric species. The final expression for the moment equations are listed below.

Moments of DR

Zeroth moment

$$\begin{aligned} \frac{d[\lambda_{DR,0}]}{dt} = & 2k_a \lambda_{DD,0}[C] - k_a \lambda_{DR,0}[C] + 2k_d \lambda_{RR,0}[CX] - k_d \lambda_{DR,0}[CX] \\ & - k_{ic} \lambda_{DR,0}^2 - k_{ic} \lambda_{DR,0} \lambda_{PR,0} \\ & - k_{id} \lambda_{DR,0}^2 - k_{id} \lambda_{DR,0} \lambda_{RR,0} - k_{id} \lambda_{DR,0} \lambda_{PR,0} \end{aligned} \quad (\text{A.10})$$

First moment

$$\begin{aligned} \frac{d[\lambda_{DR,1}]}{dt} = & 2k_a \lambda_{DD,1}[C] - k_a \lambda_{DR,1}[C] + 2k_d \lambda_{RR,1}[CX] - k_d \lambda_{DR,1}[CX] + k_p [M] \lambda_{DR,0} \\ & - k_{ic} \lambda_{DR,0} \lambda_{DR,1} + 2k_{ic} \lambda_{DR,0} \lambda_{RR,1} - k_{ic} \lambda_{PR,0} \lambda_{DR,1} \\ & - k_{id} \lambda_{DR,0} \lambda_{DR,1} - k_{id} \lambda_{DR,1} \lambda_{RR,0} - k_{id} \lambda_{DR,1} \lambda_{PR,0} \end{aligned} \quad (\text{A.11})$$

Second moment

$$\begin{aligned} \frac{d[\lambda_{DR,2}]}{dt} = & 2k_a \lambda_{DD,2}[C] - k_a \lambda_{DR,2}[C] + 2k_d \lambda_{RR,2}[CX] - k_d \lambda_{DR,2}[CX] + k_p [M] (2\lambda_{DR,1} + \lambda_{DR,0}) \\ & - k_{ic} \lambda_{DR,0} \lambda_{DR,2} + 2k_{ic} \lambda_{DR,0} \lambda_{RR,2} + 4k_{ic} \lambda_{DR,1} \lambda_{RR,1} - k_{ic} \lambda_{PR,0} \lambda_{DR,2} \\ & - k_{id} \lambda_{DR,2} \lambda_{DR,0} - k_{id} \lambda_{DR,2} \lambda_{RR,0} - k_{id} \lambda_{DR,2} \lambda_{PR,0} \end{aligned} \quad (\text{A.12})$$

Moments of RR

Zeroth moment

$$\begin{aligned} \frac{d[\lambda_{RR,0}]}{dt} = & k_a \lambda_{DR,0}[C] - 2k_d \lambda_{RR,0}[CX] \\ & - 2k_{ic} \lambda_{DR,0} \lambda_{RR,0} - 2k_{ic} \lambda_{RR,0}^2 - 2k_{ic} \lambda_{PR,0} \lambda_{RR,0} \\ & - 2k_{id} \lambda_{DR,0} \lambda_{RR,0} - 4k_{id} \lambda_{RR,0}^2 - 2k_{id} \lambda_{PR,0} \lambda_{RR,0} \end{aligned} \quad (\text{A.13})$$

First moment

$$\begin{aligned}
\frac{d[\lambda_{RR,1}]}{dt} &= k_a \lambda_{DR,1} [C] - 2k_d \lambda_{RR,1} [CX] + 2k_p [M] \lambda_{RR,0} \\
&\quad - 2k_{ic} \lambda_{DR,0} \lambda_{RR,1} - 2k_{ic} \lambda_{PR,0} \lambda_{RR,1} \\
&\quad - 2k_{id} \lambda_{DR,0} \lambda_{RR,1} - 4k_{id} \lambda_{RR,0} \lambda_{RR,1} - 2k_{id} \lambda_{PR,0} \lambda_{RR,1}
\end{aligned} \tag{A.14}$$

Second moment

$$\begin{aligned}
\frac{d[\lambda_{RR,2}]}{dt} &= k_a \lambda_{DR,2} [C] - 2k_d \lambda_{RR,2} [CX] + 2k_p [M] (2\lambda_{RR,1} + \lambda_{RR,0}) \\
&\quad + 4k_{ic} \lambda_{RR,1}^2 - 2k_{ic} \lambda_{DR,0} \lambda_{RR,2} - 2k_{ic} \lambda_{PR,0} \lambda_{RR,2} \\
&\quad - 2k_{id} \lambda_{DR,0} \lambda_{RR,2} - 4k_{id} \lambda_{RR,0} \lambda_{RR,2} - 2k_{id} \lambda_{PR,0} \lambda_{RR,2}
\end{aligned} \tag{A.15}$$

Moments of PR

Zeroth moment

$$\begin{aligned}
\frac{d[\lambda_{PR,0}]}{dt} &= k_a \lambda_{PD,0} [C] - k_d \lambda_{PR,0} [CX] \\
&\quad - k_{ic} \lambda_{PR,0} \lambda_{PR,0} - k_{ic} \lambda_{PR,0} \lambda_{DR,0} \\
&\quad + 2k_{id} \lambda_{DR,0} \lambda_{RR,0} + 4k_{id} \lambda_{RR,0} \lambda_{RR,0} - k_{id} \lambda_{PR,0} \lambda_{PR,0} \\
&\quad - k_{id} \lambda_{PR,0} \lambda_{DR,0} - 2k_{id} \lambda_{PR,0} \lambda_{RR,0}
\end{aligned} \tag{A.16}$$

First moment

$$\begin{aligned}
\frac{d[\lambda_{PR,1}]}{dt} &= k_a \lambda_{PD,1} [C] - k_d \lambda_{PR,1} [CX] + k_p [M] \lambda_{PR,0} \\
&\quad - k_{ic} \lambda_{PR,1} \lambda_{PR,0} + 2k_{ic} \lambda_{PR,0} \lambda_{RR,1} - k_{ic} \lambda_{PR,1} \lambda_{DR,0} \\
&\quad + 2k_{id} \lambda_{DR,1} \lambda_{RR,0} + 4k_{id} \lambda_{RR,1} \lambda_{RR,0} - k_{id} \lambda_{PR,1} \lambda_{PR,0} \\
&\quad - k_{id} \lambda_{PR,1} \lambda_{DR,0} - 2k_{id} \lambda_{PR,1} \lambda_{RR,0}
\end{aligned} \tag{A.17}$$

Second moment

$$\begin{aligned}
\frac{d[\lambda_{PR,2}]}{dt} &= k_a \lambda_{PD,2} [C] - k_d \lambda_{PR,2} [CX] + k_p [M] \lambda_{PR,0} + 2k_p [M] \lambda_{PR,1} \\
&\quad - k_{ic} \lambda_{PR,2} \lambda_{PR,0} + 2k_{ic} \lambda_{PR,0} \lambda_{RR,2} + 4k_{ic} \lambda_{PR,1} \lambda_{RR,1} - k_{ic} \lambda_{PR,2} \lambda_{DR,0} \\
&\quad + 2k_{id} \lambda_{DR,2} \lambda_{RR,0} + 4k_{id} \lambda_{RR,2} \lambda_{RR,0} - k_{id} \lambda_{PR,2} \lambda_{PR,0} \\
&\quad - k_{id} \lambda_{PR,2} \lambda_{DR,0} - 2k_{id} \lambda_{PR,2} \lambda_{RR,0}
\end{aligned} \tag{A.18}$$

Moments of PD

Zeroth moment

$$\begin{aligned} \frac{d[\lambda_{PD,0}]}{dt} &= -k_a \lambda_{PD,0}[C] + k_d \lambda_{PR,0}[CX] \\ &\quad + k_{ic} \lambda_{PR,0} \lambda_{DR,0} \\ &\quad + k_{id} \lambda_{DR,0}^2 + 2k_{id} \lambda_{DR,0} \lambda_{RR,0} + 2k_{id} \lambda_{DR,0} \lambda_{PR,0} \end{aligned} \quad (\text{A.19})$$

First moment

$$\begin{aligned} \frac{d[\lambda_{PD,1}]}{dt} &= -k_a \lambda_{PD,1}[C] + k_d \lambda_{PR,1}[CX] \\ &\quad + k_{ic} \lambda_{PR,1} \lambda_{DR,0} + k_{ic} \lambda_{PR,0} \lambda_{DR,1} \\ &\quad + k_{id} \lambda_{DR,0} \lambda_{DR,1} + 2k_{id} \lambda_{DR,1} \lambda_{RR,0} + 2k_{id} \lambda_{DR,1} \lambda_{PR,0} \end{aligned} \quad (\text{A.20})$$

Second moment

$$\begin{aligned} \frac{d[\lambda_{PD,2}]}{dt} &= -k_a \lambda_{PD,2}[C] + k_d \lambda_{PR,2}[CX] \\ &\quad + k_{ic} \lambda_{PR,2} \lambda_{DR,0} + k_{ic} \lambda_{PR,0} \lambda_{DR,2} + 2k_{ic} \lambda_{PR,1} \lambda_{DR,1} \\ &\quad + k_{id} \lambda_{DR,0} \lambda_{DR,2} + 2k_{id} \lambda_{DR,2} \lambda_{RR,0} + 2k_{id} \lambda_{DR,2} \lambda_{PR,0} \end{aligned} \quad (\text{A.21})$$

Moments of PP

Zeroth moment

$$\frac{d[\lambda_{PP,0}]}{dt} = \frac{k_{ic}}{2} \lambda_{PR,0}^2 + k_{id} \lambda_{PR,0}^2 + 2k_{id} \lambda_{PR,0} \lambda_{RR,0} + k_{id} \lambda_{PR,0} \lambda_{DR,0} \quad (\text{A.22})$$

First moment

$$\frac{d[\lambda_{PP,1}]}{dt} = k_{ic} \lambda_{PR,1} \lambda_{PR,0} + k_{id} \lambda_{PR,1} \lambda_{PR,0} + k_{id} \lambda_{PR,1} \lambda_{RR,0} + 2k_{id} \lambda_{PR,1} \lambda_{DR,0} \quad (\text{A.23})$$

Second moment

$$\begin{aligned} \frac{d[\lambda_{PP,2}]}{dt} &= k_{ic} \lambda_{PR,2} \lambda_{PR,0} + k_{ic} \lambda_{PR,1}^2 \\ &\quad + k_{id} \lambda_{PR,2} \lambda_{PR,0} + 2k_{id} \lambda_{PR,2} \lambda_{RR,0} + k_{id} \lambda_{PR,2} \lambda_{DR,0} \end{aligned} \quad (\text{A.24})$$

Chapter 6

6 Modelling of Atom Transfer Radical Polymerization with Bifunctional Initiators: Diffusion Effects and Case Studies*

6.1 Abstract

A mathematical model for atom transfer radical polymerization (ATRP) with bifunctional initiators was developed. The model was validated with three case studies in bulk and solution polymerization. We used only polymer yield data to estimate some of the model parameters, while others were obtained from the literature. The model fits the polymer yield data and also predicts weight average molecular weights and polydispersity indices very well. The free volume theory was also incorporated to the model to study the effect of diffusion-controlled reactions. The adjustable parameters in the free volume theory for the termination, propagation, activation and deactivation reactions were varied to show the effect on monomer conversion, polymer chain length and polydispersity index. The model shows that diffusion-limited termination reactions produce polymer with smaller polydispersity indices, while diffusion-limited propagation reactions have the opposite effect. Both models, considering and neglecting diffusion effects on the kinetic rate constants, were compared with experimental data. Even though the model predictions for monomer conversion, number average molecular weight and polydispersity index are good in both cases, the simulations indicate that diffusion-controlled reactions can be ignored for the cases studied in the three case studies described in this paper.

* This Chapter has been published: M. Al-Harhi, J. Soares, L. Simon, *Macromol. Chem. Phys.* **2006**, *207*, 469-483.

6.2 Introduction

In a previous Chapter, we developed a generic dynamic model for ATRP with bifunctional initiators and showed that the model was useful to predict monomer conversion, polymer chain length averages and polydispersity under several polymerization conditions. In the present Chapter we compare our model predictions with experimental results available in the literature.^[1-3] To our knowledge, this is the first time a fundamental polymerization kinetic model is used to fit and predict experimental ATRP results using bifunctional initiators.

Diffusion-controlled reactions are important in conventional free radical polymerization.^[4,5] However, there is no agreement in the literature about diffusion effects on LFRP. For instance, the auto-acceleration phenomenon that appears in conventional free radical polymerization seems to be absent in LFRP. Some authors suggest that only the termination constant may be affected by diffusion limitations at high monomer conversions,^[6-8] while others say that all the rate constants may be affected in controlled free radical polymerizations.^[9,10] It is difficult to evaluate the validity of these suggestions without a mathematical model that can quantify these effects. We will also investigate these two alternatives by modeling the effect of diffusion-controlled reactions in ATRP using the free volume theory.

6.3 Model development

In a typical ATRP system, alkyl halides are used as initiators, transition metals with at least two oxidation states are used as catalysts, and ligands are used to increase the solubility of the transition metal in the organic media. The polymerization involves the activation of the dormant species through halogen abstraction by the transition metal in its lower oxidation state to form active species (radicals) and the transition metal in its higher oxidation state. The polymer radicals can propagate, terminate, or deactivate via halogen transfer from the transition metal in its higher oxidation state to form dormant chains. The activation and deactivation cycle is repeated throughout the polymerization and this dynamic equilibrium is responsible for the control of the polymerization. This general feature of ATRP is common for mono-, bi-, and multifunctional initiators.

The elementary reactions for bifunctional initiators that form the basis for our model are shown in the previous chapter. Similarly the complete development of population balance and the method of moments of the given mechanism are shown in the previous chapter

6.3.1 Diffusion control

The temperature dependency of the rate constants for activation, deactivation, propagation and termination are described by Arrhenius law:

$$k_a = A_a \exp(-E_a / RT) \quad (1)$$

$$k_d = A_d \exp(-E_d / RT) \quad (2)$$

$$k_p = A_p \exp(-E_p / RT) \quad (3)$$

$$k_t = A_t \exp(-E_t / RT) \quad (4)$$

As monomer conversion increases in bulk polymerization, these reactions may become diffusion controlled. In conventional free radical polymerization, the termination rate constant decreases due to the gel effect or Trommsdorff-Smith-Norrish phenomenon. The mobility of the polymer radicals decrease and, as a result, the termination rate also decreases. This phenomenon is modeled as a decrease in the termination rate constant. At even higher monomer conversions, monomer diffusion may be affected because of the extreme viscosity of the reaction medium, reducing the propagation rate. This phenomenon is modeled as a decrease in the propagation rate constant. The free volume theory is an efficient approach to study the effect of diffusion on termination and propagation rate constants.^[4,5] In this Chapter, we used the free volume theory to quantify the importance of diffusion effects during ATRP with bifunctional initiators.

6.3.2 Free volume theory

The free volume of the reaction medium varies throughout the reaction as a function of monomer conversion. As the conversion increases, the viscosity of the reaction medium increases and its free volume decreases, therefore slowing down the diffusion of the species in the reactor. Termination reactions occur between two large polymer radicals and are limited by the rates at which the polymer radical ends meet each

other. As a result, the termination rate constant depends on the length of the polymer radical and it is inversely proportional to the viscosity of the medium. Propagation, activation and deactivation reactions become diffusion controlled when the polymerization medium becomes very viscous, at high monomer conversion. In solution polymerization the solvent acts as a diluent, which in turn decreases the viscosity of the reaction mixture, delaying or eliminating diffusion limitations.

Many models exist in the literature to explain diffusion limitations on polymerization and termination rate constants. Whereas some models consider only the diffusion effect on termination rate constants, others include this effect on all reaction rate constants. Free volume theory has been used extensively to study diffusion effects on free radical polymerization. Using this theory, all the rate constants can be correlated to the change of the free volume of the reaction media.

During polymerization, the free volume of the reaction mixture depends on the volume of the components present in the system. The total volume is calculated as,

$$v_f = \sum_{i=1}^{\text{\# of components}} [0.025 + \alpha_i(T - T_{gi})] \frac{V_i}{V_t} \quad (5)$$

where α_i is the expansion coefficient for component i , T and T_{gi} are the polymerization temperature and glass transition temperature of component i , and V_i and V_t are the volume of component i and the total volume.

Among the elementary reactions present in ATRP with bifunctional initiators, only chain termination involves reactions between two large polymer radicals. Therefore, the model for the termination rate constant is a function of the number and weight average chain lengths, r_n and r_w , of the polymer radicals. Equation (6) shows the expression used to correct the termination rate constant due to diffusion effects,^[9]

$$k_t = k_{t,0} \left(\frac{r_n}{r_w} \right)^{x/2} \exp \left[-B_t \left(\frac{1}{v_f} - \frac{1}{v_{f0}} \right) \right] \quad (6)$$

where x is monomer conversion, B_t is a dimensionless adjustable parameter, $k_{t,0}$ is the termination rate constant at the beginning of the polymerization, and v_{f0} is the fractional free-volume at the beginning of the polymerization.

The expressions for the propagation, activation and deactivation reaction rate constants are shown in the following equations,

$$k_p = k_{p,0} \exp\left[-B_p\left(\frac{1}{v_f} - \frac{1}{v_{f_0}}\right)\right] \quad (7)$$

$$k_a = k_{a,0} \exp\left[-B_a\left(\frac{1}{v_f} - \frac{1}{v_{f_0}}\right)\right] \quad (8)$$

$$k_d = k_{d,0} \exp\left[-B_d\left(\frac{1}{v_f} - \frac{1}{v_{f_0}}\right)\right] \quad (9)$$

where B_p , B_a , B_d are dimensionless adjustable parameters for propagation, activation and deactivation reactions, respectively, and the subscript “0” indicates the initial value of each reaction rate constant.

6.3.3 Model parameters

We have divided this investigation in two parts: In the first one, we show the effect of diffusion resistances on ATRP with bifunctional initiators. Even though diffusion resistances on ATRP are not expected to be very high in many practical cases, it is important to show which consequences they would have if they were relevant. We will show that some of these effects would be hard to be predicted without a fundamental polymerization model. In the second part, we use the experimental data reported in the literature ^[1-3] to validate the model.

A common difficulty in this type of modeling is the lack of reliable kinetic parameters for free radical polymerization. There is significant scatter in the literature data even for the propagation and termination rate constants of well-known monomers such as styrene. Additional problems are found for ATRP when trying to estimate the activation and deactivation rate constants. Moreover, the free volume parameters needed in Equations (6) to (9) are also hard to estimate. Our approach for the following simulations was to use the parameters available in the literature, and to estimate the

parameters that were not available based on the experimental data using a non-linear least square method.

6.4 Results and discussion

6.4.1 Diffusion effects

In the free volume theory, the rate constants vary exponentially with the total free volume of the mixture. The adjustable parameters (B_t , B_p , B_a and B_d) can be estimated by a non-linear optimization method based on experimental data. We used the proposed model for ATRP with bifunctional initiators combined with the free volume theory to study the effect of diffusion controlled reactions on the degree of polymerization (DP), monomer conversion (x) and polydispersity index (PDI) for styrene polymerization. The chemically-controlled rate constants for termination and propagation ($k_{t,0}$ and $k_{p,0}$) at 110°C were taken from the literature (see Table 6.1). The initial guesses for activation and deactivation rate constants were based on values available in the literature for similar systems. ^[6,8,9] The ratio of the initial molar concentrations of monomer, initiator and activator was 100:1:2. The free volume parameters B_t , B_p , B_a and B_d were varied over a range of values wide enough to have a significant impact on the reaction rate constants. Glass transition temperatures and thermal expansion coefficients used in this study are shown also in Table 6.1.

Since termination reactions are likely to be affected by diffusion before propagation, activation and deactivation reactions, we varied the adjustable parameter B_t without diffusion effects on the other rate constants, that is, we set the values of B_p , B_a and B_d to zero. Figure 6.1 shows that diffusion limitations on chain termination reduce the degree of polymerization (DP) and increases monomer conversion. Diffusion resistances also enhance the “livingness” of the polymer (by decreasing the termination rate) and therefore decrease the polydispersity index. The model is able to quantify this interesting phenomenon very well.

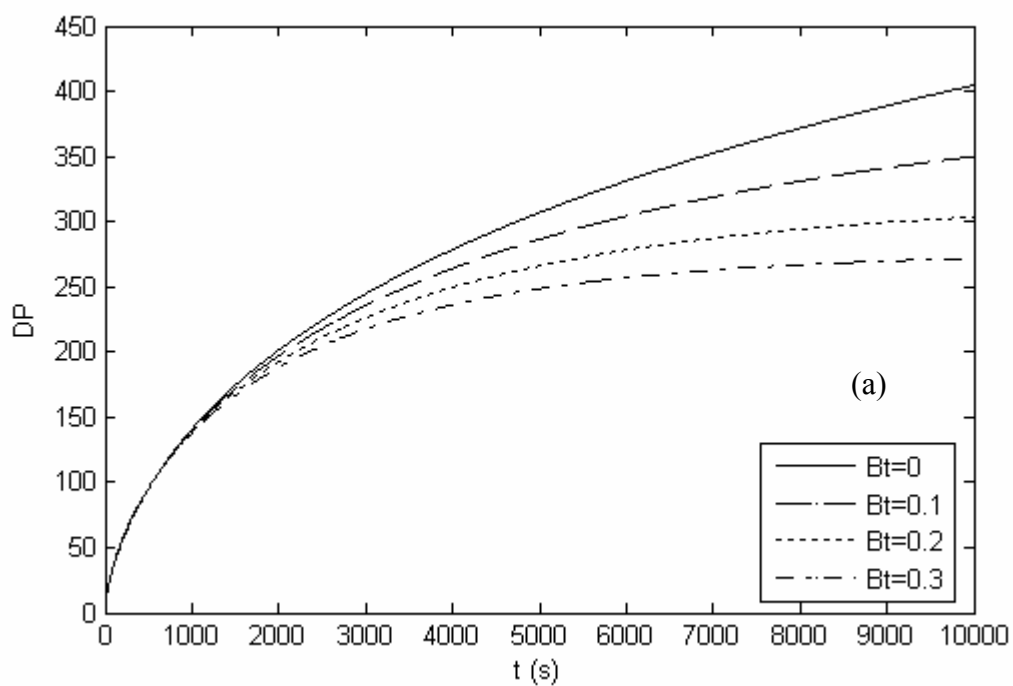
In Figure 6.2, we investigated the effect of varying the free-volume parameter for the deactivation reaction, B_d , with termination diffusion control and setting B_p and B_a to

zero (no diffusion effects for propagation or activation). The reduction of the deactivation rate constant increases both the degree of polymerization and monomer conversion. On the other hand, the polydispersity index increases. Figure 6.3 shows that the opposite is observed if the free volume parameter for the activation reaction, B_a , is varied. These observations are consistent with our knowledge of ATRP: molecular weight control is favored, that is, polymer with smaller polydispersity index is made, and molecular weight and monomer conversion decrease when we shift the equilibrium towards the dormant species. These conclusions would be very difficult to be made without the use of a fundamental mathematical model for this system.

Finally, the effect of diffusion on the propagation rate constant was studied by varying B_p with diffusion limitations for all other the reactions (B_b , B_a and B_d different from zero). The model shows that the effect of diffusion-controlled monomer propagation is to reduce both the molecular weight and monomer conversion and to increase the polydispersity index of the polymer (Figure 6.4).

Table 6.1 Parameters used in ATRP of styrene.

Parameter	Value	References
k_{p0} (L.mol ⁻¹ . s ⁻¹)	$4.266 \times 10^7 \exp(-7769.17/(RT))$	11
k_{tc0} (L.mol ⁻¹ . s ⁻¹)	$(k_{p0}^2) 1.1 \times 10^{-5} \exp(12452.2/(RT))$	12
k_{id0}	0	
$\alpha_m, \alpha_p, \alpha_s$ (K ⁻¹)	0.001, 0.00048, 0.007	13
T_{gm}, T_{gp}, T_{gs} (K)	185, 366.7, 150	13



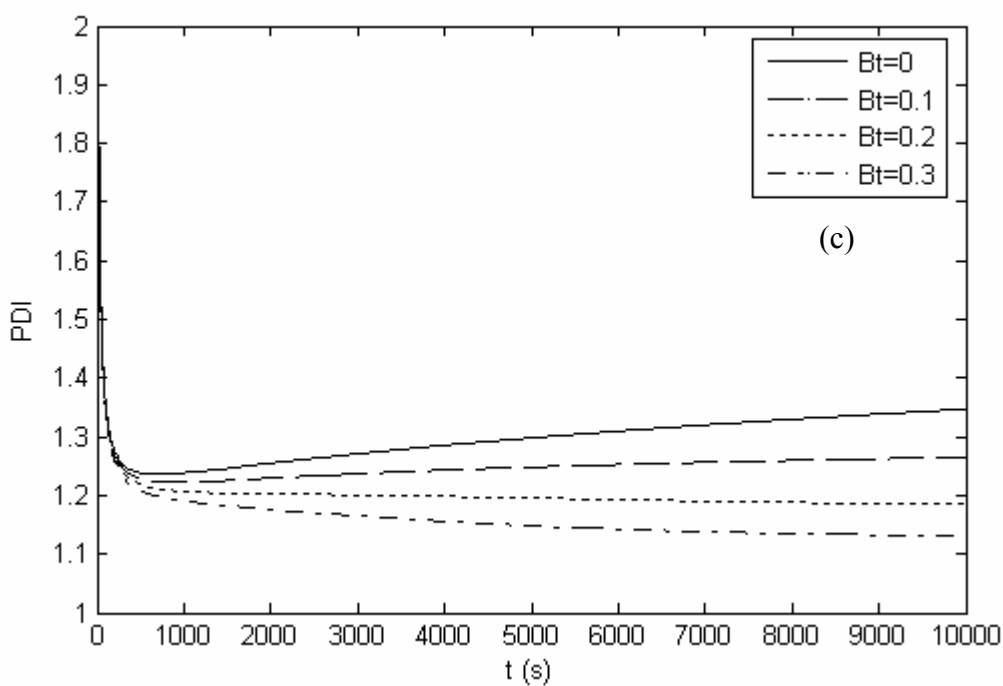
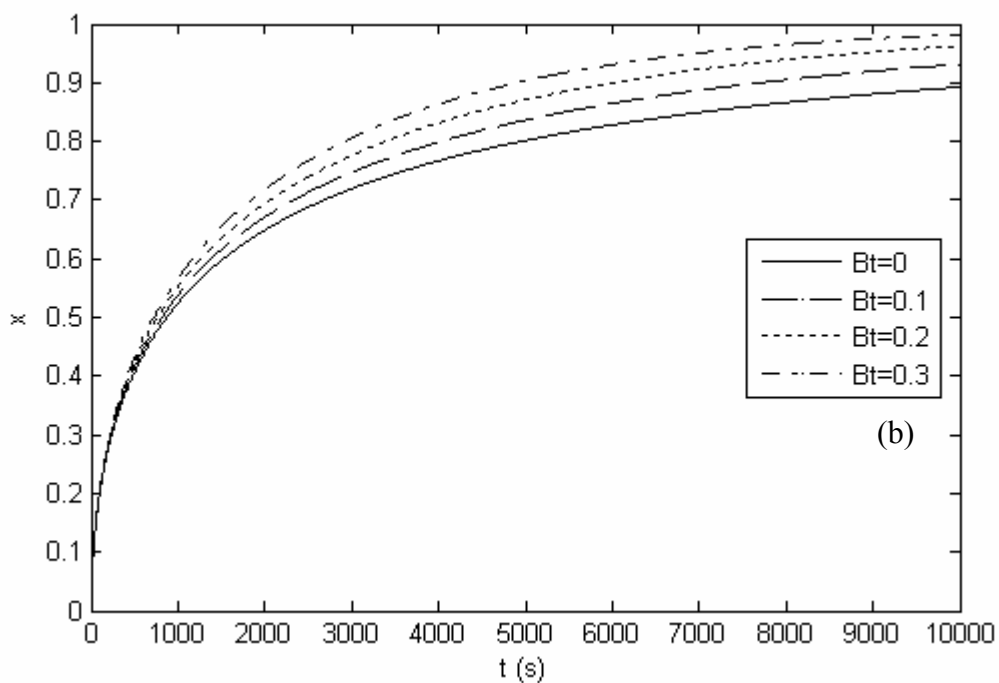
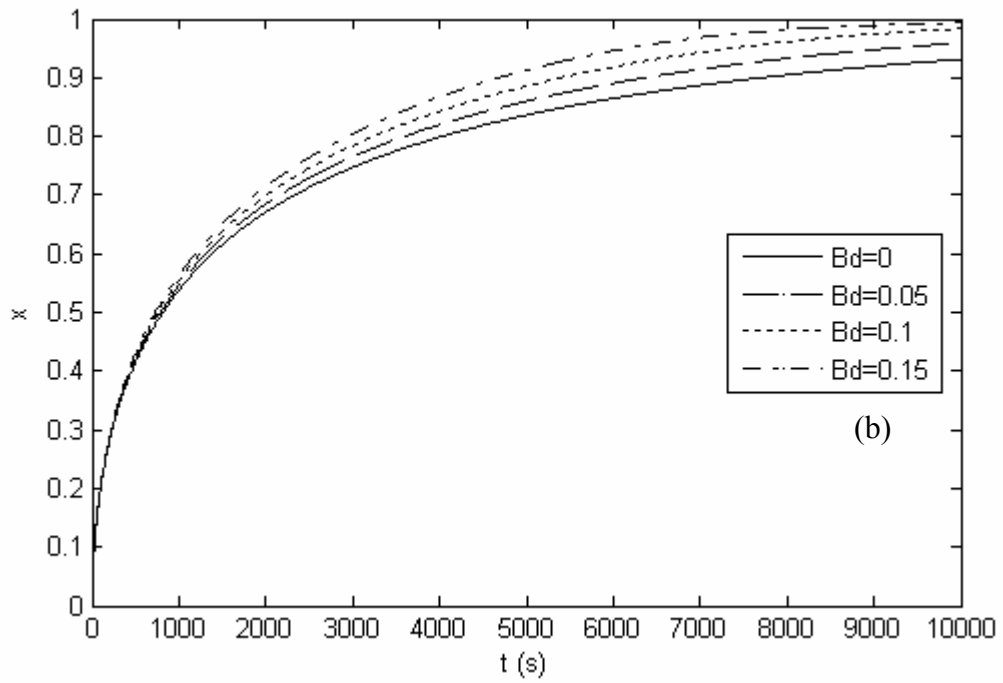
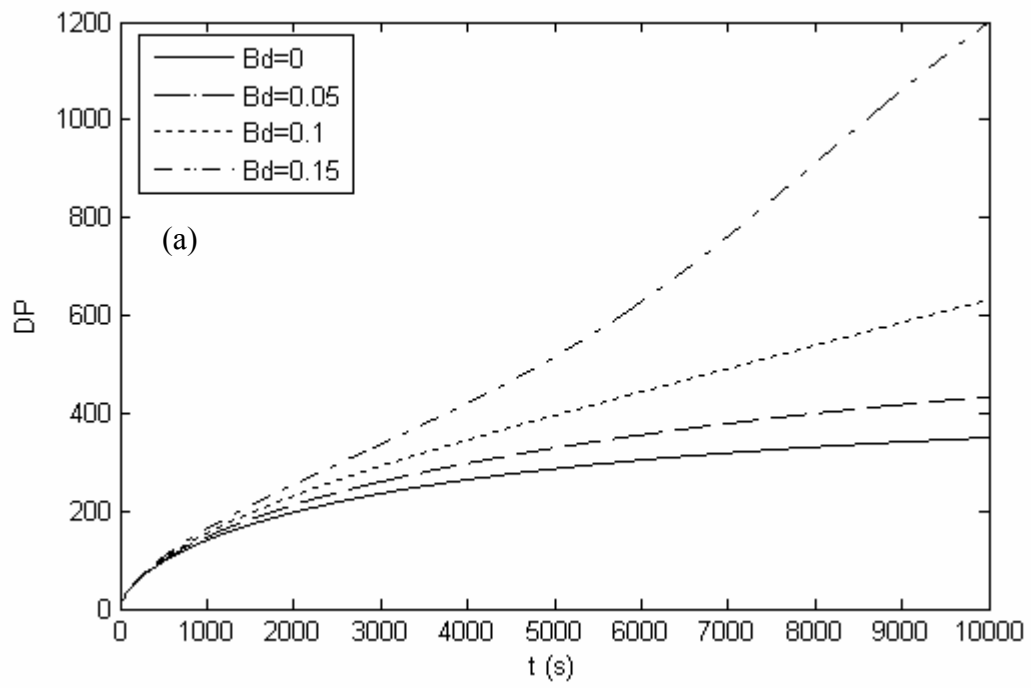


Figure 6.1 Effect of diffusion limitation on the termination rate constant: (a) degree of polymerization, (b) monomer conversion, and (c) polydispersity index. ($B_a = B_d = B_p = 0$, $k_{a0} = 0.5 \text{ L mol}^{-1} \text{ s}^{-1}$, $k_{d0} = 1 \times 10^5 \text{ L mol}^{-1} \text{ s}^{-1}$, $k_{p0} = 1578 \text{ L mol}^{-1} \text{ s}^{-1}$, $k_{tc0} = 3.475 \times 10^8 \text{ L mol}^{-1} \text{ s}^{-1}$, $k_{td0} = 0$, $[C]_0 / [I]_0 / [M]_0$ mole ratio: 2:1:100) Other parameters are shown in Table 6.1.



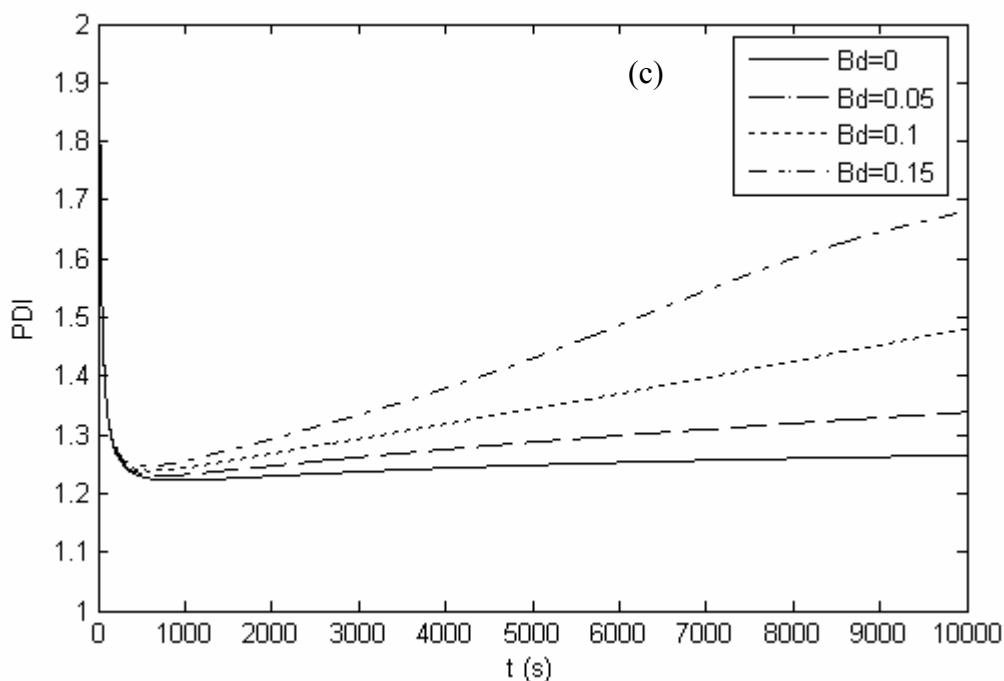
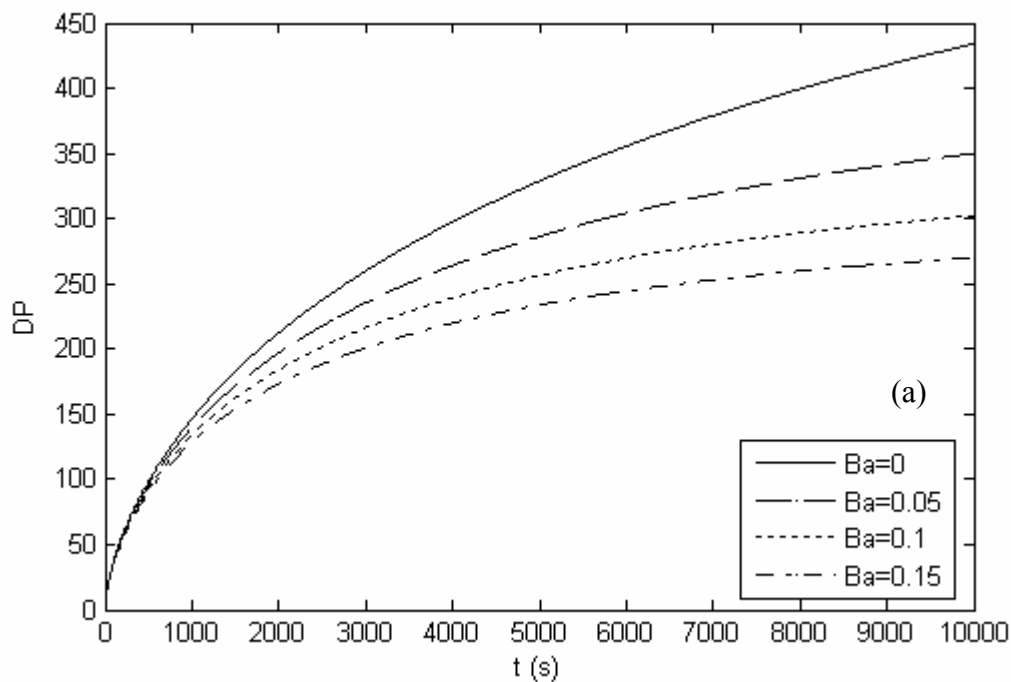


Figure 6.2 Effect of diffusion limitation on the deactivation rate constant: (a) degree of polymerization, (b) monomer conversion, and (c) polydispersity index. ($B_r=0.1$, $B_p=B_a=0$, $k_{a0}=0.5 \text{ L mol}^{-1} \text{ s}^{-1}$, $k_{d0}=1 \times 10^5 \text{ L mol}^{-1} \text{ s}^{-1}$, $k_{p0}=1578 \text{ L mol}^{-1} \text{ s}^{-1}$, $k_{ic0}=3.475 \times 10^8 \text{ L mol}^{-1} \text{ s}^{-1}$, $k_{id0}=0$, $[C]_0/[I]_0/[M]_0$ mole ratio: 2:1:100). Other parameters are shown in Table 6.1.



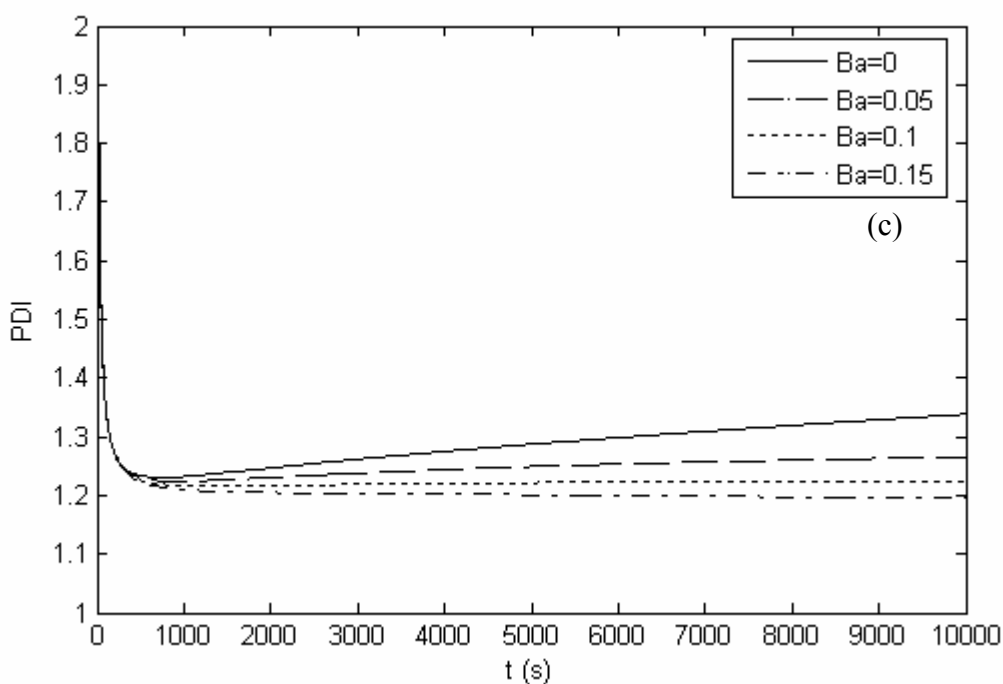
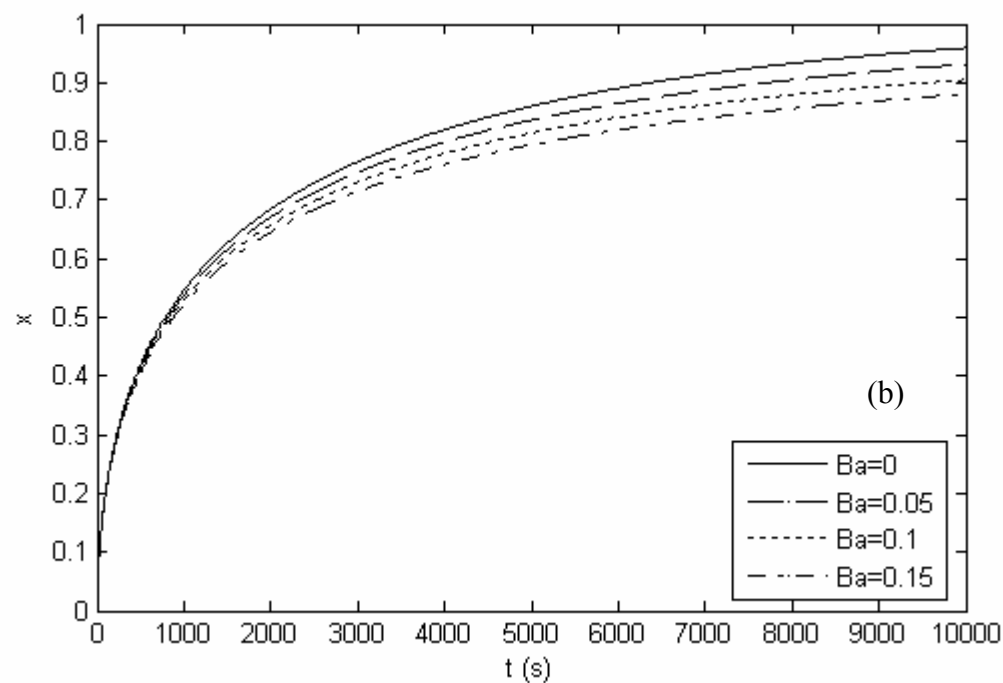
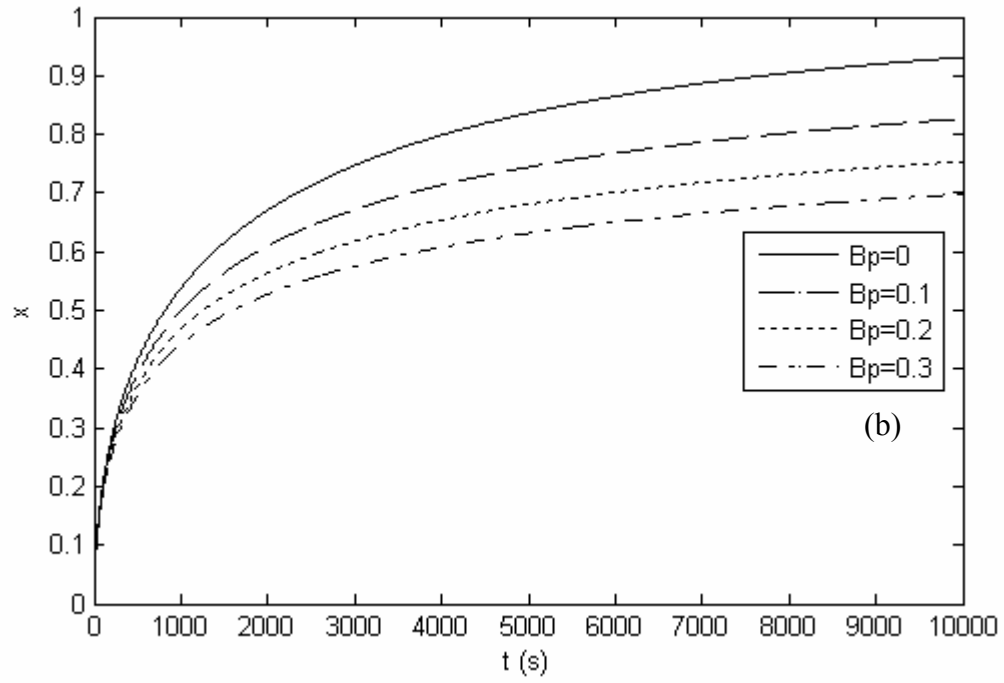
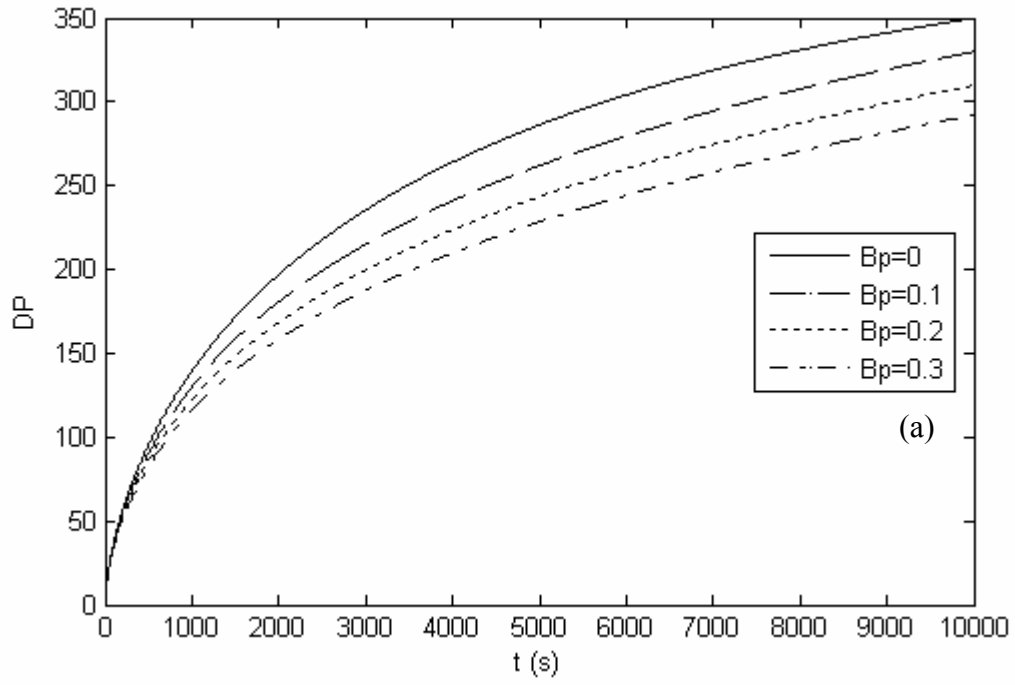


Figure 6.3 Effect of diffusion limitation on the activation rate constant: (a) degree of polymerization, (b) monomer conversion, and (c) polydispersity index. ($B_r=0.1$, $B_p=0$, $B_d=0.05$, $k_{a0}=0.5 \text{ L mol}^{-1} \text{ s}^{-1}$, $k_{d0}=1 \times 10^5 \text{ L mol}^{-1} \text{ s}^{-1}$, $k_{p0}=1578 \text{ L mol}^{-1} \text{ s}^{-1}$, $k_{tc0}=3.475 \times 10^8 \text{ L mol}^{-1} \text{ s}^{-1}$, $k_{td0}=0$, $[C]_0/[I]_0/[M]_0$ mole ratio: 2:1:100). Other parameters are shown in Table 6.1.



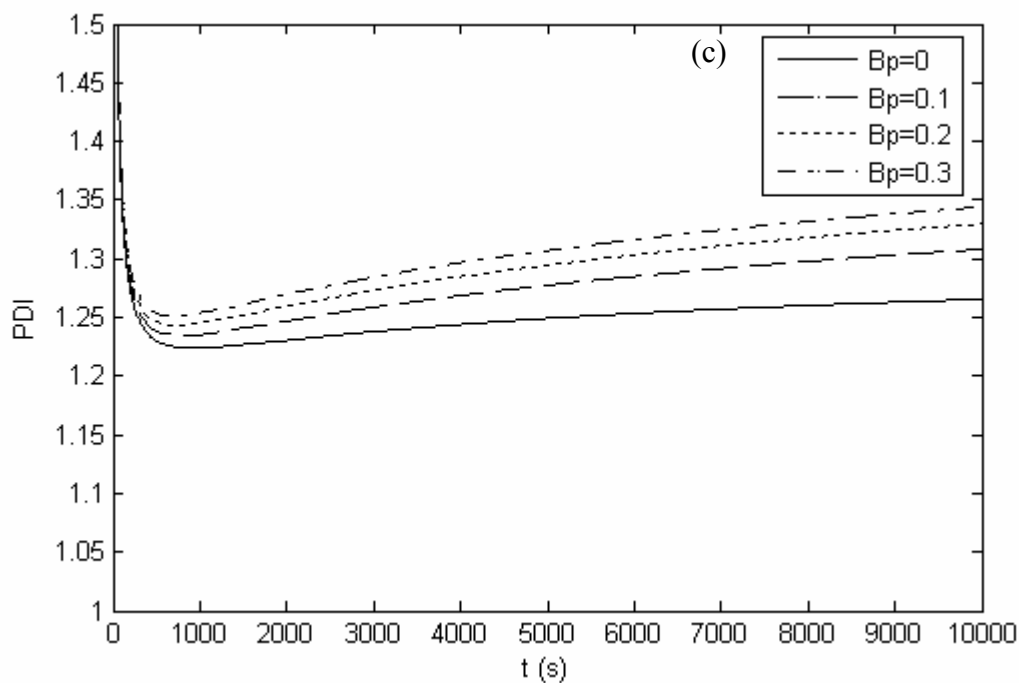


Figure 6.4 Effect of diffusion limitation on the propagation rate constant: (a) degree of polymerization, (b) monomer conversion, and (c) polydispersity index. ($B_a = B_d = 0.5$, $B_t = 0.1$, $k_{a0} = 0.5 \text{ L mol}^{-1} \text{ s}^{-1}$, $k_{d0} = 1 \times 10^5 \text{ L mol}^{-1} \text{ s}^{-1}$, $k_{p0} = 1578 \text{ L mol}^{-1} \text{ s}^{-1}$, $k_{tc0} = 3.475 \times 10^8 \text{ L mol}^{-1} \text{ s}^{-1}$, $k_{td0} = 0$, $[C]_0 / [I]_0 / [M]_0$ mole ratio: 2:1:100). Other parameters are shown in Table 6.1.

6.4.2 Case studies – model validation

The proposed model for ATRP with bifunctional initiators was validated with three case studies for polystyrene, poly(methyl methacrylate) and poly(butyl acrylate) using experimental data from the literature. Both bulk and solution polymerizations were studied. The parameters unavailable in the literature were estimated based on the experimental data. Matlab was used to estimate those unknown parameters using a non-linear least squares routine. The parameters were estimated by minimizing the square of the differences of the monomer conversion based on the following objective function,

$$\chi = \sum_{i=1}^n (x_i^{\text{exp}} - x_i^{\text{pred}})^2 \quad (10)$$

where x_i^{exp} is the experimental and x_i^{pred} is the model-predicted monomer conversion.

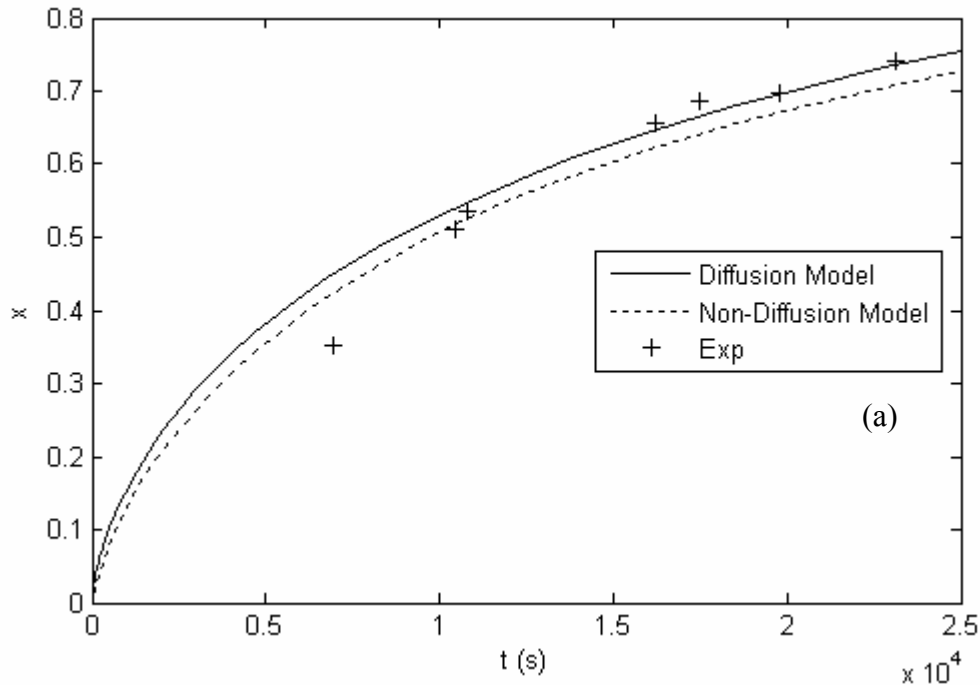
The parameters estimated using the objective function defined in Equation (10) were then used to predict polymer average molecular weight and polydispersity index. No attempt was made to fit molecular weight and polydispersity index data. The results shown in the following figures for these variables are pure model predictions using parameters obtained by fitting monomer conversion only.

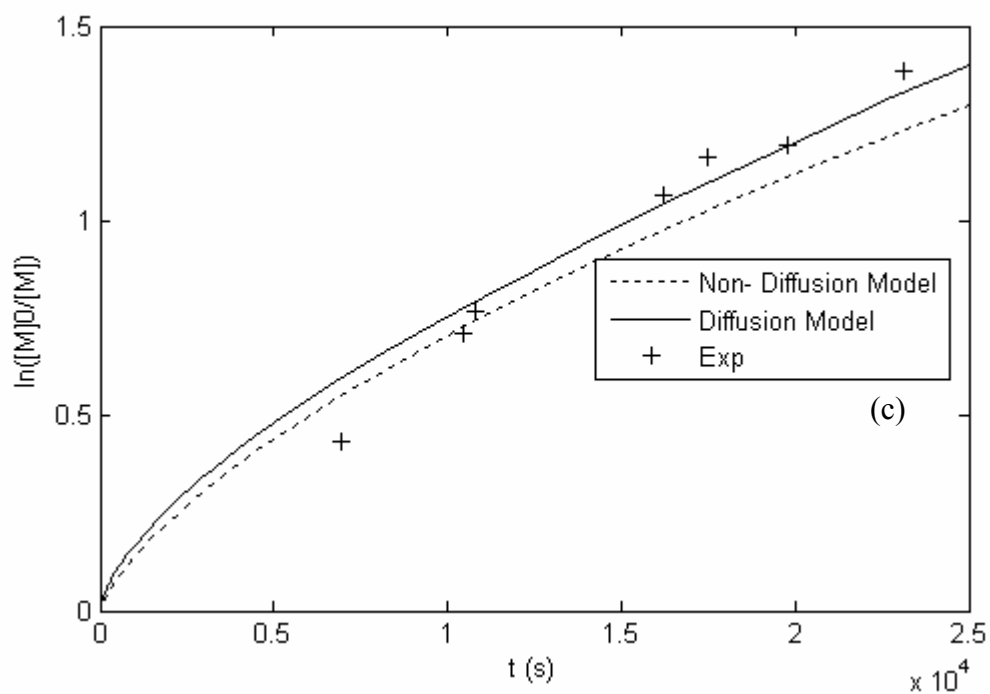
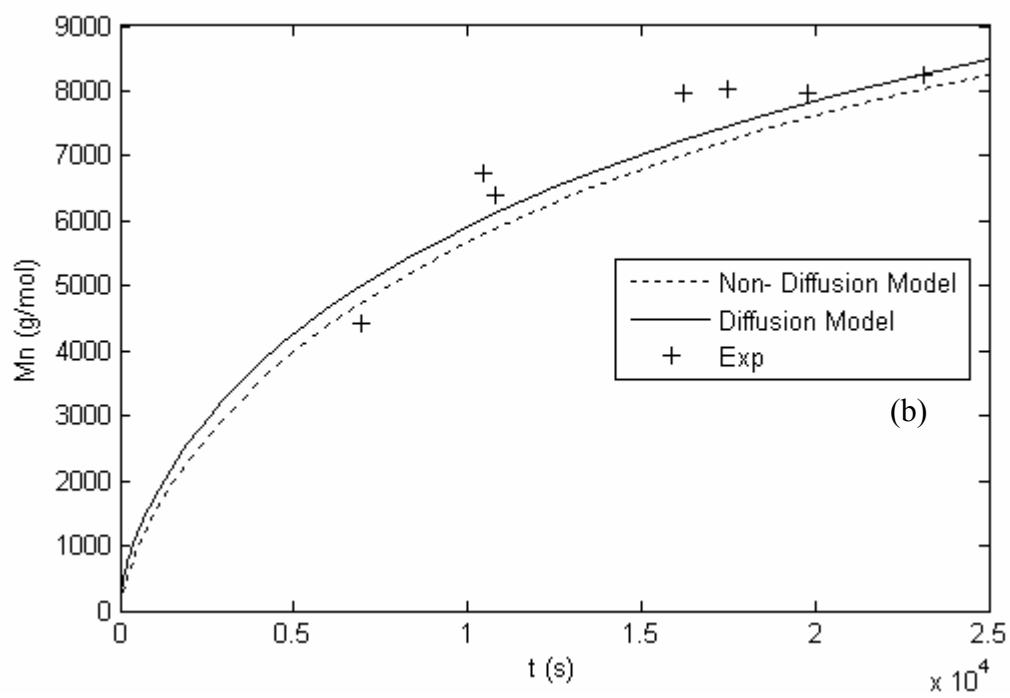
Solution Polymerization of Styrene

Hocker et al. ^[1] used α,α - dichlorotoluene (DCT) as bifunctional initiator for styrene polymerization in butyl acetate. Copper chloride and bipyridine were used as the catalyst and the ligand, respectively. The initial monomer concentration was 4.35 mol/L and the molar ratio of monomer, initiator and catalyst was 100:1:1. Monomer and solvent were kept at a 1:1 volume ratio. The polymerization temperature was 130 °C. The model was validated with the experimental data under the same conditions using the parameters shown in Table 6.1. The model is applicable for symmetrical bifunctional initiators, which is the case for DCT.

ATRP activation and deactivation rate constants are not available in the literature for this system. The parameters calculated in this study using non-linear regression based on the available experimental data were $k_a=0.0225 \text{ L}\cdot\text{mol}^{-1}\cdot\text{s}^{-1}$, and

$k_d = 8.63 \times 10^5 \text{ L.mol}^{-1}.\text{s}^{-1}$. Since this case study involves solution polymerization, we considered that the activation, deactivation and propagation reactions should not be affected by diffusion limitations. We also assumed that the termination rate constant might be affected at high conversion by diffusion limitations. We found out that, under these conditions, setting the parameters B_p , B_a and B_d to zero and B_t to 1.02 led to a good representation of the experimental data (Figure 6.5). Both diffusion and non-diffusion models were compared with the experimental results. Despite the scatter in the experimental data, both models fit the results well. Although, the non-diffusion model predictions are good, the diffusion model may fit the data slightly better for all variables shown in Figure 6.5. It is, however, hard to decide which model is more adequate based on these small differences.





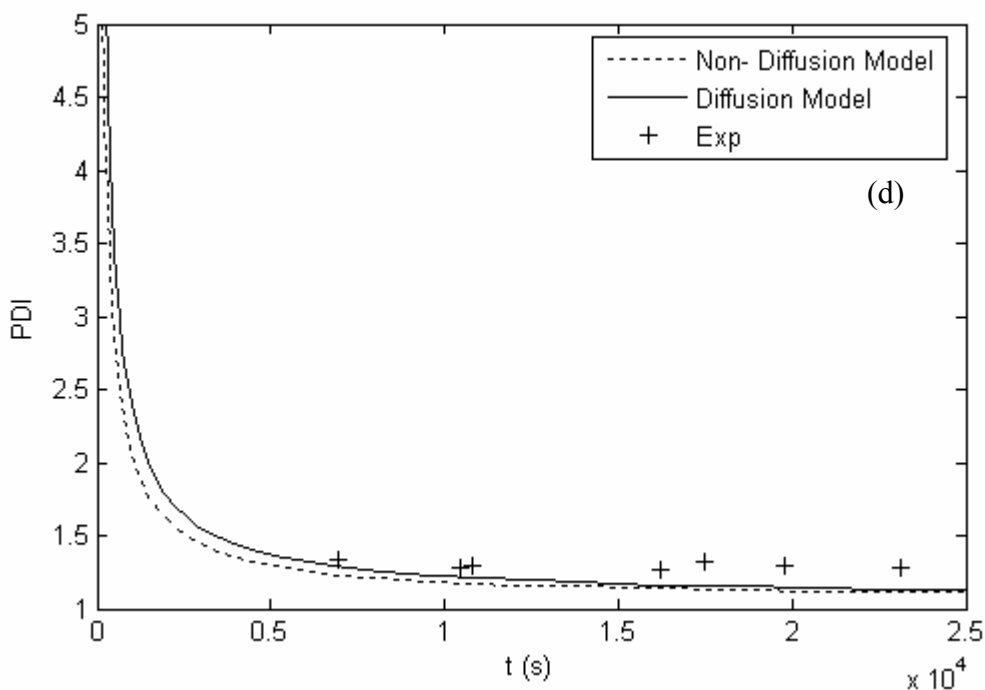


Figure 6.5 Comparison between model predictions and experimental data for styrene polymerization in butyl acetate at 130 °C with DCT as initiator: (a) monomer conversion, (b) number average molecular weight, (c) $\ln([M_0]/[M])$, and (d) polydispersity. (Polymerization conditions: $[St]_0=4.35$ mol/L, $[St]/[I]/[Cat]=100:1:1$ (molar ratio), reaction temperature $T=130$ °C. Kinetic parameters are shown in Table 6.1). Experimental data from Hocker et al. ^[1]

Solution Polymerization of Methyl Methacrylate (MMA)

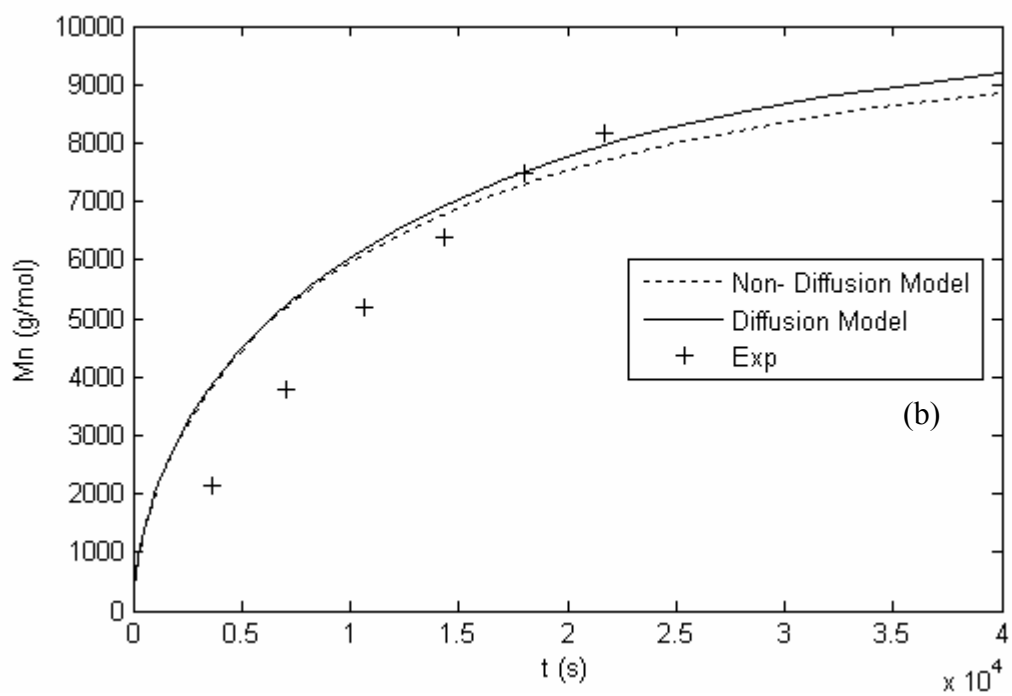
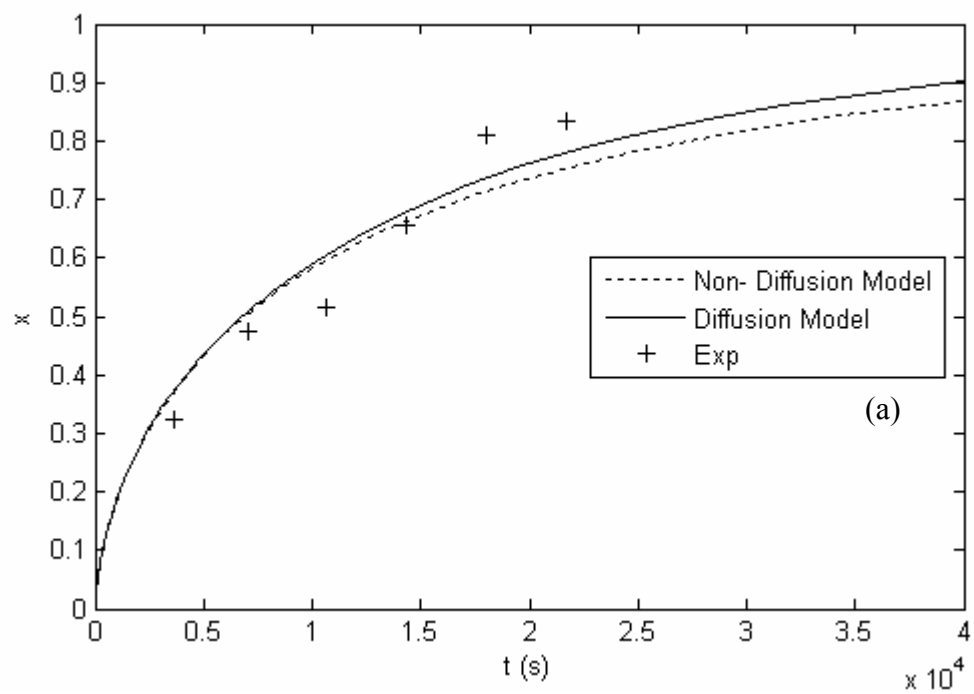
Vlcek et al. ^[2] published experimental results of ATRP of MMA with a bifunctional initiator. MMA polymerization was initiated with 1,3-bis{1-methyl-[(2,2,2-trichloroethoxy) carbonylamino]ethyl} benzene using CuCl/hexamethyltriethylenetetramine as ATRP catalyst. An amount of 18.7 mmol of MMA was polymerized at 90 °C in an equal volume of toluene as solvent. The molar ratio of monomer, initiator and catalyst was 100:1:1.

The proposed model was fitted to the experimental results using the polymerization kinetic parameters for MMA shown in Table 6.2. Since the polymerization takes place in toluene, we expected that the diffusion effects would be negligible for activation, deactivation and propagation reactions, but they might be important for chain termination. Therefore the adjustable parameters B_p , B_a , and B_d were

set to zero and B_t was estimated to fit the experimental data. Figure 6.6 shows that, under these conditions, both models fit the experimental results well. As for the case of styrene polymerization, it is difficult to decide which model is more adequate to describe the polymerization.

Table 6.2 Parameters used in solution ATRP of MMA at 90 °C.

Parameter	Value	References
k_{p0} (L.mol ⁻¹ . s ⁻¹)	1616	14
k_{tc0} (L.mol ⁻¹ . s ⁻¹)	1x10 ⁷	15
k_{td0} (L.mol ⁻¹ . s ⁻¹)	9.21x10 ⁷	15
k_{a0} (L.mol ⁻¹ . s ⁻¹)	0.081	This study
k_{d0} (L.mol ⁻¹ . s ⁻¹)	3.05x10 ⁵	This study
B_p	0	This study
B_t	1.53	This study
B_a	0	This study
B_d	0	This study
$\alpha_m, \alpha_p, \alpha_s$ (K ⁻¹)	0.001, 0.00048, 0.007	15
T_{gm}, T_{gp}, T_{gs} (K)	167, 387, 170	15



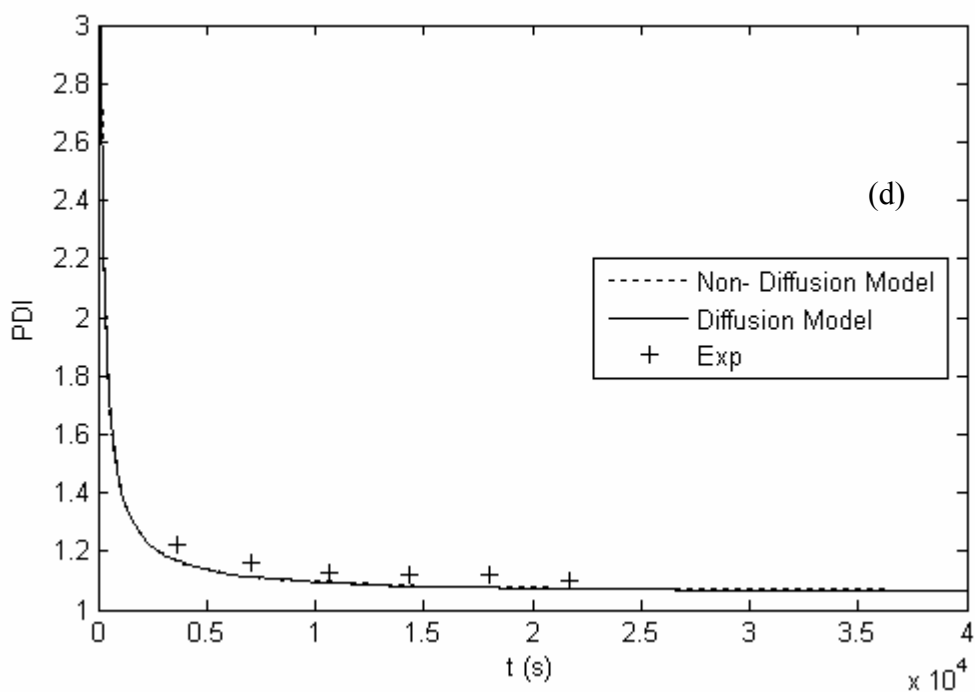
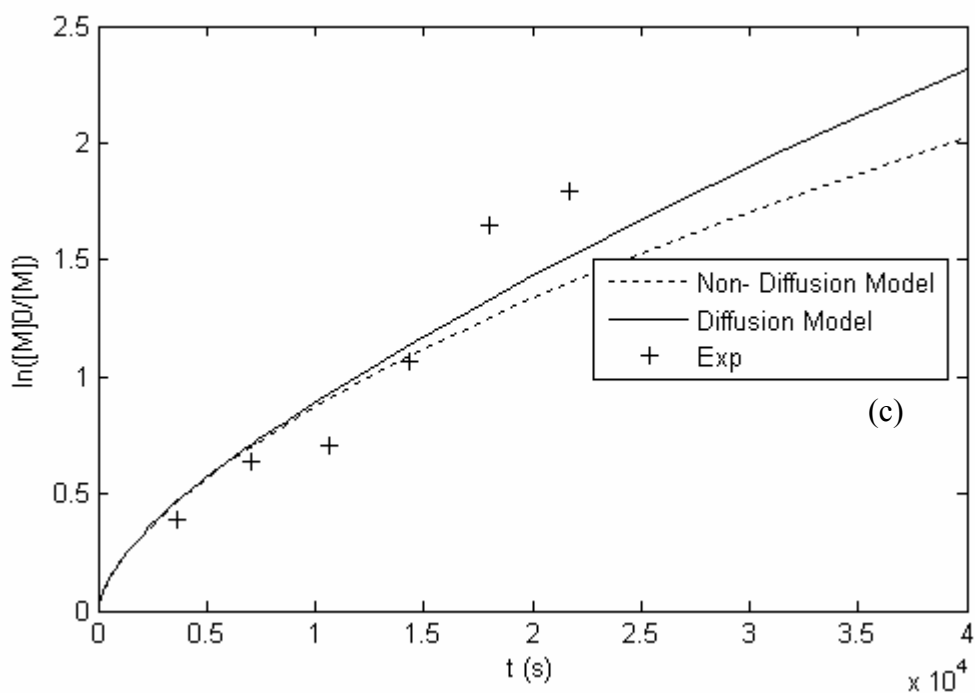


Figure 6.6 Comparison between model predictions and experimental data for ATRP of methyl methacrylate in toluene at 90 °C with 1,3-bis{1-methyl-[(2,2,2-trichloroethoxy) carbonylamino]ethyl} benzene as initiator: (a) monomer conversion, (b) number average molecular weight, (c) $\ln([M]_0/[M])$, and (d) polydispersity. (Polymerization conditions: $[MMA]_0=4.5$ mol/L, $[MMA]/[I]/[Cat]=100:1:1$ (molar ratio), reaction temperature $T=90$ °C. Kinetic parameters are given in Table 6.2). Experimental data from Vlcek et al.^[2]

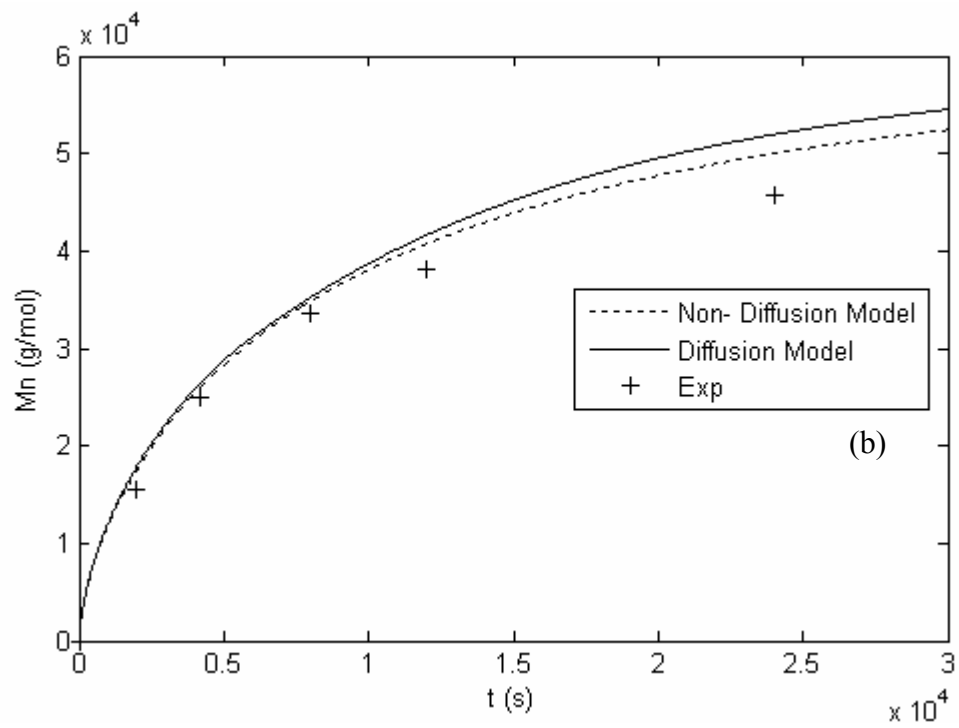
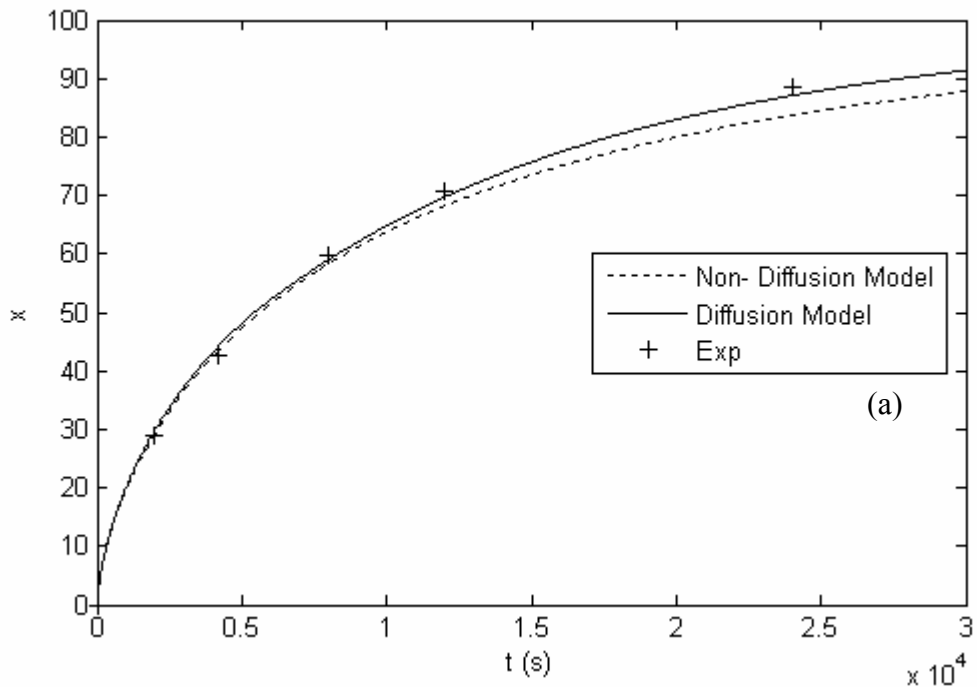
Bulk Polymerization of n-butyl acrylate (n-BA)

Matyjaszewski et. al.^[3] synthesized poly(*n*-butyl acrylate) with multifunctional initiators (bi-, tri- and tetrafunctional). To validate our model, we used their experimental data for bulk polymerization of *n*-butyl acrylate at 90 °C with the bifunctional initiator ethylene glycol bis(2-bromopropionate). The monomer, initiator and catalyst mole ratios were 465:1:1 respectively.

The model predicts the activation and deactivation constants that fit the experimental data. Since this polymerization was done in bulk, all the adjustable parameters (B_t , B_p , B_a and B_d) were estimated using the model. As for the two previous case studies, the parameter estimation is based on monomer conversion only. All the estimated parameters and the kinetic constants are shown in Table 6.3. Figure 6.7 shows the model predictions with and without diffusion limitations. Both models agree very well with the experimental results but the model with diffusion limitations is slightly better than the one that neglects diffusion effects for monomer conversion (Figures 6.7a and 6.7c). In Figure 6.7b, molecular weight versus time, the non-diffusion predictions are closer to the experimental data. Both models give similar predictions to polydispersity index (Figure 6.7d). Once again, it is not possible to discriminate with a great degree of certainty between the two models.

From a practical point of view, since the model that neglects diffusion limitations has a similar performance to but fewer adjustable parameters than the model that considers the free volume theory correction to the kinetic constants, using the simpler model is recommended. More experimental data for bulk ATRP at high monomer conversions will be required to evaluate if a diffusion-limited model is required for these systems, but the results of this investigation indicate that they can be neglected for the sake of simplicity.

It is also interesting to notice that the model predicts molecular weight averages and polydispersity index very well from the monomer conversion data and the polymerization kinetic parameters available in the literature. Therefore, one can rely on the mathematical model to predict these polymer properties and decrease the number of experiments needed to evaluate these ATRP systems.



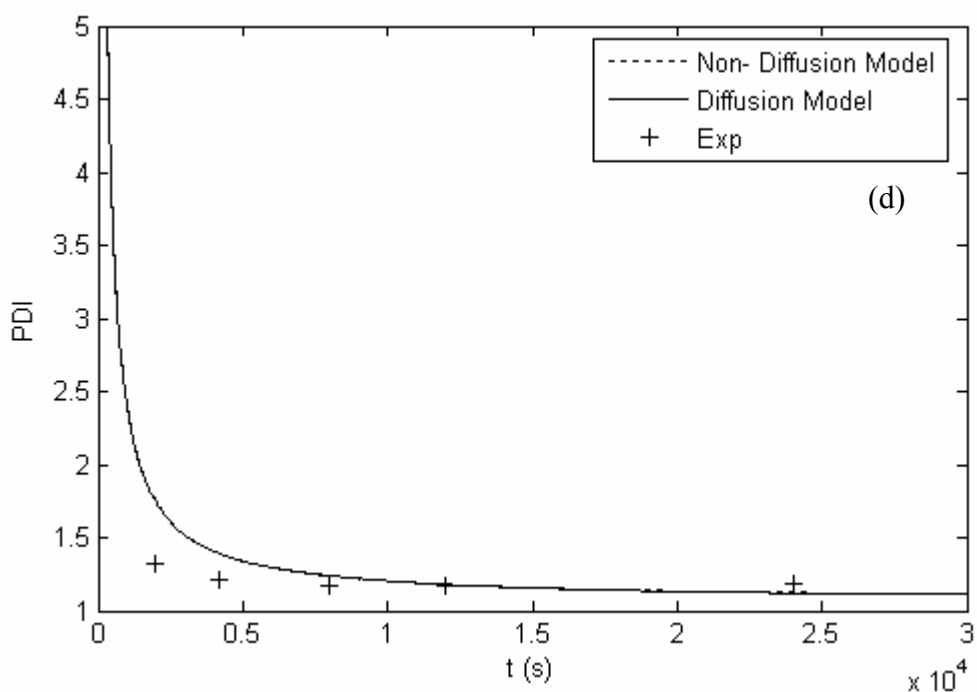
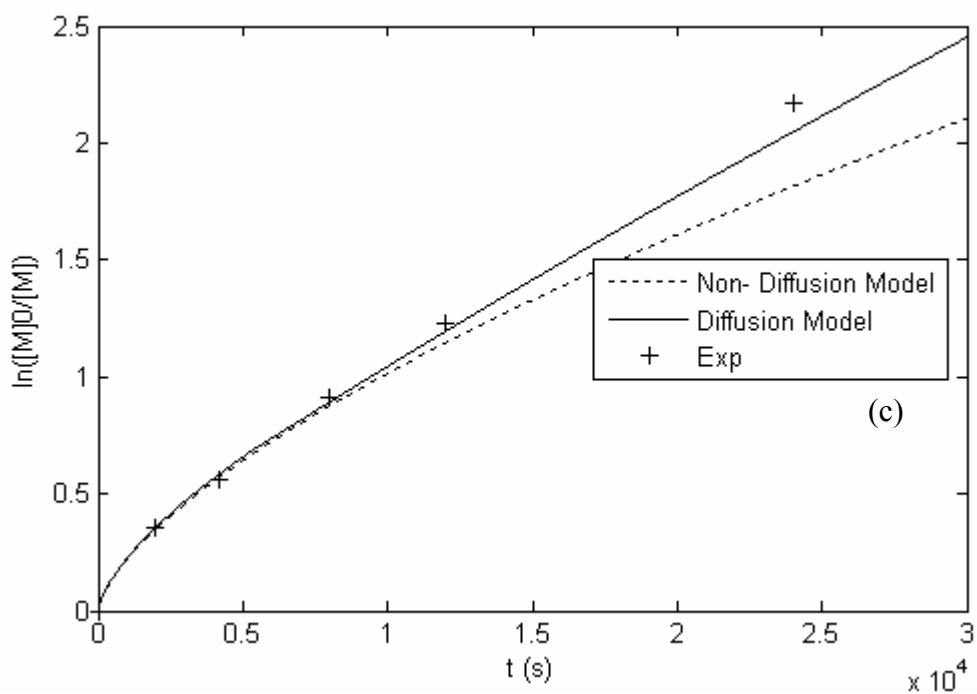


Figure 6.7 Comparison between model predictions and experimental data for n-BA polymerization in bulk at 90 °C: (a) monomer conversion, (b) number average molecular weight, (c) $\ln([M]_0/[M])$, and (d) polydispersity. (Polymerization conditions: $[M]/[I]/[Cat]=465:1:1$ (molar ratio), reaction temperature $T=90$ °C. Kinetic parameters are shown in Table 6.3). Experimental data from Matyjaszewski et. al. ^[3]

Table 6.3 Parameters used in bulk ATRP of n-BA at 90 °C.

Parameter	Value	References
k_{p0} (L.mol ⁻¹ . s ⁻¹)	3.05e4	16
k_{tc0} (L.mol ⁻¹ . s ⁻¹)	1.218e8	16
k_{td0}	0	
k_{a0} (L.mol ⁻¹ . s ⁻¹)	0.2	This study
k_{d0} (L.mol ⁻¹ . s ⁻¹)	5e8	This study
B_p	0.15	This study
B_t	5	This study
B_a	0.1	This study
B_d	0.2	This study
α_m, α_p (K ⁻¹)	1.19e-3; 0.00048;	15
T_{gm}, T_{gp} , (K)	185.15; 218;	15

6.5 Conclusions

A comprehensive mathematical model was developed for ATRP with symmetrical bifunctional initiators. The model was validated with experimental data obtained from the literature for the polymerization of styrene (solution), methyl methacrylate (solution), and n-butyl acrylate (bulk). The good agreement between experimental and simulation results show that the model can predict the time evolution of monomer conversion, molecular weight and polydispersity index. Diffusion limitations to rate constants were incorporated into the model using the free volume theory. The parameter sensitivity analysis showed that the diffusion effects enhance the livingness of the system by minimizing termination reactions. This interesting theoretical result can

only be quantified using a fundamental mathematical model such as the one proposed in this paper.

Both models, including and ignoring diffusion limitations on the rate constants, fit the experimental data for conversion well and can predict molecular weight and polydispersity index as a function of polymerization time. With the experimental data available to us in this study it is difficult to conclude which model performs better, but the model neglecting diffusion limitations seems to be preferable because of its simplicity. More experimental data for bulk polymerization at high monomer conversions is required to evaluate whether diffusion limitations may play a significant role in ATRP.

6.6 References

- [1] A. Neumann, H. Keul, H. Hocker, *Macromol. Chem. Phys.* **2000**, 201, 980.
- [2] A. Malinowska, P. Vlcek, J Kriz, L. Toman, P. Latalova, M. Janata, B. Masar, *Polymer* **2005**, 46, 5.
- [3] K. Matyjaszewski, P. Miller, J. Pyum, G. Kickelbick, S. Diamanti, *Macromolecules* **1999**, 32, 6526.
- [4] J. Vrentas, *J. Polym. Sci, Part B: Polym. Phys.* **1977**, 15, 403.
- [5] F. Marten, E. Hamielec, *ACS Symp. Ser.* **1979**, 104, 43.
- [6] M. Zhang, H. Ray, *J. Appl. Polym. Sci.* **2002**, 86, 1630.
- [7] M. Zhang, H. Ray, *J. Appl. Polym. Sci.* **2002**, 86, 1047.
- [8] A. Shipp, K. Matyjaszewski, *Macromolecules* **1999**, 32, 2948.
- [9] O. Delgadillo-Velazquez, E. Vivaldo-Lima, I. Quintero-Ortega, S. Zhu, *AIChE J.I* **2002**, 48, 11, 2597.
- [10] E. Vivaldo-Lima, A. Mendoza-Fuentes, *Polym. React. Eng.* **2002**, 4, 10, 193.
- [11] M. Buback, R. Gilbert, R. Hutchinson, B. Klumperman, F. Kuchata, B. Manders, K. O'Driscoll, G. Russell, J. Schweer, *Macromol. Chem. Phys.* **1995**, 196, 3267.
- [12] A. Hui, E. Hamielec, *J. Appl. Polym. Sci.* **1976**, 16, 749.
- [13] E. Vivaldo-Lima, E. Hamielec, P. Wood, *Polym. React. Eng.* **1994**, 2, 16.
- [14] D. Achilias, C. Kiparissides, *Macromolecules* **1992**, 25, 3739.
- [15] E. Vivaldo-Lima, R. Garcia-Perez, O. Celedon-Briones, *Rev. Soc. Quim. Mex.* **2003**, 47, 1, 22..
- [16] S. Beuermann, D. Paquet, J. McMinn, R. Hutchinson, *Macromolecules* **1992**, 29, 4206

Chapter 7

7 Dynamic Monte Carlo Simulation of ATRP with Bifunctional Initiators*

7.1 Abstract

A dynamic Monte Carlo model was developed to simulate atom-transfer radical polymerization (ATRP) with bifunctional initiators in a batch reactor. Model probabilities were calculated from polymerization kinetic parameters and reactor conditions. The model was used to predict monomer conversion, average molecular weight, polydispersity index and the complete chain length distribution (CLD) as a function of polymerization time. The Monte Carlo model was compared with simulation results from a mathematical model that uses population balances and the method of moments. We also compared polymerizations with monofunctional and bifunctional initiators to illustrate some of the advantages of using bifunctional initiators in ATRP. In addition, we used the model to investigate the effect of the control volume and several polymerization conditions on simulation time, monomer conversion, molecular weight averages and CLD. Our results indicate that computational times can be reduced without sacrificing the quality of the results if we run several simulations with small control volumes rather than one single simulation with a large control volume.

* This chapter is in print: M. Al-Harhi, J. Soares, L. Simon, *Macromol. React. Eng.* **2006**

7.2 Introduction

Previous chapters (5 and 6) contain mathematical modeling of bifunctional initiators using population balances and the method of moments. Monte Carlo simulation can give more interesting results by predicting the full molecular weight distribution as shown in the monofunctional initiator (chapter 4).

In this Chapter, Monte Carlo simulation is used to predict monomer conversion, polymerization time, molecular weight averages, polydispersity index, and the complete chain length distribution (CLD) of polymers made with ATRP with bifunctional initiators. In addition, we will compare ATRP with monofunctional and bifunctional initiators.

7.3 Model description

The dynamic Monte Carlo methodology adopted in this study is based on Gillespie's algorithm.^[1] The algorithm is defined in detail in chapter 4.

The elementary reaction steps of ATRP with bifunctional initiators used in the model are listed in chapter 5. For the sake of continuity and to connect it to the flow chart of the simulation, the mechanism is presented again in this chapter (Equations (1) to (21)).

Activation



Deactivation



Propagation



Termination



In the equations above, C is the catalyst in its lower oxidation state, CX is the catalyst in its higher oxidation state, M is the monomer, DD is a chain with two dormant ends, DR is a chain with a dormant end and a free-radical end, RR is a chain with two free-radical ends, PP is a chain with two dead ends, PD is a chain with a dormant end and a dead end, PR is a chain with a free-radical end, k_p is the propagation rate constant, k_{tc} is the rate constant of termination by combination, k_{td} is the rate constant of termination by disproportionation, k_a is the activation rate constant, k_d is the deactivation rate constant,

k_{tr} is the transfer rate constant, and the subscripts r and i indicates the number of monomer molecules in the chain.

The polymerization mechanism described in Equations (1) to (21) was used to make the flowsheet for the Monte Carlo simulation procedure adopted in this investigation, shown in Figure 7.1.

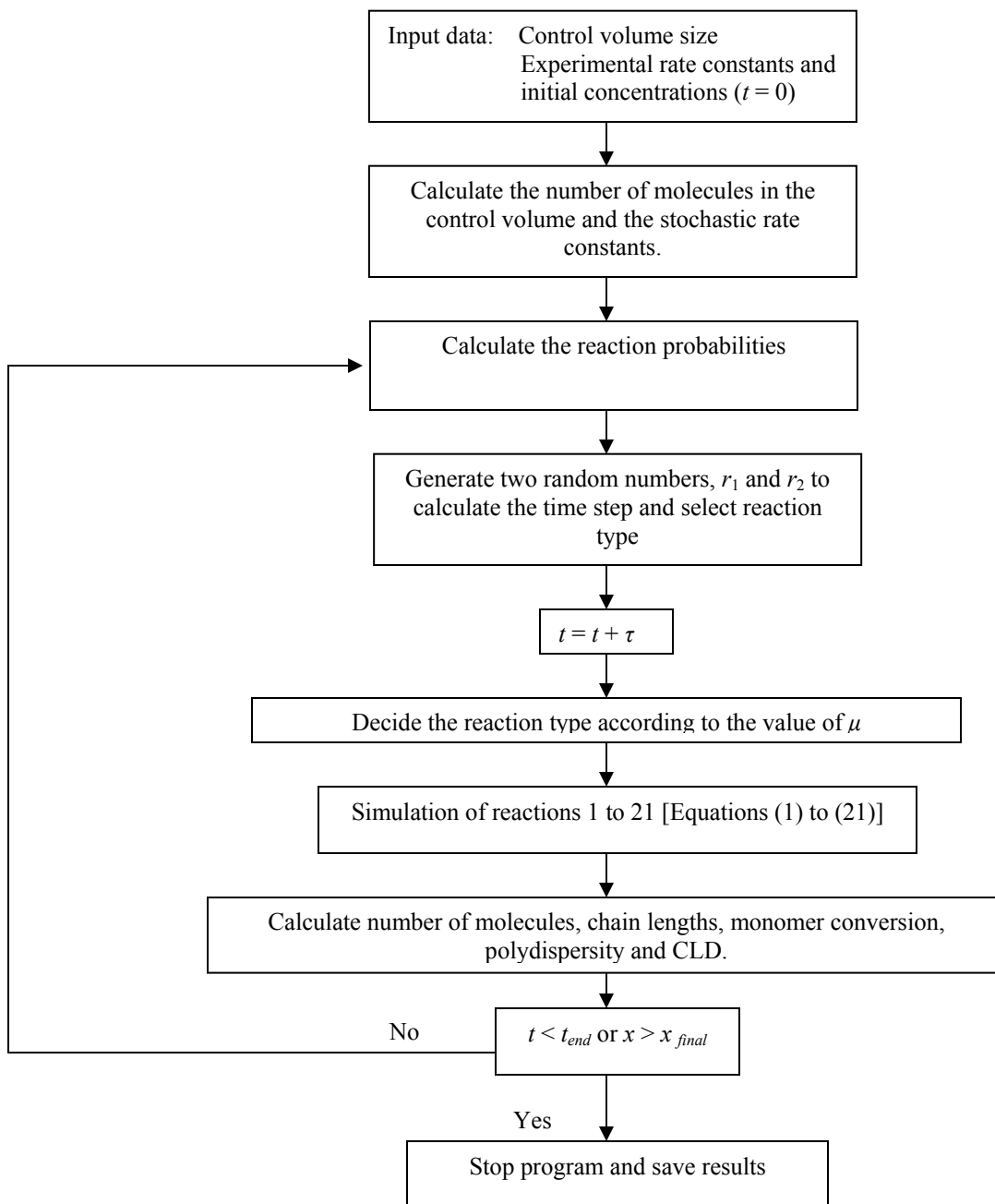


Figure 7.1 Algorithm for Monte Carlo simulation of ATRP with bifunctional initiators.

A microcomputer (Intel (R) Pentium(R) 4 with 2.8 GHz processor and 504 MB of RAM) was used in the simulations. The program was written in MATLAB version 7.

7.3.1 Kinetics parameters

Our simulation is based on probabilities calculated from polymerization kinetic parameters and reactant concentrations. In free-radical polymerization, kinetic parameters depend on monomer type and polymerization temperature. Diffusion limitations may affect the kinetic parameters, especially at high monomer conversions in bulk polymerization. The values of k_p and k_t for most commonly used monomers are in the range of 10^2 - 10^4 L/mol.s and 10^6 - 10^8 L/mol.s, respectively. [2] We will perform our simulations using parameters in this range of values.

There is more uncertainty on the values of the constants k_a and k_d for ATRP. However, recent experimental studies[3] and parameter estimations[4-6] of the equilibrium constants k_a and k_d give us an idea of the range of these parameters. In our simulations, the values of the kinetic parameters were chosen so that they fell within these ranges (see Table 7.1). All polymerization kinetic constants were kept constant during the simulations, that is, we neglected diffusion effects in all our simulations.

Table 7.1 Kinetic parameters and initial concentrations used in the simulations

Parameter	Simulation value	Reported range [2]
k_p (L mol ⁻¹ s ⁻¹)	1000	10^2 - 10^4 L/mol.s
k_{tc} (L mol ⁻¹ s ⁻¹)	1×10^7	10^6 - 10^8 L/mol.s
k_{td} (L mol ⁻¹ s ⁻¹)	0	
k_a (L mol ⁻¹ s ⁻¹)	0.1	
k_d (L mol ⁻¹ s ⁻¹)	1×10^6 (unless mentioned otherwise)	
$[M]_0$ (mol L ⁻¹)	4.35	
$[C]_0$ (mol L ⁻¹)	0.043	
$[I]_0$ (mol L ⁻¹)	0.043	

7.4 Results and discussion

7.4.1 Comparison of Monte Carlo simulation with the method of moments

We validated our Monte Carlo simulation by comparing its results with those calculated using a model based on the method of moments.^[7] Excellent agreement between both techniques for monomer conversion, number average chain length and polydispersity index is demonstrated in Figures 7.2.a to 7.2.c. The linear relation between the degree of polymerization and monomer conversion (Figure 7.2.b), and the low polydispersity index (approaching unity in Figure 7.2.c) are indications of the living polymerization mechanism in ATRP.

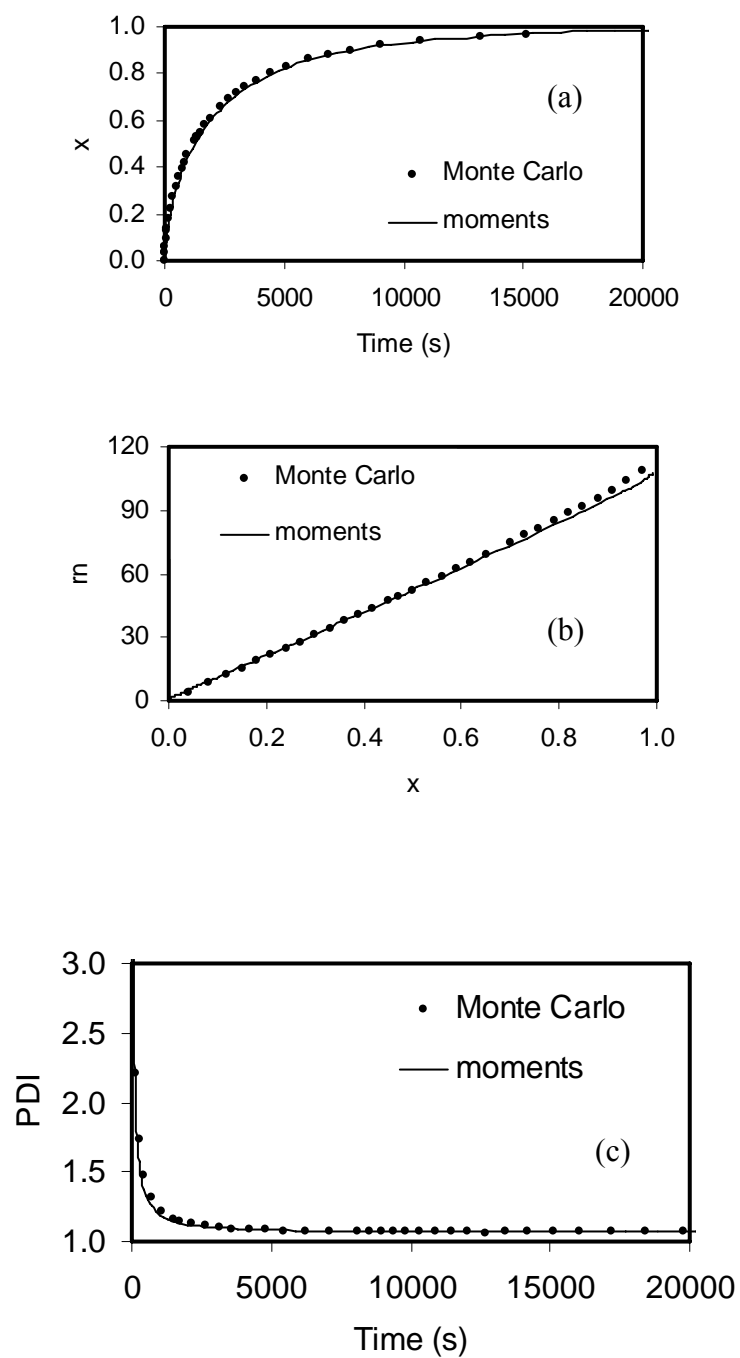


Figure 7.2 Comparison between Monte Carlo simulation and method of moments for isothermal batch polymerization: (a) monomer conversion, (b) number average chain length, (c) polydispersity index ($V = 1 \times 10^{-19}$ L).

7.4.2 Comparison between monofunctional and bifunctional initiators

The advantages of bifunctional initiators over monofunctional initiators in conventional free radical polymerization are well known.^[8] Bifunctional initiators can, for instance, be used to increase polymerization rate and polymer molecular weights simultaneously. In addition, the CLD is narrower for polymers made with bifunctional initiators. Both experimental^[9] and mathematical modeling studies^[7] confirm that these advantages are also applicable to ATRP.

Figures 7.3 to 7.6 illustrate these attractive properties of bifunctional initiators using our Monte Carlo model for ATRP. Since bifunctional initiators, unlike monofunctional initiators, can grow in both directions, they can produce polymers at higher polymerization rates and with higher average molecular weights than monofunctional initiators. The higher polymerization rate of bifunctional initiators is reflected in the higher monomer conversion for a given polymerization time in Figure 7.3, whereas Figure 7.4.a shows that polymers made with the bifunctional initiator reach higher number average chain lengths for the same polymerization time. The linear relation between number average chain length and monomer conversion (Figure 7.4.b) agrees with the living characters of these polymerizations.

Polymers made with bifunctional initiators have smaller polydispersity indices since the very beginning of the polymerization, as illustrated in Figure 7.5. Notice how it takes a much longer time for polymers made with monofunctional initiators to reach low polydispersity indices.

These results are very convincingly displayed when comparing the CLDs of polymers made by mono- and bifunctional initiators in Figure 7.6. It is also interesting to see how the CLD changes as a function of monomer conversion or polymerization time in Figure 7.7.

The termination reactions in monofunctional initiators form dead polymers that can not grow any more and broaden the distribution. On the other hand, termination reactions in bifunctional initiators do not stop the growth of the terminated chains. This phenomenon explains the low polydispersity index in the bifunctional initiators.

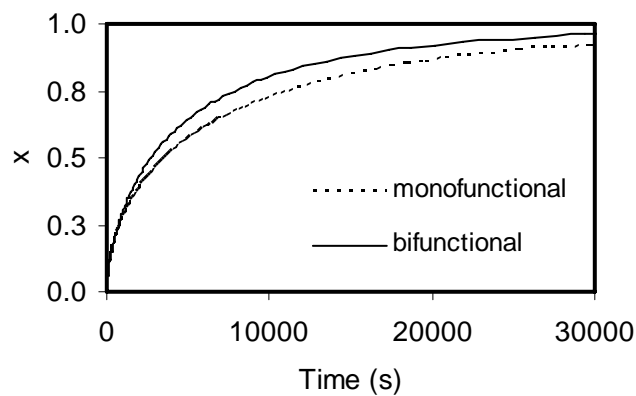


Figure 7.3 Comparison between mono- and bifunctional initiators: monomer conversion (x) as a function of time. ($V = 1 \times 10^{-19}$ L).

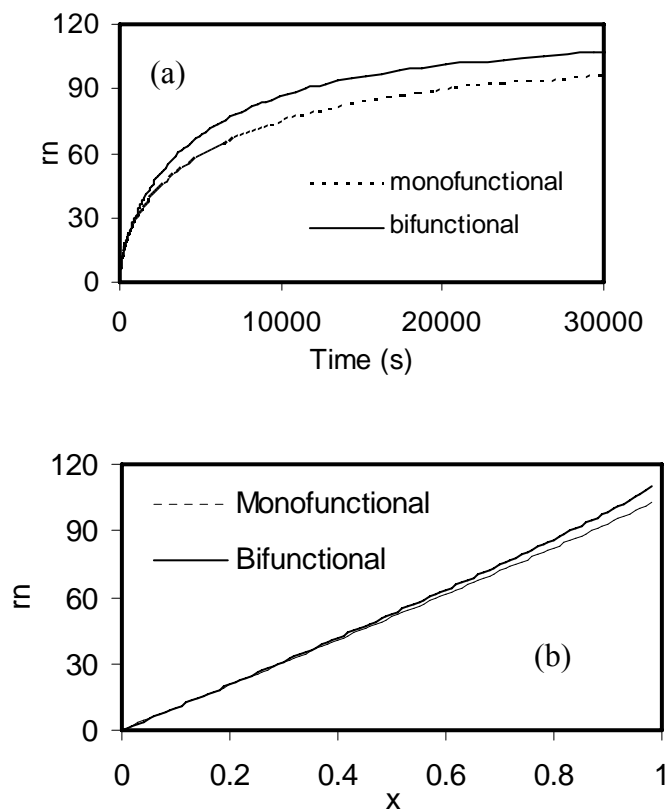


Figure 7.4 Number average chain length (r_n) as a function of (a) time and (b) conversion for polymer made with mono- and bifunctional initiators ($V = 1 \times 10^{-19}$ L).

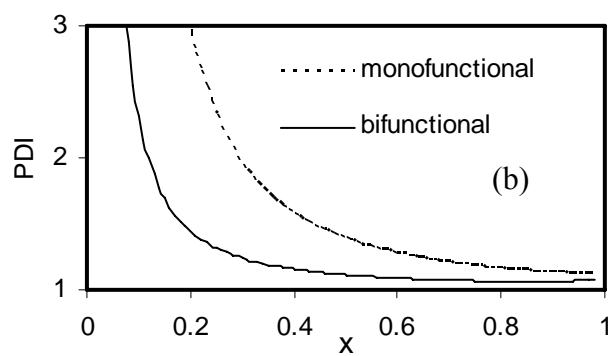
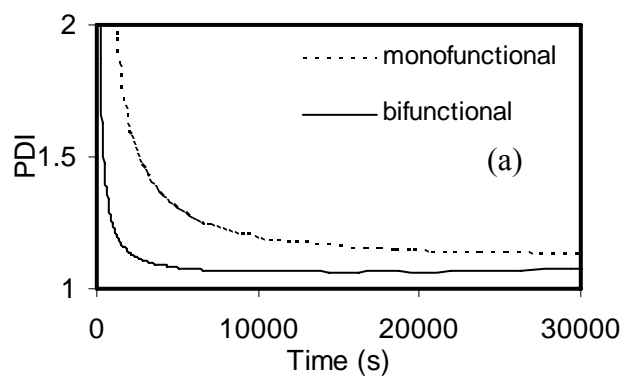


Figure 7.5 Polydispersity index (PDI) as a function of (a) time and (b) conversion for polymer made with mono- and bifunctional initiators ($V = 1 \times 10^{-19}$ L).

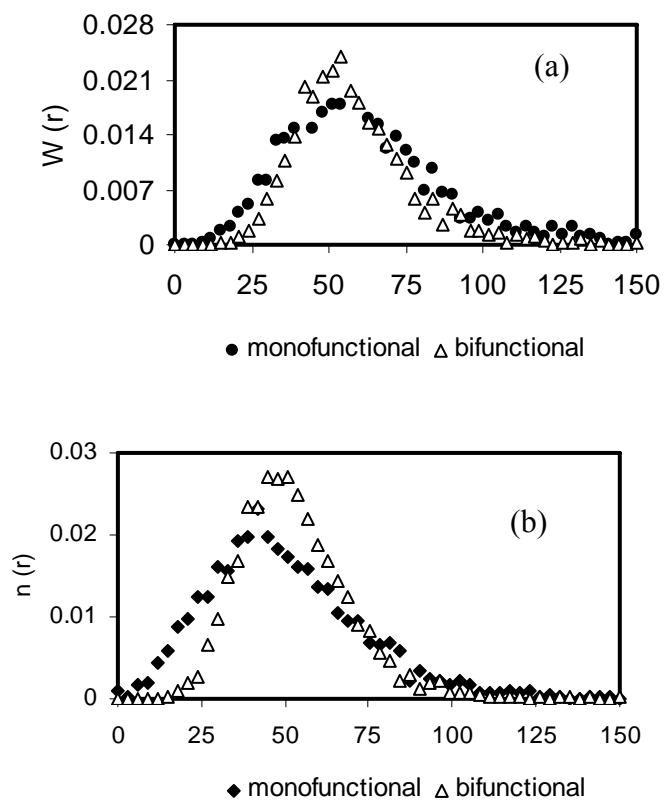


Figure 7.6 Comparison between mono- and bifunctional initiators: chain length distribution for conversion $x = 0.5$ ($V = 1 \times 10^{-19}$ L) (a) weight fraction (b) number fraction.

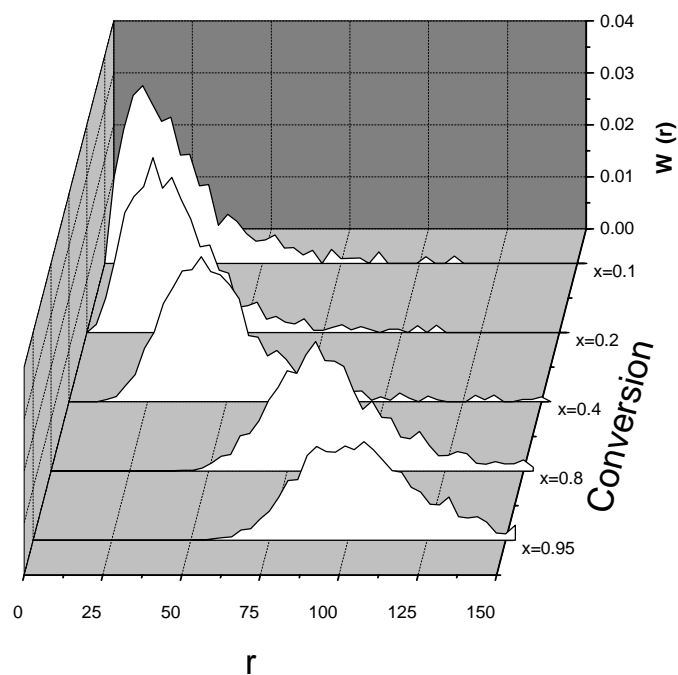


Figure 7.7 Evolution of the CLD of polymer made with a bifunctional initiator as a function of monomer conversion ($V = 1 \times 10^{-19}$ L).

7.4.3 Characteristics of the dynamic Monte Carlo simulation

Monte Carlo simulation has several advantages over other mathematical models for polymerization reactors: it is simple to implement, does not require the solution of sets of stiff differential equations, requires a minimum number of simplifying assumptions, and gives a very detailed picture of polymer microstructure. Unfortunately, Monte Carlo simulation can be time consuming and use significant computer memory. Therefore, it is important to find out conditions that minimize the computational time of Monte Carlo simulations.

In our model, the size of the control volume is one of the most important parameters affecting simulation time; as it increases, the simulation time become higher and higher, as illustrated in Figure 7.8. The simulation needs more than two hours to reach 50 % conversion when the control volume is 2×10^{-18} L. Reducing the control

volume to half that value (1×10^{-18} L) decreases the simulation time needed to reach the same conversion to approximately half an hour.

As expected, the polymerization time is not a function of the size of the control volume, as shown in Equation (9). Similarly, monomer conversion, molecular weight averages, and polydispersity index are independent of the size of the control volume. Larger control volumes simply imply that more molecules are simulated simultaneously; as a consequence, the stochastic noise decreases when the simulation volume increases. This behavior is demonstrated in Figures 7.9 to 7.11 for monomer conversion, number average chain length, and polydispersity index. The main advantage of increasing the size of the control volume is to generate smoother CLDs. The CLD in Figure 7.12 was calculated using a very small control volume (1×10^{-20} L); notice the high stochastic noise present in the results. On the other hand, Figure 7.13 shows that, for a larger control volume, the noise level in the distribution is rather small.

A similar effect can be achieved by averaging the results of several simulations done with smaller control volumes.

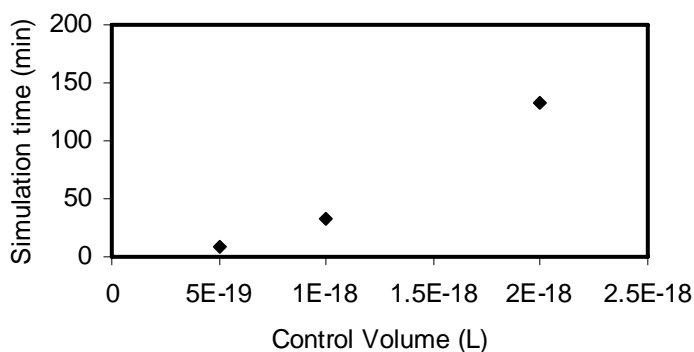


Figure 7.8 Effect of the size of the control volume on simulation time. ($x = 0.5$).

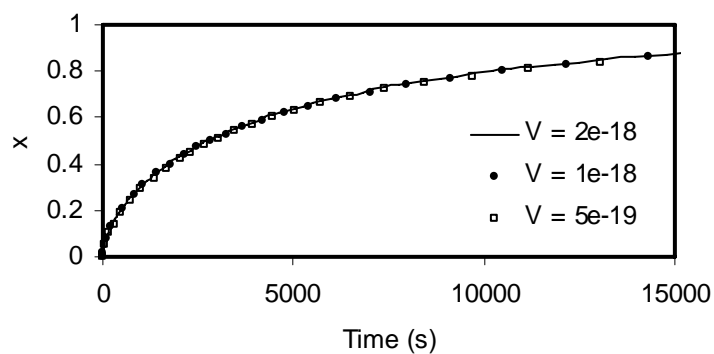


Figure 7.9 Effect of the size of the control volume on monomer conversion.

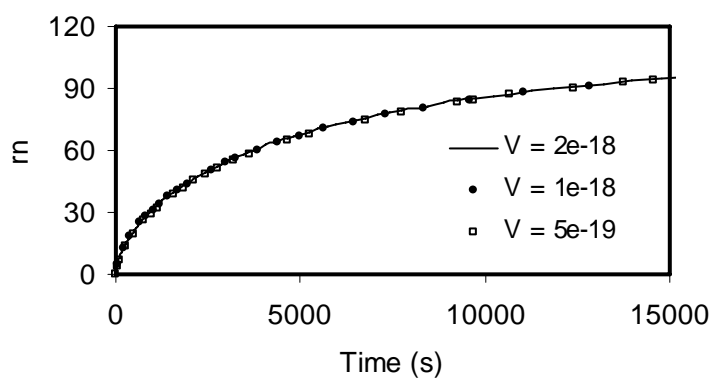


Figure 7.10 Effect of the size of the control volume on number average chain length.

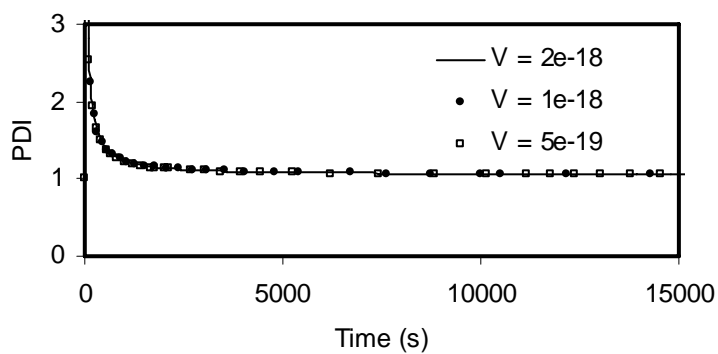


Figure 7.11 Effect of the size of the control volume on polydispersity index.

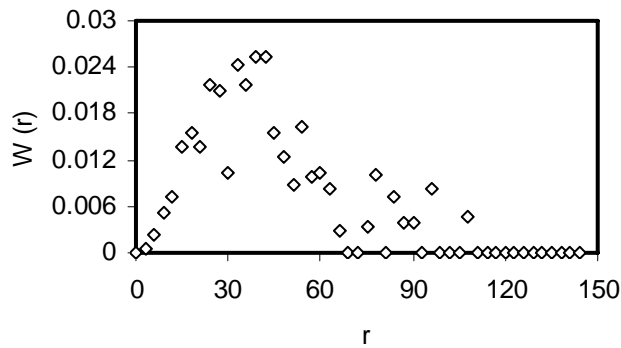


Figure 7.12 Effect of using a small control volume on the chain length distribution ($V=1 \times 10^{-20} L$, $x = 0.3$).

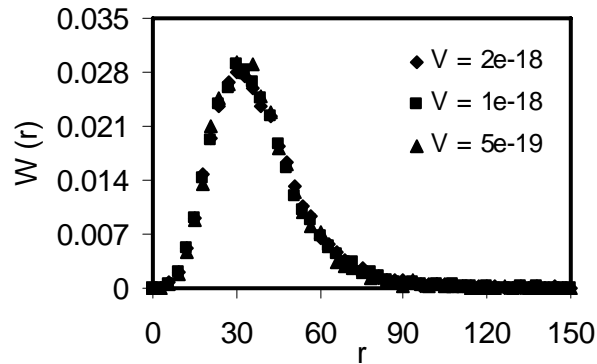


Figure 7.13 Effect of using large control volumes on the chain length distribution ($x = 0.3$).

An interesting alternative to using large control volume sizes to decrease the stochastic noise is to repeat Monte Carlo simulations with small control volumes several times and average the results of all simulations, as shown in Figure 7.14. Naturally, the seed of the random number generator routine must be changed for each simulation to ensure that the results of each subsequent simulation are different.

In order to show that smoother distributions are obtained by repeating simulations done with small volumes than the ones calculated with larger volumes, we measured the “noise level” of the distributions and computational times for both cases. We calculated the statistical noise of the CLDs with respect to a “smooth” reference distribution (w^{ref})

simulated with the large control volume of 2×10^{-18} L. The noise level in a distribution (χ_v) is defined as follows:

$$\chi_v = \sum_i^{\infty} (w_i^v - w_i^{ref})^2 \quad (31)$$

The results presented in Table 7.2 show that, as the volume increases, the noise level calculated with Equation (31) decreases. However, the simulation time increases sharply. On the other hand, Table 7.3 shows that repeating the simulation several times with a control volume of 1×10^{-19} L also reduces the noise level, but without increasing the simulation time so significantly. For instance, six repetitions lead to a noise level of $\chi_v = 1.0 \times 10^{-5}$ and a simulation time of $t = 126$ s. To achieve a similar noise level with a single simulation would require a control volume of 5×10^{-19} L (Table 7.2, $\chi_v = 1.2 \times 10^{-5}$) and the much larger simulation time of $t = 507$ s.

Figure 7.15 illustrates the effect of control volume size on both simulation time and distribution noise level and Figure 7.16 shows how the noise level and simulation time vary as a function of the number of simulation repetitions.

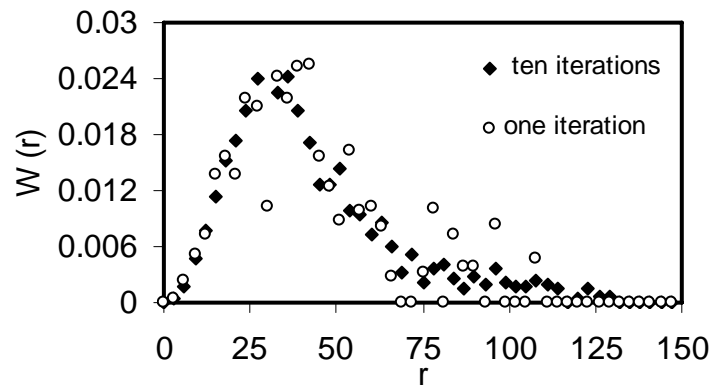


Figure 7.14 Effect of repeating the simulation several times and averaging the final results for CLD prediction ($V = 1 \times 10^{-20}$ L, $x = 0.3$).

Table 7.2 Effect of control volume on simulation time and CLD noise ($x = 0.5$)

Control Volume (L)	Simulation Time (s)	χ_v
1×10^{-20}	1.65	0.0029
1×10^{-19}	21	3.75×10^{-5}
5×10^{-19}	507	1.20×10^{-5}
1×10^{-18}	1980	5.11×10^{-6}
2×10^{-18}	7920	0

Table 7.3 Effect of number of repetitions on simulation time and CLD noise ($V = 1 \times 10^{-19}$ L, $x = 0.5$)

Number of iterations	Simulation Time (Sec.)	χ_v
0	0	
3	63	1.32×10^{-5}
6	126	1.01×10^{-5}
9	189	6.59×10^{-6}
12	252	5.99×10^{-6}
15	315	5.91×10^{-6}

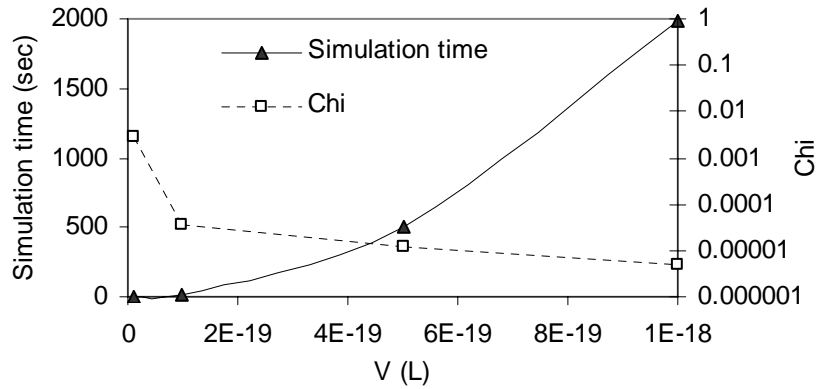


Figure 7.15 Effect of control volume size on computational time (solid line) and CLD noise (dashed line) ($x = 0.5$).

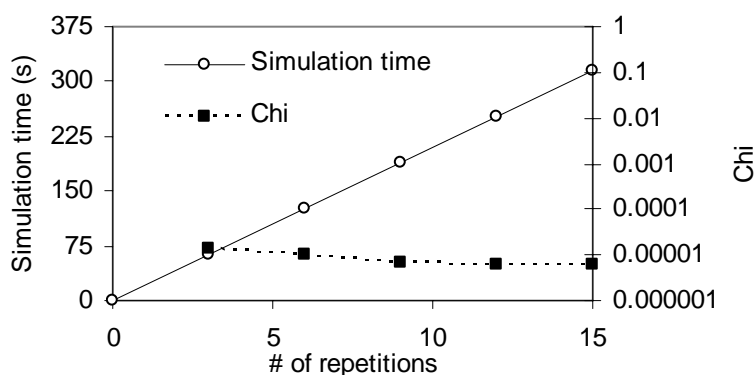


Figure 7.16 Effect of number of repetitions on computational time (solid line) and CLD noise (dashed line) ($V = 1 \times 10^{-19}$ L, $x = 0.5$).

Polymerization conditions may also affect the simulation time. In addition to the monomer type and temperature, the equilibrium rate constant ($K_{eq} = k_a/k_d$) in ATRP is function of catalyst type, polymerization temperature and monomer type. Figures 7.17 to 7.22 show the effect of K_{eq} on several simulation results; in all these simulations, the value of k_a was kept constant, while the value of k_d was varied from 10^5 to 10^7 s⁻¹. Both the simulation time and the predicted polymerization time increase when the value of the deactivation constant increases, as demonstrated in Figures 7.17 and 7.18. This behavior was expected, because keeping most of the species dormant slows down the polymerization. Monomer conversion and number average chain length increase as the deactivation constant decreases (Figures 7.19 and 7.20). Low polydispersity indices and narrow CLDs are obtained for higher deactivation constants (Figures 7.21 and 7.22).

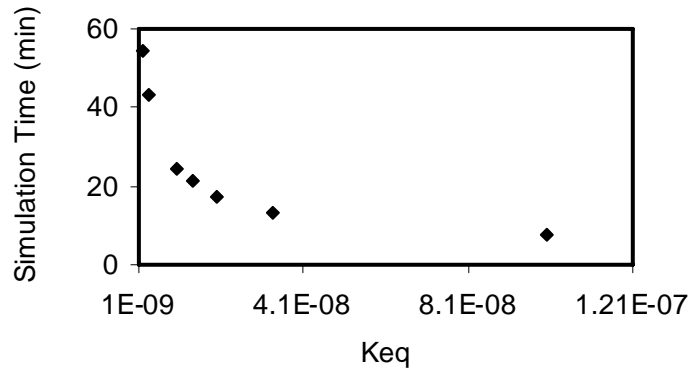


Figure 7.17 Effect of the equilibrium rate constant on simulation time. ($V = 1 \times 10^{-18}$ L, $x = 0.3$).

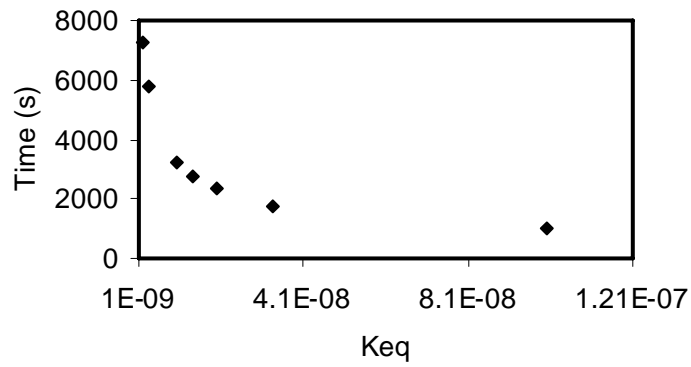


Figure 7.18 Effect of the equilibrium rate constant on polymerization time ($V = 1 \times 10^{-18}$ L, $x = 0.3$).

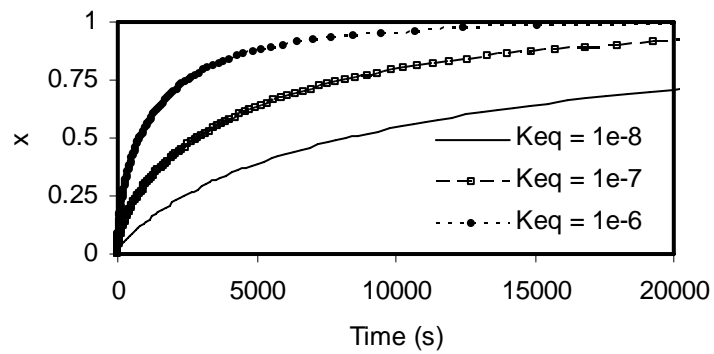


Figure 7.19 Effect of the equilibrium rate constant on monomer conversion ($V = 1 \times 10^{-18}$ L).

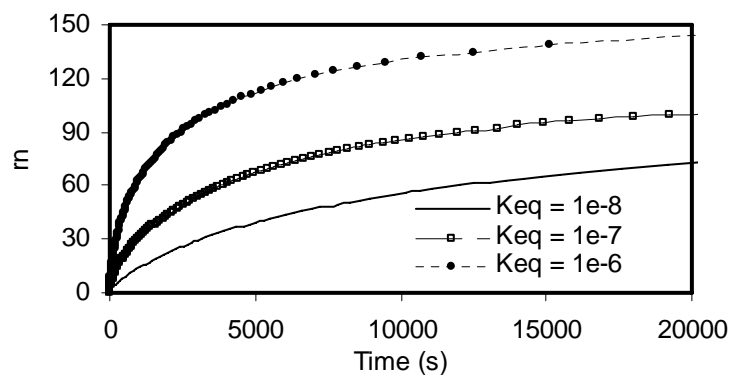


Figure 7.20 Effect of the equilibrium rate constant on number average chain length ($V = 1 \times 10^{-18} \text{ L}$).

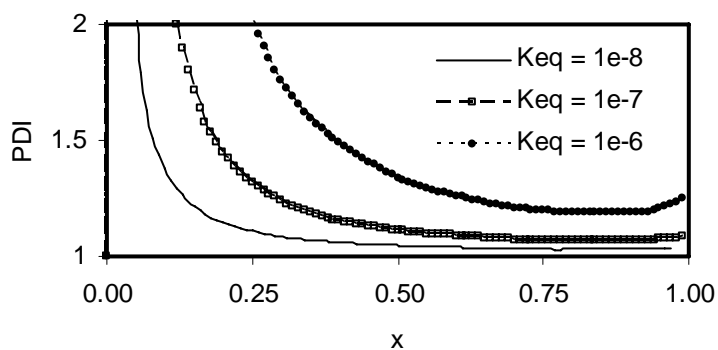


Figure 7.21 Effect of the equilibrium rate constant on polydispersity index ($V = 1 \times 10^{-18} \text{ L}$).

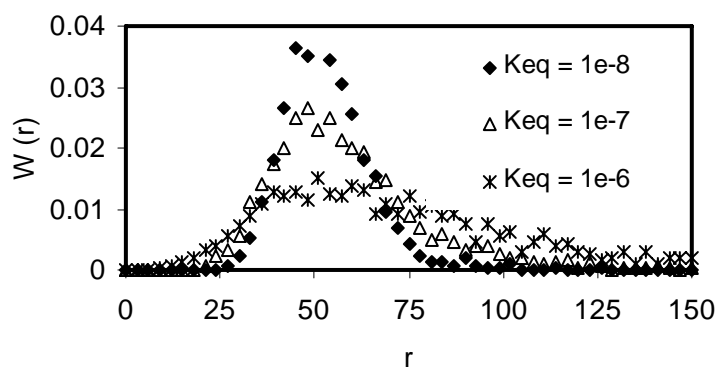


Figure 7.22 Effect of the equilibrium rate constant on chain length distribution ($V = 1 \times 10^{-18} \text{ L}$, $x = 0.5$).

The prediction of the complete CLD is the main advantage of Monte Carlo simulation over the method of moments. It is much faster to predict CLDs at low conversions than at higher conversions because the monomer concentration is high at low conversions and, hence, the propagation probability is also high. As monomer conversion increases, the probability of propagation decreases, leading to the non-linear increase in simulation time shown in Figure 7.23.

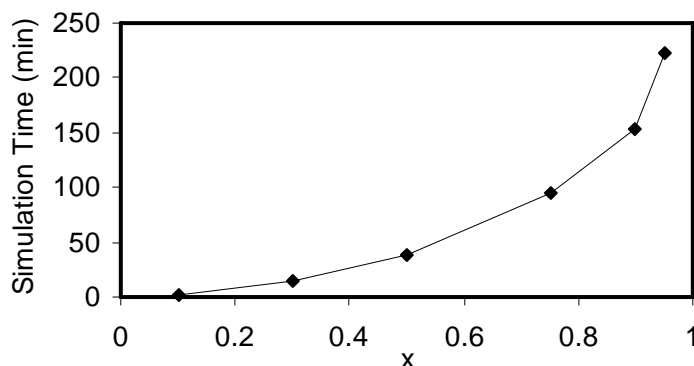


Figure 7.23 Effect of monomer conversion on simulation time ($V = 1 \times 10^{-18}$ L).

7.5 Conclusions

Dynamic Monte Carlo simulation is an efficient and powerful mathematical modeling technique to simulate ATRP with mono- and bifunctional initiators. Our Monte Carlo model was compared to another model using population balances and the method of moments with excellent agreement.

The model shows that bifunctional initiators are an excellent alternative to monofunctional initiators for ATRP because polymers made with bifunctional initiators have narrow CLDs and higher molecular weight averages.

We also examined how several polymerization conditions and model parameters affect simulation time and polymer properties. For the Monte Carlo simulation model, the selection of the proper size for the control volume is essential to obtain a smooth prediction for the CLD under a reasonable computational time. We compared two strategies to achieve this goal: in this first approach, we used single simulation runs with increasing control volume sizes until a specified noise level was achieved for their CLDs;

in the second approach we repeated simulations with a fixed control volume size as many times as required until their averaged CLD reached the noise level obtained in the first approach. For the simulation case we investigated, the second approach is clearly the faster technique.

7.6 References

- [1] D. Gillespie, J. Phys. Chem. **1979**, 81, 2340.
- [2] G. Odian, Principles of polymerization, 3rd edition, **1990**, pp. 206.
- [3] K. Ohno, A. Goto, T. Fukuda, Macromolecules **1998**, 31, 2699.
- [4] Y. Kwark, B. Novak, Macromolecules **2004**, 37, 9395.
- [5] O. Delgadillo-Velazquez, E. Vivaldo-Lima, I. Quintero-Ortega, S. Zhu, AIChE Journal, **2002**, 48,11, 2597.
- [6] M. Al-Harhi, J. Soares, L. Simon, Macromol. Chem. Phys., **2006**, 207, 469.
- [7] M. Al-Harhi, J. Soares, L. Simon, Macromol. Theory Simul, **2006**, 15, 198.
- [8] M. Villalobos, A. Hamielec, P. Wood, Journal of applied polymer science **1991**, 42, 629.
- [9] K. Matyjaszewski, P. Miller, J. Pyun, G. Kickelbick, S. Diamanti, Macromolecules **1999**, 32, 6526.

Chapter 8

8 Atom-Transfer Radical Polymerization of Styrene with Bifunctional and Monofunctional Initiators: Experimental and Mathematical Modeling Results*

8.1 Abstract

Bulk atom transfer radical polymerization (ATRP) of styrene was carried out at 110 °C using benzal bromide as bifunctional initiator and 1-bromoethyl benzene as monofunctional initiator. CuBr/2,2'-bipyridyl was used as the ATRP catalyst. The polymerization kinetic data for styrene with both initiators was measured and compared with a mathematical model based on the method of moments and another one using Monte Carlo simulation. An empirical correlation was incorporated into the model to account for diffusion-controlled termination reactions. Both models can predict monomer conversion, polymer molecular weight averages, and polydispersity index. In addition, the Monte Carlo model can also predict the full molecular weight distribution of the polymer. Our experimental results agree with our model predictions that bifunctional initiators can produce polymers with higher molecular weights and narrower molecular weight distributions than monofunctional initiators.

* This chapter has been accepted for publication: M. Al-Harhi, J. Soares, L. Simon *J. Polym.Sci., Part A Polym. Chem.*

8.2 Introduction

The basic ATRP system contains, besides the monomer(s), metal halide complexes with suitable ligands, and an initiator having a halide atom. To synthesize polymers with well-defined architectures, the use of initiators with precise functionality is essential. For example, bifunctional initiators are the best choice for ABA block copolymers. Several groups have studied ATRP with bifunctional initiators. Percec et al.^[1] used sulfonyl chlorides as bifunctional initiators to polymerize styrene, methacrylates, and acrylates. Neumann et al.^[2] used α,α -dichlorotoluene (DCT) as a bifunctional initiator to copolymerize styrene and methyl methacrylate (MMA). While the kinetic data proved that the DCT is a bifunctional initiator for styrene polymerization, DCT acts as a monofunctional initiator in MMA polymerization.

Malinowska et al.^[3] synthesized the novel bifunctional initiator (1,3-bis{1-methyl-[(2,2,2-trichloroethoxy) carbonylamino]ethyl} benzene) to polymerize MMA in bulk and solution. The resulting polymer (acting as a bifunctional macroinitiator) was used to initiate the polymerization of butylacrylate (BuA) and produce triblock copolymer with the structure BuA-*b*-MMA-*b*-BuA.

Styrene polymerization with ATRP has received considerable attention because polystyrene is inexpensive, easy to make, and it appears almost everywhere in our daily life. In fact, in Matyjaszewski's pioneering work,^[4] 1-phenylethyl chloride and copper chloride/2,2'-bipyridine were used to polymerize styrene. In the present contribution, the kinetics of bulk ATRP of styrene with monofunctional and bifunctional initiators was investigated with a detailed polymerization kinetic model, Monte Carlo simulation, and experimental polymerizations.

8.3 Experimental section

Materials. Styrene (St, 99 %) was purchased from Aldrich Chemical Co. After it was passed through an alumina column to remove the inhibitor, the styrene was stored under nitrogen atmosphere at 0°C. Copper (I) bromide (99.999 %), 2,2'-bipyridine (bpy, 99 %),

1-bromoethyl benzene (97 %), and benzal bromide (97 %) were used as received from Aldrich. Technical grade solvents were employed without further purification.

Polymerization. In a typical polymerization run, the catalyst (CuBr and 2,2'-bipyridine) and a magnetic stirrer were placed in a round-bottom flask sealed with a rubber septum and purged with nitrogen through repeated vacuum/nitrogen cycles. After the last cycle, the flask was purged with nitrogen for 10 minutes. To ensure no oxygen flowed into the flask, the monomer (styrene) was injected using a syringe and a transfer needle. The flask was immersed in an oil bath kept at 110°C. The initiator was then added with a syringe. After a specified time, the flask was removed from the oil bath and the reaction mixture diluted with THF. The solution was filtered through a column containing neutral alumina to remove the catalyst. The polymer was recovered by precipitation in methanol, followed by drying at 70 °C.

Characterization. Monomer conversion was determined by gravimetry and ¹H-NMR. Molecular weight averages and molecular weight distribution were obtained using the Waters GPC (Waters 590) system operating at room temperature. Tetrahydrofuran (THF) was used as eluent. The polymer samples were dissolved in THF (0.005 gram of sample in 1 ml of THF) and filtered using 0.45 µm filters before injecting into the GPC.

H-NMR spectra were obtained on a 300-MHz AC Bruker Fourier-transform spectrometer, in deuterated chloroform at a concentration of 10–30 mg/ml. The operating conditions were as follows: temperature of the probe, 25°C; reference, CDCl₃ assigned at ≈7.26 ppm; number of scans, 32.

8.4 Model development

8.4.1 Reaction mechanism

The basic elementary reactions in ATRP are initiation, activation, deactivation, propagation, chain termination, and transfer to small molecule. At high temperatures (110 °C and higher), styrene thermal initiation may also become significant.^[5] However, the effect of thermal initiation can generally be neglected in the presence of high initiator concentrations. Pascual et al.^[6] concluded that thermal initiation of styrene at 130 °C was

negligible in the presence of 0.02 mol/L of initiator (1-phenylethyl chloride). Matyjaszewski and co-workers have also proposed the existence of elimination reactions in the ATRP of styrene with copper bromide.^[7-9] However, they concluded that these elimination reactions occurred later in the polymerization and did not significantly affect polymer molecular weights and molecular weight distribution (MWD). The relevance of these side reactions will be examined below using Monte Carlo simulation. Monte Carlo is an ideal technique for these studies, since it is very easy to add new elementary reactions to the polymerization mechanism used in the simulation.

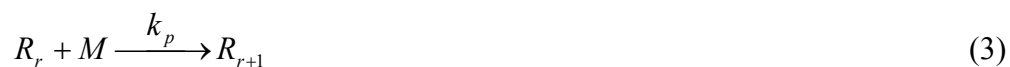
The reaction mechanism used in this study is described in the following paragraphs. Equations (1) to (5) are the main elementary reactions in the ATRP of styrene with monofunctional initiators. The side reactions (thermal initiation and elimination reactions) are described in Equations (6) to (8). Finally, Equations (9) to (26) are the main elementary reactions of ATRP of styrene with bifunctional initiators. Because this study is limited to styrene polymerization, we will consider that polymer chains terminate only by combination. In addition, we assumed that the initiation rate constant was equal to the propagation rate constant and that the activation and deactivation rate constants of the initiator molecules were equal to the ones for dormant species and polymer radicals.

The mechanism for ATRP with monofunctional initiators is given by the equations:

Equilibrium



Propagation



Transfer to monomer



Termination by combination



Thermal initiation



Elimination reactions



In Equations (1) to (8), C and CX are the catalyst in its low and high valence states, respectively, M is the monomer, R_r is a polymer radical, P_r is a dead polymer chain, D_r is a dormant polymer chain, k_p is the propagation rate constant, k_{tc} is the rate constant of termination by combination, k_a is the activation rate constant, k_d is the deactivation rate constant, k_{tr} is the transfer-to-monomer rate constant, k_{th} is the thermal initiation rate constant, and k_{el1} and k_{el2} are the elimination rate constants. The subscripts r and m indicate the number of monomer units in the chain.

Similarly, the mechanism for ATRP with bifunctional initiators is given by the elementary steps shown in chapter 5 (note that we have not included thermal initiation and elimination reactions in this mechanism):

Monomer conversion, average molecular weights, and polydispersity index are calculated from the population balances and the method of moments. The detailed derivation of the population balances and moment equations is available in the previous chapters and will not be repeated here. A dynamic Monte Carlo simulation, based on Gillespie's^[10] algorithm, is used to simulate the full molecular weight distribution of polystyrene made with ATRP. The reader is referred to Chapter 4 for more details.

8.4.2 Diffusion effects

In conventional free radical polymerization, initiation, propagation and chain termination reactions can be influenced by diffusional effects, especially at high monomer conversions in bulk polymerization. In solution polymerization, these effects are much more reduced or completely absent due to the presence of the solvent. There is

an ongoing discussion on the importance of diffusion effects in controlled free radical polymerization. While some groups ^[11-13] state that chain termination is the only diffusion-controlled reaction for these systems, others ^[14,15] claim that the initiation and propagation steps may also become diffusion-controlled. In our previous study (chapter 6),^[16] we concluded that diffusion limitations are not significant during ATRP, except for chain termination. Therefore, in the simulations present here, we will consider that only chain termination reactions may be diffusion-controlled and that the rates of the other reactions remain constant throughout the polymerization.

To account for the diffusion limitation on the termination reactions, the empirical correlation suggested by Husain and Hamielec^[17] was used in our model:

$$k_{tc} = k_{tc0} \exp[-2 \times (A_1x + A_2x^2 + A_3x^3)] \quad (9)$$

$$A_1 = 2.57 - 5.05 \times 10^{-3}T \quad (10)$$

$$A_2 = 9.56 - 1.76 \times 10^{-2}T \quad (11)$$

$$A_3 = -3.03 + 7.85 \times 10^{-3}T \quad (12)$$

Table 8.1 lists the numerical values of the kinetic rate constants used in our simulations. Only the activation and deactivation rate constants were estimated in our simulations; all the other parameters were taken directly from the previous investigations cited in Table 8.1. The termination by disproportionation rate constant is set to zero because it is not present in the styrene polymerization.

Table 8.1 Parameters used in ATRP of styrene at 110°C

Parameter	Value	Reference
k_p (L.mol ⁻¹ . s ⁻¹)	1516	18
k_{tc0} (L.mol ⁻¹ . s ⁻¹)	3.469×10^8	19
k_{td0} (L.mol ⁻¹ . s ⁻¹)	0	
k_{tr} (L.mol ⁻¹ . s ⁻¹)	0.22	19
k_a (L.mol ⁻¹ . s ⁻¹)	0.0353	This study
k_d (L.mol ⁻¹ . s ⁻¹)	4.01e5	This study
k_{th} (L ² mol ⁻² s ⁻¹)	4.58×10^{-11}	19
k_{el1} (L.mol ⁻¹ . s ⁻¹)	1×10^{-4}	8
k_{el2} (L.mol ⁻¹ . s ⁻¹)	1×10^3	8

8.5 Results and discussion

8.5.1 Effect of thermal initiation and elimination reactions

We used our model to examine the importance of thermal initiation and elimination reactions for the polymerization of styrene with monofunctional initiators. The *complete model* includes all the reactions in the ATRP mechanism, Equations (1) to (8), while the *simple model* is limited to the reactions described only in Equations (1) to (5). Figure 8.1 compares model predictions for the degree of polymerization (DP) and the chain length distribution. Both the complete and the simple model give very similar predictions, indicating that neither thermal initiation nor elimination reactions are important under these simulation conditions. This conclusion agrees with the results obtained by other groups.^[6, 9]

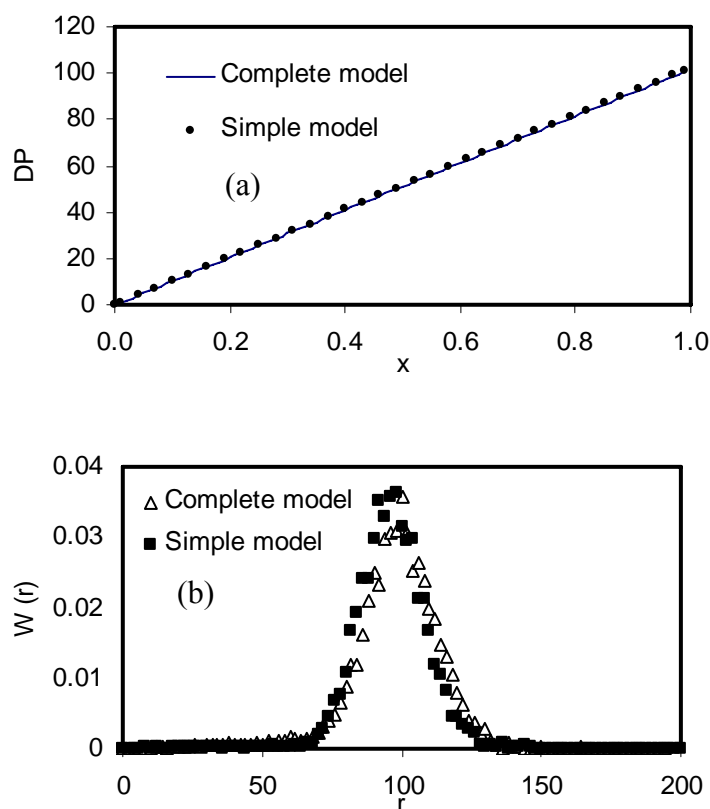


Figure 8.1 Effect of thermal initiation and elimination reactions on (a) degree of polymerization, and (b) chain length distribution. Model parameters are listed in Table 8.1.

8.5.2 Comparison of benzal bromide with 1-bromo ethyl benzene

The isothermal ATRP of styrene at 110°C in bulk was investigated using 1-bromoethyl benzene (monofunctional initiator) and benzal bromide (bifunctional initiator). Both initiators have structures resembling that of the styrene and, therefore, are good initiators for controlled ATRP of styrene, as illustrated in Figure 8.2. In this study, the benzal bromide is proposed as a symmetrical bifunctional initiator because it has two identical bromide atoms.

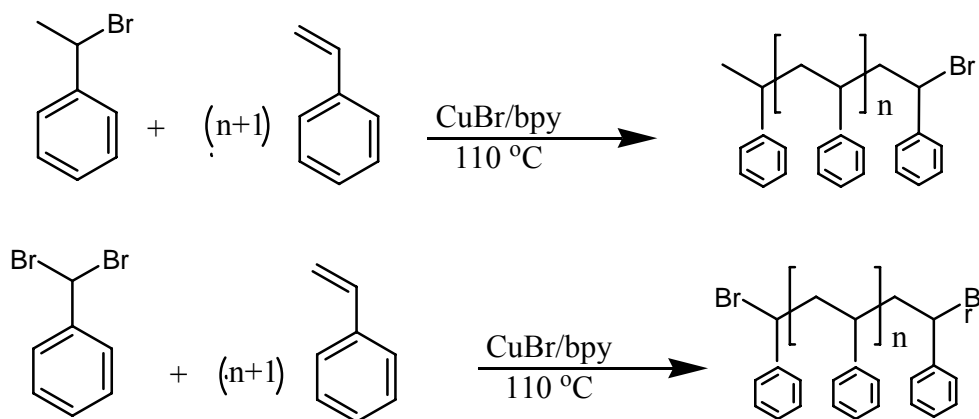


Figure 8.2 ATRP of styrene using 1-bromoethyl benzene and benzal bromide.

The equilibrium rate constants (activation and deactivation) were estimated from the experimental data using a non-linear least squares routine programmed in MATLAB. These two constants were estimated by minimizing the square of the differences between experimental and predicted monomer conversions,

$$\chi = \sum_{i=1}^n (x_i^{\text{exp}} - x_i^{\text{pred}})^2 \quad (13)$$

where x_i^{exp} is the experimental monomer conversion and x_i^{pred} is the model-predicted monomer conversion.

This parameter estimation was done for the monofunctional initiator and then those rate constants were used to predict the average molecular weight, polydispersity index, and MWD. Moreover, the same activation and deactivation constants were used to simulate styrene polymerization with the bifunctional initiator. No new data fitting was attempted (or required), in this case.

Styrene conversion was measured experimentally using gravimetry and ¹H NMR. Gravimetry is an easy and common method for conversion measurement. However, due to the fractionation of chains with very low molecular weight during polymer work up after the polymerization reaction the experimental error may be significant for lower conversions. Therefore, we used ¹H NMR to measure the conversion when the polystyrene molecular weight was low (at low conversions) and gravimetry to measure

higher conversions. More details and comparisons between these two methods will be given below.

Figures 8.4 to 8.6 compare experimental results with model predictions made with the method of moments. Figure 8.4 shows that, for a given polymerization time, bifunctional initiators lead to increased monomer conversion, as expected. The model agrees very well with the experimental data for both initiators, especially for higher conversions. For lower conversions, the induction period observed experimentally could not be represented well with our model.

Figure 8.4.a demonstrates that the number average molecular weight (M_n) of polystyrene increases linearly with monomer conversion, a typical behavior of living polymerization. Figure 8.4.b shows that the M_n of polystyrene made with the bifunctional initiator is always higher than that of polystyrene made with the monofunctional initiator for a given polymerization time because the bifunctional initiator converts monomer faster than the monofunctional initiator. Our model agrees well with the experimental data.

The dependency of the polydispersity index (PDI) on time and monomer conversion is illustrated in Figures 8.5.a and 8.5.b. PDI is kept low throughout the polymerization, as expected for a living polymerization system. Model predictions and experimental data are coincident for higher times and monomer conversions, but deviate significantly at lower monomer conversions. We believe this deviation is caused mainly by the induction period at the beginning of the polymerization (see Figure 8.4), which is not well represented by our model. This phenomena is known in conventional free radical polymerization ^[20,21] and has been observed experimentally in living free radical polymerization ^[22-23].

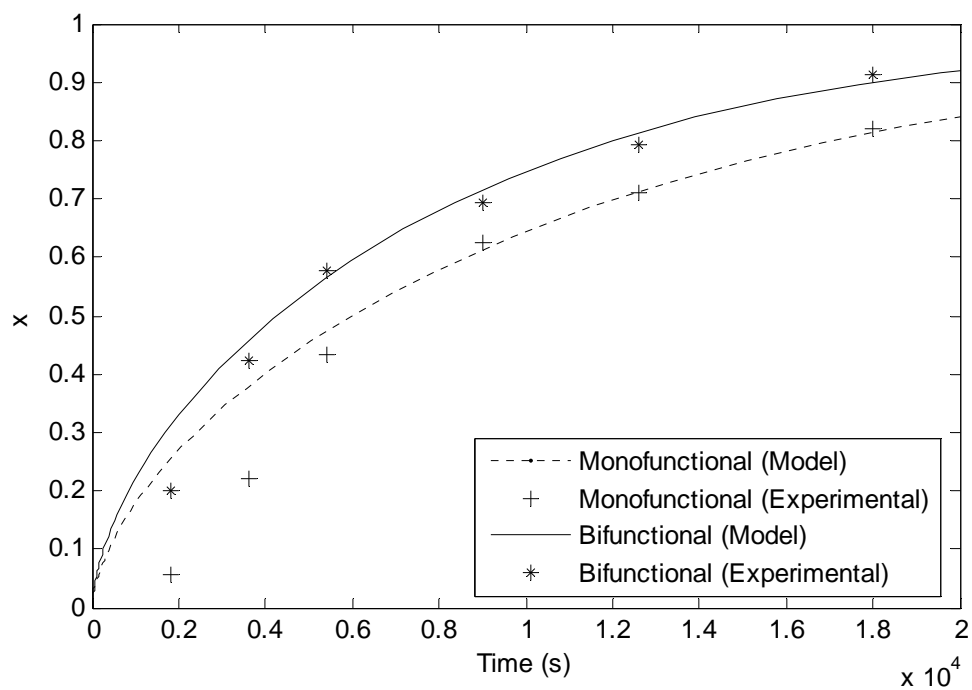


Figure 8.3 Experimental data and model predictions for monomer conversion as a function of time for the bulk ATRP of styrene with benzal bromide and 1-bromo ethyl benzene at 110 °C. Model parameters are shown in Table 8.1 and $[M]_0/[I]_0/[C]_0 = 100/1/1$.

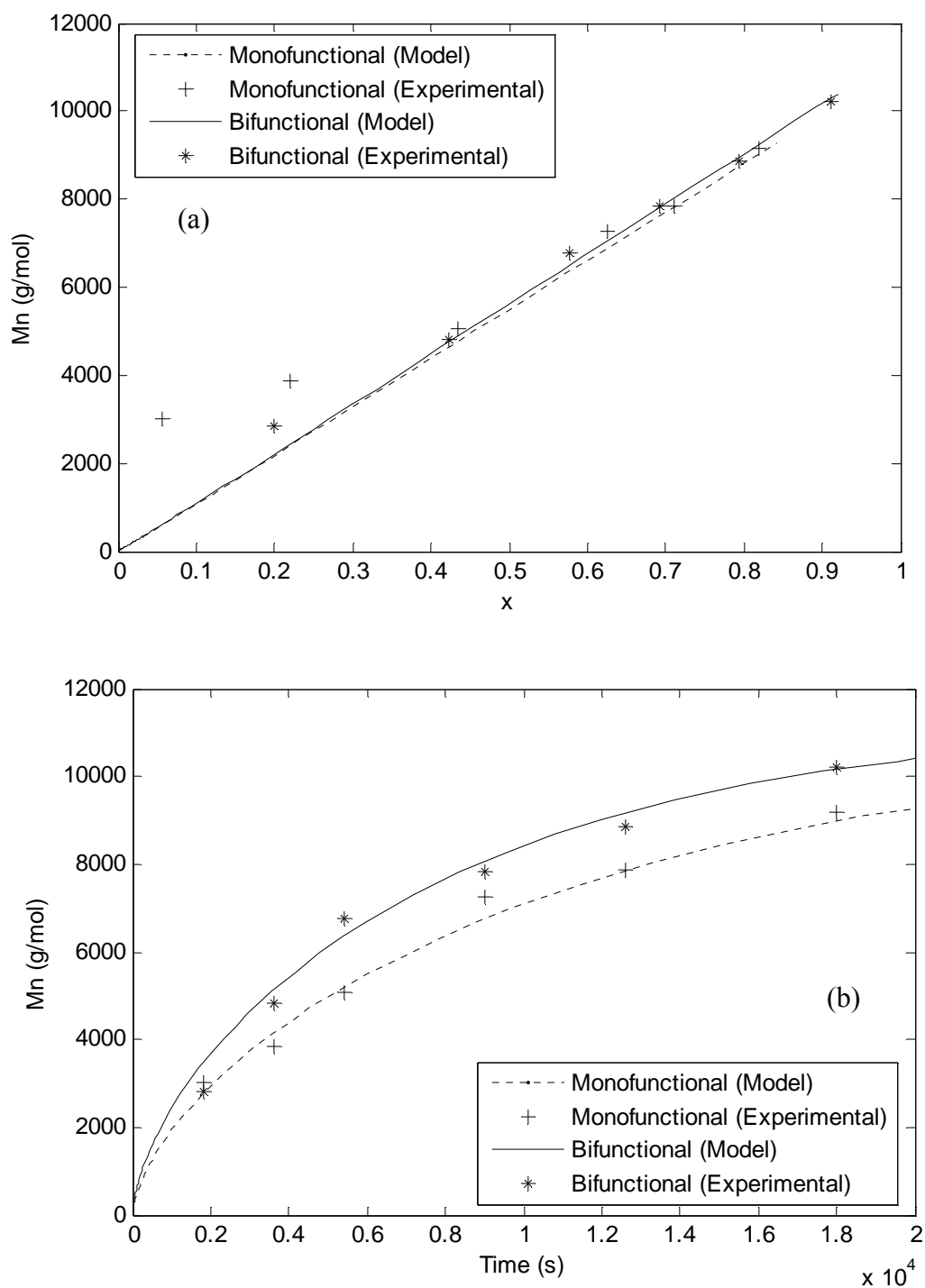


Figure 8.4 Experimental data and model predictions for (a) number average molecular weight versus conversion; (b) number average molecular weight versus time for the bulk ATRP of styrene with benzal bromide and 1-bromo ethyl benzene at 110 °C. Model parameters are shown in Table 8.1 and $[M]_0/[I]_0/[C]_0 = 100/1/1$.

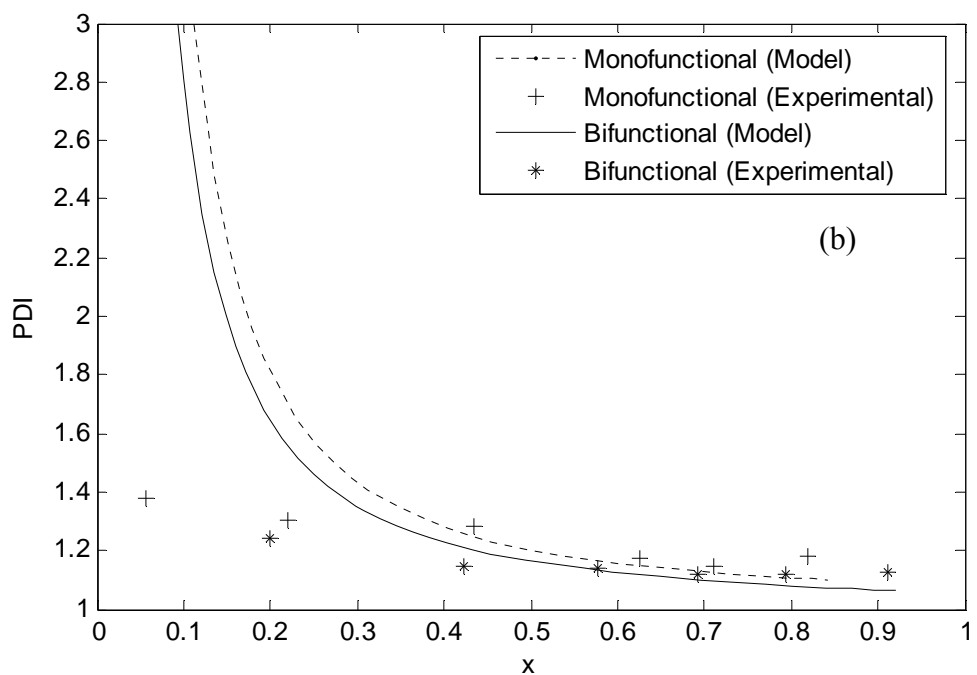
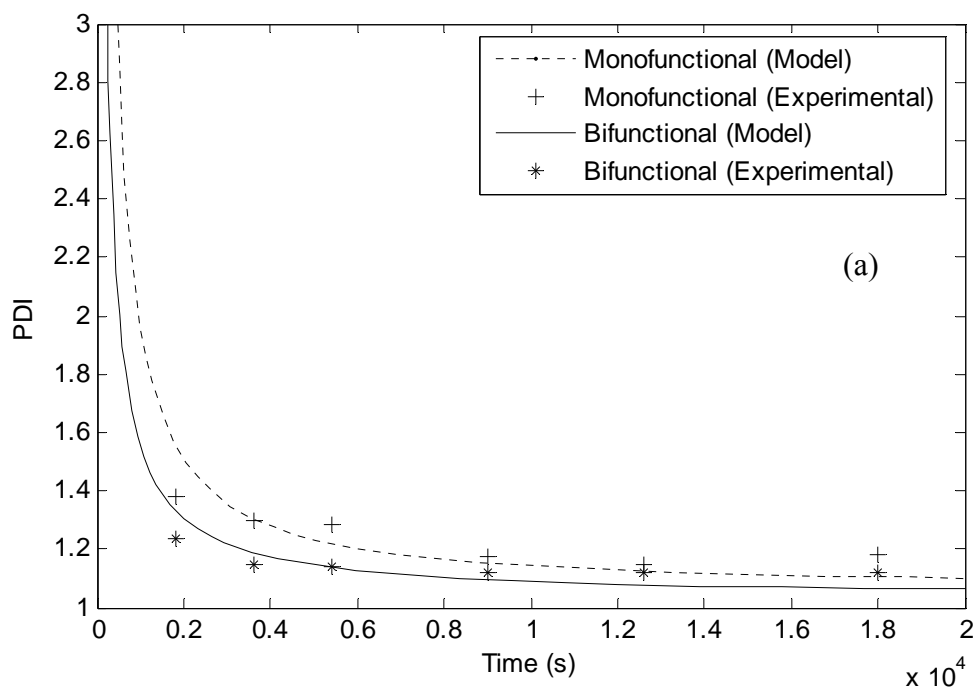


Figure 8.5 Experimental data and model predictions for (a) polydispersity index against time, (b) polydispersity index against conversion for the bulk ATRP of styrene with benzal bromide and 1-bromo ethyl benzene at 110 °C. Model parameters are shown in Table 8.1 and $[M]_0/[I]_0/[C]_0 = 100/1/1$.

In addition to the simulation results obtained with the method of moments, our Monte Carlo model predicts the full molecular weight distribution of the polymer as a function of polymerization time and monomer conversion. Under the conditions given in Table 8.1, the MWDs are predicted by Monte Carlo simulation and compared with the experimental distribution measured by GPC. Various distributions at different polymerization times with both initiators agree very well with the Monte Carlo simulation results, as depicted in Figures 8.6 and 8.7.

The agreement between experimental and Monte Carlo-simulated MWDs is very good for longer polymerization times. Predicted and measured MWDs of polystyrene made at 30 and 60 minutes of polymerization with the monofunctional initiator deviate significantly, as shown in Figure 8.6. This deviation is also observed when the method of moments is used (Figure 8.5.a) and it is most probably due to the inability of the model to predict the induction period. The MWDs of the samples made at higher polymerization times (90 to 300 minutes) are much better represented by the Monte Carlo simulations than those at short polymerization times (< 90 min).

A similar behavior is observed for the MWD of polystyrene made with the bifunctional initiator depicted in Figure 8.7: there is significant deviation between experimental and predicted MWDs of polystyrene made after 30 minutes of polymerization, but the agreement is excellent for longer polymerization times. Considering that we never tried to adjust the polymerization kinetic parameters to fit the MWDs and that we used k_a and k_d values fitted from conversion data from the monofunctional initiator to predict the behavior with the bifunctional initiator, we believe this agreement is quite remarkable.

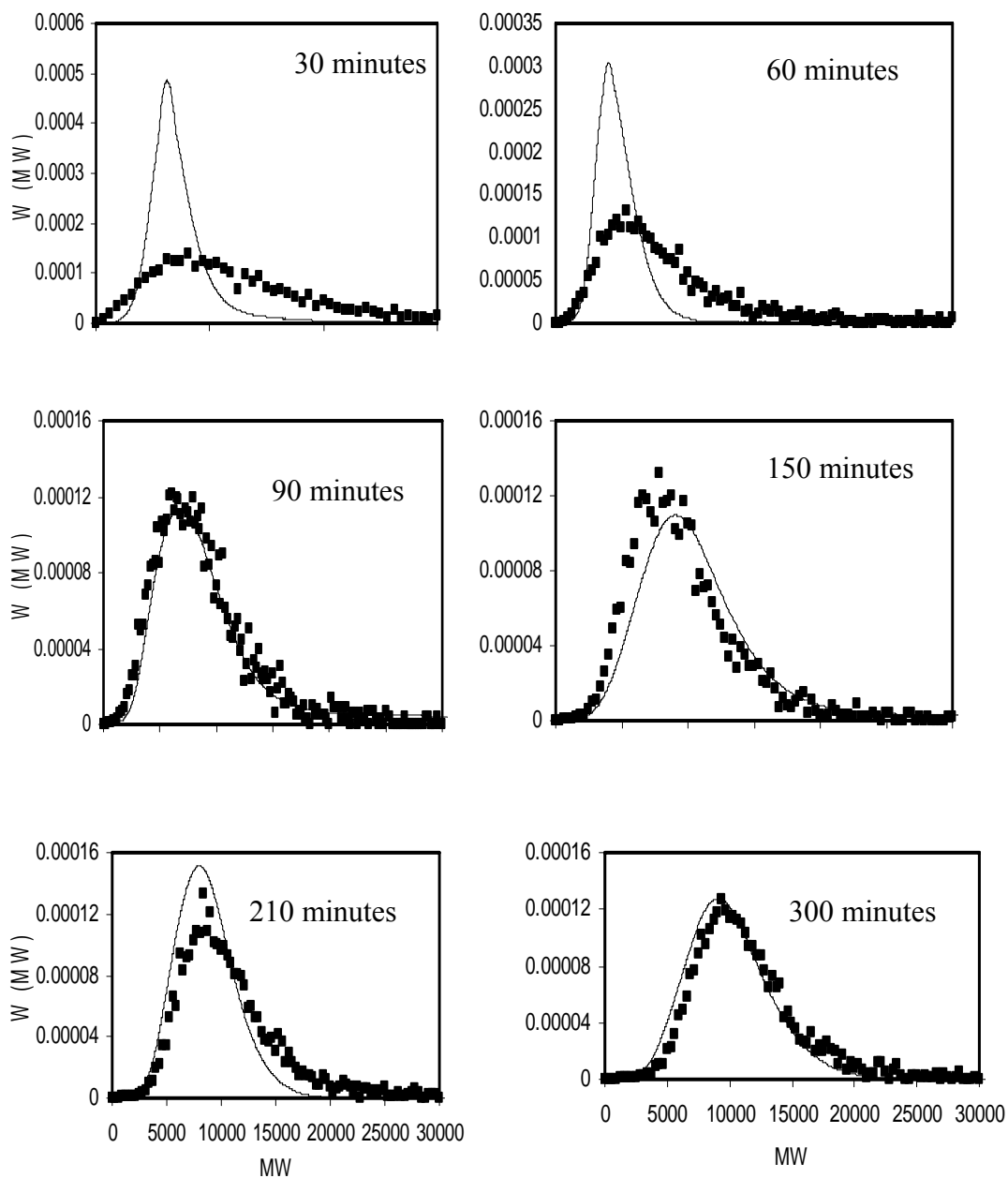


Figure 8.6 Comparison of Monte Carlo simulation (square dots) and experimental molecular weight distributions (solid line) for the bulk ATRP of styrene with 1-bromoethyl benzene at 110 °C. Model parameters are shown in Table 8.1 and $[M]_0/[I]_0/[C]_0 = 100/1/1$.

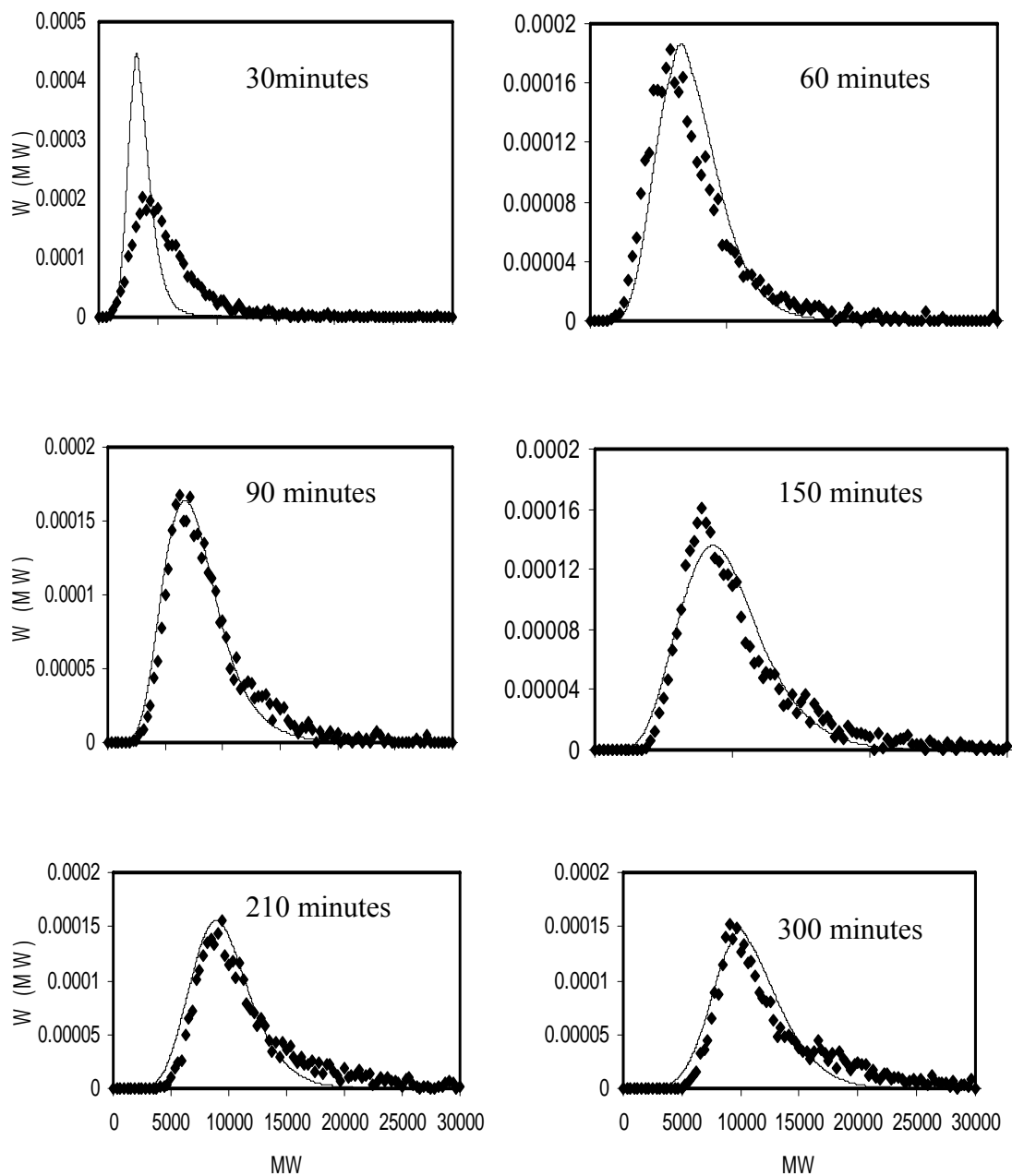


Figure 8.7 Comparison of Monte Carlo simulation (diamond dots) and experimental molecular weight distributions (solid line) for the bulk ATRP of styrene with benzal bromide at 110 °C. Model parameters are shown in Table 8.1 and $[M]_0/[I]_0/[C]_0 = 100/1/1$.

As we mentioned above, monomer conversions measured by gravimetry and by ^1H NMR do not agree well for low conversions because low molecular weight polystyrene chains are lost during polymer filtration after the polymerization. ^1H NMR spectrum was used to identify the fraction of polymer that remains in the solvent (see Figure 8.8) after it evaporates. Under this condition, ^1H -NMR is a more reliable technique to determine monomer conversion. In styrene, vinyl proton peaks appear around $\delta = 5.2$ and 5.8 ppm. As the polymerization proceeds, the vinyl proton is consumed and its magnitude in the ^1H NMR spectrum decreases. Therefore, styrene conversion by ^1H NMR can be calculated with the following equation,

$$x = 1 - \frac{\left(\frac{A_v}{A_a}\right)_{t_f}}{\left(\frac{A_v}{A_a}\right)_{sty}} \quad (14)$$

where $\left(\frac{A_v}{A_a}\right)_{t_f}$ is the ratio of the integrated area of the vinyl protons ($\delta = 5.2$ and 5.8 ppm) to the integrated area of aromatic rings ($\delta = 6.45$ - 7.09 ppm) measured after a polymerization time t_f , and $\left(\frac{A_v}{A_a}\right)_{sty}$ is the equivalent ratio for styrene monomer.

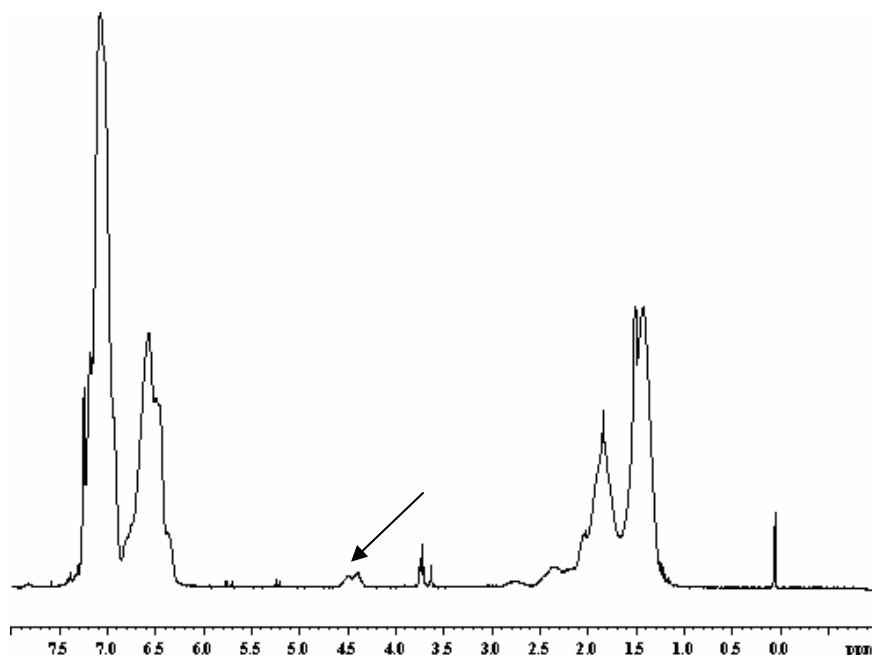


Figure 8.8 ^1H NMR spectrum of polystyrene chains obtained in the filtrate after polymerization for 30 minutes using monofunctional initiator. The arrow indicates the bromide end (dormant chain) in the polystyrene molecule ^[9].

Table 8.2 and Figure 8.9 compare monomer conversions calculated by both techniques. The deviations between the two methods at low conversions are clear evidence that the low molecular weight polystyrene chains are lost during sample filtration, leading to lower polymer yields than measured by ^1H NMR. The difference between the two techniques decreases with increasing polymerization time and, consequently, polystyrene molecular weight.

We have also collected the filtrate for more analysis to detect the polystyrene fraction. After evaporation of the solvent, the solid residue was analyzed via ^1H NMR. The spectrum is clearly that of polystyrene (6.45-7.09 ppm for aromatic ring). Moreover this polystyrene has bromide end (4.5 ppm).

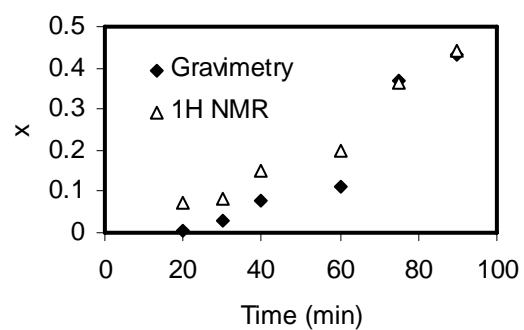


Figure 8.9 Comparison between conversion measured with gravimetry and ¹H NMR for ATRP of styrene using 1-bromo ethylbenzene as initiator at 110 °C (Data from Table 8.2).

Table 8.2 Comparison between conversion (x) measured with gravimetry and ¹H NMR for ATRP of styrene using 1-bromo ethylbenzene as initiator at 110 °C.

Time (min)	x (gravimetry)	x (NMR)
0	0	0
20	0.006	0.074
30	0.029	0.082
40	0.080	0.149
60	0.110	0.197
75	0.370	0.363
90	0.434	0.441

8.6 Conclusions

We modeled the ATRP of styrene with a mono- and a bifunctional initiator using the method of moments and Monte Carlo simulation. The method of moments was used to predict monomer conversion, average molecular weight, and polydispersity index, while the Monte Carlo model could, in addition, predict the full molecular weight distribution of the polystyrene formed as a function of monomer conversion.

We used our own polymerization experimental data to estimate the activation and deactivation constants from monomer conversion data for the monofunctional initiator. All other polymerization kinetic constants were obtained from the literature.

The modeling results agree well with the experimental data. In particular, the Monte Carlo simulation results can track the MWDs as a function of polymerization time very accurately for conversions above approximately 20%. Comparison of styrene polymerization with the two initiators shows that the bifunctional initiator produces polymers with higher conversion, higher molecular weights, and narrower molecular weight distributions than the monofunctional initiator.

8.7 References

- [1] V. Percec, H. Kim, B. Barboiu, *Macromolecules* **1997**, 30, 6702.
- [2] A. Neumann, H. Keul, H. Hocker, *Macromol. Chem. Phys.* **2000**, 201, 980.
- [3] A. Malinowska, P. Vlcek, J. Kriz, L. Toman, P. Latalova, M. Janata, B. Masar, *Polymer* **2005**, 46, 5.
- [4] J. Wang, K. Matyjaszewski, *J. Am. Chem. Soc.* **1995**, 117, 5614.
- [5] F. Mayo, *J. Amer. Chem. Soc.* **1968**, 90, 1289.
- [6] S. Pascual, B. Coutin, M. Tardi, A. Polton, J. Vairon, *Macromolecules* **2001**, 34, 5752.
- [7] J. Lutz, K. Matyjaszewski, *Macromol. Chem. Phys.* **2002**, 203, 1385.
- [8] K. Matyjaszewski, K. Davis, T. E. Patten, M. Wei, *Tetrahedron* **1997**, 53, 15321.
- [9] J. Lutz, K. Matyjaszewski, *J. Polym. Sci. Part A: Polym. Chem.* **2005**, 43, 897.
- [10] D. Gillespie, *J. Phys. Chem.* **1979**, 81, 2340.
- [11] D. Shipp, K. Matyjaszewski, *Macromolecules* **1999**, 32, 2948.
- [12] D. Peklak, A. Butte, G. Storti, M. Morbidelli, *J. Polym. Sci. Part A: Polym. Chem.* **2006**, 44, 1071.
- [13] J. Bonilla, E. Saldivar, A. Flores-Tlacuahuac, E. Vivaldo-Lima, R. Pfaendner, F. Tiscareno-Lechuga, *Polymer Reaction Engineering*, **2002**, 10, 4, 227.
- [14] O. Delgadillo-Velazquez, E. Vivaldo-Lima, I. Quintero-Ortega, S. Zhu, *AIChE J.* **2002**, 48(11), 2597.
- [15] H. Chaffey-Millar, M. Busch, T. P. Davis, M. H. Stenzel, C. Barner-Kowollik, *Macromol. Theory Simul.* **2005**, 14, 143.
- [16] M. Zhang, H. Ray, *Journal of applied polymer science* **2002**, 86, 1047.
- [17] A. Husain, A. Hamielec, *J. Appl. Polym. Sci.* **1978**, 22, 1207.
- [18] M. Buback, R. Gilbert, R. Hutchinson, B. Klumperman, F. Kuchata, B. Manders, K. O'Driscoll, G. Russell, *J. Macromol. Chem. Phys.* **1995**, 196, 3267.
- [19] A. Hui, E. Hamielec, *J. Appl. Polym. Sci.* **1972**, 16, 749.
- [20] G. Odian, *Principles of polymerization*, 3rd edition, **1990**.
- [21] A. Rudin, *The element of polymer science and engineering*, **1999**.
- [22] R. Johnson, C. Ng, C. Samson, C. Fraser, *macromolecules*, 33, **2000**, 8618.
- [23] C. Hou, R. Qu, J. Liu, L. Ying, C. Wang, *J. Appl. Polym. Sci.*, **2006**, 100, 3372.

9 Atom Transfer Radical Polymerization (ATRP) of Styrene and Acrylonitrile with Monofunctional and Bifunctional Initiators*

9.1 Abstract

A bifunctional initiator (benzal bromide) was used to initiate the bulk atom transfer radical polymerization of styrene and acrylonitrile at 90 °C with CuBr/2,2-bipyridyl. We compared these results with those of a monofunctional initiator of similar structure (1-bromoethyl benzene) under the same polymerization conditions. The monofunctional initiator worked better than the bifunctional initiator when both comonomers were added simultaneously at the beginning of the copolymerization; the bifunctional initiator was only effective when acrylonitrile was added after 20 minutes of polymerization with styrene. The styrene-acrylonitrile copolymers were characterized by gel permeation chromatography, ¹³C nuclear magnetic resonance spectroscopy, Fourier-transform infrared spectroscopy, and refractometry. Copolymer composition was monitored by both ¹³C NMR and by the change in the specific refractive index increment.

9.2 Introduction

Styrene-acrylonitrile (SAN) copolymers have important commercial applications. These copolymers have a high demand due to their superior optical, chemical, thermal and mechanical properties.^[1] SAN is typically synthesized with free radical polymerization; production can be carried out as bulk, solution, or emulsion free radical polymerization.^[2-9] Conventional free-radical polymerization allows for the efficient production of several polymer types at high yield, but lacks the precise microstructural control attained with living polymerization systems. Living polymerizations can be used to synthesize well-defined polymers with various functionalities, compositions, and chain architectures.

* This chapter has been submitted for publication: M. Al-Harhi, J. Soares, L. Simon, *Polymer*.

Controlled living free radical polymerization has been successfully used to make SAN copolymers.^[10-14]

Although several controlled radical polymerization systems have been reported by various groups,^[14-19] atom transfer radical polymerization (ATRP) remains one of the most powerful, versatile, simple, and inexpensive living polymerization techniques. The use of a range of initiators in ATRP is an effective method for introducing useful functionalities and producing polymers with novel architectures and properties. SAN was one of the copolymers studied by the Matyjaszewski group.^[19] They used several types of initiators in their studies.

A systematic study comparing monofunctional and bifunctional initiators of similar structures has not yet been reported for the case of copolymerization with ATRP. Bifunctional initiators have interesting behavior in conventional free radical polymerization.^[20] Compared to monofunctional initiators, they produce polymers with higher conversion for the same polymerization time, higher molecular weight and narrower molecular weight distribution.

In batch copolymerization, if one comonomer is consumed faster than the other, composition drift is observed. During non-living polymerization, comonomer composition drift produces copolymer chains with different intermolecular compositions. In controlled free radical polymerization (including ATRP), on the other hand, composition drift causes intramolecular comonomer composition changes and produces gradient copolymers. Comonomer reactivity ratios, comonomer feed policies, and initial comonomer compositions are the major factors that can be used to control composition drift.

In the previous chapter, we compared the bifunctional initiator benzal bromide with monofunctional initiators for the synthesis of polystyrene via ATRP.^[21] In the present chapter, we compare the synthesis of SAN copolymers with benzal bromide (bifunctional initiator) and 1-bromoethyl benzene (monofunctional initiator). The chemical structures of both initiators are shown in Figure 9.1.

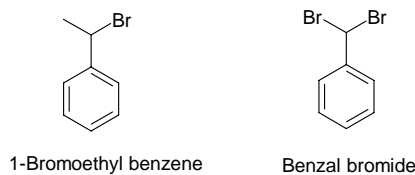


Figure 9.1 Chemical structures of the initiators used in this study.

9.3 Experimental

Materials. Styrene (>99%) inhibited with 10–15 ppm 4-*tert*-butyl catechol and acrylonitrile (AN) (99%) inhibited with 35-45 ppm monomethyl ether hydroquinone (MEHQ) were purchased from Aldrich. Both styrene and acrylonitrile were first passed through an aluminum oxide column to remove the inhibitors and then purged with nitrogen for 30 minutes. We used benzal bromide (97%) (Aldrich) as bifunctional initiator and 1-bromoethyl benzene (97%) (Aldrich) as monofunctional initiator. We used copper bromide (I) (99.999%) complex with 2-2 dipyridyl (99%), purchased from Aldrich, as the catalyst. Both initiators and the catalyst were used as received. Solvents used over the course of the experiments and characterization of the copolymers (ethanol, acetone, chloroform, tetrahydrofuran) were used as received from VWR.

Simultaneous Polymerizations. The catalyst, copper(I) bromide (0.147 g or 0.00102 moles) and ligand 2-2 dipyridyl (0.400 g or 0.00255 moles) were first placed in a round bottom flask and three cycles of nitrogen pressurization followed by vacuum were applied to remove air and moisture from the flask. The deoxygenated monomers, styrene (7.42 mL or 0.064 moles) and acrylonitrile (2.51 mL or 0.038 moles), were added in a ratio of 63 mol% styrene using disposable syringes. The mixture was stirred at room temperature until it was homogeneous. The flask was placed in an oil bath at 90 °C and the monofunctional (0.14 mL or 0.00102 moles) or bifunctional initiator (0.1697 mL or 0.00102 moles) was added to the flask using disposable syringes.

Sequential Polymerizations. The same procedure and amount of chemicals described for the Simultaneous Polymerizations were used, except that the acrylonitrile was added 20 minutes after introducing the initiators.

Polymer Characterization. Monomer conversion was determined by gravimetry. The content of the flask was first washed with tetrahydrofuran (THF) and the polymer was precipitated using a large excess of ethanol (after passing through aluminum oxide to remove the copper bromide). The precipitated polymer was filtered through filter paper and dried up to constant mass.

^{13}C NMR spectra were recorded for polymer samples dissolved in deuterated chloroform (CDCl_3), using a 300-MHz AC Bruker Fourier-transform spectrometer. The temperature of the probe was 25 °C and the number of scans was 4092. The relative amount of comonomers incorporated into the copolymer was estimated from the integrated area under the appropriate peak intensities, as discussed below.

Molecular weights were obtained using gel permeation chromatography (Waters 590) operating at room temperature with a refractive index (RI) detector on-line with a multiangle laser light-scattering photometer system. THF was filtered and used as the eluent at a flow rate of 1.0 mL/min. Samples for analysis were prepared as 0.5% solutions in THF and filtered through 0.45 μm filters prior to injection. The dn/dc values used in the calculation of molecular weights were calculated independently using a refractometer (Brice-Phoenix differential refractometer equipped with 632 nm band-pass interference filters, operated at 25 °C).

Fourier transform-infrared (FTIR) spectroscopy was used to measure the composition of the SAN copolymers. The polymer powder was dissolved in THF and a few drops of the solution were added onto a transparent KBr disk. After evaporation of the solvent, a thin polymer film was formed on the KBr disk. The samples were analyzed by FTIR and the spectra were reported after subtracting from a background spectrum for the plain KBr disk. The spectra were recorded from 400 to 4000 cm^{-1} , after 32 scans, with a resolution of 4 cm^{-1} .

Refractive index (RI) measurements were performed on all samples prior to GPC analysis to find the dn/dc ratio. Five different concentrations of the same sample (0.01

gram (and less) of SAN in 1 ml of THF) were made by dissolving the copolymer in THF. Each sample was measured on the refractometer and the results from the RI measurements were plotted against the concentration of the sample. A straight line was obtained from the graph and the multiplication of the slope of the curve and the calibration constant of the instrument gave the dn/dc .

9.4 Results and discussion

Initially, polymerizations with the mono- and bifunctional initiators were carried out by adding the two comonomers, styrene and acrylonitrile, simultaneously into the round bottom flask before placing it in the oil bath to start the copolymerization. However, the results from these tests were surprising because monomer conversion with the monofunctional initiator was higher than that with the bifunctional initiator for a given polymerization time. Since the bifunctional initiator has two bromine atoms and, hence, two active radicals, we expected that the polymer chains would grow from both ends with increased monomer conversion and producing polymers with higher molecular weight at a given polymerization time. However, this was not the case: the GPC analysis showed that samples made with the bifunctional initiator had lower molecular weights than those prepared with the monofunctional initiator. Figure 9.2 shows that monomer conversion and number average molecular weight of SAN copolymers made with the monofunctional initiator are higher than those using the bifunctional initiator.

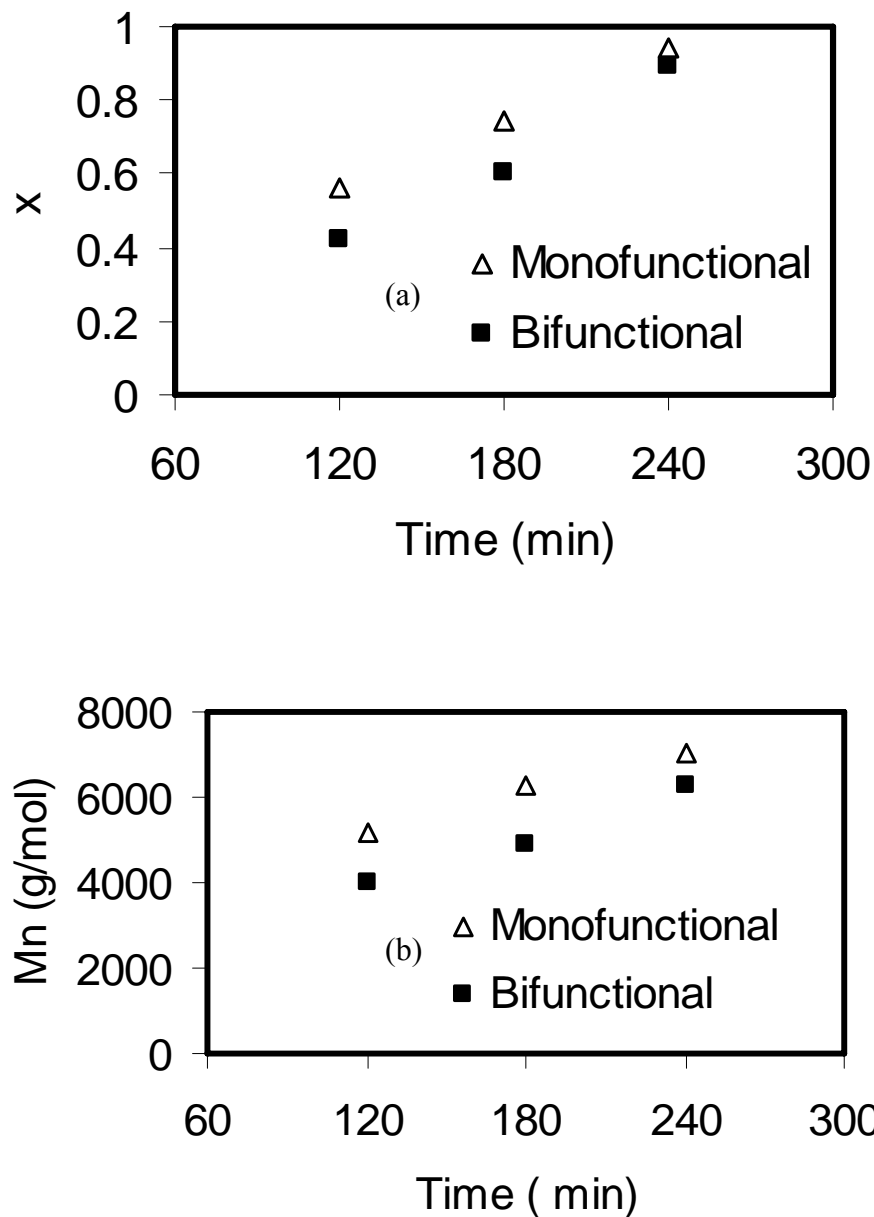


Figure 9.2 Comparison of batch ATRP of styrene and acrylonitrile using a monofunctional and a bifunctional initiator when both comonomers are added simultaneously: (a) monomer conversion, x ; (b) number average molecular weight, M_n . (Polymerization conditions: $[M]_0/[I]_0/[C]_0 = 100/1/1$. Temperature = 90 °C)

In order to help understanding such unexpected results, pure acrylonitrile was polymerized with the bifunctional (benzal bromide) and monofunctional (1-bromoethyl benzene) initiators. A five-hour polymerization (reproduced several times) with

acrylonitrile and the bifunctional initiator (the molar ratio of acrylonitrile to the initiator was 37:1) at 90 °C surprisingly produced no measurable quantities of polymer. This is not the case for the polymerization of acrylonitrile or styrene with the monofunctional initiator. In fact, the polymerization of acrylonitrile using 1-bromoethyl benzene (37:1 molar ratio of monomer to the initiator) reached complete conversion within ten minutes.

We may propose two explanations for the lack of polymerization activity of acrylonitrile with benzal bromide: 1) Side reactions between acrylonitrile and benzal bromide consume the active species or inhibit the initial activation of benzal bromide; 2) The reaction of the first acrylonitrile molecule with the benzal bromide initiator forms an unsymmetrical substituted structure that is not activate to propagate additional acrylonitrile monomers (see Figure 9.3). We realize that the mechanism described in Figure 9.3 is highly speculative and is just shown here as a conjecture to help explain the results we will discuss in the next paragraphs.

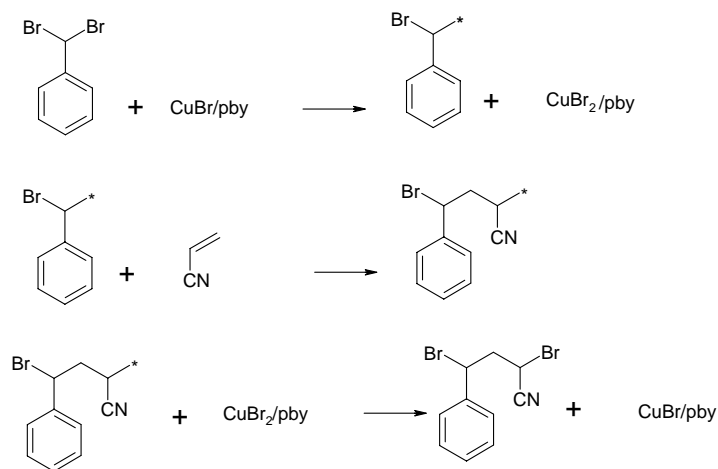


Figure 9.3 Mechanism for the formation of an unsymmetrical initiator inactive for acrylonitrile propagation.

To test this hypothesis, some changes were made in the original batch polymerization process: we started the polymerization with styrene and only added the

acrylonitrile into the flask 20 minutes after injecting the initiator (*sequential polymerization*). It should be noted that all other experimental conditions were exactly the same as for the simultaneous polymerizations described above. The sequential polymerization process allows styrene to react with the bifunctional initiator first, forming an initial block of polystyrene macroinitiator (PS). The proposed mechanism for the mono- and bifunctional initiators are shown in Figure 9.4. The monofunctional initiator forms a copolymer of the type PS-b-SAN, and the bifunctional initiator forms a copolymer of the type SAN-b-PS-b-SAN.

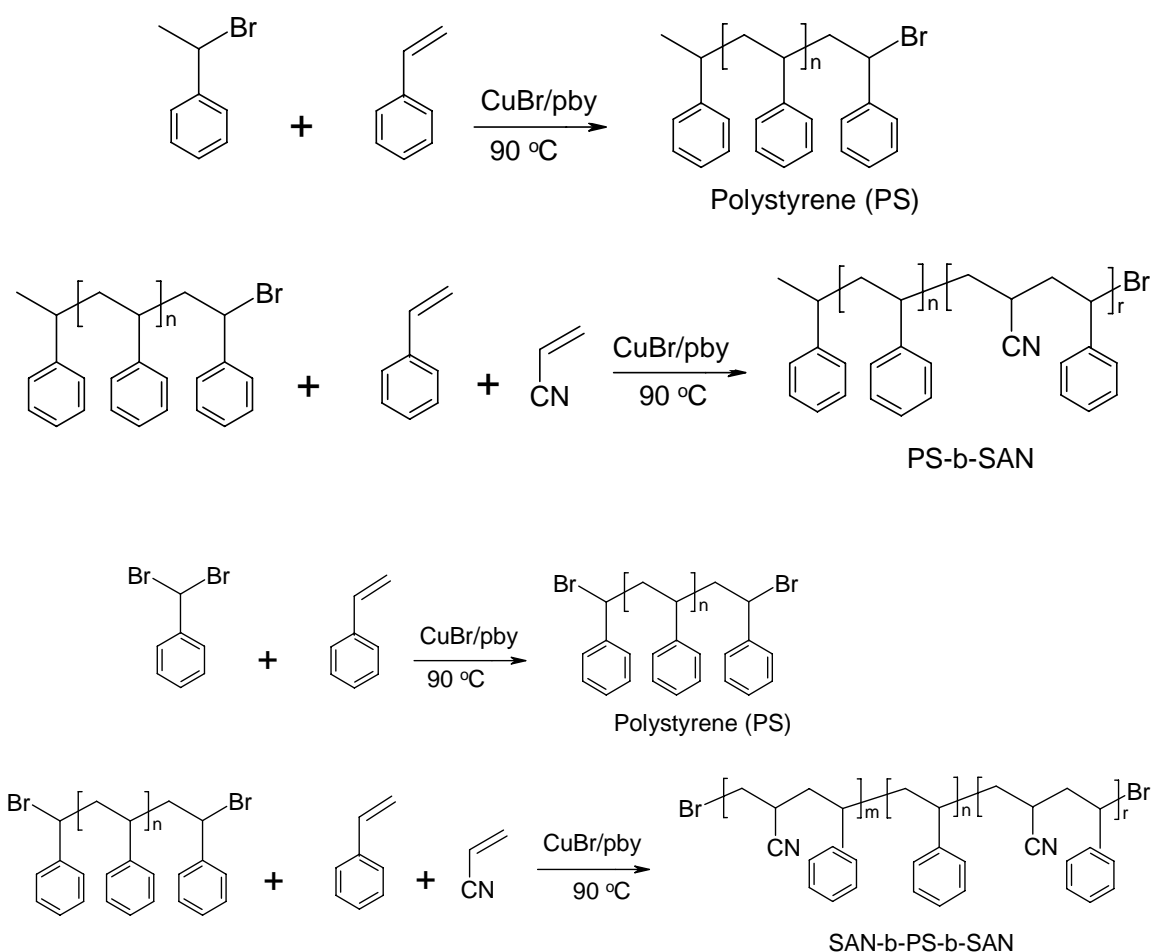
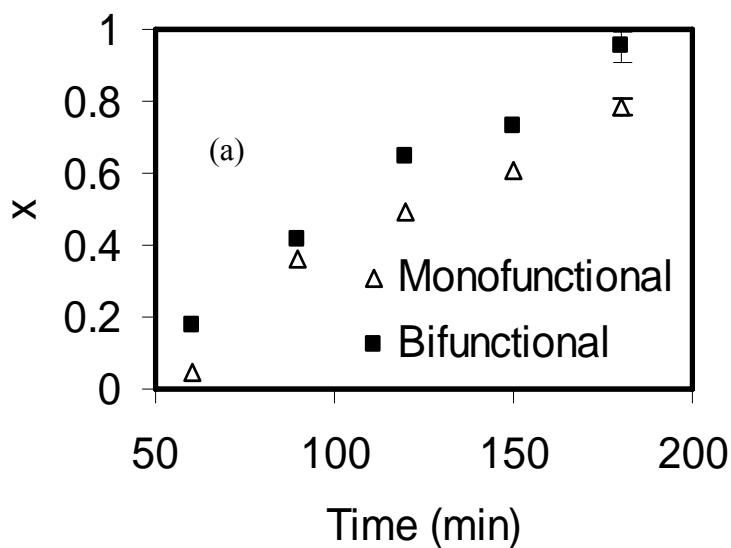


Figure 9.4 Proposed mechanism for the formation of PS-b-SAN and SAN-b-PS-b-SAN copolymer using monofunctional (top) and bifunctional (bottom) initiators in the sequential polymerization approach.

The polymerization time of 20 minutes with only styrene is required for styrene to initialize the polymerization and overcome the induction time.^[21] Figures 9.5 to 9.7 show

that this approach works well when acrylonitrile was added, the bifunctional initiators had already polymerized some styrene molecules and could continue to grow forming SAN copolymer chains. Three replicate polymerizations were done at different time intervals and the averaged results are shown in Figures 9.5 to 9.7 (example of error bar calculated as one standard deviation is shown in one of the data).

Figures 9.5 to 9.7 show that the sequential polymerizations worked well and that the bifunctional initiator behaves more closely to what we had originally expected. Figure 9.5.a shows that monomer conversion with the bifunctional initiator is higher than that with the monofunctional initiator for the same polymerization time. The linear dependence of $\ln([M]_0/[M])$ with time for both initiators, shown in Figure 9.5.b, is an evidence of living polymerization. The deviation from linearity for polymerizations with the bifunctional initiator after three hours is likely due to the high monomer conversion (95%).



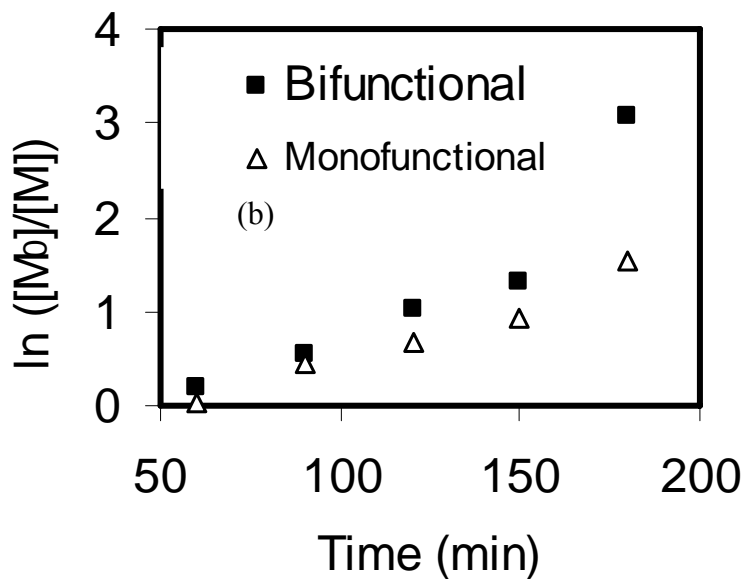


Figure 9.5 Comparison of ATRP of styrene and acrylonitrile using a monofunctional and a bifunctional initiator when acrylonitrile is added 20 minutes after the initiation of the polymerization with styrene: (a) monomer conversion, x ; and (b) $\ln([M]_0/[M])$ vs. time (Polymerization conditions: $[M]_0/[I]_0/[C]_0 = 100/1/1$).

Figure 9.6.a shows that all polymer samples made with the bifunctional initiator have higher molecular weights than the ones produced with the monofunctional initiator. Another indication that both polymerizations were controlled is the increase of polymer molecular weight with monomer conversion, as seen in Figure 9.6.b.

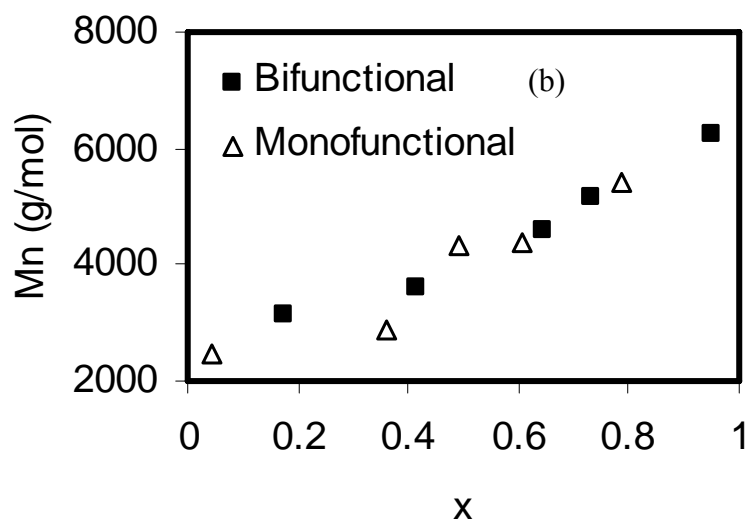
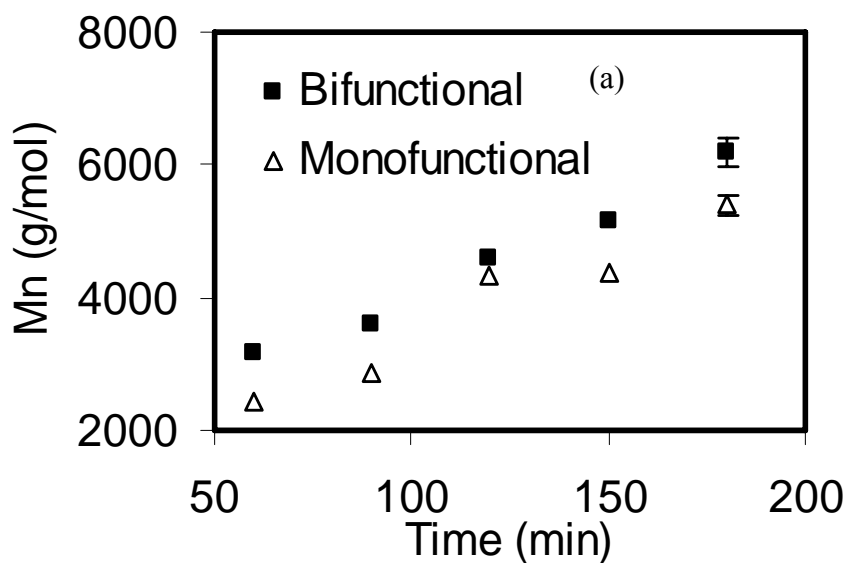


Figure 9.6 Comparison of ATRP of styrene and acrylonitrile using a monofunctional and a bifunctional initiator when acrylonitrile is added 20 minutes after the initiation of the polymerization with styrene: (a) Mn vs. time; and (b) Mn vs conversion, x (Polymerization conditions: $[M]_0/[I]_0/[C]_0 = 100/1/1$).

The polydispersity index (PDI) as a function of polymerization time and monomer conversion of all SAN copolymers is typical for ATRP (Figure 9.7). It starts slightly higher than one at low conversions and then it decreases until most of the monomer is consumed at high conversions. Generally, the bifunctional initiator produced copolymers with lower PDIs than monofunctional initiators.

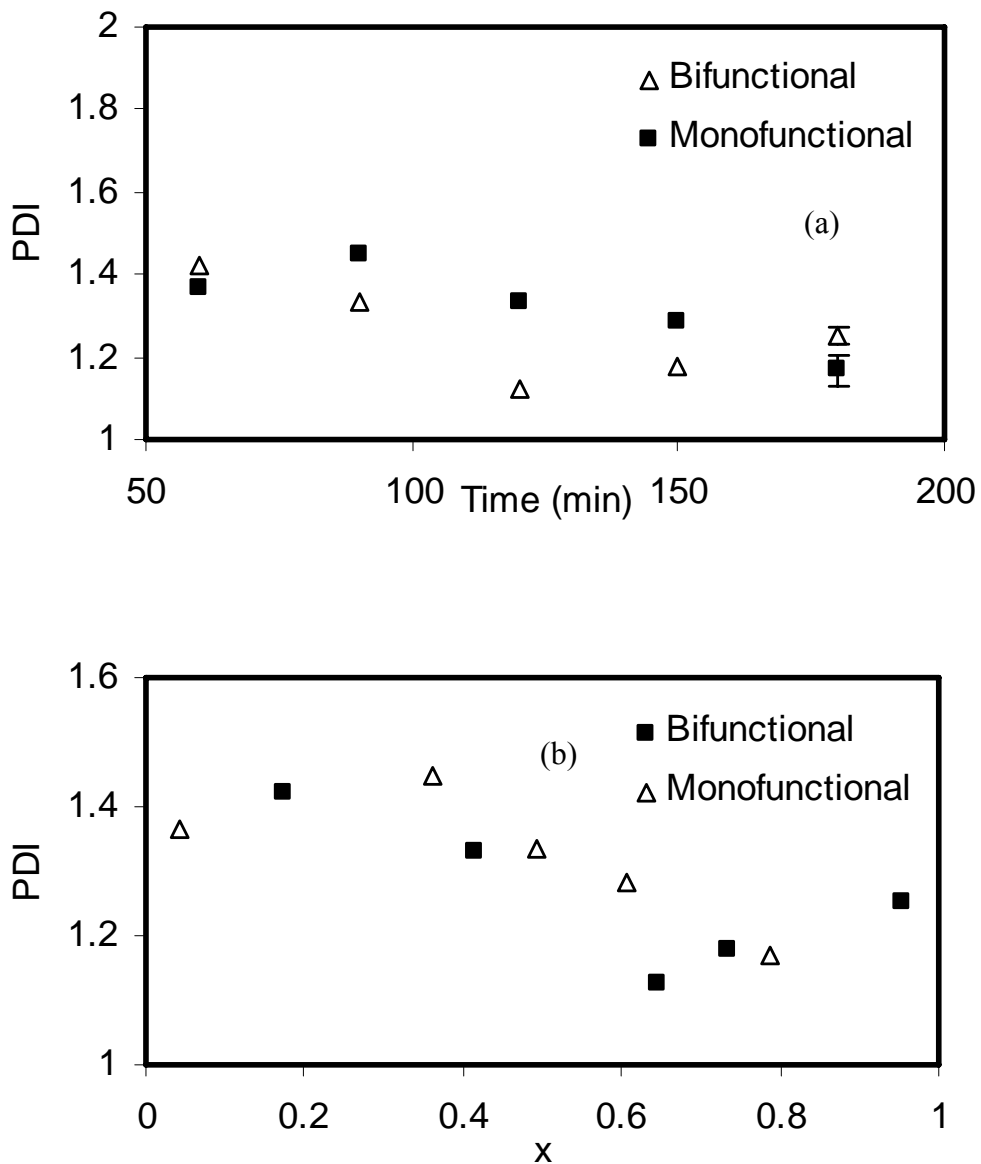


Figure 9.7 Comparison of ATRP of styrene and acrylonitrile using a monofunctional and a bifunctional initiator when styrene is added 20 minutes before acrylonitrile: (a) PDI vs. time; and (b) PDI vs. conversion, x (Polymerization conditions: $[M]_0/[I]_0/[C]_0 = 100/1/1$).

We used the azeotropic ratio for styrene and acrylonitrile for the sequential polymerizations: 63 mol-% styrene and 37 mol-% acrylonitrile. The azeotropic ratio will not lead to composition drift when both comonomers are introduced simultaneously at the beginning of the batch polymerization. However, since the acrylonitrile was introduced 20 minutes after the injection of the styrene, the initial monomer fraction deviated from the azeotropic composition and a drift was expected.

It is common to determine the average comonomer composition of copolymers with $^1\text{H-NMR}$. Unfortunately, for SAN copolymers the proton spectra are so poorly resolved that a detailed interpretation was impossible. The methylene and methine protons of the copolymer overlapped in the region 1.2–3.1 ppm. For this reason, we used $^{13}\text{C-NMR}$ instead of $^1\text{H-NMR}$ to determine copolymer average chemical composition. The $^{13}\text{C-NMR}$ spectrum of one representative copolymer sample is shown in Figure 9.8. Whereas the nitrile carbon resonance shows multiplet splitting around 120.1–121.4 ppm, the aromatic ring carbons appear in the spectra around 125–126 ppm. The relative intensities of the resonances in this region can be used to calculate the average copolymer composition. Fractions of each comonomer in the copolymer as a function of polymerization time, determined from the $^{13}\text{C-NMR}$ spectra by comparing the styrene (aromatic ring) peak with the nitrile group, are shown in Figure 9.9.

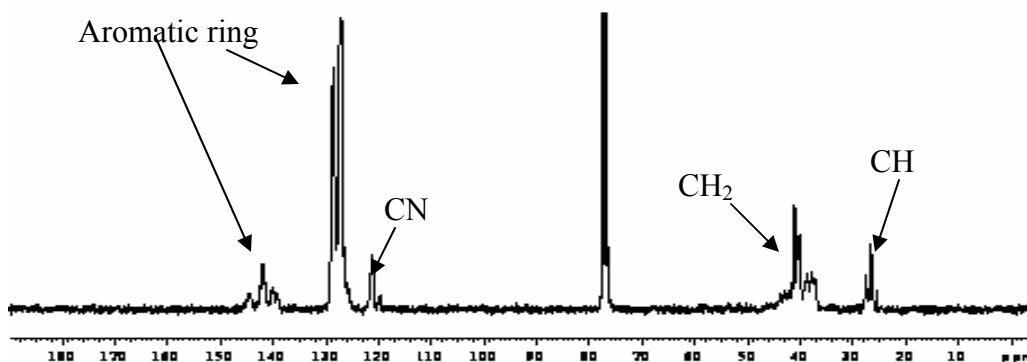


Figure 9.8 $^{13}\text{C-NMR}$ spectrum of a representative SAN copolymer made by sequential copolymerization.

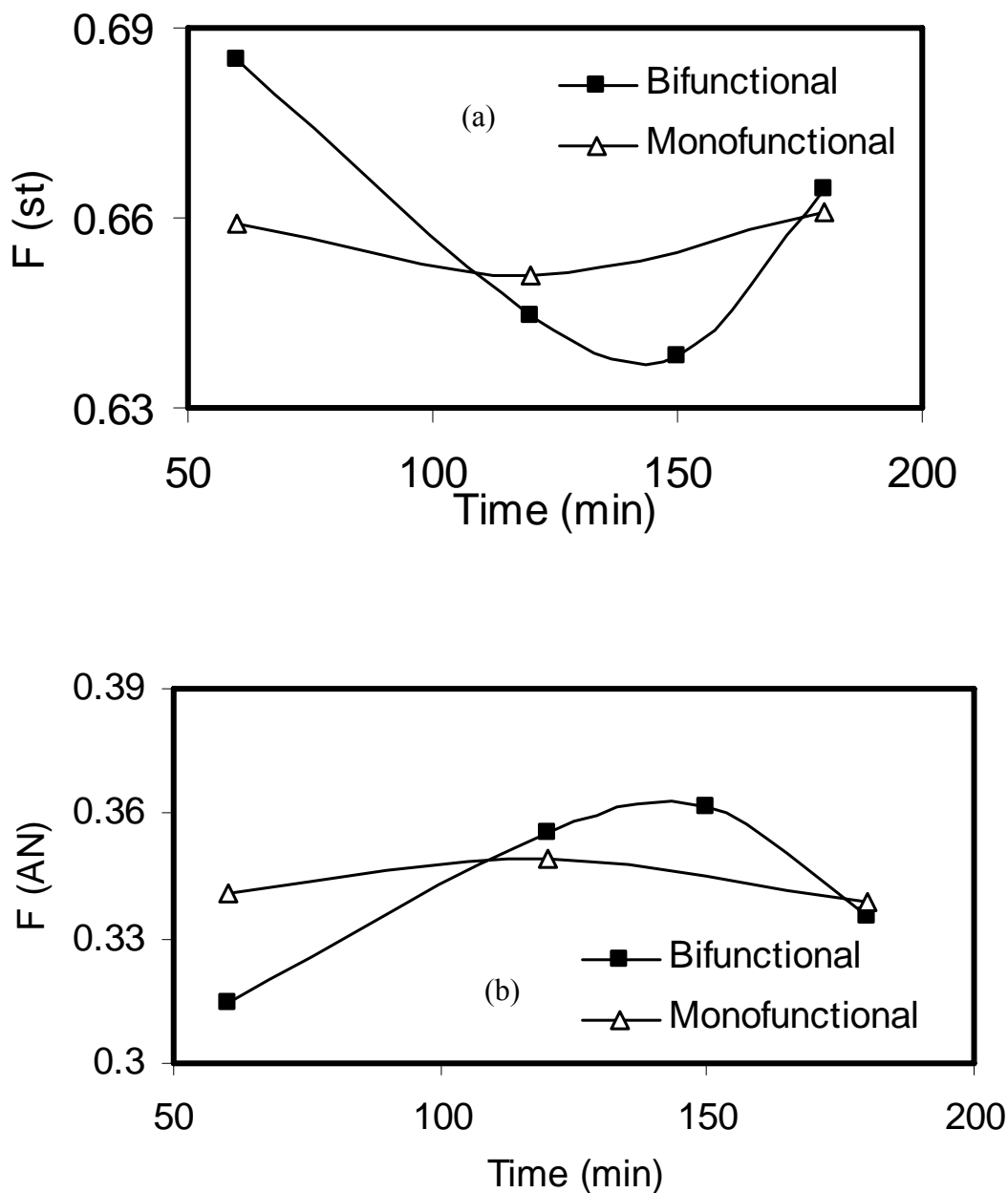


Figure 9.9 SAN copolymer composition measured with ^{13}C NMR: (a) styrene fraction vs. polymerization time for both initiators; and (b) acrylonitrile fraction vs. polymerization time for both initiators. Polymerization conditions: $[M]_0/[I]_0/[C]_0 = 100/1/1$. Temperature = 90°C

Note that the comonomer fractions in Figure 9.9 correspond to the cumulative average composition for the total polymerization time. For the case with the bifunctional initiator when acrylonitrile was injected 20 minutes after styrene injection, there is a block

of polystyrene at the middle of the chain SAN-b-PS-b-SAN. Similarly, for the monofunctional initiator there is a block of polystyrene PS-b-SAN at one of the chain ends. The composition of the SAN copolymer segments, discounting the initial polystyrene block, can be obtained by subtracting the contribution of the polystyrene block. This is possible because the length of the polystyrene block can be obtained from the styrene conversion after the initial 20 minutes of polymerization using the following equation:

$$CF_a^t = \frac{n_a^t}{n_s^t - n_s^{20} + n_a^t} \quad (1)$$

where CF is the corrected molar fraction in the copolymer and n is the number of moles,. The subscripts a and s indicate the type of the copolymer (acrylonitrile and styrene). The superscripts (t and 20) indicate the time. The corrected copolymer composition is summarized in Table 9.1. The values in Table 9.1 cannot be compared with the values obtained from the NMR test since NMR shows the cumulative composition. This was mainly done to get a sense of the range where the values would fall into.

Table 9.1 Molar fraction of acrylonitrile in the SAN copolymer. Cumulative copolymer composition (from ^{13}C NMR) and corrected fraction excluding block of polystyrene made during the first 20 minutes of polymerization.

Initiator	Polymerization Time (h)	Cumulative ^{13}C NMR Fraction of AN	Corrected Fraction of AN
Monofunctional	1	0.341	0.414
Monofunctional	2	0.349	0.355
Monofunctional	3	0.339	0.342
Bifunctional	1	0.315	0.458
Bifunctional	2	0.355	0.387
Bifunctional	2.5	0.362	0.390
Bifunctional	3	0.336	0.356

Before determining their molecular weight by GPC, it was necessary to measure the refractive index of the copolymers and to find the specific refractive increment (dn/dc). The dn/dc ratio for a copolymer varies according to the weight fraction of each comonomer incorporated into the polymeric chains:

$$\left(\frac{dn}{dc}\right)_{\text{copolymer}} = \sum \left(\frac{dn}{dc}\right)_i w_i \quad (2)$$

where n is the refractive index, c is the weight concentration (in $\text{g}_{\text{polymer}}/\text{g}_{\text{solution}}$) and the index i correspond to the homopolymer type.

The dn/dc ratio for pure polystyrene in THF is 0.185 mL/g. Acrylonitrile is not soluble in THF; therefore, there is no experimental value for its dn/dc ratio in this solvent. When the incorporation of styrene in the SAN copolymer increases, the dn/dc ratio gets closer to 0.185 mL/g. Similarly, higher acrylonitrile incorporations will cause the dn/dc ratio to deviate from 0.185 mL/g. Based on that, the copolymer composition was correlated to measurements of the dn/dc ratio. Figure 9.10 shows how the values of dn/dc vary as a function of polymerization time. The bifunctional initiator incorporated acrylonitrile faster than the monofunctional initiator and, therefore, shows a sharper decrease in the dn/dc ratio. This result supports the measures with ^{13}C NMR. The highest content of the acrylonitrile in SAN (from both ^{13}C NMR and refractometry analyses) is achieved after 2.5 hours of polymerization with the bifunctional initiator.

Generally, the comonomer composition in the copolymer can be calculated from dn/dc values using the following equation:

$$\left(\frac{dn}{dc}\right)_{\text{copolymer}} = \left(\frac{dn}{dc}\right)_{\text{monomer1}} w_1 + \left(\frac{dn}{dc}\right)_{\text{monomer2}} w_2 \quad (3)$$

where w_1 and $w_2 = (1 - w_1)$ are the weight fractions of the two comonomers in the copolymer. Unfortunately, the dn/dc of acrylonitrile in THF is unavailable because acrylonitrile is insoluble in THF. Therefore we could not use Equation (3) in this study to measure copolymer composition, but this would be a useful approach for copolymers where both dn/dc ratios are known for the respective homopolymers when an on-line refractometer is installed with the GPC.

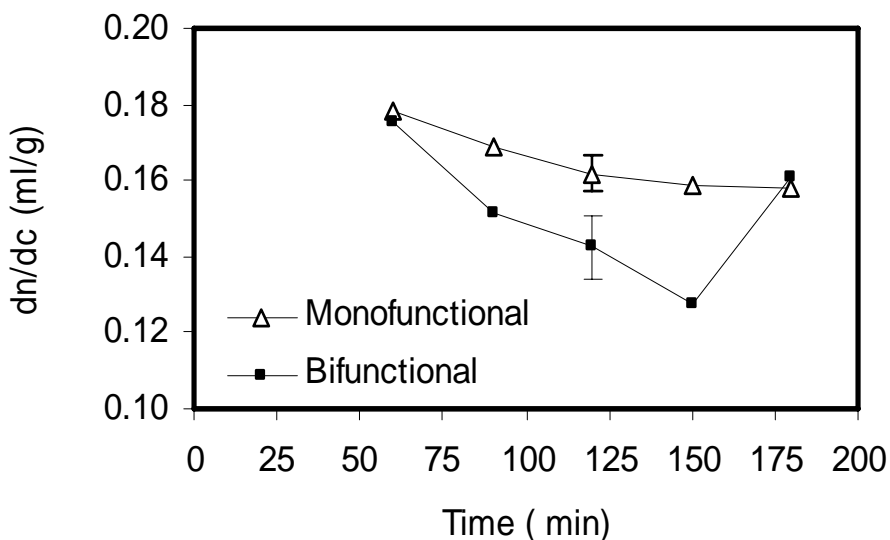


Figure 9.10 dn/dc ratios of SAN polymerized with ATRP at 90 °C using monofunctional and bifunctional initiators as a function of polymerization time. (Polymerization conditions: $[M]_0/[I]_0/[C]_0 = 100/1/1$). The error bars represent one standard deviation from two replicates done for each sample.

FTIR was also used to identify the incorporation of both comonomers into the polymeric chains. Results from FTIR confirmed, as expected, that these copolymers were composed of styrene and acrylonitrile units. The absorption band at 1601 cm^{-1} is representative of the aromatic ring of the styrene comonomer, while the one at 2235 cm^{-1} identifies the nitrile group of the acrylonitrile comonomer. Figure 9.11 compares FTIR spectra for pure polystyrene and two SAN copolymers containing different fractions of acrylonitrile. The stronger absorbance at 2235 cm^{-1} for the copolymer made with the bifunctional initiator confirms the ^{13}C NMR results that the bifunctional initiator incorporates more acrylonitrile (after 2.5 hours of polymerization) than the monofunctional initiator after 1.0 hour of polymerization (see Figure 9.9). The ratio between the nitrile peak (2235 cm^{-1}) and the phenyl peak (1601 cm^{-1}) is 0.83 after one hour of reaction and it increases to 0.915 after 2.5 hours of polymerization.

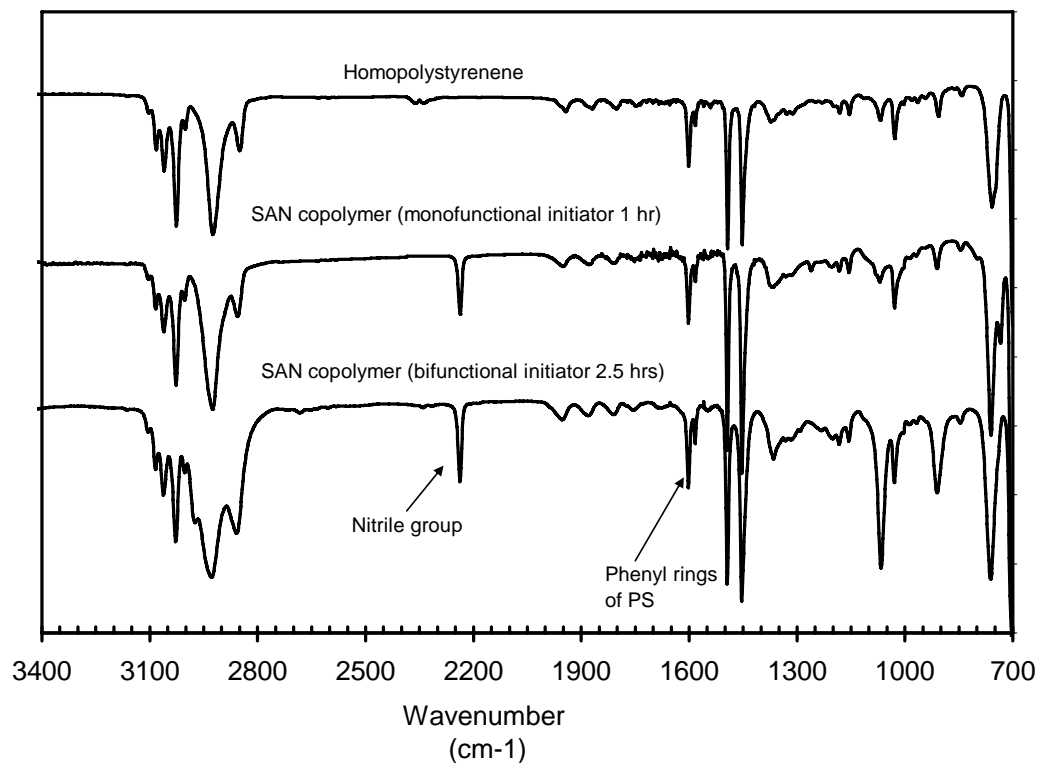


Figure 9.11 FTIR spectra for pure polystyrene and two SAN copolymer samples with different fractions of acrylonitrile. (Spectra presented in transmittance units, curves shifted horizontally for clarity).

9.5 Conclusion

Bulk atom transfer radical polymerization of styrene and acrylonitrile with a bifunctional (benzal bromide) and monofunctional initiator (1-bromoethyl benzene) was successfully conducted in this investigation. Two polymerization procedures, simultaneous and sequential polymerization, were compared. During simultaneous addition of styrene and acrylonitrile, the monofunctional initiator makes polymers with higher monomer conversion and molecular weights for the same polymerization time. This unusual result may be due to side reactions between the acrylonitrile and the benzal bromide initiator or due to the formation of species inactive for acrylonitrile polymerization after the first acrylonitrile insertion.

On the other hand, the sequential addition of comonomers (styrene first, followed by acrylonitrile after 20 minutes of polymerization) gave different results. The bifunctional

initiator produced SAN with higher conversion, higher molecular weight, and narrower molecular weight distribution than the monofunctional initiator under these polymerization conditions.

Copolymer composition as a function of time was monitored by ^{13}C NMR, FTIR, and refractometry. All these techniques indicate that composition drift is more pronounced with the bifunctional initiator is used.

9.6 References

- [1] G. P. Ziemba, Encyclopedia of Polymer Science and Technology; Mark H. F., Gaylord N. G., Bikales N. M. Eds.; Wiley: New York, **1964**,1,425.
- [2] R. F. Blanks, B. N. Shah, J. Polym. Sci., Polym. Chem. Ed. **1976**, 14,: 2589.
- [3] A. Kaim, J. Macromol. Sci., Pure Appl. Chem. **1998**, A35, 577.
- [4] D. J. Hill, J. H. O'Donnell, P. W. O'Sullivan, Macromolecules **1982**, 15, 960.
- [5] D. J. Hill, A. P.Lang, P. D. Munro, J. H. O'Donnell, Eur. Polym. J. **1992**, 28, 391.
- [6] S. Djekhaba, C. Graillat, J. Guillot, Eur. Polym. J. **1986**, 22, 729.
- [7] R. G. Fordyce, E. C. Chapin, J. Am. Chem. Soc. **1947**, 69, 581.
- [8] K. Lee, L. Gan, C. Chew, S. Ng, Polymer **1995**, 36, 3719.
- [9] P. G. Sanghvi, A. C. Patel, K. S. Gopalkrishnan, S. Devi, Eur. Polym. J. **2000**, 36, 2275.
- [10] T. Fukuda, T. Terauchi, A. Goto, Y. Tsujii, T. Miyamoto, Y. Shimizu. Macromolecules **1996**, 29,3050.
- [11] S. Brinkmann-Rengel, N. Niessner, ACS Symp Ser **2000**, 768, 394.
- [12] D. Benoit, V. Chaplinski, R. Braslau, C. J. Hawker, J. Am. Chem. Soc. **1999**, 121, 3904.
- [13] D. Fan, J. He, J. Xu, W. Tang, Y. Liu, Y. Yang, J. Polym.Sci., Part A Polym. Chem. **2006**, 44, 2260.
- [14] N. Tsarevsky, T. Sarbu, B. Belt, K. Matyjaszewski, Macromolecules **2002**, 35, 6142.
- [15] K. Matyjaszewski , J. Xia, Chem. Rev. **2001**, 101, 2921.
- [16] M. Kamigaito, T. Ando, M. Sawamoto. Chem. Rev. **2001**, 10, 13689.
- [17] M. K. Georges, R. P. Veregin, P. M. Kazmaier, G. K. Hamer, Macromolecules, **1993**, 26, 2987.
- [18] M. Rodlert, E. Harth, I. Rees, C. Hawker, J. Polym. Sci., Polym. Chem. Ed. **2000**, 38, 4749.
- [19] G. Moad, J. Chiefary, T. K. Chong, J. Krstina, R. T. A. Mayadunne, A. Postma, E. Rizzardo, S. H. Thang, Polym. Int. **2000**, 49, 993.
- [20] M. Villalobos, A. Hamielec, P. Wood, J. Appl. Polym. Sci. **1991**,42, 629.
- [21] M. Al-Harhi, L. Cheng, J. B. P. Soares, L. Simon. Polym.Sci., Part A Polym. Chem. "Atom-Transfer Radical Polymerization of Styrene with Bifunctional and Monofunctional Initiators: Experimental and Mathematical Modeling Results", accepted.

Chapter 10

10 Mathematical Modeling of Atom Transfer Radical Copolymerization *

10.1 Abstract

In this study, we developed a comprehensive mathematical model for atom transfer radical copolymerization in a batch reactor using the concept of pseudo-kinetic rate constants and the method of moments. The model describes molecular weight, monomer conversion, polydispersity index, and copolymer composition as a function of polymerization time. Experimental data for styrene and n-butyl acrylate copolymerization were obtained from the literature and compared with the model, showing good agreement between model predictions and experimental results. We have also tested the model with styrene-acrylonitrile data obtained in our laboratory. Finally, we used the model to study the effects of comonomer reactivity ratios, feed compositions, activation rate constants, and deactivation rate constants on the copolymer sequence length distribution.

10.2 Introduction

Copolymer properties are significantly influenced by comonomer composition and sequence length distribution. Controlled radical polymerization (CRP) techniques are powerful methods for synthesizing copolymers with different types of comonomer sequence length distributions. The most versatile CRP techniques are nitroxide-mediated polymerization (NMP), atom-transfer radical polymerization (ATRP), and reversible addition-fragmentation chain transfer (RAFT). Several reviews are available in the literature on these techniques.^[1-7] Even though they obey different mechanisms, all of them

* This chapter was submitted for publication: M. Al-Harhi, J. Soares, L. Simon, *J. Appl. Polym. Sci.*

are based on the dynamic equilibrium between growing polymer radicals and dormant polymer species.

ATRP has attracted much attention because it is a robust and versatile method for the copolymerization of a wide range of comonomers. ATRP can make copolymers with well defined architectures such as random, block, gradient, and graft.^[6-9]

Several mathematical models have been developed for ATRP. The method of moments was used to investigate the effects of rate constants and reactant concentrations on polymer properties.^[10,11] The free volume theory was used with the method of moments to study the effect of diffusion-controlled reactions.^[12,13] Persistent radical effects in various types of living radical polymerization, including ATRP, were investigated by Fischer^[14,15] and Souaille.^[16] The commercial software package PREDICI was used to study the kinetics of ATRP,^[17] the importance of diffusion-controlled reactions,^[18] and the kinetic modeling of the chain-end functionality.^[19] Butte et al.^[20] used the method of moments and an empirical expression for diffusion-controlled termination to develop a polymerization kinetic model for NMP and ATRP. Monte Carlo simulation was used to study ATRP with monofunctional^[21] and bifunctional initiators.^[22]

Zhang and Ray used the method of moments to model both NMP and ATRP in batch, semi-batch and continuous reactors.^[23,24] They also proposed a general model for copolymerization with ATRP. In this Chapter, we developed a mathematical model for ATRP copolymerization that combines the method of moments and the method of pseudo-kinetic constants. Our model was validated with a case study from the literature (styrene and n-butyl acrylate copolymerization) and with polymerization data obtained in our laboratories (styrene and acrylonitrile copolymerization). We have also used the model to investigate the effects of several polymerization conditions on comonomer sequence length distribution.

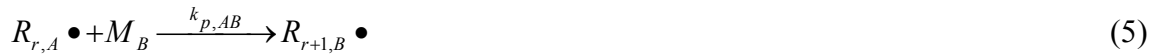
10.3 Model development

10.3.1 Polymerization mechanism

The mechanism of ATRP has all the basic elementary reactions of classical free radical polymerization: initiation, propagation, termination and transfer reactions. In addition, ATRP also includes an equilibrium reaction between active and dormant chains. This equilibrium reaction reduces the frequency of polymer radical termination or transfer reactions, thus imparting the living character of ATRP. Usually, ATRP uses an alkyl halide as the initiator and a complex of a metal halide and a ligand as the catalyst.

The proposed mechanism for ATRP for comonomers A and B is given below:

Equilibrium and propagation



Transfer to monomer



Termination by combination



Termination by disproportionation



where C is the catalyst in its lower oxidation state, CX is the catalyst in its higher oxidation state, M_A and M_B are the comonomers, D is the dormant chain, $R \bullet$ is the polymer radical, P is a dead chain, and r and m are chain lengths.

10.3.2 Pseudo-Kinetic constants

Compared to homopolymerizations, copolymerizations involve more polymerization kinetic steps, requiring more complex population balances. The mathematical treatment can be simplified by using the method of pseudo-kinetic constants developed by Hamielec in the early eighties.^[25] Using the terminal model^[26] for copolymerization, the equations for the pseudo-kinetic rate constants for propagation, k_p , chain transfer, k_{tr} , termination by disproportionation, k_{td} , and termination by combination, k_{tc} , are given by the following equations:

$$k_p = \sum_{i=1}^N \sum_{j=1}^N k_{p,ij} \phi_i f_j \quad (19)$$

$$k_{tr} = \sum_{i=1}^N k_{tr,ij} \phi_i f_j \quad (20)$$

$$k_{td} = \sum_{i=1}^N \sum_{j=1}^N k_{td,ij} \phi_i \phi_j \quad (21)$$

$$k_{tc} = \sum_{i=1}^N \sum_{j=1}^N k_{tc,ij} \phi_i \phi_j \quad (22)$$

where N is the number of comonomers, and k_{pij} , $k_{tr,ij}$, $k_{td,ij}$, $k_{tc,ij}$ are the kinetic rate constants for propagation, chain transfer to monomer, termination by disproportionation and termination by combination, respectively. The subscripts i and j are used to designate the type of polymer radical and monomer.

The mole fraction of polymer radical i (ϕ_i) is given by:

$$\phi_i = \frac{[R_i \bullet]}{\sum_{i=1}^N [R_i \bullet]} \quad (23)$$

The mole fraction of monomer j in the monomer mixture (f_j) is given by :

$$f_j = \frac{[M_j]}{\sum_{j=1}^N [M_j]} \quad (24)$$

The validity of the pseudo-kinetic rate constant method has been investigated for conventional free radical polymerization using the terminal model.^[25,27-29] However, to our knowledge, this is the first time that the pseudo-kinetic rate constant method is applied to ATRP.

In addition to the pseudo-kinetic constants defined in Equations (19) to (22), two additional constants (activation and deactivation) should be defined for ATRP. The expression for the pseudo-kinetic rate constant for deactivation is simple to formulate:

$$k_d = \sum_{i=1}^N k_{d,i} \phi_i \quad (25)$$

However, the pseudo-kinetic rate constant for activation is a function of the fraction of dormant chains in the reactor. The molar balances for dormant chains terminated with monomer A or B are:

$$\frac{d[D_{r,A}]}{dt} = -k_{a,A}[D_{r,A}][C] + k_{d,A}[R_{r,A}\bullet][CX] \quad (26)$$

$$\frac{d[D_{r,B}]}{dt} = -k_{a,B}[D_{r,B}][C] + k_{d,B}[R_{r,B}\bullet][CX] \quad (27)$$

We can calculate the concentrations of dormant chains terminated with monomer A or B by making the steady-state approximation for Equations (26) and (27):

$$[D_{r,A}] = \frac{k_{d,A}}{k_{a,A}[C]} [R_{r,A}\bullet][CX] \quad (28)$$

$$[D_{r,B}] = \frac{k_{d,B}}{k_{a,B}[C]} [R_{r,B}\bullet][CX] \quad (29)$$

The molar fraction of dormant chains terminated in monomer i (Γ_i) is given by:

$$\Gamma_i = \frac{[D_i]}{\sum_{i=1}^N [D_i]} \quad (30)$$

Substituting Equation (28) and (29) in Equation (30) leads to the following expressions for binary copolymers,

$$\Gamma_A = \frac{[R\bullet_A]}{[R\bullet_A] + K[R\bullet_B]} \quad (31)$$

and,

$$\Gamma_B = \frac{[R\bullet_B]}{[R\bullet_B] + \frac{1}{K}[R\bullet_A]} \quad (32)$$

where K is the ratio of the equilibrium constants:

$$K = \frac{K_{eq,A}}{K_{eq,B}} = \frac{k_{a,A}/k_{d,A}}{k_{a,B}/k_{d,B}} \quad (33)$$

Note that, when $K_{eq,A} = K_{eq,B} = 1$, the molar ratio of dormant chains (Γ_i) is equal to the molar ratio of polymer radicals (ϕ_i).

Now, the pseudo-kinetic rate constant for activation can be formulated as a function of the fraction of dormant chains:

$$k_a = \sum_{i=1}^N k_{a,i} \Gamma_i \quad (34)$$

10.3.3 Polymerization rate constants

The cross termination rate constants (k_{tab} and k_{tba}) were calculated using the following correlation,^[30] unless mentioned otherwise:

$$\phi_t = k_{t,AB} / [2(k_{t,AA}k_{t,BB})^{1/2}] \quad (35)$$

The cross propagation rate constants ($k_{p,AB}$ and $k_{p,BA}$) were from the reactivity ratios r_A and r_B and the values of $k_{p,AA}$ and $k_{p,BB}$:

$$r_A = \frac{k_{p,AA}}{k_{p,AB}}, \quad r_B = \frac{k_{p,BB}}{k_{p,BA}} \quad (36)$$

All polymerization rate constants available for conventional free-radical polymerization were obtained from the literature, as indicated below. The activation and deactivation rate constants, particular to ATRP, were estimated by fitting the monomer conversion versus polymerization time data, as also explained below.

10.3.4 Method of moment equations

Molar balances in a batch reactor were derived for polymer radicals, dormant chains, dead polymers and monomer based on the reaction mechanism shown above. In a batch reactor, the concentration of such species varies with time, as explained in Appendix A. The method of moments was used to calculate the average chain lengths of the polymer chains. The j^{th} moments of polymer radicals, dormant chains, and dead polymers are defined below:

$$[\lambda_{R,j}] = \sum_{r=1}^{\infty} r^j [R_r \bullet] \quad (37)$$

$$[\lambda_{D,j}] = \sum_{r=1}^{\infty} r^j [D_r] \quad (38)$$

$$[\lambda_{PP,j}] = \sum_{r=2}^{\infty} r^j [PP_r] \quad (39)$$

$$[\lambda_{P,j}] = \sum_{r=2}^{\infty} r^j [P_r] \quad (40)$$

Applying the method of moments to the molar balance equations produces a set of ordinary differential equations for zeroth, first and second moments for polymer radicals, dormant chains and dead polymers. The final model equations are shown in Table 10.1 and their derivations are presented in Appendix A.

Table 10.1 The final model equations used in the model and their initial conditions

Species	Mathematical equations	Initial condition
Radicals (zeroth moment)	$\frac{d[\lambda_{R,0}]}{dt} = k_f[\lambda_{D,0}][C] - k_b[\lambda_{R,0}][CX]$ $- k_t[\lambda_{R,0}][\lambda_{R,0}] - k_{tr}[M][\lambda_{R,0}]$	0
Radicals (first moment)	$\frac{d[\lambda_{R,1}]}{dt} = k_p[\lambda_{R,0}][M] + k_f[\lambda_{D,1}][C] - k_b[\lambda_{R,1}][CX]$ $- k_t[\lambda_{R,1}][\lambda_{R,0}] - k_{tr}[M][\lambda_{R,1}]$	0
Radicals (second moment)	$\frac{d[\lambda_{R,2}]}{dt} = k_p[\lambda_{R,0}][M] + 2k_p[\lambda_{R,1}][M]$ $+ k_f[\lambda_{D,2}][C] - k_b[\lambda_{R,2}][CX]$ $- k_t[\lambda_{R,0}][\lambda_{R,2}] - k_{tr}[M][\lambda_{R,2}]$	0
Dormant (zeroth moment)	$\frac{d[D_r]}{dt} = -k_a[D_r][C] + k_d[R_r \bullet][CX]$	$[I_0]$
Dormant (first moment)	$\frac{d[\lambda_{D,1}]}{dt} = -k_f[\lambda_{D,1}][C] + k_b[\lambda_{R,1}][CX]$	0
Dormant (second moment)	$\frac{d[\lambda_{D,2}]}{dt} = -k_f[\lambda_{D,2}][C] + k_b[\lambda_{D,2}][CX]$	0

Dead polymers via combination (zeroth moment)	$\frac{d[\lambda_{PP,0}]}{dt} = \frac{k_{tc}}{2}[\lambda_{R,0}][\lambda_{R,0}]$	0
Dead polymers via combination (first moment)	$\frac{d[\lambda_{PP,1}]}{dt} = k_{tc}[\lambda_{R,1}][\lambda_{R,0}]$	0
Dead polymers via combination (second moment)	$\frac{d[\lambda_{PP,2}]}{dt} = k_{tc}[\lambda_{R,0}][\lambda_{R,2}] + k_{tc}[\lambda_{R,1}][\lambda_{R,1}]$	0
Dead polymers via disproportionation (zeroth moments)	$\frac{d[\lambda_{P,0}]}{dt} = k_{td}[\lambda_{R,0}][\lambda_{R,0}] + k_{tr}[M][\lambda_{R,0}]$	0
Dead polymers via disproportionation (first moments)	$\frac{d[\lambda_{P,1}]}{dt} = k_{td}[\lambda_{R,0}][\lambda_{R,1}] + k_{tr}[M][\lambda_{R,1}]$	0
Dead polymers via disproportionation (second moments)	$\frac{d[\lambda_{P,2}]}{dt} = k_{td}[\lambda_{R,0}][\lambda_{R,2}] + k_{tr}[M][\lambda_{R,2}]$	0
Consumption of monomer A	$\frac{dM_A}{dt} = -k_{AA}M_A[\lambda_{R,0,A}] - k_{BA}M_A[\lambda_{R,0,B}]$	$[M_A]$
Consumption of monomer B	$\frac{dM_B}{dt} = -k_{BB}M_B[\lambda_{R,0,B}] - k_{AB}M_B[\lambda_{R,0,A}]$	$[M_B]$
Activator	$[C] = [C]_0 - [CX]$	$[C_0]$
Dactivator	$[CX] = [I]_0 - [\lambda_{R,0}]$	0

The polydispersity index of the polymer is given by:

$$PD = \frac{r_w}{r_n} \quad (41)$$

where r_n is the number average chain length, given by,

$$r_n = \frac{[\lambda_{R,1}] + [\lambda_{D,1}] + [\lambda_{P,1}] + [\lambda_{PP,1}]}{[\lambda_{R,0}] + [\lambda_{D,0}] + [\lambda_{P,0}] + [\lambda_{PP,0}]} \quad (42)$$

and r_w is the weight average chain length, given by,

$$r_w = \frac{[\lambda_{R,2}] + [\lambda_{D,2}] + [\lambda_{P,2}] + [\lambda_{PP,2}]}{[\lambda_{R,1}] + [\lambda_{D,1}] + [\lambda_{P,1}] + [\lambda_{PP,1}]} \quad (43)$$

Average molecular weights (number and weight) can be calculated by multiplying the average chain lengths by the average molecular weight of the repeating unit.

The set of ordinary differential equations (ODE) listed in Table 10.1 were solved simultaneously using MATLAB. Since the resultant ODE system is stiff, we used the MATLAB's ode15s routine for its solution.

10.4 Results and discussion

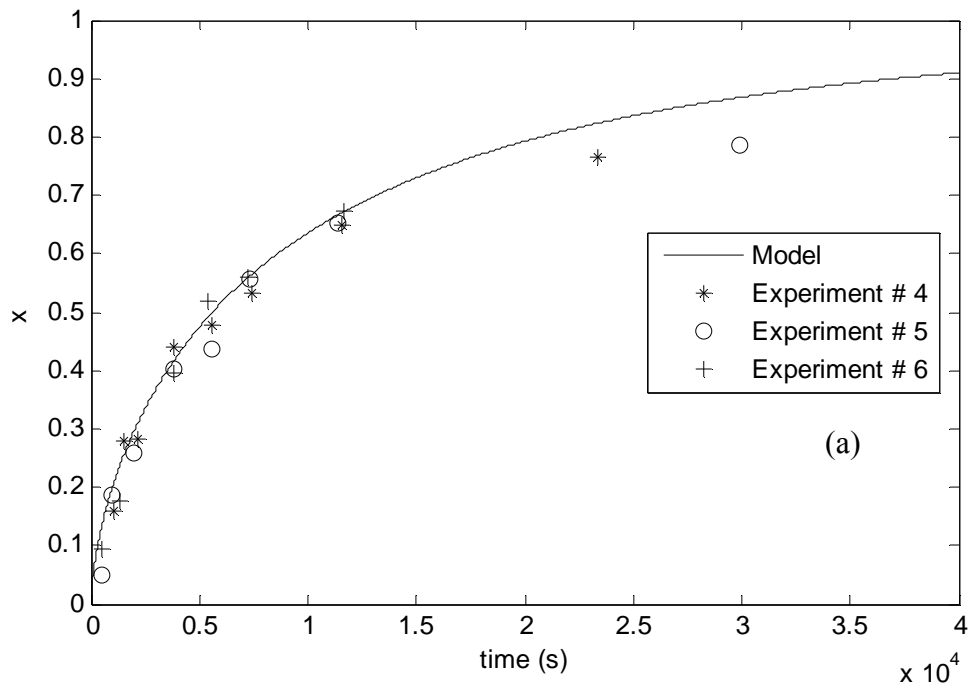
10.4.1 Model validation

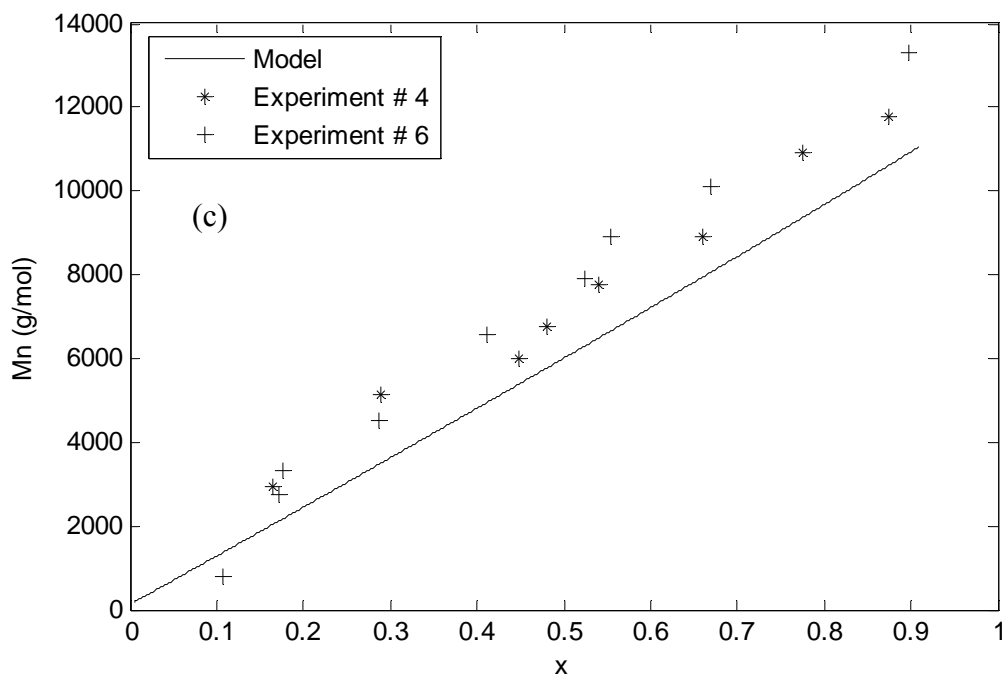
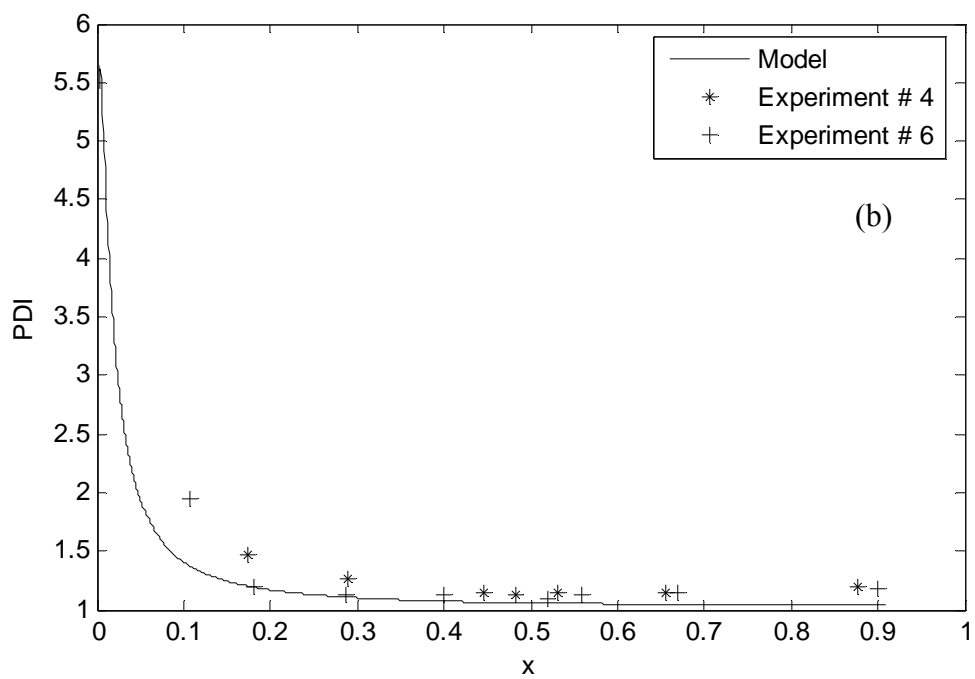
We compared the predictions of our model shown in Table 10.1 with two sets of experimental data, one from results published by Arehart et al.^[31] and the other from our own experimental results^[32]

Arehart et al.^[31] used CuBr, 4'-di(5-nonyl)-2,2'-bipyridine (dNbpy) as catalyst and methyl 2-bromopropionate (MBP) as initiator to copolymerize styrene and n-butyl acrylate (n-BA) at 110 °C. Zhang and Ray^[23] validated their model of atom transfer copolymerization with Arehart et al. results. Because rate constants for activation and deactivation were not available, Zhang and Ray estimated those parameters based on the experimental data reported by Arehart et al. To compare our model (using pseudo-kinetic rate constants) with Zhang and Ray's model, we used the same values they reported for these parameters (Appendix B).

In our model, we assumed that the activation rate constant of the initiator molecules is the same as that of the dormant chains. In other words, we assumed that the activation and deactivation rate constants are the same for both initiation and propagation steps. We have also neglected some side reactions such as thermal polymerization and diffusion-controlled effects. These assumptions may cause deviations between experimental results and simulations at high conversions. Nevertheless, we noticed that the agreement between model predictions and experiments was rather satisfactory.

Our model prediction agrees very well with the monomer conversion data shown in Figure 10.1.a. The polydispersity index is also well represented with our model, as shown in Figure 10.1.b. Reasonable agreement is obtained for the number average molecular weight, as indicated in Figure 10.1.c. Finally, the cumulative copolymer composition predicted with the model tracks the experimental results very closely, as shown in Figure 10.1.d.





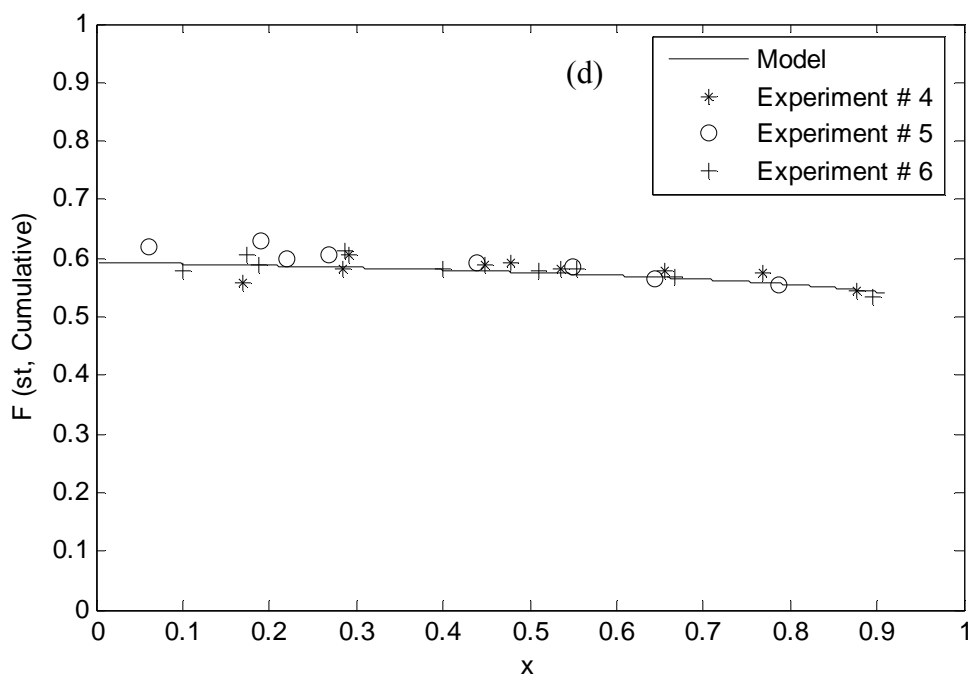
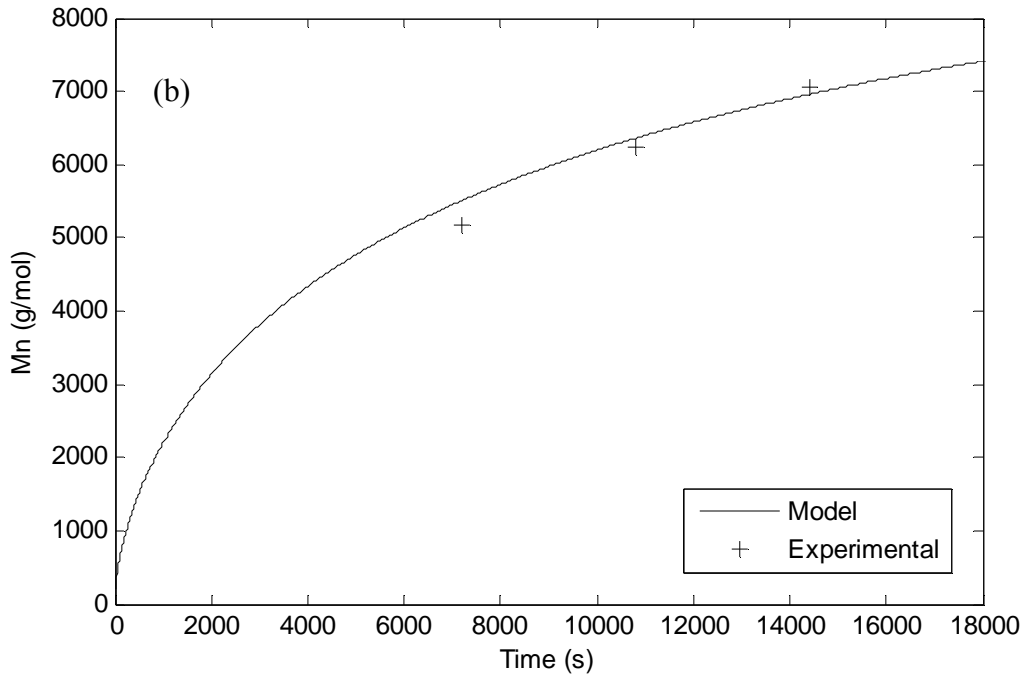
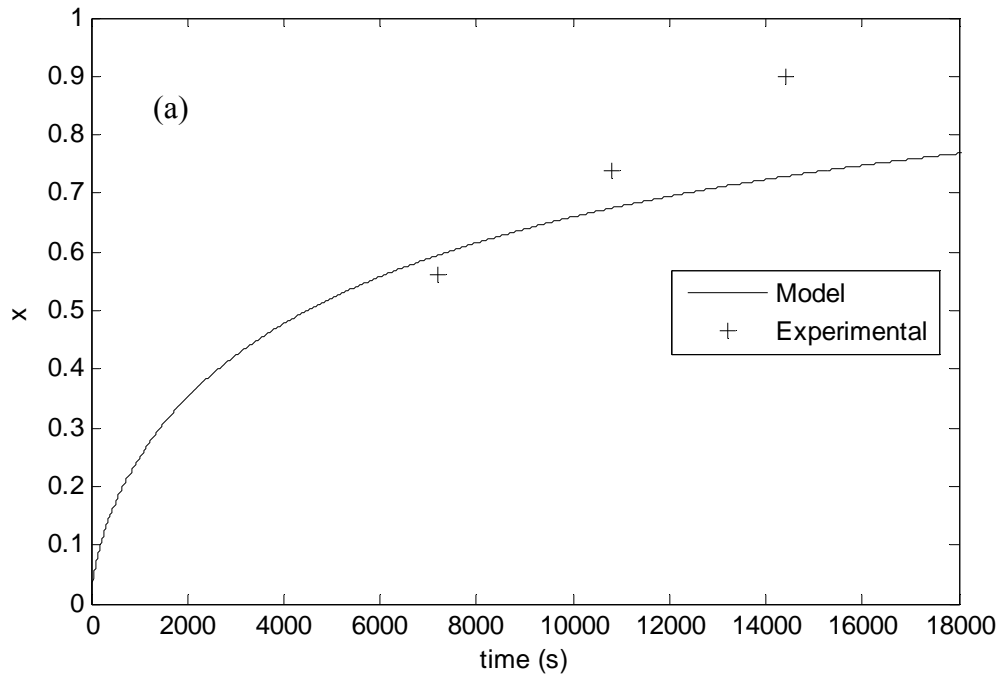


Figure 10.1 Comparison between model predictions and experimental data for the batch copolymerization of styrene and n-butyl acrylate from Arehart et al. ⁽³¹⁾: (a) monomer conversion, (b) polydispersity, (c) number average molecular weight, and (d) cumulative copolymer composition.

The second validation that was applied to our model is bulk atom transfer radical copolymerization of styrene and acrylonitrile (SAN). The experimental data were generated in our lab and discussed in Chapter 9. ^[32] The polymerization was carried out isothermally at 90 °C using 1-bromomethyl benzene as ATRP initiator and copper bromide/ 2,2'-bipyridine as ATRP catalyst. The molar ratio of monomer, initiator and catalyst were 100:1:1. The molar ratio of styrene to acrylonitrile is 0.63 to 0.37 which is the azeotropic ratio of SAN system. The activation and deactivation rate constants of both monomers were estimated in this study. The other rate constants are used as reported in the literature for free radical copolymerization of SAN. All the parameters used in this case study are reported in Appendix B. The cross termination constants were estimated using equation 35. As shown in Figure 10.2, a good agreement between the model prediction and the experimental data is obtained.



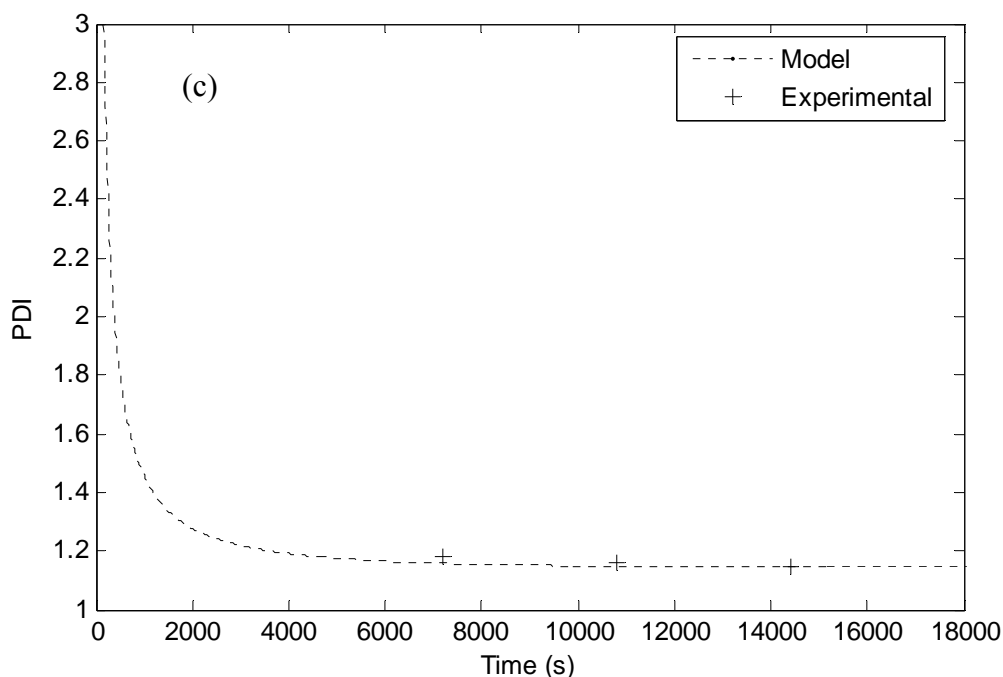


Figure 10.2 Comparison between model predictions and experimental data for the batch copolymerization of SAN (from Chapter 9) ⁽³¹⁾: (a) monomer conversion, (b) number average molecular weight, (c), and polydispersity index.

10.4.2 Effect of ATRP parameters on copolymer sequence lengths

Copolymerization is the best way to produce materials with properties that are intermediate between the properties of the respective homopolymers. It is an important process from a commercial point of view because it can produce new polymers with completely different properties. An unlimited number of polymeric structures with a wide range of properties and applications can be synthesized via copolymerization of a few different types of comonomers. One way to categorize copolymers is based on their architecture. They are classified as statistical, alternating, block, and graft.

All monomers that can be homopolymerized using ATRP can also be copolymerized easily with the same method. ATRP produces polymer chains with very narrow intermolecular chemical composition distribution (CCD) –and also narrow intramolecular CCD, provided care is taken to avoid comonomer composition drift – because of its living nature. On the other hand, chains produced via conventional free

radical polymerization have broader CCD due to termination reactions. In ATRP and other living polymerization mechanisms, it is possible to change the composition of the polymer backbone from random to gradient by varying the composition of the comonomer during the polymerization.

Living polymerization allows the formation of gradient copolymers in which the comonomer composition varies continuously from one end of the chain to the other (narrow interchain, but broad intrachain CCD). This will happen naturally if the polymerization is performed in a batch reactor and the two comonomers have significantly different reactivity ratios. The concentration of the most reactive comonomer will decrease steadily from the “beginning” to the “end” of the chain, since the concentration of the fast comonomer in the reactor will drop faster than the concentration of the slow comonomer, a phenomenon known as composition drift. The controlled addition of comonomers during a semi-batch polymerization will allow the formation of polymers that have even more intricate microstructures.

In conventional free radical polymerization, it is known that the initial feed concentrations and the reactivity ratios play an important role in the control of the copolymer composition.^[33] We used our model to study the comonomer sequence length distribution during ATRP. To study the effect of the reactivity ratios, the model was applied to three ATRP systems at 110 °C, namely, styrene-*n*-butyl acrylate ($r_{st} = 0.79$ and $r_{n-BA} = 0.26$), styrene-methyl methacrylate ($r_{st} = 0.52$ and $r_{MMA} = 0.46$) and styrene-acrylonitrile ($r_{St} = 0.36$ and $r_{AN} = 0.078$). The kinetic parameters used in this comparison are shown in Appendix B. The initial comonomer feed ratios of styrene to the other monomers were 0.25:0.75 for all simulations. The molar ratio of initiator, catalyst and both comonomers was 1:1:100 for all simulations.

Figure 10.3 plots the ratio of instantaneous copolymer composition versus the total conversion for the three systems. The larger the difference between the reactivity ratios of the comonomers, the higher the composition drift and, therefore, the higher the likelihood of forming gradient copolymers.

The initial monomer feed was also varied for the copolymerization of styrene and *n*-butyl acrylate to illustrate its effect on composition drift (Figure 10.4). It is obvious that the

chance of forming gradient copolymers increases when there is a larger difference in comonomer feed ratio. However no composition drift occurs when the reactivity ratios are equal to one (Figure 10.5). So the composition of the copolymer is constant throughout the polymerization and equal to the monomer feed composition.

The main difference between conventional free radical polymerization and controlled free radical polymerization is the equilibrium reaction between the polymer radicals and the dormant chains. The effect of the rate constants of activation (k_a) and deactivation (k_d) on copolymer composition was also studied using our model for ATRP. As expected, Figure 10.6 demonstrates that neither k_a nor k_d affect the instantaneous copolymer composition. Therefore, it can be concluded that copolymer composition in ATRP is a function only of the comonomer reactivity ratios and the initial monomer feed concentrations, as in conventional free radical polymerization. We can also conclude from our model that the Mayo-Lewis equation for terminal model is applicable in ATRP, similar to conventional free radical.

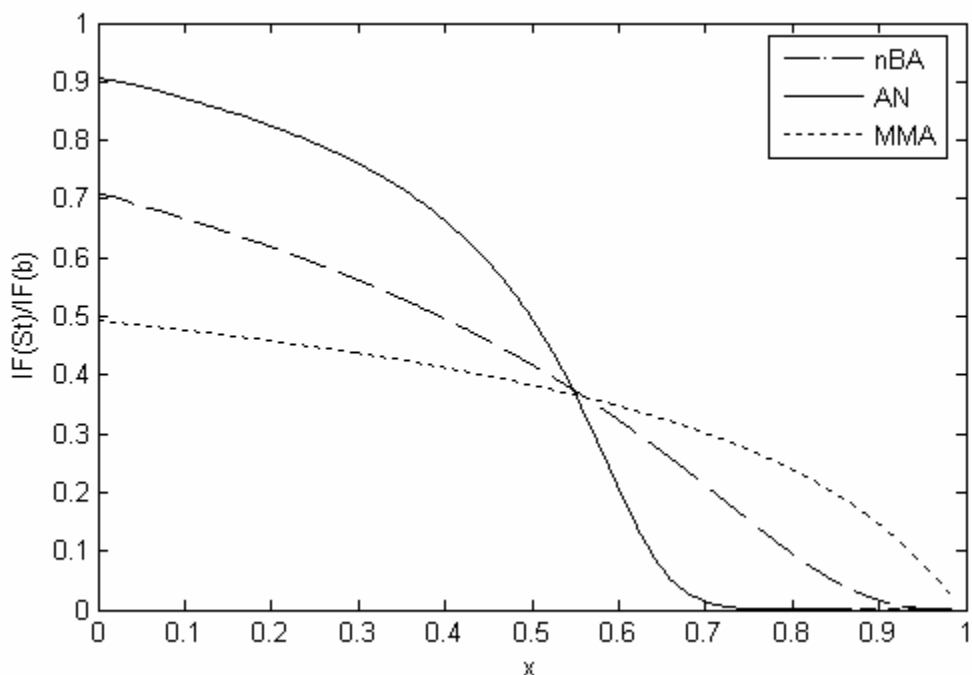


Figure 10.3 Total comonomer conversion versus the ratio of instantaneous copolymer composition (IF) for three ATRP systems at 110 °C. The initial feed monomers are $f_{0,St}=0.25$, $f_{0,b}=0.75$. (The subscript b stands for the second monomer that copolymerizes with styrene: AN, n-BA or MMA)

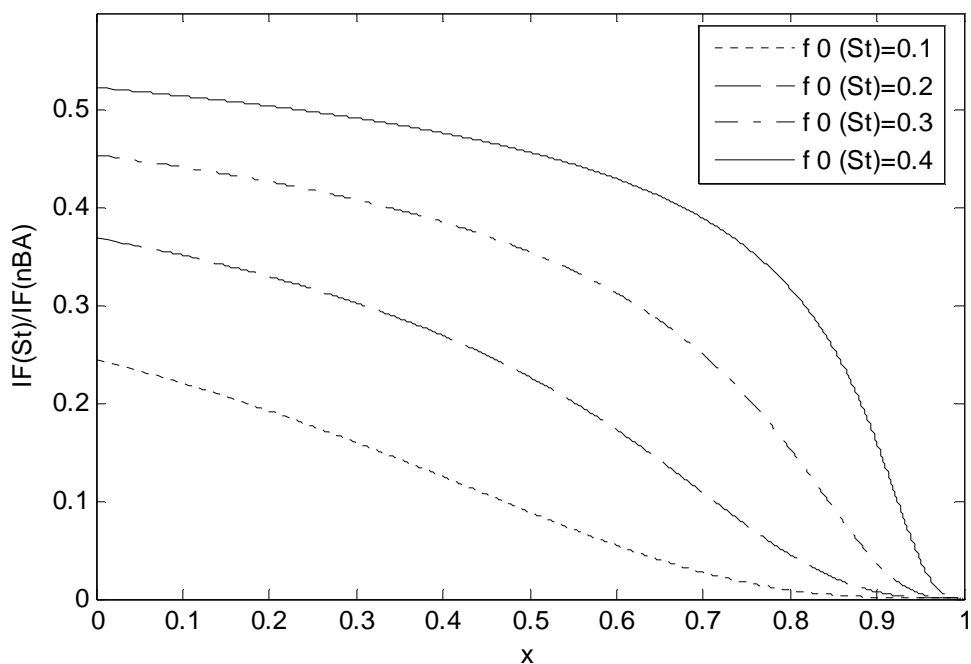


Figure 10.4 Ratio of instantaneous copolymer composition (IF) as a function of total comonomer conversion for the copolymerization of styrene and n-butyl acrylate at 110 °C with various initial feed monomer.

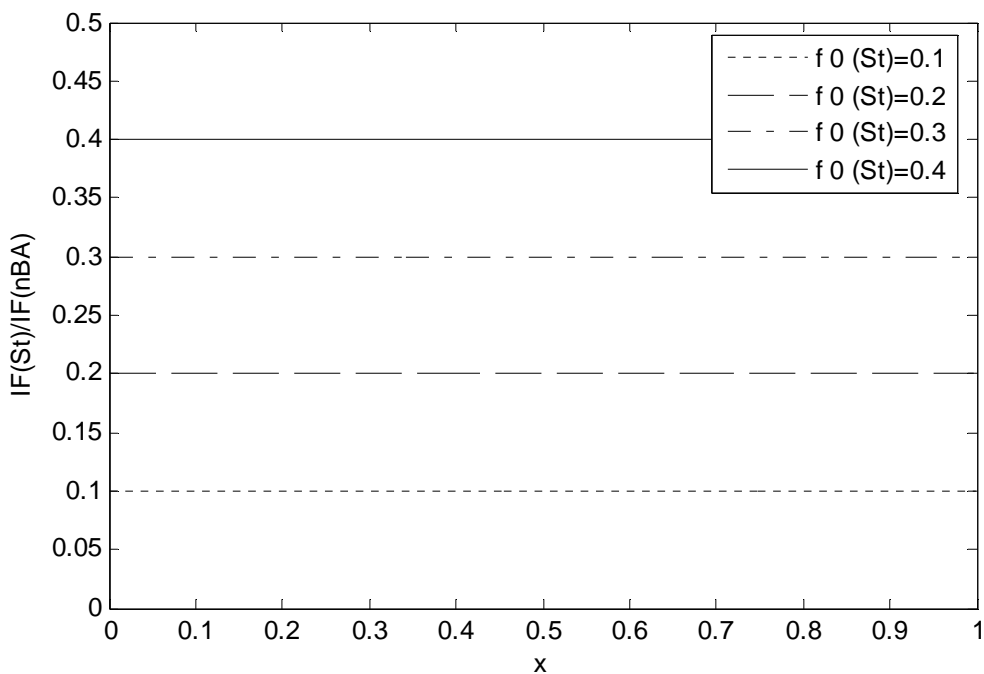


Figure 10.5 Ratio of instantaneous copolymer composition (IF) as a function of total comonomer conversion for fictitious comonomers with reactivity ratios equal to one and various initial feed monomer.

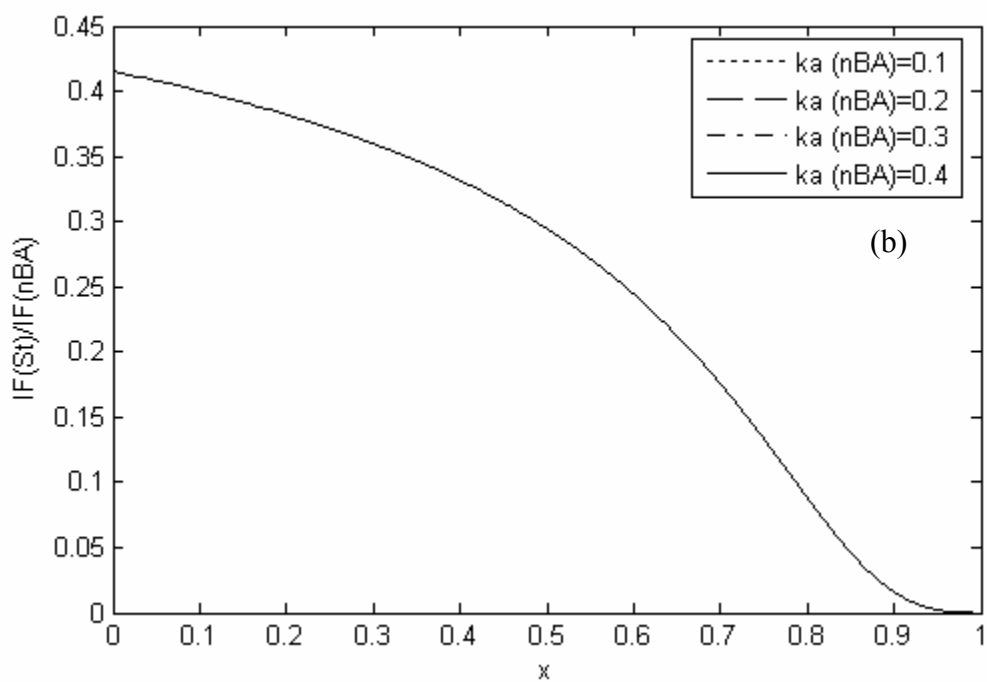
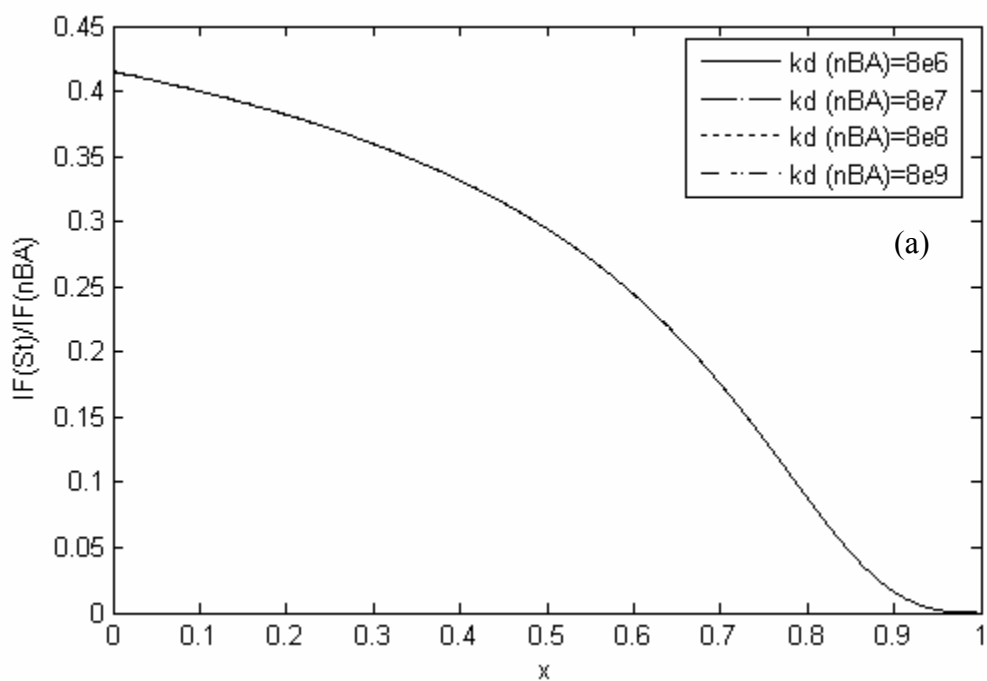


Figure 10.6 Ratio of instantaneous copolymer composition (IF) as a function of total comonomer conversion for the copolymerization of styrene and n-butyl acrylate: (a) various values of k_d and (b) various values of k_a .

10.5 Conclusions

We developed a polymerization kinetic model for the simulation of atom transfer radical copolymerization using the method of moments and the concept of pseudo-kinetic constants. The pseudo-kinetic rate constant method reduces the model complexity to the level of that for a homopolymerization model. The model can predict the monomer conversion average molecular weights, polydispersity index, and copolymer composition. The reliability of the model was assessed by comparison with an experimental data from the literature (copolymerization of styrene and n-butyl acrylate) and from our lab (copolymerization of styrene and acrylonitrile). The model proved that the copolymer composition in the atom transfer radical copolymerization is independent of the ATRP parameters. Therefore the Mayo-Lewis terminal model is applicable in ATRP.

10.6 References

- [1] J. Chiefary, YK. Chong, F. Ercole, C. Moad, G. Moad, E. Rizzardo, SH. Thang, *Macromolecules* **1998**, 31, 5559.
- [2] G. Moad, J. Chiefary, YK. Chong, J. Krstina, RTA. Mayadunne, A. Postma, E. Rizzardo, SH. Thang, *Polym Int* **2000**, 49, 993.
- [3] MK. Georges, RPN. Veregin, PM. Kazmaier, GK. Hamer, *Macromolecules* **1993**, 26, 2987.
- [4] D. Benoit, V. Chaplinski, R. Braslau, CJ. Hawker, *J Am Chem Soc* **1999**, 121, 3904.
- [5] M. Rodlert, E. Harth, I. Rees, CJ. Hawker, *J Polym Sci, Polym Chem Ed* **2000**, 38, 4749.
- [6] K. Matyjaszewski, J. Xia, *Chem Rev* **2001**, 101, 2921.
- [7] M. Kamigaito, T. Ando, M. Sawamoto, *Chem Rev* **2001**, 101, 3689.
- [8] K. Davis, K. Matyjaszewski, *Statistical, gradient, block and graft copolymers by controlled/living radical polymerization*, 2002.
- [9] T. Davis, K. Matyjaszewski, *Handbook of radical polymerization*, 2002, pp 523.
- [10] S. Zhu, *Macromol. Theory Simul.* **1999**, 8, 29.
- [11] M. Al-Harhi, J. Soares, L. Simon, *Macromol. Theory Simul.* **2006**, 15, 198.
- [12] O. Delgadillo-Velazquez, E. Vivaldo-Lima, I. Quintero-Ortega, S. Zhu, *AICHe J.I* **2002**, 48, 11, 2597.
- [13] M. Al-Harhi, J. Soares, L. Simon, *Macromol. Chem. Phys.*, **2006**, 207, 469.
- [14] H. Fischer, *Macromolecules* **1997**, 30, 5666.
- [15] H. Fischer, *J. Polym. Sci. Part A: Polym. Chem.* **1999**, 37, 1885.
- [16] M. Souaille, *J. Polym. Sci. Part A : Polym Chem.* **1999**, 37, 1885.
- [17] D. Shipp, K. Matyjaszewski, *Macromolecules*, **2000**, 33, 1553.
- [18] D. Shipp, K. Matyjaszewski, *Macromolecules*, **1999**, 32, 2948.
- [19] J. Lutz, K. Matyjaszewski, *Macromol. Chem. Phys.* **2002**, 203, 1385.
- [20] A. Butte, G. Storti, M. Morbidelli, *Chem. Eng. Sci.* **1999**, 54, 3225.
- [21] M. Al-Harhi, J. Soares, L. Simon, *Macromol. Mat. Sci.*, 2006, 291, 993.
- [22] M. Al-Harhi, J. Soares, L. Simon, *Macromol. Rec. Eng.*, "Dynamic Monte Carlo Simulation of ATRP with Bifunctional Initiators", accepted.
- [23] M. Zhang, H. Ray, *J. appl. polym. sci.* **2002**, 86, 1630.
- [24] M. Zhang, H. Ray, *J. appl. polym. sci.* **2002**, 86, 1047.

- [25] Hamielec, A. ;MacGregor, J. in Polymer Reaction Engineering' (Eds K. H. Reichert and W. Geiseler), Hanser Publishers, New York, **1983**, 21.
- [26] Morris, L. M.; Davis, T. P.; Chaplin, R. P. *Polymer* **2000**, 42, 941.
- [27] T. Broadhead, A. Hamielec, J. MacGregor, *Macromol. Chem. Suppl.* **1985**, 10, 105.
- [28] A. Hamielec, J. MacGregor, A. Penlidis, *Macromol. Chem., Macromol. Symp.* **1985**, 10, 521.
- [29] H. Tobita, A. Hamielec, *Macromolecules* **1989**, 22, 3098.
- [30] A. Keramopoulos, C. Kiparissides, *Macromolecules* **2002**, 35, 4155.
- [31] S. Arehart, K. Matyjaszewski, *Macromolecules* **1999**, 32, 2221.
- [32] Al-Harathi M., Sardashti A., Soares J. B. P., Simon L. C. *Polymer*. "Atom transfer radical polymerization (ATRP) of styrene and acrylonitrile with monofunctional and bifunctional initiators", submitted.
- [33] F. R. Mayo, F. M. Lewis, *J. Am. Chem. Soc.* **1944**, 66, 1594.
- [34] Buback, M.; Gilbert, R.; Hutchinson, R.; Klumperman, B.; Kuchata, F; Manders, B.; O'Driscoll, K.; Russell, G. Schweer, J. *Macromol. Chem. Phys.* **1995**, 196, 3267.
- [35] S. Jr. Beuermann, D. Paquet, J. McMin, R. Hutchinson, *Macromolecules* **1996**, 29, 4206
- [36] J. Brandrub, E. Immergut, E. Grulke, Eds. *Polymer Handbook*, 4th ed.; Wiley: New York, **1999**.
- [37] Hui, A. W.; Hamielec, A. E. *J. Appl Polym. Sci* 1976, 16, 749.
- [38] Ohno, K.; Goto, A.; Fukuda T.; Xia, J.; Matyjazewski, K. *Macromolecules* **1998**, 31, 2699.
- [39] I. M. Yaraskavitch, J. L. Brash, A. E. Hamielec, *Polymer* **1987**, 28, 489.
- [40] L. H. Garcia-Rubio, M. G. Lord, J. F. MacGregor, A. E. Hamielec, *Polymer* **1985**, 26, 2001.
- [41] T. P. Pittman-Bejger, *Real-Time Control and Optimization of Batch Free-Radical Copolymerization Reactors*. Ph.D. Thesis, University of Minnesota, **1982**.
- [42] K. S. Balaraman, V. M. Nadkarni, R. A. Mashelkar, *Chem. Eng. Sci.* **1986**, 41,1357.
- [43] Achilias, D. S.; Kiparissides, C., *Macromolecules* **1992**, 25,3739.
- [44] H. Suzuki, V. B. Mathot, *Macromolecules* **1989**, 22, 1380.

Appendices

Appendix A

Population balances

The molar population balances for ATRP in a batch reactor are given by the following equations:

Dormant chains :

$$\frac{d[D_r]}{dt} = -k_d[D_r][C] + k_d[R_r \bullet][CX] \quad (A1)$$

Polymer radicals :

$$\begin{aligned} \frac{d[R_r \bullet]}{dt} = & k_p[R_{r-1} \bullet]M - k_p[R_r \bullet]M \\ & - k_{tr}[R_r \bullet]M - k_t[\lambda_{R,0}][R_r \bullet] \\ & + k_a[\lambda_{D,r}][C] - k_d[R_r \bullet][CX] \end{aligned} \quad (A2)$$

Dead polymer from transfer and disproportionation reactions:

$$\frac{d[P_r]}{dt} = k_{tr}[R_r \bullet]M + k_{td}[R_r \bullet][\lambda_{R,0}] \quad (A3)$$

Dead polymer from combination reactions:

$$\frac{d[PP_r]}{dt} = \frac{k_{tc}}{2} \sum_{i=1}^{r-1} [R_i \bullet][R_{r-i} \bullet]$$

Assuming the long chain approximation (monomer is consumed mainly by propagation reactions), the monomer concentration varies as a function of the residence time in the batch reactor according to the following equation:

$$\frac{dM}{dt} = -k_p M [\lambda_{R,0}] \quad (A4)$$

The non-polymeric species in the system are described with the following equations:

$$[C] = [C]_0 - [CX] \quad (A5)$$

$$[CX] = [I]_0 - [\lambda_{D,0}] \quad (A6)$$

Method of Moments

Number (r_n) and the weight (r_w) average chain lengths are calculated using the method of moments. The j^{th} moments of the chain length distributions for the several polymer species present in the reactor are given by the equations:

$$[\lambda_{D,j}] = \sum_{r=1}^{\infty} r^j [D_r] \quad (\text{A7})$$

$$[\lambda_{R,j}] = \sum_{r=1}^{\infty} r^j [R_r] \quad (\text{A8})$$

$$[\lambda_{P,j}] = \sum_{r=1}^{\infty} r^j [P_r] \quad (\text{A9})$$

$$[\lambda_{PP,j}] = \sum_{r=1}^{\infty} r^j [PP_r] \quad (\text{A10})$$

The zeroth moment of the dormant species (D) is given by :

$$[\lambda_{D,0}] = \sum_{r=1}^{\infty} [D_r] = D_1 + \sum_{r=2}^{\infty} D_r \quad (\text{A11})$$

Therefore

$$\frac{d[\lambda_{D,0}]}{dt} = \frac{d[D_1]}{dt} + \sum_{r=2}^{\infty} \frac{d[D_r]}{dt} \quad (\text{A12})$$

The population balances equation (equation A1) was substituted in the above equations. After some simplifications the equation for the zeroth moment of the distribution of chain length for the dormant species was obtained:

$$\frac{d[\lambda_{D,0}]}{dt} = -k_a [\lambda_{D,0}] [C] + k_d [\lambda_{R,0}] [CX] \quad (\text{A13})$$

Similarly, the first moment of dormant species is given by,

$$[\lambda_{D,1}] = \sum_{r=1}^{\infty} r [D_r] = D_1 + \sum_{r=2}^{\infty} r D_r \quad (\text{A14})$$

and:

$$\frac{d[\lambda_{D,1}]}{dt} = \frac{d[D_1]}{dt} + \sum_{r=2}^{\infty} r \frac{d[D_r]}{dt} \quad (\text{A15})$$

Substituting the population balances, and simplifying the resulting expression, we obtain:

$$\frac{d[\lambda_{D,1}]}{dt} = -k_a [\lambda_{D,1}] [C] + k_d [\lambda_{R,1}] [CX] \quad (\text{A16})$$

The second moment of dormant species is given by,

$$[\lambda_{D,2}] = \sum_{r=1}^{\infty} r^2 [D_r] = D_1 + \sum_{r=2}^{\infty} r^2 D_r \quad (\text{A17})$$

and:

$$\frac{d[\lambda_{D,2}]}{dt} = \frac{d[D_1]}{dt} + \sum_{r=2}^{\infty} r^2 \frac{d[D_r]}{dt} \quad (\text{A18})$$

Substituting the population balances and simplifying the resulting expression, we obtain:

$$\frac{d[\lambda_{D,2}]}{dt} = -k_a[\lambda_{D,2}][C] + k_d[\lambda_{D,2}][CX] \quad (\text{A19})$$

Similarly, the method of moments was applied to the other species and we obtain the following equations:

Polymer Radicals:

Zeroth moments

$$\frac{d[\lambda_{R,0}]}{dt} = k_a[\lambda_{D,0}][C] - k_d[\lambda_{R,0}][CX] - k_t[\lambda_{R,0}][\lambda_{R,0}] - k_{tr}[M][\lambda_{R,0}] \quad (\text{A20})$$

First moments

$$\begin{aligned} \frac{d[\lambda_{R,1}]}{dt} = & k_p[\lambda_{R,0}][M] + k_a[\lambda_{D,1}][C] - k_d[\lambda_{R,1}][CX] \\ & - k_t[\lambda_{R,1}][\lambda_{R,0}] - k_{tr}[M][\lambda_{R,1}] \end{aligned} \quad (\text{A21})$$

Second moments

$$\begin{aligned} \frac{d[\lambda_{R,2}]}{dt} = & k_p[\lambda_{R,0}][M] + 2k_p[\lambda_{R,1}][M] + k_a[\lambda_{D,2}][C] - k_d[\lambda_{R,2}][CX] \\ & - k_t[\lambda_{R,0}][\lambda_{R,2}] - k_{tr}[M][\lambda_{R,2}] \end{aligned} \quad (\text{A22})$$

Dead Polymers:

Zeroth moments

Dead polymers via combination

$$\frac{d[\lambda_{PP,0}]}{dt} = \frac{k_{tc}}{2} [\lambda_{R,0}][\lambda_{R,0}] \quad (\text{A23})$$

Dead polymers via disproportionation

$$\frac{d[\lambda_{P,0}]}{dt} = k_{td}[\lambda_{R,0}][\lambda_{R,0}] + k_{tr}[M][\lambda_{R,0}] \quad (\text{A24})$$

First moments

Dead polymers via combination

$$\frac{d[\lambda_{PP,1}]}{dt} = k_{tc}[\lambda_{R,1}][\lambda_{R,0}] \quad (\text{A25})$$

Dead polymers via disproportionation

$$\frac{d[\lambda_{P,1}]}{dt} = k_{td}[\lambda_{R,0}][\lambda_{R,1}] + k_{tr}[M][\lambda_{R,1}] \quad (\text{A26})$$

Second moments

Dead polymers via combination

$$\frac{d[\lambda_{PP,2}]}{dt} = k_{tc}[\lambda_{R,0}][\lambda_{R,2}] + k_{tc}[\lambda_{R,1}][\lambda_{R,1}] \quad (\text{A27})$$

Dead polymers via disproportionation

$$\frac{d[\lambda_{P,2}]}{dt} = k_{td}[\lambda_{R,0}][\lambda_{R,2}] + k_{tr}[M][\lambda_{R,2}] \quad (\text{A28})$$

Appendix B

Physical and kinetic parameters in the copolymerization simulations.

Table 10.2 Kinetic rate constants and physical properties for the styrene -n-butyl acrylate copolymerization.

Parameter	Value	Reference
k_{p11}	$4.266 \times 10^7 \exp(-7769/RT)$ (L/mol s)	34
k_{p22}	$7.37 \times 10^5 \exp(-2299/RT)$ (L/mol s)	35
r_1	0.79;	36
r_2	0.26	36
k_{tc11}	$(k_{p11})^2 \times 1.1 \times 10^{-5} \exp(12452.2/RT)$ (L/mol s)	37
k_{td22} and k_{td11}	0	35
k_{tc22}	$k_{p22} / 2.5 \times 10^{-4}$ (L/mol s)	35
k_{tr11}	$k_{p11} \times 2.198 \times 10^{-1} \exp(-2820/T)$ (L/mol s)	37
k_{tr22}	$k_{p22} \times 1.3 \times 10^{-4}$ (L/mol s)	35
Cross termination (k_{tc12} and k_{tc21})	$7.681 \times 10^9 \exp(-2690.42/RT)$ (L/mol s)	23
Cross transfer (k_{tr12} and k_{tr21})	$2.997 \times 10^4 \exp(-7835.8/RT)$ (L/mol s)	23
k_{a1}	0.45 (L/mol s)	38
k_{a2}	0.055 (L/mol s)	23
k_{d1}	1.15×10^7 (L/mol s)	38
k_{d2}	8×10^7 (L/mol s)	23
MW_1	104.14 (g/mol)	
MW_2	128.17 (g/mol)	

Table 10.3 Kinetic rate constants and physical properties for the styrene-acrylonitrile copolymerization.

Parameter	Value	Reference
k_{p11}	$4.266 \times 10^7 \exp(-7769/RT)$ (L/mol s)	34
k_{p22}	$1.05 \times 10^8 \exp(-3663/RT)$ (L/mol s)	39
r_1	0.36	40
r_2	0.078	40
k_{tc11}	$(k_{p11})^2 \times 1.1 \times 10^{-5} \exp(12452.2/RT)$ (L/mol s)	37
k_{tc22}	$3.30 \times 10^{12} \exp(-5400/RT)$ (L/mol s)	41
k_{td11} and k_{td22}	0	30
Φ_t	$16[(1 - f_{1,0}) \times 0.0625 + r_1 f_{1,0}] / [(1 - f_{1,0}) + r_1 f_{1,0}]$	42
k_{tr11}	$k_{p11} \times 2.198 \times 10^{-1} \exp(-2820/T)$ (L/mol s)	37
k_{tr12}	$6.92 \times 10^7 \exp(-12670/RT)$ (L/mol s)	41
k_{tr22}	$4.62 \times 10^4 \exp(-5837/RT)$ (L/mol s)	30
k_{tr21}	$2.30 \times 10^5 \exp(-5837/RT)$ (L/mol s)	30
k_{a1}	0.15	This study
k_{a2}	0.595	This study
k_{d1}	2.65×10^5	This study
k_{d2}	5.01×10^8	This study
MW_1	104.14 (g/mol)	
MW_2	53.06 (g/mol)	

Table 10.4 Kinetic rate constants and pPhysical properties for the styrene-methyl methacrylate copolymerization.

Parameter	Value	Reference
k_{p11}	$4.266 \times 10^7 \exp(-7769/RT)$ (L/mol s)	34
k_{p22}	$4.92 \times 10^5 \exp(-4353/RT)$ (L/mol s)	43
r_1	0.52	44
r_2	0.46	44
k_{ic11}	$(k_{p11})^2 \times 1.1 \times 10^{-5} \exp(12452.2/RT)$ (L/mol s)	37
k_{id22}	$9.80 \times 10^7 \exp(-701/RT)$ (L/mol s)	43
k_{id11}	0	30
k_{ic22}	0	30
Φ_t	25	30
MW_1	104.14 (g/mol)	
MW_2	100.13 (g/mol)	

Chapter 11

11 Dynamic Monte Carlo Simulation of Graft Copolymers Made with ATRP and Metallocene Catalysts*

11.1 Abstract

The synthesis of polyolefin graft copolymers made with coordination polymerization was studied by dynamic Monte Carlo simulation. Narrow molecular weight distribution macromonomers, containing terminal vinyl groups made with atom-transfer radical polymerization (ATRP), were incorporated randomly into the polyolefin backbone. In addition to average molecular weights and polydispersity index, the model predicts the complete molecular weight distribution (MWD) and branching density of the graft copolymer. The effect of the concentration of macromonomers on the grafting efficiency was also studied.

11.2 Introduction

Polyolefins are the largest volume commodity polymers produced in the world and many researchers in industry and academia are actively studying the production of new polyolefins for specialty applications. For instance, some researchers are seeking coordination catalysts that can efficiently copolymerize olefins and polar comonomers; others are trying to copolymerize olefins with macromonomers (polymer chains containing a terminal vinyl group) made by coordination and other polymerization mechanisms to make block or graft copolymers.

* This chapter is in print: M. Al-Harhi, J. Soares, L. Simon, *Macromol. Symp.* **2006**

Controlled polymerization is an excellent method to produce macromonomers with well-defined, uniform molecular architectures. Indeed, living (or controlled) free-radical polymerization (LFRP) is a vibrant area of polymer reaction engineering. The three most common types of LFRP are reversible addition-fragmentation chain transfer (RAFT),^[1,2] nitroxide-mediated polymerization (NMP)^[3-5] and atom-transfer radical polymerization (ATRP).^[6,7]

We can combine two different polymerization mechanisms, such as coordination and living polymerization, to produce polymers with unique graft microstructures. In this approach, one polymer is made with one type of polymerization mechanism in a first step, and the other type of polymerization mechanism is used to prepare the final polymer. Two main techniques have been tried: *graft-to* and *grafting-from* approaches.

In the *graft-to* approach (Figure 11.1), macromonomers with narrow MWD (B) are prepared using a suitable living polymerization technique. These macromonomers are then modified chemically to introduce vinyl groups at their chain ends. Finally, a metallocene catalyst is used to copolymerize the macromonomers and the olefin monomer (A).

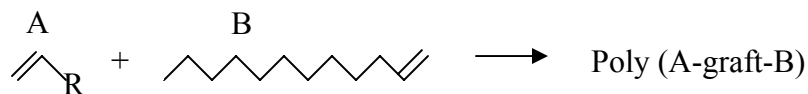


Figure 11.1 *Grafting-to* approach.

In the *grafting-from* approach (Figure 11.2), a metallocene catalyst is used to produce polyolefin copolymers (A+B) having reactive comonomer units (B) that can be modified to become controlled free radical initiators. The resulting polymeric initiators can be used to initiate living polymerization reactions from the backbone of the previously formed polymer.

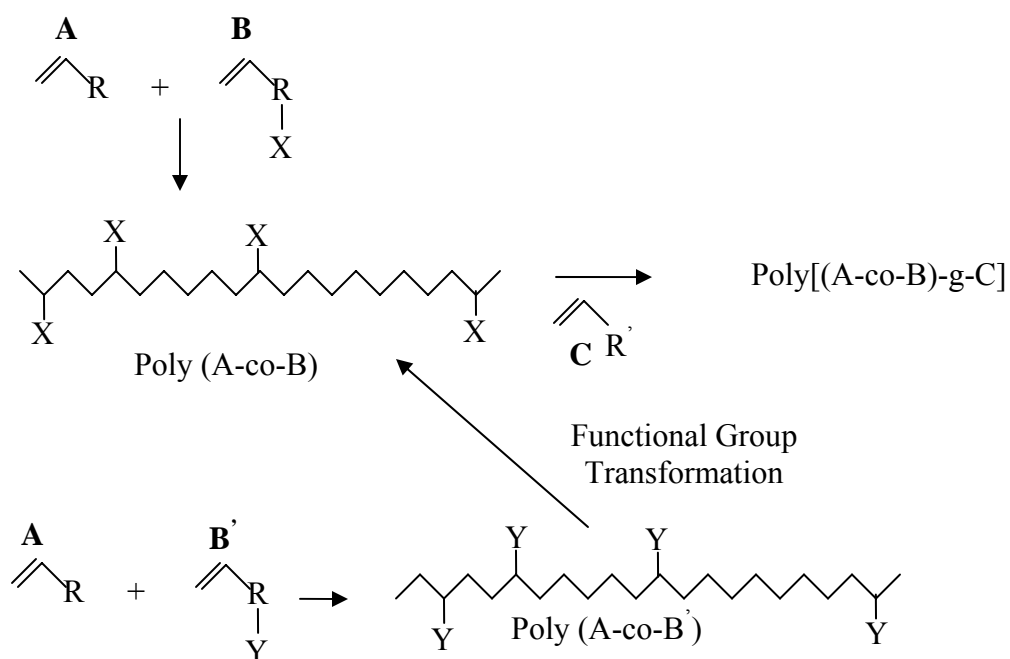


Figure 11.2 *Graft-from* approach.

Graft copolymers with well defined side chains have been produced by combining anionic and coordination polymerizations.^[8-11] Anionic polymerization was used to produce macromonomers with narrow MWD, while metallocene polymerization was used to produce the grafted chains (graft-to approach). Similarly, nitroxide-mediated polymerization was used to synthesize macromonomers that were grafted to a polymer backbone using metallocene catalysts.^[12,13]

The graft-to method was also used to produce poly(propene-*g*-styrene) copolymers. Polystyrene macromonomer with different molecular weights were synthesized by ATRP and metallocenes were used to copolymerize them with propene.^[14]

Matyjaszewski et al. used the graft-from method to incorporate n-butyl acrylate (BA) and methyl methacrylate (MMA) into linear polyethylene. Ethylene and 10-undecen-1-ol were copolymerized using a metallocene catalyst and the resulting copolymer chains were modified to become ATRP macroinitiators. The resultant multifunctional macroinitiator was used to initiate the BA and MMA polymerization.^[15]

Even though these interesting polymers have been studied experimentally by several researchers, little has been done to describe their microstructures with a detailed mathematical model. Zhu published an interesting paper showing some analytical solutions to describe random grafting.^[16] Monte Carlo simulation is a powerful technique to predict the microstructure of polymers produced with any polymerization mechanism. In addition, because there is no need to solve systems of differential equations, Monte Carlo models are generally easier to develop and implement than models using population balances, albeit at a higher computational time. Monte Carlo simulation has been widely used to study coordination polymerization,^[17-19] free radical polymerization,^[20,21] and living polymerization.^[22-27]

In this chapter, we developed a Monte Carlo model to describe the synthesis of polyolefin graft copolymers made with ATRP and coordination polymerization with the graft-to approach. The simulation considers two types of macromonomers: *ex-situ* macromonomers produced by ATRP, and *in-situ* macromonomers produced during coordination polymerization. The first type of macromonomer is called *ex-situ* because they are produced in a separate reactor using ATRP, before being copolymerized with an olefin by coordination polymerization; the second type is called *in-situ* because macromonomers are produced in the same reactor during the polymerization of the olefin with a coordination catalyst.

11.3 Model development

11.3.1 ATRP mechanism

The elementary reactions that constitute the polymerization mechanism of ATRP are discussed in detail in chapter 4.

11.3.2 Coordination polymerization mechanism

The main elementary reactions involved in the copolymerization of olefins and *ex-situ* macromonomers with coordination catalysts are:

Initiation:



Propagation:



In-situ macromonomer insertion:



Ex-situ macromonomer insertion:



β -Hydride elimination and in-situ macromonomer formation:



Transfer to monomer and in-situ macromonomer formation:



In Equations (1) to (6), $P_{r,i,j}$ is a living polymer chain of chain length r having i in-situ macromonomer branches and j ex-situ macromonomer branches, C^* is the catalyst, $D_{r,i,j}^-$ is a dead polymer chain with a terminal vinyl group (in-situ macromonomer) of chain length r and i and j in-situ and ex-situ macromonomers, respectively, S_z^- is an ex-situ macromonomer, M is an olefin monomer.

11.3.3 Principles of Monte Carlo simulation

The Monte Carlo model we developed is based on the procedure suggested by Gillespie. [28] The detailed explanation of this algorithm is available in chapter 4.

A flowsheet summarizing the Monte Carlo simulation procedure used in this investigation is shown in Figure 11.3.

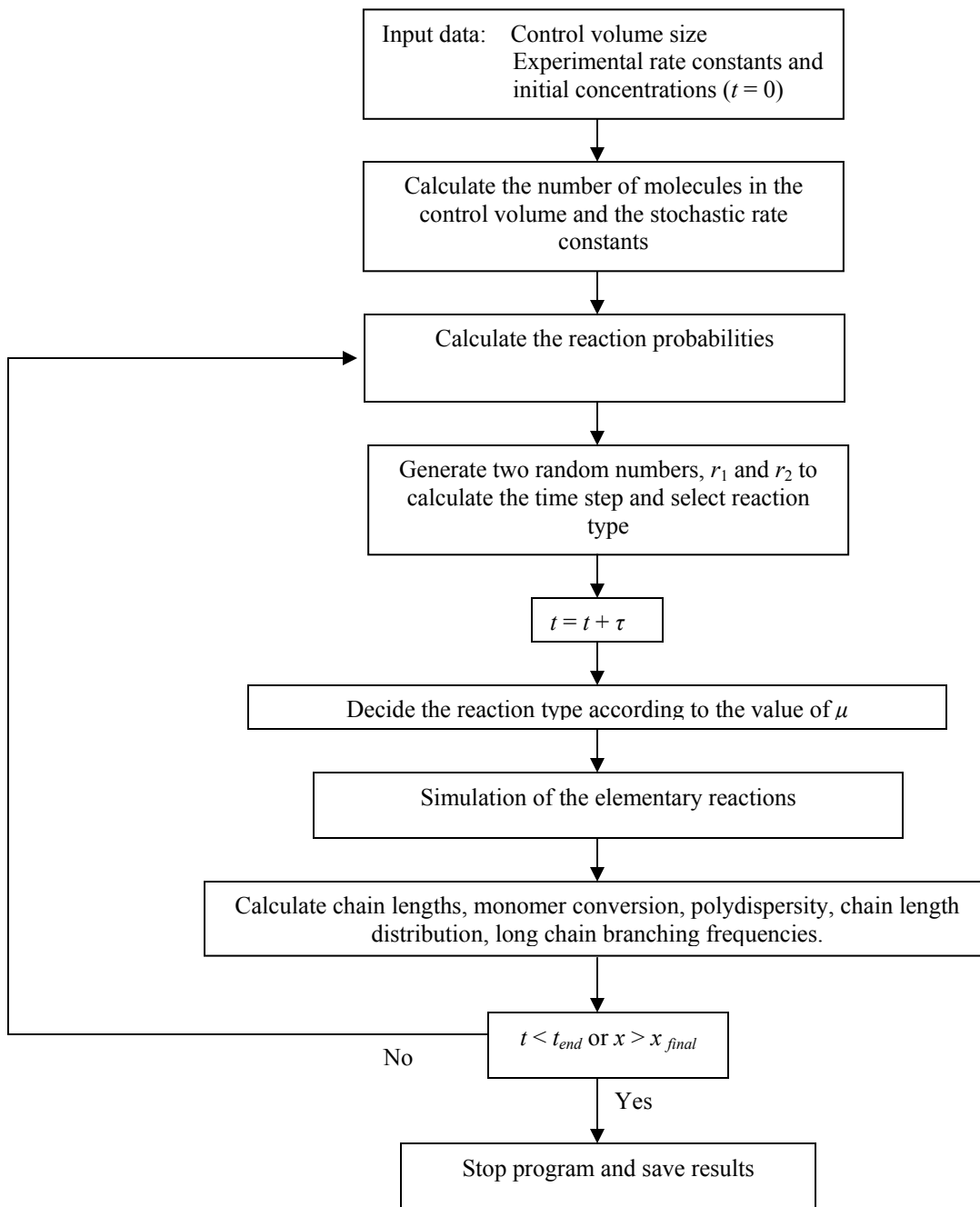


Figure 11.3 Algorithm for Monte Carlo simulation.

A microcomputer (Intel® Pentium® 4 with 2.8 GHz processor and 504 MB of RAM) was used in the simulations. The program was written in Visual Basic version 6.

11.4 Modeling macromonomer formation

Practically, there are two ways to produce macromonomers with ATRP: 1) modify the terminal functional group (halide atom) to a terminal double bond through a post-polymerization reaction, or 2) use initiators that have two functionalities (a halide atom and a terminal double bond) such as allyl bromides or allyl chlorides (Figure 11.4).



Figure 11.4 Allyl bromide (left) and allyl chloride (right).

ATRP can produce polymers with controlled molecular weights and narrow molecular weight distributions. The molecular weight can be controlled either by changing the molar ratio of monomer to initiator or by varying polymerization time, as it was discussed in the previous Chapters.

11.5 Modeling of graft copolymer formation

Some coordination polymerization catalysts can copolymerize olefins with chains containing terminal vinyl groups (macromonomers). Constrained geometry catalysts (CGC) are among the best coordination catalysts having high reactivity towards macromonomer incorporation. These macromonomers can be of two types: 1) in-situ macromonomers, generated via β -hydride elimination and chain transfer to ethylene directly in the reactor, and 2) ex-situ macromonomers, synthesized in a separate reactor and added at the beginning of the polymerization. In our case, we will assume that the ex-situ macromonomer was made with ATRP and can be considered monodisperse.

The ATRP ex-situ macromonomer is fed to the reactor with several concentrations in batch mode. The concentration of the ex-situ macromonomer decreases with the polymerization time, as they are incorporated into the polymer chains. The in-situ macromonomers are produced throughout the polymerization and their concentration

increases with time. Naturally, the incorporation of both macromonomer types produces a polymer having long chain branches of ex-situ and in-situ types.

The values of the polymerization kinetic parameters used in this study are summarized in Table 11.1. These values were estimated from experimental results published in a previous study in our laboratory. ^[29] The rate constant for the incorporation of ex-situ and in-situ macromonomers is assumed to be the same, for simplicity, in the following simulations. The monomer concentration was kept constant at 1.0 mol/L because we assumed semi-batch monomer feed in our simulations.

Table 11.1 Summary of polymerization kinetic parameters.

Kinetic parameter	Value
k_i	373.22 L/(mol.s)
k_p	373.22 L/(mol.s)
$k_\beta + k_{tm}$	0.0824 s ⁻¹
k_{LCB} / k_p	0.0248
k_S / k_p	0.0248

As the polymerization starts, the ex-situ macromonomer chains start copolymerizing with ethylene and incorporating into the living chains. This incorporation decreases with time, since the concentration of ex-situ macromonomers is decreasing and, therefore, the number of incorporated ex-situ macromonomer branches per chain also decreases, as shown in Figure 11.5.

On the other hand, the concentration of in-situ macromonomers increases with time because of the chain transfer reactions that take place in coordination polymerization. As a result, their branching frequency also increases with time, as depicted in Figure 11.6.

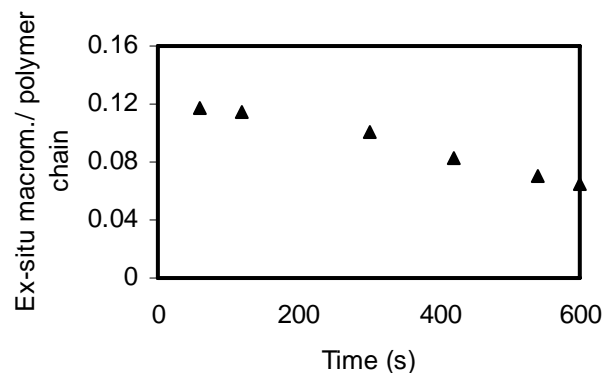


Figure 11.5 Average number of ex-situ macromonomer branches per polymer chain as a function of time.

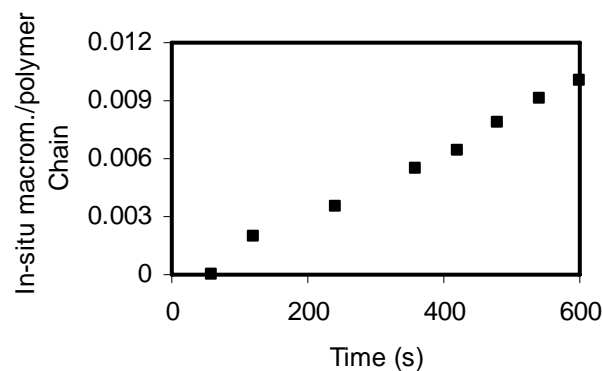


Figure 11.6 Average number of in-situ macromonomer branches per polymer chain as a function of time.

One of the most important information that Monte Carlo simulation can predict is the complete chain length distribution (CLD). As the concentration of in-situ macromonomer increases, its probability to be incorporated into the living chains increases. Therefore, the grafting density increases and this affects the CLD. Flory's most probable distribution, used to describe the CLD of linear polymers made with single-site coordination catalysts, is no longer applicable to graft copolymers. Figure 11.7 shows

how the polydispersity index varies with polymerization time and with the initial concentration of ex-situ macromonomer in the reactor. Notice how, for a given polymerization time, polymers made with a higher ex-situ macromonomer concentration have a higher polydispersity index. In addition, the polydispersity index increases with polymerization time, since the concentration of in-situ macromonomer also increases with polymerization time. This gives us two variables to control the molecular weight and polydispersity index of the final product.

Figure 11.8 shows how the CLD broadens when the initial concentration of ex-situ macromonomer is increased for a given polymerization time.

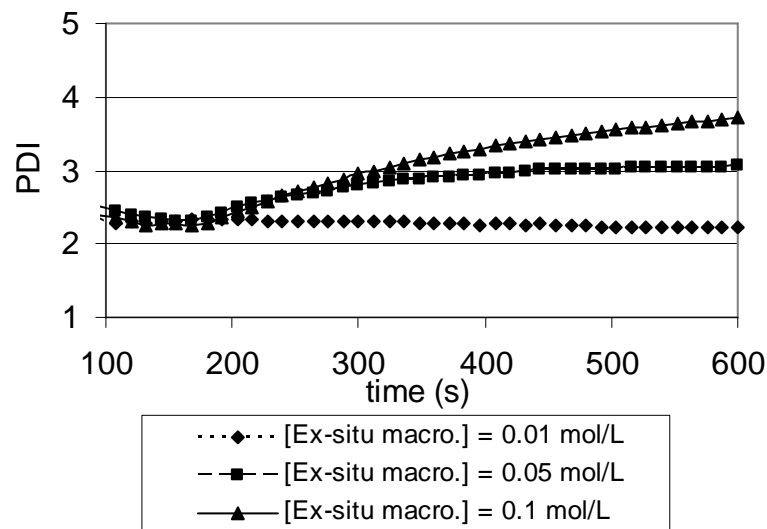


Figure 11.7 Effect of ex-situ macromonomer concentration and polymerization time on polydispersity index.

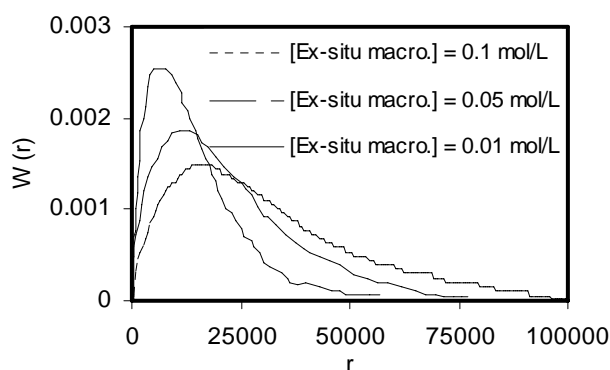


Figure 11.8 Effect of ex-situ macromonomer concentration on the CLD for ten minutes of polymerization

11.6 Conclusion

Monte Carlo simulation was used to describe the microstructure of polymers made with a combination of coordination polymerization and ATRP. ATRP was used in the first step to produce monodisperse macromonomers that were subsequently copolymerized with ethylene using a coordination catalyst in semi-batch mode. The model is general and can be used to describe any system, provided that the proper rate constants are used.

In this study, we use rate constants of styrene polymerization with ATRP to prepare the ex-situ macromonomers and rate constants of ethylene polymerization with CGC for the grafting polymerization.

The chain length distribution and the grafting density were the most important microstructural details predicted in this study. We showed that the frequency of ex-situ branching decreased with polymerization time, while the frequency of in-situ branched increased linearly with polymerization time. The effects of these grafting reactions on the CLD of the final polymer were also demonstrated.

11.7 References

- [1] J. Chiefary, YK. Chong, F. Ercole, C. Moad, G. Moad, E. Rizzardo, SH. Thang, *Macromolecules*, **1998**, 31, 5559.
- [2] G. Moad, J. Chiefary, YK. Chong, J. Krstina, RTA. Mayadunne, A. Postma, E. Rizzardo, SH. Thang, *Polym. Int.*, **2000**, 49, 993.
- [3] MK. Georges, RPN. Veregin, PM. Kazmaier, GK. Hamer, *Macromolecules*, **1993**, 26, 2987.
- [4] D. Benoit, V. Chaplinski, R. Braslau, CJ. Hawker, *J. Am. Chem. Soc.*, **1999**, 121, 3904.
- [5] M. Rodlert, E. Harth, I. Rees, CJ. Hawker, *J. Polym. Sci. Polym. Chem. Ed.*, **2000**, 38, 4749.
- [6] K. Matyjaszewski, J. Xia, *Chem. Rev.*, **2001**, 101, 2921.
- [7] M. Kamigaito, T. Ando, M. Sawamoto, *Chem. Rev.*, **2001**, 101, 3689.
- [8] K. Senoo, K. Endo, *Polymer* **1999**, 40, 5977.
- [9] O. Henschke, A. Neubauer, M. Arnold, *Macromolecules*, **1997**, 30, 8097.
- [10] C. Batis, G. Karanikolopoulos, M. Pitsikalis, N. Hadjichristidis, *Macromolecules*, **2000**, 33, 8925.
- [11] T. Chung, H. Lu, R. Ding, *Macromolecules*, **1997**, 30, 1272.
- [12] U. Stehling, E. Malmstrom, R. Waymouth, C. Hawker, *Macromolecules*, **1998**, 31, 4396.
- [13] J. Lahitte, F. Peruch, S. Plentz-Meneghetti, F. Isel, P. Lutz, *Macromol. Chem. Phys.*, **2002**, 203, 2583.
- [14] U. Schulze, T. Nagy, H. Komber, G. Pompe, J. Pionteck, B. Ivan, *Macromolecules*, **2003**, 36, 4719.
- [15] Y. Inoue, T. Matsugi, N. Kashiwa, K. Matyjaszewski, *Macromolecules*, **2004**, 37, 3651.
- [16] S. Zhu, *Macromolecules*, **1998**, 31, 7519.
- [17] L. Simon, J. Soares, R. de Souza, *AIChE Journal*, **2000**, 46, 1234.
- [18] L. Simon, C. Williams, J. Soares, R. de Souza, *Chemical Engineering Science*, **2001**, 56, 4181.
- [19] L. Simon, J. Soares, *Industrial and Engineering Chemistry Research*, **2005**, 44, 2461.
- [20] H. Tobita, *Macromol. Theory Simul.*, **2003**, 12, 32.
- [21] J. He, H. Zhang, Y. Yang, *Macromol. Theory Simul.*, **1993**, 2, 747.
- [22] J. He, L. Li, Y. Yang, *Macromol. Theory Simul.*, **2000**, 9, 463.
- [23] J. He, H. Zhang, J. Chen, Y. Yang, *Macromolecules*, **1997**, 30, 8010.

- [24] L. Li, J. He, Y. Yang, Chem. J. Chin. Univ., **2000**, 21, 1146.
- [25] H. Tobita, Macromol. Theory Simul. **2006**, 15, 23.
- [26] M. Al-Harhi, J. Soares, L. Simon, Macromol. Mat. Eng., **2006**, 291, 993.
- [27] M. Al-Harhi, J. Soares, L. Simon, Macromol. Reac. Eng., “Dynamic Monte Carlo Simulation of ATRP with Bifunctional Initiators”, accepted.
- [28] D. Gillespie, J. Phys. Chem., **1979**, 81, 2340.
- [29] D. Beigzadeh, Ph.D. thesis, University of Waterloo, Waterloo, Ontario, Canada, **2000**.

Chapter 12

12 Amphiphilic Copolymers of PS and PEGMA using ATRP*

12.1 Abstract

Two atom transfer radical polymerization (ATRP) steps were used to produce polystyrene-poly(ethylene glycol methacrylate) (PS-PEGMA) amphiphilic copolymers. In the first step, PS macroinitiators were synthesized with two types of initiators (monofunctional and bifunctional). In the second step, the produced PS macroinitiators were used to polymerize PEGMA macromonomers. Due to the reactivity of PEGMA, the resultant PS-PEGMA product can be crosslinked to create polymer structures that vary from amphiphilic block copolymers to amphiphilic crosslinked copolymers. ¹H NMR and GPC were used to characterize the resultant amphiphilic copolymers. A comparison between the two macroinitiators showed that the bifunctional initiator can reach high conversion with less crosslinking side reaction.

12.2 Introduction

Block copolymers are interesting for both academic and industrial applications. Two comonomers (even immiscible ones) can be connected covalently to form polymers with entirely new properties. These types of copolymers have interesting applications as compatibilizers, stabilizers, and emulsifiers.

Living polymerization is the most common method to synthesize block copolymers. Over the past decade, tremendous effort has been given to living free radical polymerization because of its many advantages over other living polymerization

* This chapter was submitted for publication: M. Al-Harhi, J. Soares, L. Simon, *Macromol. Rapid Commun.*

techniques.^[1-7] Among the several techniques of living free radical polymerizations, atom transfer radical polymerization (ATRP) has become one of the most promising ones.^[6-9] Diblock copolymers can be formed with ATRP by sequential addition of the two comonomers. The first comonomer makes macroinitiator chains that can be used with the second comonomer to grow an AB block copolymer. Similarly, ABA triblock copolymers can be formed using bifunctional initiators.^[10]

Polymers that contain hydrophobic and hydrophilic segments in the same chain are called amphiphilic polymers. Based on their architecture and chemical composition, they can self-assemble into micelles, vesicles and a variety of other morphologies.^[11-15]

Polyethylene glycol (PEG) has been widely used in the pharmaceutical industry due to its unique physical and biochemical properties, such as nontoxicity, nonimmunogenesis, nonantigenicity, excellent biocompatibility, and miscibility with many solvents. In addition, polyethylene glycol is soluble in water; this is one of its most important properties. Due to polyethylene glycol's nonadhesion to proteins,^[16-23] the dissipation of active chemicals takes place not only by melting within the body but also by dissolving in the body fluids. Polyethylene glycol methacrylate (PEGMA) macromonomers are one of the PEG derivatives that are attractive materials for biomedical applications.

Several groups reported research to produce and characterize amphiphilic copolymers that contain polyethylene glycol segments.^[25-29] They can also be polymerized to form brush-type polymers.^[30-37] Homopolymerization of PEGMA produces a brush-type polymer composed of hydrophobic backbones (polymethacrylate) and hydrophilic side chains (poly(ethylene glycol)).^[37] This type of amphiphilic copolymer is in the shape of graft copolymer and can be formed by conventional free radical polymerization.

In the present study we used ATRP to produce amphiphilic copolymers with novel molecular structures. Both monofunctional and bifunctional polystyrene (PS) macroinitiators were used to polymerize PEGMA.

12.3 Experimental

Materials. Styrene (St, 99%) (Aldrich) was passed through an alumina column to remove the inhibitors and stored under nitrogen atmosphere at 0 °C. Poly(ethylene glycol) methyl ether methacrylate ($M_n \sim 1,100$), copper (I) bromide (99.999%), 2,2'-bipyridine(bpy, 99%), 1-bromo-ethyl benzene (97%), benzal bromide (97%) were used as received (Aldrich). Technical grade solvents were used as received (VWR) without further pretreatment.

Polymerization. Polystyrene macroinitiators were synthesized using 1-bromo ethyl benzene (monofunctional initiator) and benzal bromide (bifunctional initiator). ATRP of PEGMA in 3:1 of xylene (volume ratio) using polystyrene macroinitiators was carried out at 110 °C with molar ratio PEGMA/PS/CuBr/bipy of 17/1/1/2.5. Samples were taken periodically during the polymerization for NMR analysis. Initially, those samples have high catalyst content; they must be left to settle for a certain time in the NMR tube in the presence of the chloroform. The clear supernatant solution is then transferred to a new NMR tube for analysis. At the end of the polymerization, the reaction mixture was dissolved in dichloromethane and left in air until the copper catalyst was completely oxidized. The resulting copper (II) complex is insoluble in the polymer solution and is easily removed by filtration.

Characterization. ^1H NMR was used to measure PEGMA conversion. ^1H -NMR spectra were obtained on a 300-MHz AC Bruker Fourier-Transform spectrometer in deuterated chloroform at a concentration of 10–30 mg/ml. The operating conditions were as follows: temperature of the probe: 25°C; number of scans: 64.

Molecular weight distributions were obtained using gel permeation chromatography (Waters 590) operating at room temperature with a refractive index (RI) detector and a multiangle laser light-scattering photometer system. THF was filtered and used as the eluent at a flow rate of 1.0 mL/min. Samples for analysis were prepared as 0.5% solutions in THF and filtered through 0.45 μm filters prior to injection.

12.4 Results and discussion

Polystyrene macroinitiators were synthesized by atom transfer radical polymerization of styrene in bulk using two different initiators. Benzal bromide was used as bifunctional initiator to form bifunctional polystyrene macroinitiators and 1-bromo ethyl benzene was used as monofunctional initiator to form monofunctional polystyrene macroinitiators. The molar ratio of initiator/CuBr/bpy was 1/1/3. The initiator/styrene ratio was calculated from the desired molecular weight of the macroinitiator. The monofunctional macroinitiator and the bifunctional macroinitiator have average number molecular weights of 3150 and 4267 g/mol, respectively.

As mentioned earlier, the main objective of this study is to synthesis amphiphilic copolymer samples with novel microstructures. ^1H NMR is the best characterization technique that can prove this objective. Figure 12.1 shows ^1H NMR spectra for the samples that were taken periodically from the polymerization reactor. The chemical shifts around 7 ppm are assigned to aromatic protons in polystyrene. The chemical shifts at 3.38 ppm and 3.6-4.2 ppm are assigned to the protons of the methoxyl group (OCH_3) and methylene protons ($\text{OCH}_2\text{-CH}_2$) of the polyethylene glycol brush. Interesting information that can be extracted from the NMR spectrum is the conversion of PEGMA that can be determined by keeping track of the double bond peaks. The peak for methyl (CH_3) protons near the double bond appears around 1.9 ppm and the peak strength decreases with polymerization time, which indicates the consumption of the double bond. Similarly, the conversion can be calculated from the peaks of the methylene (CH_2) near the double bond (at 5.54 and 6.1 ppm). The following equation was used to calculate the conversion,

$$x = 1 - \frac{\left(\frac{A_v}{A_a}\right)_{t_f}}{\left(\frac{A_v}{A_a}\right)_{\text{PEGMA}}} \quad (1)$$

where $\left(\frac{A_v}{A_a}\right)_{t_f}$ is the ratio of the integrated area of the vinyl protons to the integrated area of the protons of the aromatic rings measured after a polymerization time t_f , and $\left(\frac{A_v}{A_a}\right)_{PEGMA}$ is the equivalent ratio for the PEGMA macromonomer.

Figure 12.2 summarizes the conversion of PEGMA polymerization using both macroinitiators. The conversion of PEGMA using bifunctional macroinitiator is higher than the conversion using the monofunctional macroinitiator. This agrees with the results expected from bifunctional initiators due to the presence of two functionalities.

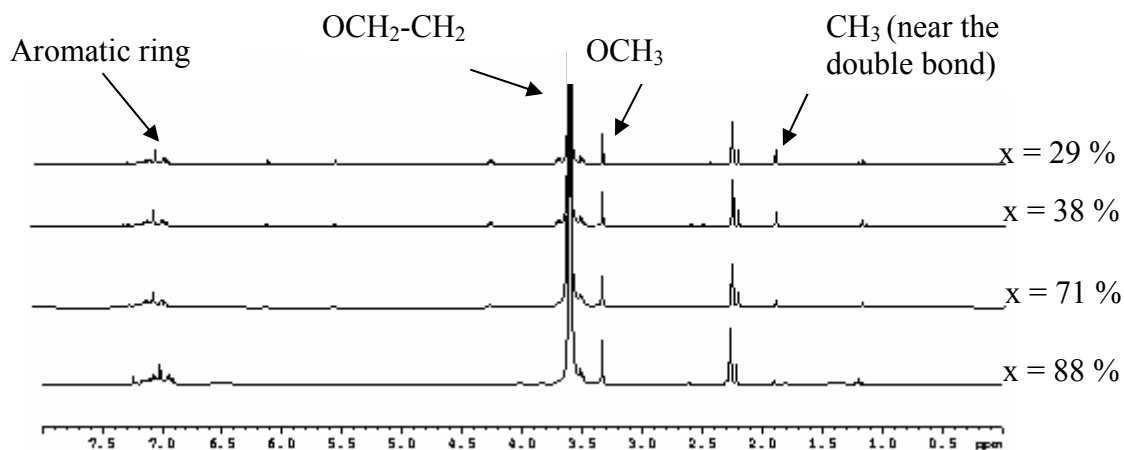


Figure 12.1 ^1H NMR spectra for PEGMA polymerized with PS macroinitiator at different conversion (x). (Polymerization conditions: $[\text{PEGMA}]_0/[\text{PS}]_0/[\text{C}]_0 = 17/1/1$ (molar ratio). PEGMA/xylene = 3:1 (volume ratio) Temperature = 110°C).

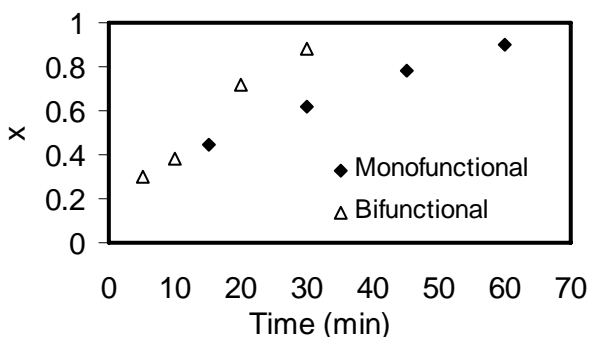


Figure 12.2 Conversion of PEGMA as a function of time using monofunctional and bifunctional macroinitiators. (Polymerization conditions: $[\text{PEGMA}]_0/[\text{PS}]_0/[\text{C}]_0 = 17/1/1$ (molar ratio). PEGMA/xylene = 3:1 (volume ratio) Temperature = 110°C).

Ideally, the formed amphiphilic copolymer should be a block copolymer as suggested in the reaction mechanism shown in Figure 12.3. However, it is known that poly(ethylene glycol) derivatives can suffer side reactions. For instance, the oxyethylene unit in poly(ethylene glycol) and their derivatives can participate in chain transfer to polymer reactions.^[39-41] The longer the oxyethylene chain (which is the case in PEGMA), the higher the probability of this reaction taking place. The presence of chain transfer to polymer can lead to crosslinking, which was, indeed, observed in this study. Crosslinking will increase the polydispersity index and the average molecular weights, as shown in Figures 12.4 and 12.5. The comparison between the two macroinitiators in Figure 12.4 shows that the bifunctional macroinitiators produce polymers with lower polydispersity index.

There are two reasons for this result. The first reason is that bifunctional initiators generally make polymers with narrower molecular distributions than monofunctional initiators as discussed in the previous chapters. The second reason is specific for this system and related to crosslinking. It takes more time for monofunctional initiators to reach a certain monomer conversion than bifunctional initiators. Therefore, the PEGMA will be exposed to the polymerization conditions for a longer time (for the same conversion) when a monofunctional initiator is used; this longer time will enhance crosslinking through side reactions such as transfer to polymer and, as a result, the polydispersity index will increase.

This conclusion is supported by the results presented in Figure 12.5, where the molecular weight starts increasing very fast at high conversions. For example, at 88% conversion of PEGMA, the bifunctional macroinitiator produces polymer with average molecular weight of 46000 g/mol. On the other hand, at 90 % conversion of PEGMA, the monofunctional macroinitiator produces polymer with average molecular weight of almost 66000 g/mol. Although the difference in the conversion is only 2%, the difference in molecular weight is very high because it takes only 30 minutes to achieve 88% conversion with the bifunctional initiator, while it takes one hour to reach 90% conversion with the monofunctional initiator.

Figure 12.5 shows the average molecular weight against conversion. Both macroinitiators show M_n increasing almost linearly with the conversion. Usually this

conclusion is an indication of the livingness of the system. However in this case, it is not absolutely true because the polydispersity index is not as low as living system and the values of the experimental M_n is far away from the theoretical values that can be calculated from the following equation

$$M_n = \text{conversion} \times \frac{[PEGMA]_0}{[PS]_0} \times MW_{PEGMA} + MW_{PS} \quad (2)$$

Three plausible reasons can be explored to explain the deviation between the experimental and the theoretical values (Figure 12.6):

- 1) Termination of the growing chains, although this reason would cause a significant difference. Therefore, it is probably not the main reason.
- 2) Crosslinking (as discussed before), although it is important it would not explain the deviation when the PDI is low (For example the first points has PDI around 1.2).
- 3) Solubility and the miscibility of the polystyrene and xylene in the melt of PEGMA. The last reason leads to termination of some of the polystyrene macroinitiators before they attack the PEGMA. This was clear by measuring the molecular weight of the unreacted fraction of polystyrene. Although the initial average molecular weight of the polystyrene fed to the reactor was 3150 g/mol (in the case of monofunctional case), the GPC measurement of the polystyrene fraction after the copolymerization reaction showed that it has average molecular weight higher than 3150 g/mol. That means the actual initial molar concentration of the PEGMA to PS was not 1:17 as desired in the experiment.

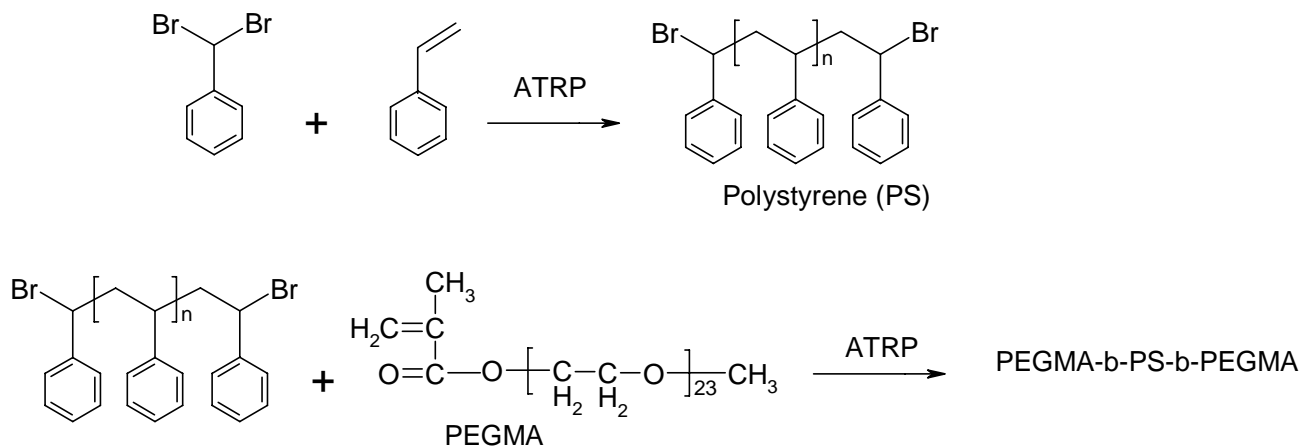


Figure 12.3 Ideal mechanism to form amphiphilic block copolymer of polystyrene and PEGMA.

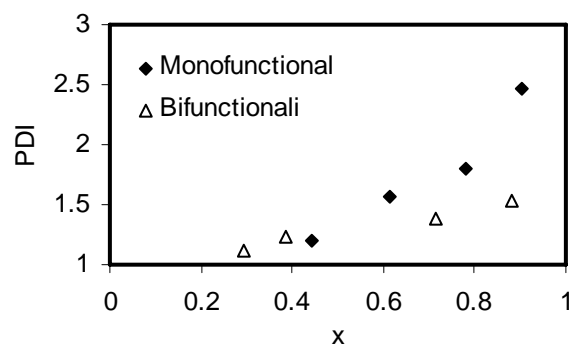


Figure 12.4 Polydispersity index versus conversion of PEGMA using monofunctional and bifunctional macroinitiators. (Polymerization conditions: $[PEGMA]_0/[PS]_0/[C]_0 = 17/1/1$ (molar ratio). PEGMA/xylene = 3:1 (volume ratio) Temperature = 110 °C).

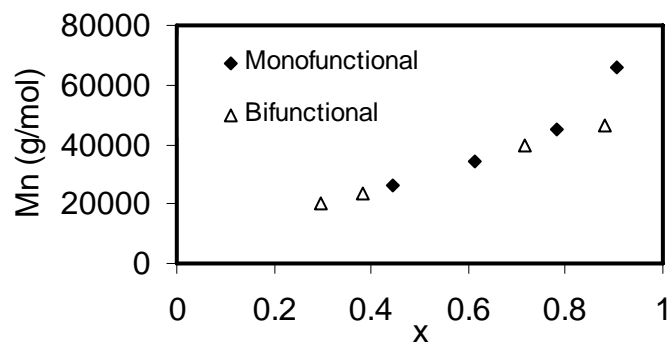


Figure 12.5 Number average molecular weight versus conversion of PEGMA using monofunctional and bifunctional macroinitiators. (Polymerization conditions: $[PEGMA]_0/[PS]_0/[C]_0 = 17/1/1$ (molar ratio). PEGMA/xylene = 3:1 (volume ratio) Temperature = 110 °C).

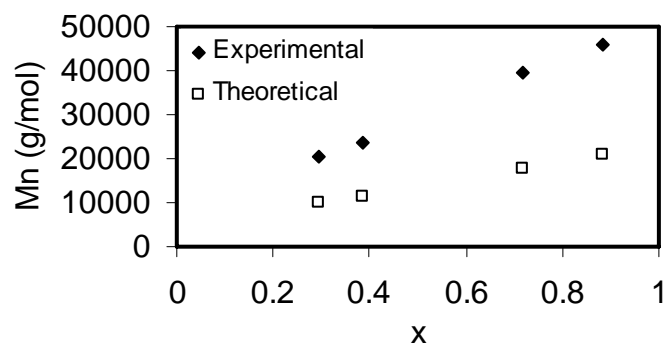


Figure 12.6 Comparison of experimental and theoretical molecular weights of PEGMA polymerized with polystyrene bifunctional macroinitiator. (Polymerization conditions: $[PEGMA]_0/[PS]_0/[C]_0 = 17/1/1$ (molar ratio). PEGMA/xylene = 3:1 (volume ratio) Temperature = 110 °C).

12.5 Conclusion

In this chapter, ATRP was used to synthesise amphiphilic copolymer. The hydrophobic segment is polystyrene and the hydrophilic segment is PEGMA. The resultant copolymer drifts from a block copolymer to a crosslinked copolymer. This drift can be monitored with GPC which indicates the presence of crosslinking from the PDI values. A comparison between two polystyrene macroinitiators (monofunctional and bifunctional) showed that the bifunctional initiators produces polymers with higher conversion and less crosslinking.

12.6 References

- [1] J. Chiefary, YK. Chong, F. Ercole, C. Moad , G. Moad, E. Rizzardo, SH. Thang, *Macromolecules* **1998**, 31, 5559.
- [2] G. Moad, J. Chiefary, YK. Chong, J. Krstina, RTA. Mayadunne, A. Postma, E. Rizzardo, SH.Thang *Polym Int* **2000**, 49, 993.
- [3] MK. Georges, RPN. Veregin, PM. Kazmaier, GK. Hamer, *Macromolecules* **1993**, 26, 2987.
- [4] D. Benoit, V. Chaplinski, R. Braslau, CJ. Hawker, *J Am Chem Soc* **1999**, 121, 3904.
- [5] M. Rodlert, E. Harth, I. Rees, CJ. Hawker, *J Polym Sci, Polym Chem Ed* **2000**, 38, 4749.
- [6] K. Matyjaszewski, J. Xia, *Chem Rev* **2001**,101, 2921.
- [7] M. Kamigaito, T. Ando, M. Sawamoto, *Chem Rev* **2001**, 101, 3689.
- [8] K. Davis, K. Matyjaszewski, *Statistical, gradient, block and graft copolymers by controlled/living radical polymerization*, **2002**.
- [9] T. Davis, K. Matyjaszewski, *Handbook of radical polymerization*, 2002, pp 523.
- [10] [19] X. Zhang, K. Matyjaszewski, *Macromolecules* **1999**, 32, 1763.
- [11] S. Forster, T. Plantenberg *Angew. Chem., Int. Ed.* **2002**, 41,688.
- [12] Z. Gao, S. K. Varshney, S. Wong, A. Eisenberg *Macromolecules***1994**, 27, 7923.
- [13] M. Nakano, H. Matsuoka, H. Yamaoka, A. Poppe, D. Richter *Macromolecules* **1999**, 32, 697.
- [14] L. Zhang, A. Eisenberg, *Science* **1995**, 268, 1728.
- [15] R. Xu, M. A. Winnik, G. Riess, B. Chu, M. D. Croucher *Macromolecules* **1992**, 25, 644.
- [16] Y. Nakayama, M. Miyamura, Y. Hirano, K. Goto, T. Matsuda *Biomaterials* **1999**, 20, 963.
- [17] S. Jo, K. Park *Biomaterials* **2000**, 21, 605.
- [18] P. Wang, K. L. Tan, E. T. Kang *J. Biomater. Sci., Polym. Ed.* **2000**, 11, 169.
- [19] F. Zhang, E.T. Kang, K. G. Neoh, P. Wang, K. L. Tan, *Biomaterials* **2001**, 22, 1541.
- [20] Y. X. Qiu, D. Klee, W. Pluster, B. Severich, H. Hocker *J. Appl. Polym. Sci.* **1996**, 61, 2373.
- [21] S. H. Y. Cheo, P. Wang, K. L. Tan, C. C. Ho, E. T. Kang *J. Mater. Sci.: Mater. Med.* **2001**, 12, 377.
- [22] S. Belfer, R. Fainshtain, Y. Purinson, J. Gilron, M. Nystrom, M. Manttari *J. Membr. Sci.* **2004**, 239, 55.
- [23] Y. Liu, J. Y. Lee, E. T. Kang, P. Wang, K. L. Tan. *React. Funct. Polym.* **2001**, 47, 201.
- [24] B. Reining, H. Keul, H. Hocker, *polymer*, **2002**, 43, 7145.
- [25] M. Mukkaram, A. Harald, D. Stover, *Macromolecules*, **2004**, 37, 5219.
- [26] L. Zhongyu, L. Pengpeng, H. Julina, *Journal of Polymer Science, Part A: Polymer Chemistry*, 44, **2006**, 4361.
- [27] A. Napoli, N. Tirelli, G. Kilcher, A. Hubbell, *Macromolecules*, 34, **2001**, 8913.

- [28] J. Katja, C. Xianyi, K. Jorgen, B. Walther, *Macromolecules*, 31, **1998**, 538.
- [29] D. Neugebauer, Y. Zhang, T. Pakula, K. Matyjaszewski, *Polymer*, 44, **2003**, 6863.
- [30] S. J. Holder, N. A. A. Rossi, C. T. Yeoh, G. G. Durand, M. J. Boerakkerb, N. A. Sommerdijk *J. Mater. Chem.* **2003**, 13, 2771.
- [31] D. Neugebauer, Y. Zhang, T. Pakula, S. S. Sheiko, K. Matyjaszewski *Macromolecules* **2003**, 36, 6746.
- [32] D. Neugebauer, Y. Zhang, T. Pakula, K. Matyjaszewski, *Polymer* **2003**, 44, 6863.
- [33] M. M. Ali, H. D. Stover, *Macromolecules* **2004**, 37, 5219.
- [34] L. Bes, S. Angot, A. Limer, D. M. Haddleton, *Macromolecules* **2003**, 36, 2493.
- [35] S. Han, M. Hagiwara, T. Ishizone, *Macromolecules* **2003**, 36, 8312.
- [36] T. Ishizone, S. Han, S. Okuyama, S. Nakahama, *Macromolecules* **2003**, 36, 42.
- [37] D. Neugebauer, M. Theis, T. Pakula, G. Wegner, K. Matyjaszewski, *Macromolecules* **2006**, 39, 584.
- [38] Al-Harhi M., Cheng L., Soares J. B. P., Simon L. C. J. *Polym.Sci., Part A Polym. Chem.* "Atom-Transfer Radical Polymerization of Styrene with Bifunctional and Monofunctional Initiators: Experimental and Mathematical Modeling Results", Accepted.
- [39] S. Okamura, K. Katagiri, T. Motoyama *J. Polym. Sci.*, 43, **1960**, 509.
- [40] U. S. Nandi, G. Sudesh Kumar, G. C Bhaduri, *Indian J. Chem.* 20°, **1981**, 759.
- [41] P. Fritzsche, A. Schneider, *Acta Polym.* 30, **1979**, 270.

Chapter 13

13 Conclusions and Recommendations

ATRP is one of the most promising techniques in controlled free radical polymerization. Its development during the last years has led to the synthesis of a wide variety of polymers with well-defined microstructures. Many research groups around the world are trying to better understand this living polymerization process and to take it to the next stage of industrial applications. Mathematical models, the main focus of this thesis, are crucial in this development effort.

This thesis contributed to the literature in the field of ATRP with nine journal papers and four conference presentations and posters. Six of the journal papers have already been published or accepted for publication. The other three are submitted for publication. The major contributions of this thesis will be summarized in the next paragraphs.

Conclusions

For the first time, dynamic Monte Carlo models were developed and implemented to simulate ATRP with both monofunctional and bifunctional initiators. Population balances and the method of moments were also used to develop mathematical models for ATRP with both initiator types. The models were validated with experimental case studies obtained in our laboratories or available in the literature. The agreement between the model predictions and the experimental data was very good. Both models, Monte Carlo and method of moments, can predict monomer conversion, average molecular weights and polydispersity index as a function of polymerization time in batch reactors. Moreover, the Monte Carlo model can predict the full molecular weight distribution at any polymerization time and monomer conversion.

We have also systematically examined how several parameters for dynamic Monte Carlo simulation affect computational time and the precision of the simulation results. To the best of our knowledge, this is the first time such a study has been

published for polymerization systems. As a result, we were able to provide useful insights on how the time of Monte Carlo simulations can be decreased without increasing the noise level significantly.

Another major contribution of this thesis is the systematic investigation of the advantages of using bifunctional initiators in ATRP. Experimental and modeling comparisons with monofunctional initiators showed that bifunctional initiators can produce polymers with higher monomer conversion, higher molecular weights, and narrower molecular weight distribution for the same polymerization time.

I also extended the ability of ATRP to synthesize polymers with novel structures by producing amphiphilic copolymers. Two different types of the amphiphilic copolymers were produced using a polystyrene macroinitiator and polyethylene glycol methacrylate macromonomer. This new polymer may have potential for new applications on biomedical systems.

Recommendations

Although this thesis covered a wide range of ATRP modeling, it can be extended in future work to model multifunctional initiators or star copolymers using both the method of moments and Monte Carlo simulation. In this case the model will be complex (but not impossible) and few assumptions are necessary to simplify it for models similar to the ones that were developed here. PREDICI (commercial software) can be more useful in such complex models. It has been used so far in ATRP with monofunctional initiators. It can be applied to multifunctional systems and compared with other models.

In the case of copolymerization, Monte Carlo simulation will be so useful to study the copolymer sequence and monitor the gradient copolymers. More effort in the experimental part will be needed to validate such model. Similarly the proposed model for graft copolymer needs big effort in the experimental part.

More work can be done in relation to the parameters used for simulation. The estimation can be extended to non isothermal cases to determine the Arrhenius

parameters. In this case more experimental data may be necessary to get accurate estimation.

Another direction in the modeling of living free radical polymerizations is the modeling of continuous reactors. The literature has only studies on the monofunctional systems using the method of moments. It can be extended to multifunctional initiators. Monte Carlo simulation can be used also in both monofunctional and multifunctional systems.

As far as the experimental efforts are concerned, more characterization can be done to study the physical properties of the prepared polymers. Living polymerizations are unique to produce gradient copolymers. More effort is required to study this type of polymers and compare it with the other copolymer types. Several copolymerization systems can be used to investigate this study. Similarly for the amphiphilic copolymers, more morphological tests (such as TEM and SEM) can be used to determine their microstructure shapes.